Nucleosome Assembly by the Chaperonosome

-

Complex of a Chaperone-Bound Histone Octamer

Ivan Corbeski

ISBN 978-90-393-7207-4

Doctoral Thesis
Nucleosome Assembly by the Chaperonosome - Complex of a Chaperone-Bound Histone Octamer

Ivan Corbeski
NMR Spectroscopy Research Group,
Bijvoet Center for Biomolecular Research
Department of Chemistry, Faculty of Science
Utrecht University, Netherlands
October 2019

Cover and lay-out design: Ivan Corbeski and ProefschriftMaken
Printed in the Netherlands by ProefschriftMaken | www.proefschriftmaken.nl

Nucleosome Assembly by the Chaperonosome

Complex of a Chaperone-Bound Histone Octamer

Nucleosoom Assemblage door het Chaperonosoom:
Complex van een Chaperonne Gebonden Histon Octameer

(met een samenvatting in het Nederlands)

Proefschrift

ter verkrijging van de graad van doctor aan de Universiteit Utrecht
op gezag van de rector magnificus, prof.dr. H.R.B.M. Kummeling,
ingevolge het besluit van het college voor promoties in het openbaar
te verdedigen op woensdag 16 oktober 2019 des middags te 12.45 uur

door

Ivan Corbeski
geboren op 10 september 1986
te Skopje, Noord-Macedonië

Promotor:

Prof.dr. R. Boelens

Copromotor:

Dr. H. van Ingen

The research described in this thesis is part of the ManiFold project, a Marie Curie Initial Training Network and Innovative Doctoral Programme at Utrecht University, The Netherlands, that is funded by the 7th Framework Programme of the European Union.

Dedicated to my parents and brother.

For all the hard workers,

people who bring peace,

the chaperones out there.

This is my gift to the world.

Table of Contents

“I used to be blind, but now I can see”

John 9:25

“Better sooner than later, but better later than never”

I.C.

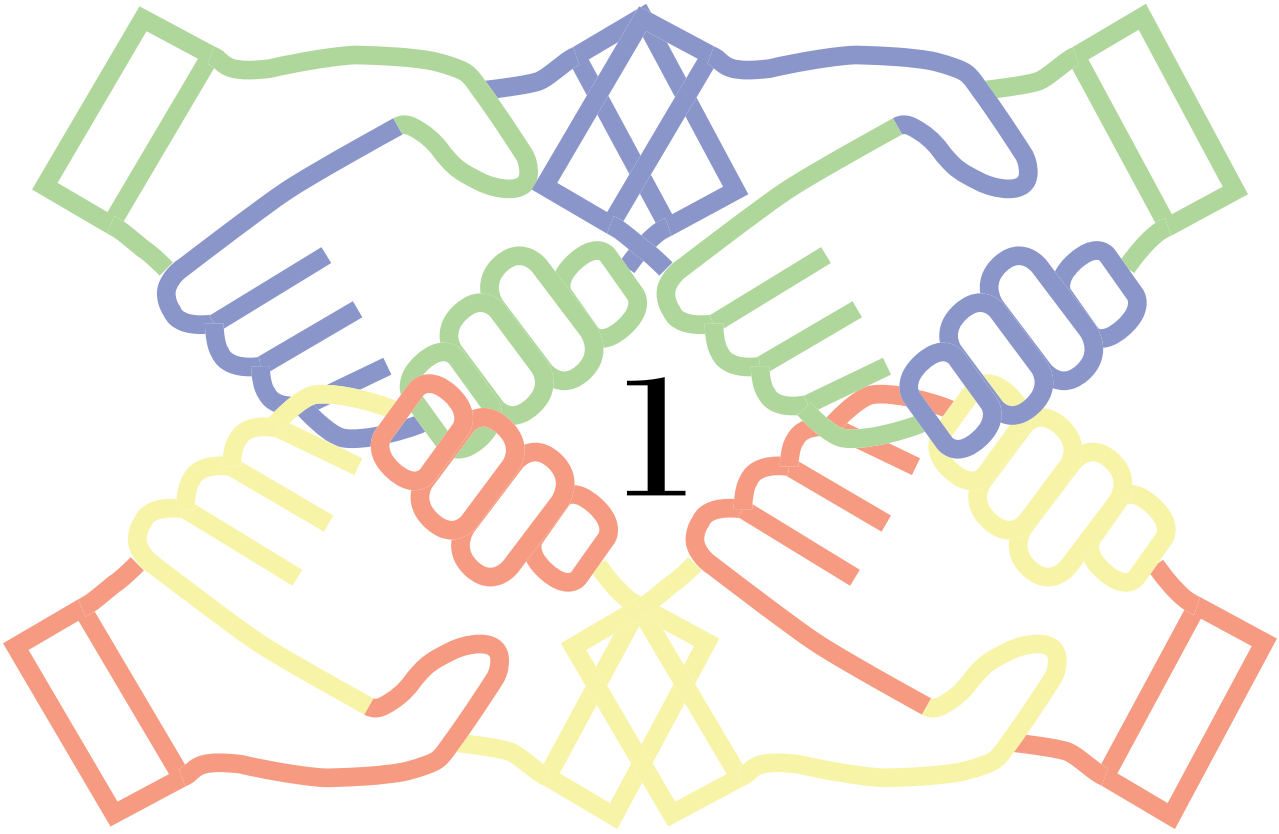
1

Chapter 1

Introduction

HISTONES & THE NUCLEOSOME

In eukaryotes, deoxyribonucleic acid (DNA) is organized into chromatin in a dynamic manner that enables it to be accessed for processes such as replication, transcription and repair. Histones are the main structural proteins associated with DNA in eukaryotic cells. They are basic proteins formed by a common histone-fold domain that is involved in histone-histone and histone-DNA interactions, and extended and flexible tails that play an important role in chromatin regulation. Histones must be assembled, replaced or exchanged to preserve or change the chromatin organization according to cellular needs. They can be divided into two groups: the core histones and the linker histones.

Histones are amongst some of the very first proteins studied and the most abundant proteins in the cell nucleus, yet the plethora of their modifications and their role in the regulation of chromatin were scrutinized only within the last few decades. In 1884, Albrecht Kossel was the first to describe and name these proteins he isolated through acid-extractions from red blood cells of geese (1). In the process, he uncovered their basic nature and association with nucleic acids for which, in conjunction with his work on nucleic acids, he received the 1910 Nobel Prize in Physiology or Medicine for his studies on the chemical composition of the cell nucleus. Over the century that followed others described DNA as carrier of the genome (2), the double-helical structure of DNA (3), association of histone post-translational modifications with chromatin function (4), epigenetics (5) and the histone code (6), fractionation of histones (7-12), composition and structural characterization of the histones and histone octamer (13-18), and identification and structural characterization of the nucleosome as chromatin subunit (7-12,19-24).

HISTONE STRUCTURE

The four core histones H2A, H2B, H3, and H4 are small highly basic proteins, ranging between 11 and 16 kDa, with more than 20% of their amino acid composition being lysines and arginines. They represent some of the most conserved proteins in eukaryotes, highlighting the importance of their role in organizing DNA (25). The histone fold domain is characterized by a long central helix flanked by two shorter helices (Figure 1A). The four different core histones contain additional N- and C-terminal extensions that are specific to each histone. Most notably, they all have an extended basic N-terminal tail. Whereas isolated histones are not folded, the core histones fold into the so-called histone fold as dimers (Figure 1B). The helical bundles form a hydrophobic dimerization interface according to a handshake motif through which the core histones form obligate heterodimers, H2A-H2B and H3-H4, with similar structures. Two H3-H4 dimers can further associate to form an $(H3\text{-}H4)_2$ tetramer through a four-helix bundle involving the $\alpha 2$-$\alpha 3$-helices from each copy of histone H3, and stabilized by both hydrophilic and hydrophobic interactions.

Two H2A-H2B dimers and one $(H3\text{-}H4)_2$ tetramer (or two H3-H4 dimers) can assemble into a histone octamer *in vitro* and *in vivo* (Figure 1C). This structure was first determined in the absence of DNA (15). In the histone octamer, each H2A-H2B dimer is bound to one side of the $(H3\text{-}H4)_2$ tetramer by a structurally similar four-helix bundle formed by the $\alpha 2$-$\alpha 3$-helices

of H2B and H4. This interaction is further aided by the H2A docking domain, a unique C-terminal extension in H2A, which interacts with the $(H3\text{-}H4)_2$ tetramer. Additionally, the two symmetrically related H2A-H2B dimers interact with each other through a small interface comprised of the L1-loop of each H2A. The histone octamer is only stable in the presence of DNA or if the positive charges of the histones are neutralized in high-salt buffer.

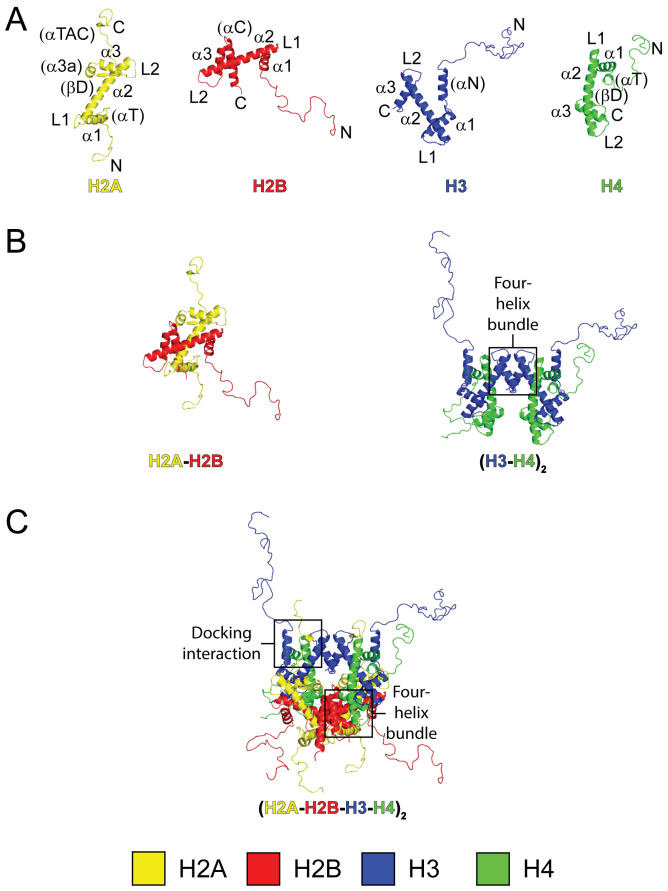

Figure 1. Hierarchical view of histone organization. Histones are depicted in cartoon representation. Structures are taken from Protein Data Bank (PDB, www.rcsb.org) (26) identifier (ID) 2PYO and the histone tails are added by modeling. (A) The four different major core histones with annotation of secondary structure elements: α1-α3 = the three alpha-helices forming the histone fold domain, L1/L2 = the two loops connecting the α1-α2/α2-α3-helices, N = N-terminus, C = C-terminus. In brackets: additional secondary structure elements specific to each histone with naming as in Ref. (27), in particular: βD and αTAC in H2A forming the H2A docking domain, αC in H2B is an additional C-terminal alpha-helix, αN in H3 is an additional N-terminal alpha-helix, βD in H4 forms the H4 docking sequence. All four histones have N-terminal tail domains, H2A has additionally a C-terminal tail. (B) A combination of the H2A and H2B or of the H3 and H4 histone fold domains form the H2A-H2B or H3-H4 histone fold dimers. Two H3-H4 dimers associate via a four-helix bundle formed by the α2-α3-helices of each H3 to form an $(H3\text{-}H4)_2$ tetramer. (C) Two H2A-H2B dimers and one $(H3\text{-}H4)_2$ tetramer associate into a histone octamer stabilized by an additional four-helix bundle between the α2-α3-helices of H2B and H4 and by an interaction between the H2A docking domain and the H3 αN-helix. The N-terminal histone tails extend beyond the folded α-helical core of the histone octamer.

NUCLEOSOME STRUCTURE

The histone octamer forms the protein core of the nucleosome, the fundamental repeating unit of chromatin (22,28) (Figure 2). As such, the octamer fulfills two conflicting functions in the cell. It has to bind and bend the DNA to achieve compaction and partial charge neutralization, but it also has to be able to release specific segments of DNA in a concerted manner to allow the access of DNA-processing enzymes at the appropriate time. This is achieved through the modular nature of the histone octamer: it forms a basic protein core with evenly spaced DNA-binding sites (29) (Figure 2A).

The DNA wrapped around a histone octamer is called nucleosomal DNA (Figure 2B). About 145-147 base pairs (bp) of DNA are needed to bind the octamer, creating the nucleosome core particle (NCP). The nucleosomal DNA is bound in a left-handed superhelix that forms a disc-shaped structure. In conventional terminology, each location where the major groove of the DNA double helix faces towards the center of the disc is designated a "superhelix location" (SHL) number from SHL = 0 at the nucleosomal dyad (center of the nucleosomal DNA) to SHL = ± 7 for the very last region of the nucleosomal DNA (24). Along the two-fold axis, the nucleosomal DNA can be divided into two gyres of approximately 72 bp each. Nucleosomal DNA can be extended on each entry-exit site by an arbitrary length of DNA that will protrude out of the core particle. This is called linker DNA. Histone-DNA particles containing >150 bp of DNA are referred to as mononucleosomes and contain linker DNA. If the DNA is long enough, nucleosomal arrays can form with nucleosomes consisting of ~146-165 bp of DNA wrapped around each histone octamer at ~160-210 bp intervals.

The second type of histone proteins, next to the core histones, are linker histones such as H1 and H5, that can bind to the linker DNA (30) (Figure 2C). Linker histones are much less conserved proteins and do not bear structural similarity to the core histones. Linker histones are monomeric proteins composed of a globular core and long and basic N- and C-terminal tails. A linker histone binds and stabilizes the linker DNA of a mononucleosome to form a so-called chromatosome (Figure 2D). Recently, high-resolution structures of a chromatosome have been solved, highlighting how linker histones promote a closed conformation of the protruding linker DNA ends (31-36).

Within the core particle, the main contacts between histones and DNA are made through the structurally conserved histone-fold domains of the histone octamer. The histone dimers bind to roughly 30 bp of DNA each and are linked in a stable yet flexible manner to form a basic protein core with evenly spaced DNA-binding sites to organize a total of ~120 bp of the nucleosomal DNA (29). The histone octamer surface is largely basic and presents regularly spaced arginine side chains that anchor into the minor groove of the DNA every 10 bp. These arginine-anchors form strong electrostatic interactions with the phosphate backbone of the DNA to impose a tight bending of the DNA in a sequence independent manner. Notably, the structure of the nucleosome core particle showed that the actual path of nucleosomal DNA around the histone octamer was remarkably similar to the path predicted from the earlier structure of the octamer alone (16-18,24). Comparison of the histone octamer structure without and with DNA demonstrated also that both the histone fold domains within each core histone (secondary structure) and the various interaction interfaces between histones observed in the histone octamer (tertiary structure) remained largely unchanged in the nucleosome. These findings show that the determinants for wrapping nucleosomal DNA reside mainly in the core

histone octamer. The remaining ~13 bp at each nucleosomal DNA entry-exit site are bound by the αN-helix of H3. The latter interactions are important for maintaining the stability of the nucleosome (37).

In the eukaryotic cell, many levels of folding are required to allow the DNA, of about two meters length in the case of the human genome, to be packaged in a typical interphase nucleus (38). The first level of compaction is the formation of nucleosomes. They are typically spaced at ~160-210 bp intervals. The folding and further compaction of these so-called nucleosome arrays requires the histone tails and the linker histones (39-42). The core histone tails, particularly of H3 and H4, mediate both intra- and inter-nucleosome interactions by interacting with DNA and the acidic patch, a negatively charged binding interface on the nucleosome surface formed from six H2A and two H2B residues (43,44). The ultimate higher-level organization is called chromatin, a complex superstructure.

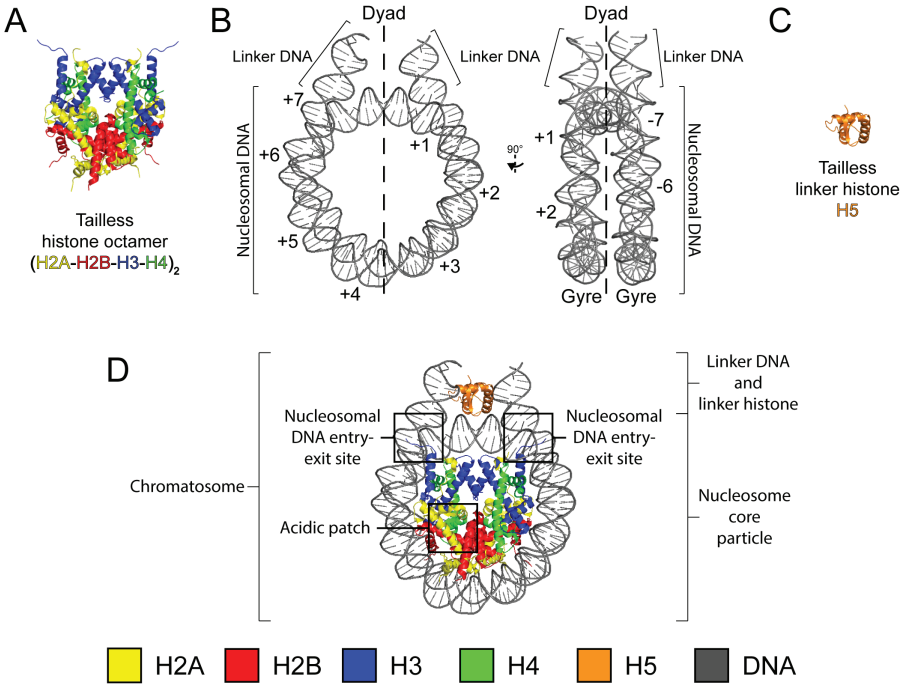

Figure 2. Structural illustration of the chromatosome and its components that make up the nucleosome core and linker region. Structures are taken from PDB ID 4QLC. (A) Histone fold region of the tailless histone octamer. (B) Nucleosomal DNA and linker DNA with a total length of 167 bp. Along the two-fold axis, the nucleosomal DNA (145-147 bp) can be divided into two gyres (approximately 72 bp each). The superhelix location (SHL) designation represents the position of each major groove facing inward. The dyad (center of the nucleosomal DNA) is defined as position SHL=0. The numbers 1-7 highlight the SHLs on the nucleosomal DNA. Linker DNA is the extranucleosomal DNA. (C) The structure of the folded globular domain of linker histone H5. (D) The crystal structure of the chromatosome containing the globular domain of H5 and linker DNA connected through the nucleosomal DNA entry-exit site with the nucleosome core particle containing the tailless histone octamer. The globular domain of the linker histone sits on the dyad of the nucleosome and interacts with both linker DNAs. Location of the acidic patch of one H2A-H2B dimer is indicated. Note that a second acidic patch formed by the other H2A-H2B dimer is situated on the opposite side of the chromatosome.

HISTONE-BASED REGULATION OF CHROMATIN

The histones contain long and basic N-terminal tails of about 15-30 amino acids that protrude out of the nucleosome surface. The tails are generally invisible in structural studies using X-ray crystallography and electron microscopy due to their high flexibility (e.g. see Figure 2A). The N-terminal tails are the main sites of several covalent post-translational modifications (PTMs), including acetylation, methylation and phosphorylation, which are involved in the regulation of access to the underlying DNA and chromatin dynamics (45). The combinatorial nature of histone PTMs has been hypothesized to function as a "histone code" that considerably extends the information potential of the genetic code (6), and which is used in two ways: (i) as a short-term signal, for instance to activate/repress a specific gene in response to cellular demands or to signal for DNA repair after DNA damage, or (ii) as a stable marking system that could be used during cellular differentiation to determine specific chromatin states that are inherited in an epigenetic manner. It was proposed that this epigenetic system represents a regulatory mechanism that has an impact on most, if not all, chromatin processes, directly affecting cell fate and development of both health and disease. The key players of underlying changes in chromatin architecture have been identified as epigenetic modifiers of chromatin and are categorized as: (i) writers, that introduce various chemical modifications on DNA and histones; (ii) readers, specialized protein domains that identify and interpret the modifications; and (iii) erasers, dedicated enzymes that remove the modifications. The effect of histone PTMs and modifications of the DNA on chromatin structure and gene activity can be indirect by recruiting chromatin factors, or direct by changing histone tail interactions within the higher-order chromatin structure (46-48).

Importantly, the synthesis of core histones is highly regulated and balanced. In fact, in the yeast *Saccharomyces cerevisiae* it was shown that overexpression of either H2A-H2B or H3-H4 leads to frequent chromosome loss (49). Therefore, the stoichiometry between histone pairs has to be controlled to ensure the maintenance of genome integrity. In proliferating cells, the bulk of synthesis of the major histones occurs during the S phase of the cell cycle and is coupled to DNA synthesis in order to ensure the assembly of the newly replicated DNA as chromatin. However, a lower level of histone synthesis also takes place outside of S phase, especially of histone variants, such as H2A.X, H2A.Z, H3.3, and CENP-A, which are important for epigenetic regulation and constitutively expressed in small quantities throughout the cell cycle (50-53). These variants are incorporated in replication-independent nucleosome assembly pathways that are distinct from replication-coupled chromatin assembly.

STEPWISE NUCLEOSOME ASSEMBLY

The most extensively studied *in vitro* determinant of nucleosome assembly/disassembly in solution is salt concentration (54-58). In 100-200 mM NaCl, the NCP has been shown to have the same general hydrodynamic shape expected from its crystal structure (55). As the salt concentration is raised above 600 mM NaCl, the nucleosome disassembles through sequential release of H2A-H2B, followed by dissociation of $(H3\text{-}H4)_2$ from the DNA (59). Thus, in contrast to the extremely stable molecular interfaces within H2A-H2B and H3-H4, the interfaces between H2A-H2B and H3-H4 in the nucleosome are

considerably less stable. In addition to the salt concentration in the solution, conformational changes and alterations in the dynamics of the nucleosome can also be caused by drug binding, post-translational modifications, and binding of chromatin-associated proteins such as linker histones and remodeling factors (60-63). The nucleosome assembly pathway is the reverse of the nucleosome disassembly pathway and is thought to consist of a sequential deposition of H3-H4 followed by H2A-H2B (46,64). The stepwise deposition of H3-H4 followed by H2A-H2B onto DNA to form chromatin was demonstrated by showing that a micrococcal nuclease resistant H3-H4-DNA complex could be isolated and converted to mature chromatin by the addition of H2A-H2B (65). However, NCPs do not form spontaneously if histones and DNA are mixed under physiological conditions but instead form insoluble aggregates. Hence, in order to achieve nucleosome assembly under physiological conditions, additional factors are necessary to mediate this process. These factors are a special family of molecular chaperones: histone chaperones.

HISTONE CHAPERONES

In vivo, there is a crucial need for an ordered deposition of histones onto DNA to form nucleosomes, not only during DNA replication, but also during gene expression or when a cell encounters DNA damage. During cell metabolism, histones are not continuously associated with DNA. Newly synthesized histones have to be transported to the nucleus and targeted to the required location, whereas old or damaged histones have to be discarded. In addition, cellular processes involving DNA can require transient histone eviction and replacement. In some phases of the cell cycle histone storage is important (66). As histones are highly basic proteins, their presence in the cell could lead to deleterious effects through promiscuous interactions with DNA or other proteins, and aggregation. Thus, under most circumstances, when histones are not in association with DNA, they are bound to histone chaperones (67). These proteins prevent unintended interactions of histones with other factors and help to control histone supply and incorporation into chromatin. Thus, histone chaperones are key factors for securing an intact chromatin. After all, it was found that the two most abundant histone chaperones in the yeast *Saccharomyces cerevisiae* are, taken together, present in copy numbers equal to the number of nucleosomes in the cell (68).

A molecular chaperone is a protein that associates with a target protein and prevents its unspecific interactions, thereby avoiding the production of inactive or aggregated forms. Histone chaperones are a class of proteins responsible for: (i) binding of the basic histones, (ii) shielding them from nonspecific interactions with DNA and other factors, (iii) their nuclear import, and (iv) facilitating their deposition onto DNA either by directly transferring them to DNA or by handing them over to other chaperones (69-72). Histone chaperones are thus crucial for the process of nucleosome assembly and disassembly (Figure 3).

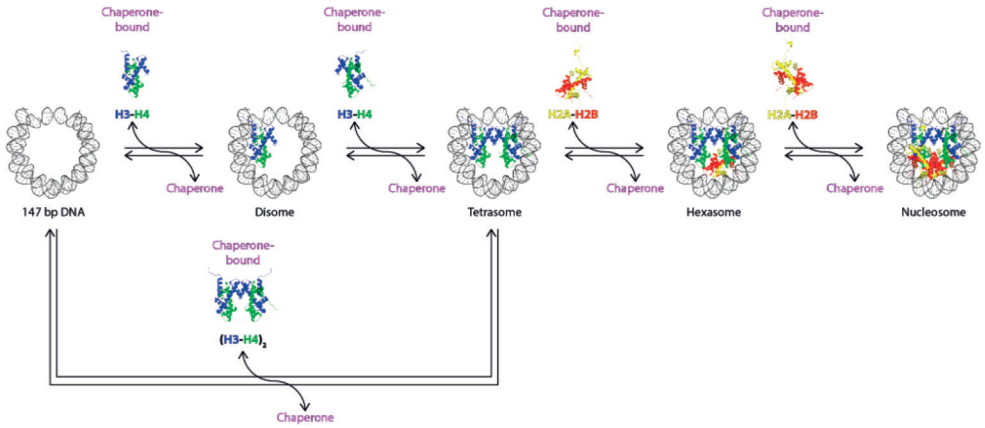

Figure 3. Illustration of the chaperone-mediated nucleosome assembly and disassembly process. Structures of tailless histones and nucleosomal DNA are taken from PDB ID 2PYO. In the nucleosome assembly process from left to right, nucleosomal DNA of 147 bp length is wrapped by a sequential addition of H3-H4 and H2A-H2B dimers to form the nucleosome via several stable intermediates. In an alternative route, instead of two sequential additions of H3-H4 dimers, one $(H3\text{-}H4)_2$ tetramer can be added in one step. The nucleosome disassembly from right to left is the reverse of the assembly process. Each step is mediated by a histone chaperone. The histone complexes are either bound to a chaperone or to DNA. Note that *in vivo* several additional factors can contribute to nucleosome assembly and disassembly which are left out here for simplicity. These factors include the histone tails, post-translational modifications, histone variants, linker DNA and linker histones, DNA-processing enzymes such as DNA and ribonucleic acid (RNA) polymerases, and chromatin remodeling factors.

Histones appear constantly under surveillance by specific chaperones potentially involved in each step of the histone metabolism including folding, nuclear transport, incorporation into defined chromatin structures, storage, and post-translational modification (73). Throughout its lifetime, an individual histone may be passed between different chaperones that dictate its movement within the cell, its assembly into specific chromatin locations and its covalent modifications. Histone chaperones can also provide a connection with other regulators of cellular metabolism and are involved in integrating and possibly transferring information concerning the cellular status.

Since histones are found as H2A-H2B and H3-H4 pairs, or monomeric linker histones, histone chaperones have preferential affinity for one of these histone species. Histone chaperones are structurally diverse with few common structural features (74) (Figure 4). A proteome-wide functional analysis showed that nuclear and chromatin binding proteins are predicted to be enriched in intrinsically disordered regions (IDRs) (75,76). This suggests that IDRs may play an important role in regulating the cellular and nuclear processes related to chromatin assembly and regulation. IDRs and acidic stretches are found in most histone chaperones and may play key roles in histone binding and charge shielding. A prime example is the prothymosin-α histone chaperone of linker histone H1 that forms a purely electrostatically driven ultrahigh-affinity complex in which both chaperone and histone (tail domain) remain largely disordered (77). The extent in which IDRs in histone chaperones contribute to binding affinity and specificity in general is not well understood due to difficulties in the structural characterization of these IDRs (78).

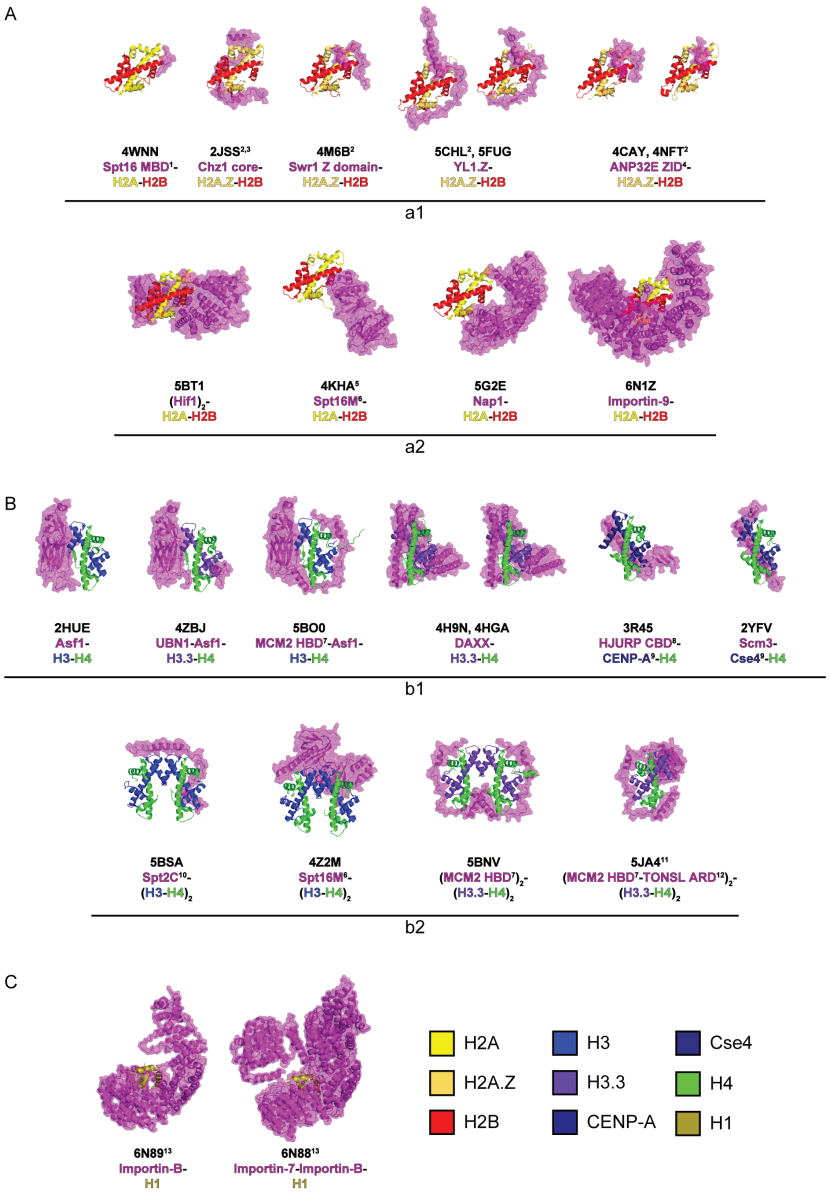

Figure 4. Histone chaperone-histone complexes. Annotations: [1]Minimal binding domain; [2]H2B-H2A.Z chimera; [3]NMR structure; [4]H2A.Z interacting domain; [5]Spt16M-H2B chimera; [6]Middle domain; [7]Histone binding domain; [8]CENP-A binding domain; [9]Histone H3-like centromeric protein; [10]Conserved C terminus; [11]The biological unit is a dimer, shown is the monomeric asymmetric unit; [12]Ankyrin repeat domain; [13]Cryo EM structure. The structures were obtained by X-ray crystallography and shown are the biological units, unless indicated otherwise. Structures are shown in cartoon representation, the chaperones (all magenta) additionally in transparent surface representation. The PDB ID and the composition of the complex with name of the histone chaperone (name of the domain or fragment indicated where applicable) and histone complex are listed below each structure. (A) Histone chaperones of H2A-H2B or variants thereof. a1: small chaperone protein fragments or polypeptides. a2: folded chaperone proteins or protein domains. (B) Histone chaperones of H3-H4 or variants thereof. b1: histone chaperones binding the H3-H4 dimer. b2: histone chaperones binding the $(H3\text{-}H4)_2$ tetramer. (C) Histone chaperones of linker histone H1.

Several H2A-H2B specific chaperones use IDRs to bind key DNA interaction sites on the histones, as shown by the structures of the histone chaperone-histone complexes of Spt16 (79) and H2A.Z-H2B chaperones Chz1 (80), Swr1 (81), YL1 (82,83), and ANP32E (84,85). Spt16, Swr1 and ANP32E interact with the patch of H2B that is made up of its α1- and α2-helices (α1-α2-patch), whereas Chz1 interacts with the α1-α2-patch of H2A.Z and YL1 interacts with both of the patches which are key interaction sites for DNA in the nucleosome (Figure 4A, a1). Swr1, YL1, and ANP32E interact additionally with the H2A.Z specific αC-helix, explaining their specificity for this histone variant. Structured H2A-H2B chaperones are Hif1 (86), Spt16 (middle domain) (87), Nap1 (88), and Importin-9 (89) (Figure 4A, a2). Hif1 interferes with DNA and H3-H4 binding to H2A-H2B in the nucleosome. The Spt16 middle domain binds to the α1-α2-region of H2B, albeit caution should be taken as for the interpretation of this interaction as the structure was obtained by using a fusion construct between the chaperone domain and H2B which might have artificially enforced the interaction. Nap1 covers most of the H2A-H2B DNA interaction surface. Importin-9 is a nuclear import receptor and wraps around the globular core region of H2A-H2B to form an extensive interface.

For H3-H4, several structured and unstructured chaperones have been identified (Figure 4B). H3-H4 represents a special case as it can form stable $(H3\text{-}H4)_2$ tetramers. Hence, there are chaperones that can bind H3-H4 dimers (Figure 4B, b1) and/or $(H3\text{-}H4)_2$ tetramers (Figure 4B, b2). Asf1 is a structured protein and binds to the α2- and α3-helices of H3 and hence prevents tetramerization of H3-H4 (90). Asf1 can form co-chaperone complexes with chaperones that bind to the DNA interaction surface of H3-H4 such as UBN1 and MCM2, which use IDRs to bind in particular to the α1-α2-patch of H3 (91-94). Furthermore, UBN1 is a chaperone specific to the variant H3.3 due to its special composition of amino acids that make up its α1-α2-patch while MCM2 can bind both canonical and variant H3. Another H3.3 chaperone is DAXX which envelops H3.3-H4 to form an extensive interface whereas it is predominantly unfolded in the absence of its histone binding partner (95-97). Finally, chaperones HJURP and Scm3 bind dimers containing the histone H3-like centromeric proteins CENP-A and Scm3, respectively (98-100). Both HJURP and Scm3 interfere with H3-H4 tetramerization and DNA binding.

Histone chaperones Spt2 and Spt16 (middle domain) specifically recognize the $(H3\text{-}H4)_2$ tetramer and bind to its periphery, mimicking the trajectory of nucleosomal DNA (101,102). Two copies of histone chaperone MCM2 can also bind the $(H3\text{-}H4)_2$ tetramer, covering its DNA and H2A-H2B interaction surfaces (92). This complex of $(H3\text{-}H4)_2$ with MCM2 can be recognized by the protein TONSL which binds the H4 N-terminal tail and is part of a homologous recombination complex (103).

Finally, Importin-7 and Importin-β form a cradle to chaperone and transport linker histone H1 into the cell nucleus (104) (Figure 4C). Interestingly, transient and nonspecific electrostatic interactions form and shape the complex and the H1 tail serves as a zipper that closes and stabilizes it through so-called "fuzzy" interactions (105).

The activity of histone chaperones is typically measured by their ability to mediate histone deposition onto DNA *in vitro*. However, *in vivo*, some chaperones are restricted to handling histones at earlier stages in the delivery pathway and only a few chaperones are recognized as actual deposition factors. It remains unclear what functional properties are required to assemble nucleosomes, but shared features include the ability to deposit H3-H4 onto DNA.

Studies on histone chaperone Nap1 have led to a thermodynamic model of nucleosome assembly (106). Nap1 has a very high affinity for histones with K_D values of ~10 nM and ~20 nM for H2A-H2B and H3-H4, respectively. Of the two histone pairs, H3-H4 interacts stronger with DNA with a K_D value of ~2 nM. Hence, the model postulates that Nap1 carries out nucleosome assembly by regulating the concentration of free histones, in particular by maintaining a low concentration of free histones due to its high-affinity binding. Maintaining a low concentration of free histones prevents unspecific histone-DNA interactions that would lead to aggregation and instead promotes specific and productive interactions that lead to nucleosome assembly. An additional Nap1 study refined this model by also analyzing affinities of the components involved with stable intermediates of the nucleosome assembly process (107). In particular, Nap1 promotes nucleosome assembly not by delivering histones, but through disfavoring nonnucleosomal interactions between H2A-H2B dimers and DNA, both *in vitro* and *in vivo*, thereby ensuring that nucleosome assembly goes via sequential deposition of H3-H4 followed by H2A-H2B onto DNA (see Figure 3). Together, these studies led to the current paradigm in which nucleosome assembly depends on the elimination of competing, nonnucleosomal histone-DNA interactions by histone chaperones.

In addition to preventing non-native interactions, histone chaperones may also promote nucleosome assembly by direct delivery of histone dimers to the DNA, as has been proposed for chaperones Hif1 (86), CAF1 (108), and FACT (109). Yet, the mechanisms of how these chaperones transition from histone binding, in which the functional DNA binding surfaces are shielded, to histone release for deposition onto DNA, remain unclear.

A HISTONE CHAPERONE IN DNA DOUBLE-STRAND BREAK REPAIR BY NON-HOMOLOGOUS END JOINING

DNA packaging into nucleosomes and higher-order chromatin structures restricts DNA accessibility for DNA repair. This led to the Access-Repair-Restore (ARR) model which integrates nucleosome dynamics in the repair process and constitutes a foundation for studying DNA damage response (DDR) related chromatin changes (110,111). This model postulates that chromatin has to be disassembled, at least partially, prior to binding of repair factors on damaged DNA, and then reassembled after the repair process is completed. Restoring chromatin organization and its original information, the so-called epigenome, is key for maintaining cell identity.

Recently it has become clear that histone variants and chromatin-associated proteins are integral components of the DDR. In particular, histone variants and their specific chaperones and associated remodelers fulfill important roles during all steps of the DDR: they contribute to early DNA damage signaling, DNA repair, fine-tuning and amplification of checkpoint signals, restoration of chromatin organization after repair, and finally, turning off of checkpoint signals. To take this into account, the ARR model has been expanded to include a "priming" step of chromatin that involves histone variant replacement with the assistance of histone chaperones followed by a concerted repair and restoration process, emphasizing the direct link between chaperone-mediated nucleosome assembly and DNA repair (110).

DNA double-strand breaks (DSBs) are common events in eukaryotic cells. There are an estimated 10-50 DSBs per cell and cell cycle (112,113). There are two major pathways for repairing them: homologous recombination (HR) and non-homologous end joining (NHEJ). NHEJ is active throughout the cell cycle, whereas repair of DSBs via HR occurs only in late S and G2 phases when a sister chromatid is available for accurate, template-mediated repair (114). In non-dividing haploid cells or in diploid cells that are not in S phase, a homology donor is not nearby and NHEJ is the repair pathway (115).

In mitotic cells, DSBs are all pathologic except the specialized subset of physiologic DSBs created during variable (diversity) joining (V(D)J) recombination in the development of T and B cells in the vertebrate immune system (116-118). Major pathologic causes of DSBs include replication across a nick, giving rise to chromatid breaks during S phase. Such DSBs are ideally repaired by HR using the nearby sister chromatid. All of the remaining pathologic forms of DSBs are repaired primarily by NHEJ because they mostly occur outside of S phase. These causes include reactive oxygen species (ROS) from oxidative metabolism, ionizing radiation (IR), and action of DNA processing enzymes (119).

NHEJ (sometimes referred to as classical or cNHEJ) is the major pathway for repair of IR-induced DSBs in human cells (117,118). A characteristic is the damage or loss of bases, as well as production of DNA single strand breaks (SSBs) that frequently terminate in non-ligatable end groups (120,121). The presence of SSBs on both DNA strands can yield a DSB. Moreover, IR-induced DSBs are frequently surrounded by other DNA lesions, such as base damage, that together make IR-induced DSBs difficult to repair and one of the most cytotoxic forms of DNA damage. Consequently, NHEJ in response to IR-induced DNA damage requires flexibility to respond to complex and variable types of DSBs. This also requires the removal of the histones from the damage site and neighboring DNA regions for complete processing of the DNA damage.

To reduce toxicity and genome instability, DSB repair by NHEJ requires detection and tethering of DSB ends, processing of DNA termini to remove non-ligatable end groups, and ligation, and all without releasing the DNA ends. DNA end detection is initiated by the Ku70/80 heterodimer (Ku) (122), followed by recruitment of core NHEJ factors including DNA-dependent protein kinase catalytic subunit (DNA-PKcs) (123,124), the XRCC4-DNA ligase IV (X4L4) complex (125), and XRCC4-like factor (XLF) (126). Loss of any of these core NHEJ factors is associated with radiation sensitivity and defective V(D)J recombination and immune defects (127-132). NHEJ occurs in three distinct stages (see also Figure 5): (i) detection of the DSB by Ku and subsequent tethering by DNA-PKcs to form the DNA-PKcs-Ku-DNA complex (termed DNA-PK), (ii) processing of the lesions to remove damaged DNA and non-ligatable end groups at the termini of the DSB to facilitate ligation, and (iii) ligation of the DNA ends by X4L4 that functions in complex with XLF (133). Apart from DSB detection by Ku, the order of recruitment of the different NHEJ proteins may be flexible and not all NHEJ components may be required for repair of all types of lesions (134,135). Thus, a model is emerging in which NHEJ may take place within a dynamic, multi-protein complex (136).

Ku also interacts with accessory factors such as Aprataxin and Polynucleotide kinase Like Factor (APLF). Recently, APLF has emerged as an important scaffolding protein in NHEJ (137). APLF is largely an intrinsically disordered protein that binds Ku, DNA-PK, and X4L4 within an extended flexible NHEJ core complex that supports DNA accessibility while possibly providing flexible attachment of the core repair complex to chromatin. APLF has an N-terminal forkhead

associated (FHA) domain to interact with phosphorylated X4 (138,139), while interacting with Ku80 via its middle domain (140,141), and poly-(ADP-ribose) (PAR) via its C-terminal PAR-binding zinc finger (PBZ) domains (142-145). Furthermore, APLF acts as a histone chaperone and binds to histones via its unstructured C-terminal acidic domain (146), and the C-terminal ~150 amino acids of APLF have been associated with 3'-5'-exonuclease activity (139,147). APLF stimulates the rate of NHEJ early after damage and the rate of X4L4-mediated ligation, and promotes the retention of X4 at DSBs *in vivo* (140,148). Despite its involvement in the multiple steps of NHEJ, the basis for the regulatory and structural activities of APLF has been unknown. In particular, its histone chaperone activity has not been integrated into the model of NHEJ thus far.

Since APLF is positioned in the core repair complex at the break site, its histone chaperone activity may play a role in restoration of chromatin after DSB repair. For example, APLF could store the original histones and subsequently promote nucleosome formation after DNA repair. Such preservation of the original histones is essential to maintain the epigenetic status of chromatin through the repair process. Furthermore, APLF could contribute to DNA damage-induced chromatin relaxation and compaction, which are thought to be sequential events in the repair process. After rapid relaxation of chromatin to facilitate efficient detection of DNA lesions (149-151), chromatin is transiently condensed to promote DNA damage signaling (151,152). APLF could have a function in this chromatin compaction step by depositing specific histone variants at or near the break site. The histone chaperone function of APLF might be crucial for this.

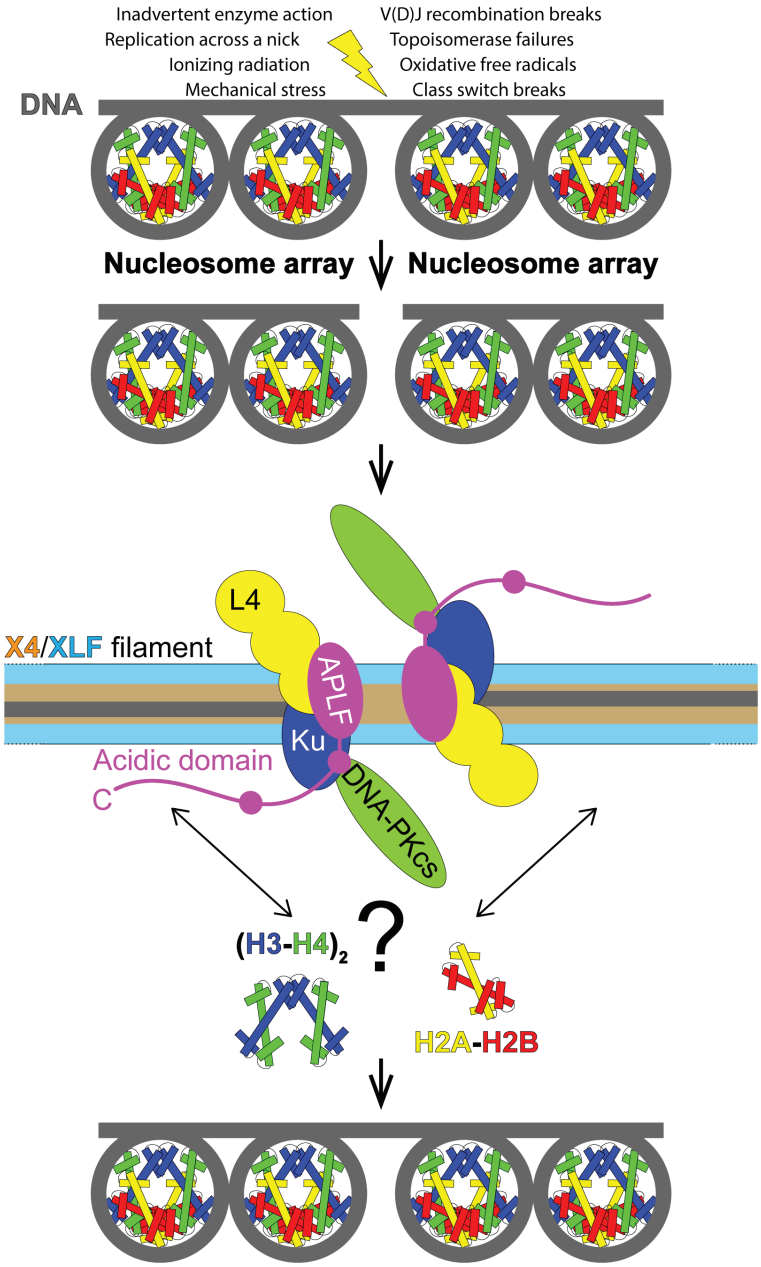

Figure 5. The architecture of DNA double-strand break (DSB) repair by NHEJ. DSBs are detected by the Ku70/80 heterodimer (Ku), which interacts with multiple components of the NHEJ machinery, including DNA-PKcs, XLF, and APLF, recruiting them to DSBs. Once the DSB is detected, various enzymes may be involved in processing of the DSB ends, for example, removal of non-ligatable end groups and gap filling by DNA polymerases (not shown for simplicity). Schematic representation of DNA pairing by the Ku-nucleated XRCC4 and DNA ligase IV (X4L4)/XLF filament. DNA-PKcs is tethered by Ku (153). The APLF-FHA domain interacts with X4 (154). At the same time, APLF residues in its central region bridge Ku80 and DNA-PKcs. The Ku-nucleated X4/XLF filament maintains DNA end alignment (155,156). The role of APLF is to scaffold X4L4 with the Ku/DNA-PKcs assembly. Aligned DNA ends are stabilized by the Ku-X4L4-XLF-APLF complex. X4L4 is present at the break site as a multi-protein complex with XLF. The break is resealed by L4.

SCOPE OF THIS THESIS

This thesis describes a detailed investigation, using a variety of biochemical and biophysical methods, of the histone chaperone activity of the APLF acidic domain ($APLF^{AD}$) with the goal of understanding the function of this activity in NHEJ DNA repair.

Chapter 2 is adapted from a protocol published in the book *Bacterial Chromatin: Methods and Protocols* (157). Here, we describe in detail the use of microscale thermophoresis (MST) to study protein interactions in general, and the interaction of $APLF^{AD}$ with histone complexes H2A-H2B and $(H3\text{-}H4)_2$ in particular. We put emphasis on the step-by-step optimization of experimental conditions and provide strategies to detect and overcome experimental issues.

Chapter 3 is adapted from a publication in the journal *Nucleic Acids Research* (158). Here, we complement the MST data from **Chapter 2** by investigating the molecular basis of the histone chaperone function of $APLF^{AD}$, in particular for the histone complex H2A-H2B, using a combination of nuclear magnetic resonance (NMR) spectroscopy, crosslinking, isothermal titration calorimetry (ITC), and a functional histone chaperone assay. We present a structural model of the H2A-H2B-$APLF^{AD}$ complex and its functional implications in NHEJ DNA repair.

Chapter 4 is in preparation for submission for publication. Here, we carry on with the investigation of the histone chaperone function of $APLF^{AD}$ by including the histone complex H3-H4 as well as the histone octamer complex. Using a combination of analytical gel filtrations, native and crosslinking mass spectrometry, ITC, NMR spectroscopy, small-angle X-ray scattering, and a functional histone chaperone assay, we build a structural model of the histone octamer-$APLF^{AD}$ complex, the major discovery of this work. Based on this, we propose a new paradigm of histone chaperone function and implement that in a sophisticated nucleosome assembly mechanism.

In **Chapter 5**, we discuss the major findings of our investigations and detail the implications of our discoveries. We discuss the chaperone-histone interactions involved in the histone octamer-$APLF^{AD}$ complex, its limitations, mechanisms, and functions in DNA repair. We discuss how other histone chaperones function and make a link of our findings to a different type of molecular chaperone involved in protein folding. Finally, we propose future perspectives for histone chaperone research.

REFERENCES

1. Kossel, A. (1884) Ueber einen peptonartigen Bestandtheil des Zellkerns. *Z Physiol Chem*, **8**, 511-515.
2. Avery, O.T., Macleod, C.M. and McCarty, M. (1944) Studies on the Chemical Nature of the Substance Inducing Transformation of Pneumococcal Types : Induction of Transformation by a Desoxyribonucleic Acid Fraction Isolated from Pneumococcus Type Iii. *J Exp Med*, **79**, 137-158.
3. Watson, J.D. and Crick, F.H. (1953) Molecular structure of nucleic acids; a structure for deoxyribose nucleic acid. *Nature*, **171**, 737-738.
4. Allfrey, V.G., Faulkner, R. and Mirsky, A.E. (1964) Acetylation and Methylation of Histones and Their Possible Role in the Regulation of Rna Synthesis. *Proc Natl Acad Sci U S A*, **51**, 786-794.
5. Turner, B.M. (1993) Decoding the nucleosome. *Cell*, **75**, 5-8.
6. Jenuwein, T. and Allis, C.D. (2001) Translating the histone code. *Science*, **293**, 1074-1080.
7. Johns, E.W., Phillips, D.M., Simson, P. and Butler, J.A. (1960) Improved fractionations of arginine-rich histones from calf thymus. *Biochem J*, **77**, 631-636.
8. Johns, E.W. and Butler, J.A. (1962) Further fractionations of histones from calf thymus. *Biochem J*, **82**, 15-18.
9. Phillips, D.M. and Johns, E.W. (1965) A Fractionation of the Histones of Group F2a from Calf Thymus. *Biochem J*, **94**, 127-130.
10. Johns, E.W. (1967) A method for the selective extraction of histone fractions f2(a)1 and f2(a)2 from calf thymus deoxyribonucleoprotein at pH7. *Biochem J*, **105**, 611-614.
11. Johns, E.W. (1968) The fractionation of the histones of group F2(b) from calf thymus. *Eur J Biochem*, **4**, 437-441.
12. Johns, E.W. and Diggle, J.H. (1969) A method for the large scale preparation of the avian erythrocyte specific histone F2C. *Eur J Biochem*, **11**, 495-498.
13. D'Anna, J.A., Jr. and Isenberg, I. (1974) A histone cross-complexing pattern. *Biochemistry*, **13**, 4992-4997.
14. Roark, D.E., Geoghegan, T.E. and Keller, G.H. (1974) A two-subunit histone complex from calf thymus. *Biochem Biophys Res Commun*, **59**, 542-547.
15. Arents, G., Burlingame, R.W., Wang, B.C., Love, W.E. and Moudrianakis, E.N. (1991) The nucleosomal core histone octamer at 3.1 A resolution: a tripartite protein assembly and a left-handed superhelix. *Proc Natl Acad Sci U S A*, **88**, 10148-10152.
16. Arents, G. and Moudrianakis, E.N. (1993) Topography of the histone octamer surface: repeating structural motifs utilized in the docking of nucleosomal DNA. *Proc Natl Acad Sci U S A*, **90**, 10489-10493.
17. Moudrianakis, E.N. and Arents, G. (1993) Structure of the histone octamer core of the nucleosome and its potential interactions with DNA. *Cold Spring Harb Symp Quant Biol*, **58**, 273-279.
18. Arents, G. and Moudrianakis, E.N. (1995) The histone fold: a ubiquitous architectural motif utilized in DNA compaction and protein dimerization. *Proc Natl Acad Sci U S A*, **92**, 11170-11174.
19. Olins, A.L. and Olins, D.E. (1974) Spheroid chromatin units (v bodies). *Science*, **183**, 330-332.
20. Kornberg, R.D. (1974) Chromatin structure: a repeating unit of histones and DNA. *Science*, **184**, 868-871.
21. Kornberg, R.D. and Thomas, J.O. (1974) Chromatin structure; oligomers of the histones. *Science*, **184**, 865-868.
22. Oudet, P., Gross-Bellard, M. and Chambon, P. (1975) Electron microscopic and biochemical evidence that chromatin structure is a repeating unit. *Cell*, **4**, 281-300.
23. Richmond, T.J., Finch, J.T., Rushton, B., Rhodes, D. and Klug, A. (1984) Structure of the nucleosome core particle at 7 A resolution. *Nature*, **311**, 532-537.
24. Luger, K., Mader, A.W., Richmond, R.K., Sargent, D.F. and Richmond, T.J. (1997) Crystal structure of the nucleosome core particle at 2.8 A resolution. *Nature*, **389**, 251-260.
25. Hansen, J.C. (2002) Conformational dynamics of the chromatin fiber in solution: determinants, mechanisms, and functions. *Annu Rev Biophys Biomol Struct*, **31**, 361-392.
26. Berman, H.M., Westbrook, J., Feng, Z., Gilliland, G., Bhat, T.N., Weissig, H., Shindyalov, I.N. and Bourne, P.E. (2000) The Protein Data Bank. *Nucleic Acids Res*, **28**, 235-242.
27. Chantalat, L., Nicholson, J.M., Lambert, S.J., Reid, A.J., Donovan, M.J., Reynolds, C.D., Wood, C.M. and Baldwin, J.P. (2003) Structure of the histone-core octamer in KCl/phosphate crystals at 2.15 A resolution. *Acta Crystallogr D Biol Crystallogr*, **59**, 1395-1407.
28. Kornberg, R.D. (1977) Structure of chromatin. *Annu Rev Biochem*, **46**, 931-954.
29. Luger, K. and Richmond, T.J. (1998) DNA binding within the nucleosome core. *Curr Opin Struct Biol*, **8**, 33-40.
30. Fyodorov, D.V., Zhou, B.R., Skoultchi, A.I. and Bai, Y. (2018) Emerging roles of linker histones in regulating chromatin structure and function. *Nat Rev Mol Cell Biol*, **19**, 192-206.
31. Ramakrishnan, V., Finch, J.T., Graziano, V., Lee, P.L. and Sweet, R.M. (1993) Crystal structure of globular domain of histone H5 and its implications for nucleosome binding. *Nature*, **362**, 219-223.
32. Zhou, B.R., Jiang, J., Feng, H., Ghirlando, R., Xiao, T.S. and Bai, Y. (2015) Structural Mechanisms of Nucleosome Recognition by Linker Histones. *Mol Cell*, **59**, 628-638.

33. Bednar, J., Garcia-Saez, I., Boopathi, R., Cutter, A.R., Papai, G., Reymer, A., Syed, S.H., Lone, I.N., Tonchev, O., Crucifix, C. *et al.* (2017) Structure and Dynamics of a 197 bp Nucleosome in Complex with Linker Histone H1. *Mol Cell*, **66**, 384-397 e388.
34. Garcia-Saez, I., Menoni, H., Boopathi, R., Shukla, M.S., Soueidan, L., Noirclerc-Savoye, M., Le Roy, A., Skoufias, D.A., Bednar, J., Hamiche, A. *et al.* (2018) Structure of an H1-Bound 6-Nucleosome Array Reveals an Untwisted Two-Start Chromatin Fiber Conformation. *Mol Cell*, **72**, 902-915 e907.
35. Zhou, B.R., Jiang, J., Ghirlando, R., Norouzi, D., Sathish Yadav, K.N., Feng, H., Wang, R., Zhang, P., Zhurkin, V. and Bai, Y. (2018) Revisit of Reconstituted 30-nm Nucleosome Arrays Reveals an Ensemble of Dynamic Structures. *J Mol Biol*, **430**, 3093-3110.
36. Zhou, Y.B., Gerchman, S.E., Ramakrishnan, V., Travers, A. and Muyldermans, S. (1998) Position and orientation of the globular domain of linker histone H5 on the nucleosome. *Nature*, **395**, 402-405.
37. Iwasaki, W., Miya, Y., Horikoshi, N., Osakabe, A., Taguchi, H., Tachiwana, H., Shibata, T., Kagawa, W. and Kurumizaka, H. (2013) Contribution of histone N-terminal tails to the structure and stability of nucleosomes. *FEBS Open Bio*, **3**, 363-369.
38. Horn, P.J. and Peterson, C.L. (2002) Molecular biology. Chromatin higher order folding--wrapping up transcription. *Science*, **297**, 1824-1827.
39. Zlatanova, J. and Doenecke, D. (1994) Histone H1 zero: a major player in cell differentiation? *FASEB J*, **8**, 1260-1268.
40. Zlatanova, J. and van Holde, K. (1996) The linker histones and chromatin structure: new twists. *Prog Nucleic Acid Res Mol Biol*, **52**, 217-259.
41. Zlatanova, J., Caiafa, P. and Van Holde, K. (2000) Linker histone binding and displacement: versatile mechanism for transcriptional regulation. *FASEB J*, **14**, 1697-1704.
42. Zlatanova, J., Seebart, C. and Tomschik, M. (2008) The linker-protein network: control of nucleosomal DNA accessibility. *Trends Biochem Sci*, **33**, 247-253.
43. Pepenella, S., Murphy, K.J. and Hayes, J.J. (2014) Intra- and inter-nucleosome interactions of the core histone tail domains in higher-order chromatin structure. *Chromosoma*, **123**, 3-13.
44. Kalashnikova, A.A., Porter-Goff, M.E., Muthurajan, U.M., Luger, K. and Hansen, J.C. (2013) The role of the nucleosome acidic patch in modulating higher order chromatin structure. *J R Soc Interface*, **10**, 20121022.
45. Strahl, B.D. and Allis, C.D. (2000) The language of covalent histone modifications. *Nature*, **403**, 41-45.
46. Annunziato, A.T. and Hansen, J.C. (2000) Role of histone acetylation in the assembly and modulation of chromatin structures. *Gene Expr*, **9**, 37-61.
47. Eberharter, A. and Becker, P.B. (2002) Histone acetylation: a switch between repressive and permissive chromatin. Second in review series on chromatin dynamics. *EMBO Rep*, **3**, 224-229.
48. Shahbazian, M.D. and Grunstein, M. (2007) Functions of site-specific histone acetylation and deacetylation. *Annu Rev Biochem*, **76**, 75-100.
49. Meeks-Wagner, D. and Hartwell, L.H. (1986) Normal stoichiometry of histone dimer sets is necessary for high fidelity of mitotic chromosome transmission. *Cell*, **44**, 43-52.
50. Henikoff, S. (2008) Nucleosome destabilization in the epigenetic regulation of gene expression. *Nat Rev Genet*, **9**, 15-26.
51. Probst, A.V., Dunleavy, E. and Almouzni, G. (2009) Epigenetic inheritance during the cell cycle. *Nat Rev Mol Cell Biol*, **10**, 192-206.
52. Yuan, G. and Zhu, B. (2013) Histone variants and epigenetic inheritance. *Biochim Biophys Acta*, **1819**, 222-229.
53. Buschbeck, M. and Hake, S.B. (2017) Variants of core histones and their roles in cell fate decisions, development and cancer. *Nat Rev Mol Cell Biol*, **18**, 299-314.
54. Ausio, J., Seger, D. and Eisenberg, H. (1984) Nucleosome core particle stability and conformational change. Effect of temperature, particle and NaCl concentrations, and crosslinking of histone H3 sulfhydryl groups. *J Mol Biol*, **176**, 77-104.
55. Czarnota, G.J. and Ottensmeyer, F.P. (1996) Structural states of the nucleosome. *J Biol Chem*, **271**, 3677-3683.
56. Dong, F., Nelson, C. and Ausio, J. (1990) Analysis of the changes in the structure and hydration of the nucleosome core particle at moderate ionic strengths. *Biochemistry*, **29**, 10710-10716.
57. Eisenberg, H. and Felsenfeld, G. (1981) Hydrodynamic studies of the interaction between nucleosome core particles and core histones. *J Mol Biol*, **150**, 537-555.
58. Yager, T.D. and van Holde, K.E. (1984) Dynamics and equilibria of nucleosomes at elevated ionic strength. *J Biol Chem*, **259**, 4212-4222.
59. Yager, T.D., McMurray, C.T. and van Holde, K.E. (1989) Salt-induced release of DNA from nucleosome core particles. *Biochemistry*, **28**, 2271-2281.
60. Chaires, J.B. (1983) Daunomycin inhibits the B leads to Z transition in poly d(G-C). *Nucleic Acids Res*, **11**, 8485-8494.
61. Guschin, D., Chandler, S. and Wolffe, A.P. (1998) Asymmetric linker histone association directs the asymmetric rearrangement of core histone interactions in a positioned nucleosome containing a thyroid hormone response element. *Biochemistry*, **37**, 8629-8636.

62. Lee, K.M. and Hayes, J.J. (1998) Linker DNA and H1-dependent reorganization of histone-DNA interactions within the nucleosome. *Biochemistry*, **37**, 8622-8628.
63. Zhou, K., Gaullier, G. and Luger, K. (2019) Nucleosome structure and dynamics are coming of age. *Nat Struct Mol Biol*, **26**, 3-13.
64. Fletcher, T.M. and Hansen, J.C. (1996) The nucleosomal array: structure/function relationships. *Crit Rev Eukaryot Gene Expr*, **6**, 149-188.
65. Smith, S. and Stillman, B. (1991) Stepwise assembly of chromatin during DNA replication in vitro. *EMBO J*, **10**, 971-980.
66. Woodland, H.R. and Adamson, E.D. (1977) The synthesis and storage of histones during the oogenesis of Xenopus laevis. *Dev Biol*, **57**, 118-135.
67. Loyola, A. and Almouzni, G. (2004) Histone chaperones, a supporting role in the limelight. *Biochim Biophys Acta*, **1677**, 3-11.
68. McCullough, L., Connell, Z., Petersen, C. and Formosa, T. (2015) The Abundant Histone Chaperones Spt6 and FACT Collaborate to Assemble, Inspect, and Maintain Chromatin Structure in Saccharomyces cerevisiae. *Genetics*, **201**, 1031-1045.
69. Liu, W.H. and Churchill, M.E. (2012) Histone transfer among chaperones. *Biochem Soc Trans*, **40**, 357-363.
70. Burgess, R.J. and Zhang, Z. (2013) Histone chaperones in nucleosome assembly and human disease. *Nat Struct Mol Biol*, **20**, 14-22.
71. Li, Q., Burgess, R. and Zhang, Z. (2013) All roads lead to chromatin: multiple pathways for histone deposition. *Biochim Biophys Acta*, **1819**, 238-246.
72. Park, Y.J. and Luger, K. (2008) Histone chaperones in nucleosome eviction and histone exchange. *Curr Opin Struct Biol*, **18**, 282-289.
73. Pardal, A.J., Fernandes-Duarte, F. and Bowman, A.J. (2019) The histone chaperoning pathway: from ribosome to nucleosome. *Essays Biochem*, **63**, 29-43.
74. Hammond, C.M., Stromme, C.B., Huang, H., Patel, D.J. and Groth, A. (2017) Histone chaperone networks shaping chromatin function. *Nat Rev Mol Cell Biol*, **18**, 141-158.
75. Ward, J.J., Sodhi, J.S., McGuffin, L.J., Buxton, B.F. and Jones, D.T. (2004) Prediction and functional analysis of native disorder in proteins from the three kingdoms of life. *J Mol Biol*, **337**, 635-645.
76. Tompa, P. (2012) Intrinsically disordered proteins: a 10-year recap. *Trends Biochem Sci*, **37**, 509-516.
77. Borgia, A., Borgia, M.B., Bugge, K., Kissling, V.M., Heidarsson, P.O., Fernandes, C.B., Sottini, A., Soranno, A., Buholzer, K.J., Nettels, D. *et al.* (2018) Extreme disorder in an ultrahigh-affinity protein complex. *Nature*, **555**, 61-66.
78. Warren, C. and Shechter, D. (2017) Fly Fishing for Histones: Catch and Release by Histone Chaperone Intrinsically Disordered Regions and Acidic Stretches. *J Mol Biol*, **429**, 2401-2426.
79. Kemble, D.J., McCullough, L.L., Whitby, F.G., Formosa, T. and Hill, C.P. (2015) FACT Disrupts Nucleosome Structure by Binding H2A-H2B with Conserved Peptide Motifs. *Mol Cell*, **60**, 294-306.
80. Zhou, Z., Feng, H., Hansen, D.F., Kato, H., Luk, E., Freedberg, D.I., Kay, L.E., Wu, C. and Bai, Y. (2008) NMR structure of chaperone Chz1 complexed with histones H2A.Z-H2B. *Nat Struct Mol Biol*, **15**, 868-869.
81. Hong, J., Feng, H., Wang, F., Ranjan, A., Chen, J., Jiang, J., Ghirlando, R., Xiao, T.S., Wu, C. and Bai, Y. (2014) The catalytic subunit of the SWR1 remodeler is a histone chaperone for the H2A.Z-H2B dimer. *Mol Cell*, **53**, 498-505.
82. Latrick, C.M., Marek, M., Ouararhni, K., Papin, C., Stoll, I., Ignatyeva, M., Obri, A., Ennifar, E., Dimitrov, S., Romier, C. *et al.* (2016) Molecular basis and specificity of H2A.Z-H2B recognition and deposition by the histone chaperone YL1. *Nat Struct Mol Biol*, **23**, 309-316.
83. Liang, X., Shan, S., Pan, L., Zhao, J., Ranjan, A., Wang, F., Zhang, Z., Huang, Y., Feng, H., Wei, D. *et al.* (2016) Structural basis of H2A.Z recognition by SRCAP chromatin-remodeling subunit YL1. *Nat Struct Mol Biol*, **23**, 317-323.
84. Obri, A., Ouararhni, K., Papin, C., Diebold, M.L., Padmanabhan, K., Marek, M., Stoll, I., Roy, L., Reilly, P.T., Mak, T.W. *et al.* (2014) ANP32E is a histone chaperone that removes H2A.Z from chromatin. *Nature*, **505**, 648-653.
85. Mao, Z., Pan, L., Wang, W., Sun, J., Shan, S., Dong, Q., Liang, X., Dai, L., Ding, X., Chen, S. *et al.* (2014) Anp32e, a higher eukaryotic histone chaperone directs preferential recognition for H2A.Z. *Cell Res*, **24**, 389-399.
86. Zhang, M., Liu, H., Gao, Y., Zhu, Z., Chen, Z., Zheng, P., Xue, L., Li, J., Teng, M. and Niu, L. (2016) Structural Insights into the Association of Hif1 with Histones H2A-H2B Dimer and H3-H4 Tetramer. *Structure*, **24**, 1810-1820.
87. Hondele, M., Stuwe, T., Hassler, M., Halbach, F., Bowman, A., Zhang, E.T., Nijmeijer, B., Kotthoff, C., Rybin, V., Amlacher, S. *et al.* (2013) Structural basis of histone H2A-H2B recognition by the essential chaperone FACT. *Nature*, **499**, 111-114.
88. Aguilar-Gurrieri, C., Larabi, A., Vinayachandran, V., Patel, N.A., Yen, K., Reja, R., Ebong, I.O., Schoehn, G., Robinson, C.V., Pugh, B.F. *et al.* (2016) Structural evidence for Nap1-dependent H2A-H2B deposition and nucleosome assembly. *EMBO J*, **35**, 1465-1482.

89. Padavannil, A., Sarkar, P., Kim, S.J., Cagatay, T., Jiou, J., Brautigam, C.A., Tomchick, D.R., Sali, A., D'Arcy, S. and Chook, Y.M. (2019) Importin-9 wraps around the H2A-H2B core to act as nuclear importer and histone chaperone. *Elife*, **8**.
90. English, C.M., Adkins, M.W., Carson, J.J., Churchill, M.E. and Tyler, J.K. (2006) Structural basis for the histone chaperone activity of Asf1. *Cell*, **127**, 495-508.
91. Ricketts, M.D., Frederick, B., Hoff, H., Tang, Y., Schultz, D.C., Singh Rai, T., Grazia Vizioli, M., Adams, P.D. and Marmorstein, R. (2015) Ubinuclein-1 confers histone H3.3-specific-binding by the HIRA histone chaperone complex. *Nat Commun*, **6**, 7711.
92. Huang, H., Stromme, C.B., Saredi, G., Hodl, M., Strandsby, A., Gonzalez-Aguilera, C., Chen, S., Groth, A. and Patel, D.J. (2015) A unique binding mode enables MCM2 to chaperone histones H3-H4 at replication forks. *Nat Struct Mol Biol*, **22**, 618-626.
93. Richet, N., Liu, D., Legrand, P., Velours, C., Corpet, A., Gaubert, A., Bakail, M., Moal-Raisin, G., Guerois, R., Compper, C. *et al.* (2015) Structural insight into how the human helicase subunit MCM2 may act as a histone chaperone together with ASF1 at the replication fork. *Nucleic Acids Res*, **43**, 1905-1917.
94. Wang, H., Wang, M., Yang, N. and Xu, R.-M. (2015) Structure of the quaternary complex of histone H3-H4 heterodimer with chaperone ASF1 and the replicative helicase subunit MCM2. *Protein & Cell*, **6**, 693-697.
95. Elsasser, S.J., Huang, H., Lewis, P.W., Chin, J.W., Allis, C.D. and Patel, D.J. (2012) DAXX envelops a histone H3.3-H4 dimer for H3.3-specific recognition. *Nature*, **491**, 560-565.
96. Liu, C.P., Xiong, C., Wang, M., Yu, Z., Yang, N., Chen, P., Zhang, Z., Li, G. and Xu, R.M. (2012) Structure of the variant histone H3.3-H4 heterodimer in complex with its chaperone DAXX. *Nat Struct Mol Biol*, **19**, 1287-1292.
97. DeNizio, J.E., Elsasser, S.J. and Black, B.E. (2014) DAXX co-folds with H3.3/H4 using high local stability conferred by the H3.3 variant recognition residues. *Nucleic Acids Res*, **42**, 4318-4331.
98. Zhou, Z., Feng, H., Zhou, B.R., Ghirlando, R., Hu, K., Zwolak, A., Miller Jenkins, L.M., Xiao, H., Tjandra, N., Wu, C. *et al.* (2011) Structural basis for recognition of centromere histone variant CenH3 by the chaperone Scm3. *Nature*, **472**, 234-237.
99. Cho, U.S. and Harrison, S.C. (2011) Recognition of the centromere-specific histone Cse4 by the chaperone Scm3. *Proc Natl Acad Sci U S A*, **108**, 9367-9371.
100. Hu, H., Liu, Y., Wang, M., Fang, J., Huang, H., Yang, N., Li, Y., Wang, J., Yao, X., Shi, Y. *et al.* (2011) Structure of a CENP-A-histone H4 heterodimer in complex with chaperone HJURP. *Genes Dev*, **25**, 901-906.
101. Chen, S., Rufiange, A., Huang, H., Rajashankar, K.R., Nourani, A. and Patel, D.J. (2015) Structure-function studies of histone H3/H4 tetramer maintenance during transcription by chaperone Spt2. *Genes Dev*, **29**, 1326-1340.
102. Tsunaka, Y., Fujiwara, Y., Oyama, T., Hirose, S. and Morikawa, K. (2016) Integrated molecular mechanism directing nucleosome reorganization by human FACT. *Genes Dev*, **30**, 673-686.
103. Saredi, G., Huang, H., Hammond, C.M., Alabert, C., Bekker-Jensen, S., Forne, I., Reveron-Gomez, N., Foster, B.M., Mlejnkova, L., Bartke, T. *et al.* (2016) H4K20me0 marks post-replicative chromatin and recruits the TONSL-MMS22L DNA repair complex. *Nature*, **534**, 714-718.
104. Ivic, N., Potocnjak, M., Solis-Mezarino, V., Herzog, F., Bilokapic, S. and Halic, M. (2019) Fuzzy Interactions Form and Shape the Histone Transport Complex. *Mol Cell*.
105. Fuxreiter, M. (2018) Fuzziness in Protein Interactions-A Historical Perspective. *J Mol Biol*, **430**, 2278-2287.
106. Andrews, A.J., Downing, G., Brown, K., Park, Y.J. and Luger, K. (2008) A thermodynamic model for Nap1-histone interactions. *J Biol Chem*, **283**, 32412-32418.
107. Andrews, A.J., Chen, X., Zevin, A., Stargell, L.A. and Luger, K. (2010) The histone chaperone Nap1 promotes nucleosome assembly by eliminating nonnucleosomal histone DNA interactions. *Mol Cell*, **37**, 834-842.
108. Mattiroli, F., Gu, Y., Yadav, T., Balsbaugh, J.L., Harris, M.R., Findlay, E.S., Liu, Y., Radebaugh, C.A., Stargell, L.A., Ahn, N.G. *et al.* (2017) DNA-mediated association of two histone-bound complexes of yeast Chromatin Assembly Factor-1 (CAF-1) drives tetrasome assembly in the wake of DNA replication. *Elife*, **6**.
109. Wang, T., Liu, Y., Edwards, G., Krzizike, D., Scherman, H. and Luger, K. (2018) The histone chaperone FACT modulates nucleosome structure by tethering its components. *Life Science Alliance*, **1**.
110. Soria, G., Polo, S.E. and Almouzni, G. (2012) Prime, repair, restore: the active role of chromatin in the DNA damage response. *Mol Cell*, **46**, 722-734.
111. Smerdon, M.J. (1991) DNA repair and the role of chromatin structure. *Curr Opin Cell Biol*, **3**, 422-428.
112. Haber, J.E. (1999) DNA recombination: the replication connection. *Trends Biochem Sci*, **24**, 271-275.
113. Vilenchik, M.M. and Knudson, A.G. (2003) Endogenous DNA double-strand breaks: production, fidelity of repair, and induction of cancer. *Proc Natl Acad Sci U S A*, **100**, 12871-12876.
114. Rothkamm, K., Kruger, I., Thompson, L.H. and Lobrich, M. (2003) Pathways of DNA double-strand break repair during the mammalian cell cycle. *Mol Cell Biol*, **23**, 5706-5715.
115. Moore, J.K. and Haber, J.E. (1996) Cell cycle and genetic requirements of two pathways of nonhomologous end-joining repair of double-strand breaks in Saccharomyces cerevisiae. *Mol Cell Biol*, **16**, 2164-2173.

116. Helmink, B.A. and Sleckman, B.P. (2012) The response to and repair of RAG-mediated DNA double-strand breaks. *Annu Rev Immunol*, **30**, 175-202.
117. Mahaney, B.L., Meek, K. and Lees-Miller, S.P. (2009) Repair of ionizing radiation-induced DNA double-strand breaks by non-homologous end-joining. *Biochem J*, **417**, 639-650.
118. Lieber, M.R. (2010) The mechanism of double-strand DNA break repair by the nonhomologous DNA end-joining pathway. *Annu Rev Biochem*, **79**, 181-211.
119. Riballo, E., Kuhne, M., Rief, N., Doherty, A., Smith, G.C., Recio, M.J., Reis, C., Dahm, K., Fricke, A., Krempler, A. *et al.* (2004) A pathway of double-strand break rejoining dependent upon ATM, Artemis, and proteins locating to gamma-H2AX foci. *Mol Cell*, **16**, 715-724.
120. Cadet, J., Ravanat, J.L., TavernaPorro, M., Menoni, H. and Angelov, D. (2012) Oxidatively generated complex DNA damage: tandem and clustered lesions. *Cancer Lett*, **327**, 5-15.
121. Georgakilas, A.G., O'Neill, P. and Stewart, R.D. (2013) Induction and repair of clustered DNA lesions: what do we know so far? *Radiat Res*, **180**, 100-109.
122. Grundy, G.J., Moulding, H.A., Caldecott, K.W. and Rulten, S.L. (2014) One ring to bring them all--the role of Ku in mammalian non-homologous end joining. *DNA Repair (Amst)*, **17**, 30-38.
123. Gottlieb, T.M. and Jackson, S.P. (1993) The DNA-dependent protein kinase: requirement for DNA ends and association with Ku antigen. *Cell*, **72**, 131-142.
124. Gell, D. and Jackson, S.P. (1999) Mapping of protein-protein interactions within the DNA-dependent protein kinase complex. *Nucleic Acids Res*, **27**, 3494-3502.
125. Mari, P.O., Florea, B.I., Persengiev, S.P., Verkaik, N.S., Bruggenwirth, H.T., Modesti, M., Giglia-Mari, G., Bezstarosti, K., Demmers, J.A., Luider, T.M. *et al.* (2006) Dynamic assembly of end-joining complexes requires interaction between Ku70/80 and XRCC4. *Proc Natl Acad Sci U S A*, **103**, 18597-18602.
126. Yano, K., Morotomi-Yano, K., Wang, S.Y., Uematsu, N., Lee, K.J., Asaithamby, A., Weterings, E. and Chen, D.J. (2008) Ku recruits XLF to DNA double-strand breaks. *EMBO Rep*, **9**, 91-96.
127. Zha, S., Guo, C., Boboila, C., Oksenych, V., Cheng, H.L., Zhang, Y., Wesemann, D.R., Yuen, G., Patel, H., Goff, P.H. *et al.* (2011) ATM damage response and XLF repair factor are functionally redundant in joining DNA breaks. *Nature*, **469**, 250-254.
128. van der Burg, M., van Dongen, J.J. and van Gent, D.C. (2009) DNA-PKcs deficiency in human: long predicted, finally found. *Curr Opin Allergy Clin Immunol*, **9**, 503-509.
129. Nijnik, A., Dawson, S., Crockford, T.L., Woodbine, L., Visetnoi, S., Bennett, S., Jones, M., Turner, G.D., Jeggo, P.A., Goodnow, C.C. *et al.* (2009) Impaired lymphocyte development and antibody class switching and increased malignancy in a murine model of DNA ligase IV syndrome. *J Clin Invest*, **119**, 1696-1705.
130. Woodbine, L., Neal, J.A., Sasi, N.K., Shimada, M., Deem, K., Coleman, H., Dobyns, W.B., Ogi, T., Meek, K., Davies, E.G. *et al.* (2013) PRKDC mutations in a SCID patient with profound neurological abnormalities. *J Clin Invest*, **123**, 2969-2980.
131. Lee, P.P., Woodbine, L., Gilmour, K.C., Bibi, S., Cale, C.M., Amrolia, P.J., Veys, P.A., Davies, E.G., Jeggo, P.A. and Jones, A. (2013) The many faces of Artemis-deficient combined immunodeficiency - Two patients with DCLRE1C mutations and a systematic literature review of genotype-phenotype correlation. *Clin Immunol*, **149**, 464-474.
132. Girard, P.M., Kysela, B., Harer, C.J., Doherty, A.J. and Jeggo, P.A. (2004) Analysis of DNA ligase IV mutations found in LIG4 syndrome patients: the impact of two linked polymorphisms. *Hum Mol Genet*, **13**, 2369-2376.
133. Wang, C. and Lees-Miller, S.P. (2013) Detection and repair of ionizing radiation-induced DNA double strand breaks: new developments in nonhomologous end joining. *Int J Radiat Oncol Biol Phys*, **86**, 440-449.
134. Yano, K. and Chen, D.J. (2008) Live cell imaging of XLF and XRCC4 reveals a novel view of protein assembly in the non-homologous end-joining pathway. *Cell Cycle*, **7**, 1321-1325.
135. Gu, J. and Lieber, M.R. (2008) Mechanistic flexibility as a conserved theme across 3 billion years of nonhomologous DNA end-joining. *Genes Dev*, **22**, 411-415.
136. Williams, G.J., Hammel, M., Radhakrishnan, S.K., Ramsden, D., Lees-Miller, S.P. and Tainer, J.A. (2014) Structural insights into NHEJ: building up an integrated picture of the dynamic DSB repair super complex, one component and interaction at a time. *DNA Repair (Amst)*, **17**, 110-120.
137. Hammel, M., Yu, Y., Radhakrishnan, S.K., Chokshi, C., Tsai, M.S., Matsumoto, Y., Kuzdovich, M., Remesh, S.G., Fang, S., Tomkinson, A.E. *et al.* (2016) An Intrinsically Disordered APLF Links Ku, DNA-PKcs, and XRCC4-DNA Ligase IV in an Extended Flexible Non-homologous End Joining Complex. *J Biol Chem*, **291**, 26987-27006.
138. Iles, N., Rulten, S., El-Khamisy, S.F. and Caldecott, K.W. (2007) APLF (C2orf13) is a novel human protein involved in the cellular response to chromosomal DNA strand breaks. *Mol Cell Biol*, **27**, 3793-3803.
139. Kanno, S., Kuzuoka, H., Sasao, S., Hong, Z., Lan, L., Nakajima, S. and Yasui, A. (2007) A novel human AP endonuclease with conserved zinc-finger-like motifs involved in DNA strand break responses. *EMBO J*, **26**, 2094-2103.

140. Grundy, G.J., Rulten, S.L., Zeng, Z., Arribas-Bosacoma, R., Iles, N., Manley, K., Oliver, A. and Caldecott, K.W. (2013) APLF promotes the assembly and activity of non-homologous end joining protein complexes. *EMBO J*, **32**, 112-125.
141. Shirodkar, P., Fenton, A.L., Meng, L. and Koch, C.A. (2013) Identification and functional characterization of a Ku-binding motif in aprataxin polynucleotide kinase/phosphatase-like factor (APLF). *J Biol Chem*, **288**, 19604-19613.
142. Ahel, I., Ahel, D., Matsusaka, T., Clark, A.J., Pines, J., Boulton, S.J. and West, S.C. (2008) Poly(ADP-ribose)-binding zinc finger motifs in DNA repair/checkpoint proteins. *Nature*, **451**, 81-85.
143. Eustermann, S., Brockmann, C., Mehrotra, P.V., Yang, J.C., Loakes, D., West, S.C., Ahel, I. and Neuhaus, D. (2010) Solution structures of the two PBZ domains from human APLF and their interaction with poly(ADP-ribose). *Nat Struct Mol Biol*, **17**, 241-243.
144. Li, G.Y., McCulloch, R.D., Fenton, A.L., Cheung, M., Meng, L., Ikura, M. and Koch, C.A. (2010) Structure and identification of ADP-ribose recognition motifs of APLF and role in the DNA damage response. *Proc Natl Acad Sci U S A*, **107**, 9129-9134.
145. Fenton, A.L., Shirodkar, P., Macrae, C.J., Meng, L. and Koch, C.A. (2013) The PARP3- and ATM-dependent phosphorylation of APLF facilitates DNA double-strand break repair. *Nucleic Acids Res*, **41**, 4080-4092.
146. Mehrotra, P.V., Ahel, D., Ryan, D.P., Weston, R., Wiechens, N., Kraehenbuehl, R., Owen-Hughes, T. and Ahel, I. (2011) DNA repair factor APLF is a histone chaperone. *Mol Cell*, **41**, 46-55.
147. Li, S., Kanno, S., Watanabe, R., Ogiwara, H., Kohno, T., Watanabe, G., Yasui, A. and Lieber, M.R. (2011) Polynucleotide kinase and aprataxin-like forkhead-associated protein (PALF) acts as both a single-stranded DNA endonuclease and a single-stranded DNA 3' exonuclease and can participate in DNA end joining in a biochemical system. *J Biol Chem*, **286**, 36368-36377.
148. Rulten, S.L., Fisher, A.E., Robert, I., Zuma, M.C., Rouleau, M., Ju, L., Poirier, G., Reina-San-Martin, B. and Caldecott, K.W. (2011) PARP-3 and APLF function together to accelerate nonhomologous end-joining. *Mol Cell*, **41**, 33-45.
149. Khurana, S., Kruhlak, M.J., Kim, J., Tran, A.D., Liu, J., Nyswaner, K., Shi, L., Jailwala, P., Sung, M.H., Hakim, O. *et al.* (2014) A macrohistone variant links dynamic chromatin compaction to BRCA1-dependent genome maintenance. *Cell Rep*, **8**, 1049-1062.
150. Timinszky, G., Till, S., Hassa, P.O., Hothorn, M., Kustatscher, G., Nijmeijer, B., Colombelli, J., Altmeyer, M., Stelzer, E.H., Scheffzek, K. *et al.* (2009) A macrodomain-containing histone rearranges chromatin upon sensing PARP1 activation. *Nat Struct Mol Biol*, **16**, 923-929.
151. Burgess, R.C., Burman, B., Kruhlak, M.J. and Misteli, T. (2014) Activation of DNA damage response signaling by condensed chromatin. *Cell Rep*, **9**, 1703-1717.
152. Ayrapetov, M.K., Gursoy-Yuzugullu, O., Xu, C., Xu, Y. and Price, B.D. (2014) DNA double-strand breaks promote methylation of histone H3 on lysine 9 and transient formation of repressive chromatin. *Proc Natl Acad Sci U S A*, **111**, 9169-9174.
153. Walker, J.R., Corpina, R.A. and Goldberg, J. (2001) Structure of the Ku heterodimer bound to DNA and its implications for double-strand break repair. *Nature*, **412**, 607-614.
154. Cherry, A.L., Nott, T.J., Kelly, G., Rulten, S.L., Caldecott, K.W. and Smerdon, S.J. (2015) Versatility in phospho-dependent molecular recognition of the XRCC1 and XRCC4 DNA-damage scaffolds by aprataxin-family FHA domains. *DNA Repair (Amst)*, **35**, 116-125.
155. Hammel, M., Rey, M., Yu, Y., Mani, R.S., Classen, S., Liu, M., Pique, M.E., Fang, S., Mahaney, B.L., Weinfeld, M. *et al.* (2011) XRCC4 protein interactions with XRCC4-like factor (XLF) create an extended grooved scaffold for DNA ligation and double strand break repair. *J Biol Chem*, **286**, 32638-32650.
156. Reid, D.A., Keegan, S., Leo-Macias, A., Watanabe, G., Strande, N.T., Chang, H.H., Oksuz, B.A., Fenyo, D., Lieber, M.R., Ramsden, D.A. *et al.* (2015) Organization and dynamics of the nonhomologous end-joining machinery during DNA double-strand break repair. *Proc Natl Acad Sci U S A*, **112**, E2575-2584.
157. Corbeski, I., Horn, V., van der Valk, R.A., le Paige, U.B., Dame, R.T. and van Ingen, H. (2018) Microscale Thermophoresis Analysis of Chromatin Interactions. *Methods Mol Biol*, **1837**, 177-197.
158. Corbeski, I., Dolinar, K., Wienk, H., Boelens, R. and van Ingen, H. (2018) DNA repair factor APLF acts as a H2A-H2B histone chaperone through binding its DNA interaction surface. *Nucleic Acids Res*, **46**, 7138-7152.


2

Chapter 2

Microscale thermophoresis analysis of chromatin interactions

Based on the published protocol: Corbeski, I.[*,1], Horn, V.[*,2], van der Valk, R.A.[2], le Paige, U.B.[2], Dame, R.T.[2] and van Ingen, H.[2] (2018) Microscale Thermophoresis Analysis of Chromatin Interactions. *Methods Mol Biol*, 1837, 177-197.

[1] NMR Spectroscopy, Bijvoet Center for Biomolecular Research, Utrecht University, The Netherlands.

[2] Macromolecular Biochemistry, Leiden Institute of Chemistry, Leiden University, The Netherlands.

* These authors contributed equally.

ABSTRACT

Architectural DNA-binding proteins are key to the organization and compaction of genomic DNA inside cells. The activity of architectural proteins is often subject to further modulation and regulation through the interaction with a diverse array of other protein factors. Detailed knowledge on the binding modes involved is crucial for our understanding of how these protein-protein and protein-DNA interactions shape the functional landscape of chromatin in all kingdoms of life: bacteria, archaea and eukarya.

Microscale thermophoresis (MST) is a biophysical technique that has seen increasing application in the study of biomolecular interactions thanks to its solution-based nature, its rapid application, modest sample demand, and the sensitivity of the thermophoresis effect to binding events. Here, we describe the use of MST in the study of chromatin interactions, with emphasis on the way in which these experiments are set up and the diverse types of information they reveal. These aspects are illustrated on the sequential binding of core histone complexes to histone chaperone APLF. Special emphasis is given to the key steps in the design, execution and analysis of MST experiments in the context of the provided example.

1. INTRODUCTION

Biophysical characterization of functional chromatin interactions has typically relied thus far on band-shift assays (electrophoretic mobility shift assays (EMSA)) for protein-DNA interactions, as well as on common biophysical techniques such as surface plasmon resonance (SPR) spectroscopy, isothermal titration calorimetry (ITC) and nuclear magnetic resonance (NMR) spectroscopy (1-3). Thorough characterization of binding modes and binding affinities is often a critical step preceding subsequent structural and functional studies. This calls for a flexible technique which is fast and can characterize interactions in solution with reasonable throughput and modest sample demands. Microscale thermophoresis (MST) fulfills these criteria and thus provides an efficient option for the analysis of biological interactions.

1.1 MST

Analogous to electrophoresis, thermophoresis is the flow or directed movement of molecules along a temperature gradient (4). Technological advances have made it possible to use small temperature gradients (typically 2-6 °C) and detect the resulting micrometer-scale movements, allowing the application in molecular biology as microscale thermophoresis (MST) (5). MST typically requires fluorescent labeling of the protein of interest for high sensitivity of detection. Samples are loaded onto glass capillaries and a specific spot is heated by an infrared laser (see Figure 1A). The resulting temperature gradient causes thermophoresis of the labeled molecule, typically away from the heated spot, which is observed through a decrease in fluorescence in the heated region (see Figure 1B). Since thermophoresis is sensitive to molecular size, charge and hydration shell (6), changes in these properties due to binding will cause changes

in thermophoresis. For analysis of interactions, MST curves are recorded as titration series with increasing amounts of ligand and normalized with respect to their initial equilibrium fluorescence (F_{norm}) (Figure 1B). A binding curve is extracted by plotting the F_{norm} values at the end of the laser on-period (phase IV, Figure 1B), which captures binding induced changes both in thermophoresis and in the intrinsic temperature dependence of the fluorophore (indicated by the arrow "Thermophoresis + T-Jump" in Figure 1B). Both effects can also be analyzed separately. Since the observed F_{norm} values are the population weighted averages of the unbound and bound molecules, standard methods can be used to fit the binding curve and extract the binding affinity. Furthermore, MST can be performed in virtually every buffer (7) and other characteristics such as thermodynamic properties, binding stoichiometry and enzyme kinetics can be extracted with customized experimental designs (8).

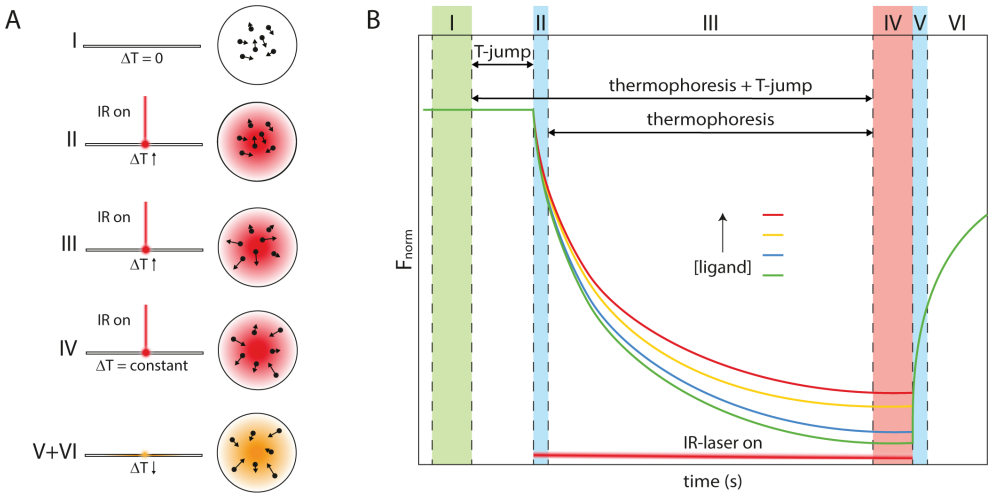

Figure 1. Principle of MST. Schematic depiction of the MST experiment **(A)** and MST time trace **(B)**. In (A), the capillaries (left) and particles in a cross-section thereof (right) during different stages of the experiment (I-VI) are shown. Starting from equilibrium (phase I), infrared (IR) laser irradiation is started which induces a temperature gradient (phase II), causing particles to move out or into the heated volume (thermophoresis, phase III). When thermophoresis is counter balanced by mass diffusion, a steady state is reached (phase IV). When the laser is switched off, the particle concentration re-equilibrates (phase V+VI). In (B), a four sample titration series is shown, relative ligand concentration indicated. Each sample is characterized by a distinct thermophoresis curve. The rapid changes in normalized fluorescence in phases II and V are caused by the temperature dependence in fluorescence (T-jump). Binding curves can be extracted by plotting F_{norm} values for regions "Thermophoresis + T-jump" (I vs. IV), "Thermophoresis" (start of III vs. IV), or "T-jump" (I vs. start of III).

1.2 MST OF CHROMATIN SYSTEMS

The study of chromatin function is strongly connected to protein-DNA and protein-protein interactions that modulate the chromatin state. An increasing number of studies has employed MST to investigate binding events in chromatin related systems (see for instance (9-13)), and some of the earliest examples have been included in reviews (1,14-16). A variety of

labeling strategies have emerged, in particular for the study of protein-nucleosome interactions. Fluorescent nucleosomes have been constructed using Cy5-labeled DNA (16) or AlexaFluor647-labeled histone H3 (17). Furthermore, MST has been used to derive insights in protein binding mechanisms, e.g. demonstration of cooperative binding (18) or determination of binding sites from a comparison of different deletion mutants (19).

Here, we describe in detail the use of MST to study chromatin interactions. We put particular emphasis on the step-by-step optimization of experimental conditions. We present an example on the interaction of chromatin architectural proteins, in this case complexes of histone proteins, with a binding partner, a histone chaperone, which illustrates the additional information MST can provide on the binding mechanism, the sensitivity of the thermophoretic effect and the merits of custom data analysis. With these, we provide a first-hand report on assay issues that can be observed for chromatin-related samples and strategies to detect and overcome them.

2. MATERIALS

2.1 FLUORESCENT LABELING

1. Monolith NT™ Protein Labeling Kit RED/GREEN/BLUE, either NT-647-NHS, which reacts with solvent exposed primary amines, or NT-647-MALEIMIDE, which reacts with sulfhydryl groups to form dye-protein conjugates (NanoTemper Technologies) (see Note 1).
2. Variable speed benchtop microcentrifuge.
3. 1.5-2 mL microcentrifuge tubes.
4. 10 mL assay buffer (see Note 2).
5. 100% dimethylsulfoxide (DMSO).
6. Eppendorf heating block capable of reaching 95 °C.

Prepare all solutions using water (resistivity 18.2 MΩ×cm and organic content less than five parts per billion) and analytical grade reagents.

2.2 MST

1. MST instrument Monolith NT.115 equipped with "Red" channel (NanoTemper Technologies) (see Note 3).
2. Capillaries: NT.115 standard, hydrophobic, hydrophilic (see Note 4) or premium treated capillaries, or the NT.115™ Capillary Selection Set (NanoTemper Technologies).
3. Personal computer with dedicated NT Control and MO Affinity Analysis software (version 2.1.5). Custom analysis scripts are available upon request from the corresponding author of the underlying publication of this chapter.

4. Small volume reaction tubes (e.g. as found in the labeling kit, or 200 µL PCR tubes).
5. Calibrated pipettes in the range 2-1,000 µL.
6. NanoDrop™ Spectrophotometer (Thermo Scientific).
7. Aluminum foil.

2.3 Stock solutions

1. At least 100 µL of 20 µM of biomolecule to be labelled (see Note 5).
2. 100 µL of biomolecule to be titrated with a concentration 20 times the expected dissociation constant (see Note 5).
3. 10 mL of assay buffer.
4. 10-100 mg/mL bovine serum albumin (BSA).
5. 5-10% Tween-20.
6. 4 M NaCl.

3. Methods

3.1 Design of MST experiment: choice of fluorescent labeling

The MST experiment can be performed with either of the interaction partners fluorescently labeled (see Note 6). Proteins and peptides can be labeled either with the manufacturer's labeling kits or with other widely available fluorophores and coupling strategies (see also Note 1). DNA molecules are readily labeled using custom oligo synthesis using commercially available labeled nucleotides, or using modifications of the termini for coupling of dyes. For the applications described below, proteins were labeled using the manufacturer supplied labeling kits.

Protein labeling

1. Prepare a solution of pure protein at a concentration of 20 µM in a volume of 100 µL.
2. Prepare the spin column for buffer exchange into labeling buffer, using the manufacturer supplied spin columns and instructions (see Note 7). Resuspend the dried labeling buffer in 3 mL water. Prepare column A by resuspending the slurry. Remove excess storage solution by placing the column in a 1.5-2 mL microcentrifuge tube and centrifuging at 1,500 g for 1 minute. Wash the column three times with 300 µL labeling buffer.

3. Exchange the protein to labeling buffer by placing the protein solution from step 1 at the center of the resin. Be careful not to disturb the resin. Place the column in a new microcentrifuge tube and centrifuge at 1,500 g for 2 minutes.
4. Dissolve the solid fluorescent dye in 30 µL DMSO (yielding a ~470 µM solution) and mix thoroughly by vortexing (see Note 8). Prepare 100 µL 20-60 µM dye solution in Labeling Buffer (see Note 9) and take 100 µL 20 µM protein solution in Labeling Buffer. Add the dye to the protein in a 1:1 volume ratio for a final 1:1 to 3:1 molar ratio of dye to protein in a 200 µL volume. Incubate the reaction for 30 minutes at room temperature and in the dark (see Note 10). Proceed with step 5 in the meantime.
5. Prepare the gravity flow column for purification of labeled protein and removal of unreacted dye (see Note 11). Pour off the storage solution in column B and wash the column three times with 3 mL assay buffer (see Note 2) in a 15 mL tube using the supplied adapter through gravity flow.
6. Separate the labeled protein obtained at step 4 from unreacted dye. Apply the labeling reaction mixture to the center of column B from step 5. Let the sample enter the bed completely, then add 300 µL assay buffer and discard the flow-through (see Note 12). Place the column in a new 15 mL tube. Add 600 µL assay buffer and collect the eluate in ~50 µL fractions (one drop at a time) in appropriate tubes, e.g. 1.5 mL microcentrifuge tubes.
7. Verify the presence of labeled protein in elution fractions by determining their fluorescence intensity and their capillary scan signal shape (see section 3.2 below) in the MST instrument. According to the gel filtration principle, larger particles will elute prior to smaller particles (see Note 13). At 20% LED power, 10 nM labeled protein should yield fluorescence intensities of approximately 100-200 counts (see Note 14 and section 3.2).
8. Pool the fractions that contain labeled protein and shield them from light.
9. Determine the protein and dye concentrations and derive the labeling efficiency by measuring the absorbance at 280 (A_{280}) and 650 nm (A_{650}) in a suitable spectrophotometer, e.g. using a NanoDrop™ Spectrophotometer (Thermo Scientific) and applying the Lambert-Beer law (see Note 15).
10. Aliquot the labeled protein as 10 µL aliquots (e.g. into 200 µL PCR tubes), flash-freeze in liquid nitrogen and store for several weeks to months at -80 °C (see Note 5 and 16).

3.2 Optimization of experimental conditions

Optimization of experimental conditions is paramount to obtain high-quality data and derive accurate binding parameters, which is in particular due to the sensitivity of the MST experiment to protein adsorption to exposed surfaces and protein aggregation. To avoid such experimental artifacts, the correct capillary type has to be chosen, and the buffer composition needs to be optimized to ensure a homogeneous state of the sample, free from aggregation. Here, we outline this procedure step-by-step (see Figure 2), but we note that some parameters are interrelated and that addition of ligand may result in the need for further optimization.

1. Set the machine to the desired temperature and wait for temperature equilibration (see Note 17 and 18).

2. Make a calibration curve of the dye alone at the set temperature. To this purpose, prepare 20 µL 200 nM dye solution in assay buffer in a capped, small volume reaction tube to avoid evaporation (e.g. 200 µL PCR tubes) and label this tube 1. Label 8 more PCR tubes 2 through 9. Add 10 µL assay buffer in each tube 2-9. Add 10 µL from tube 1 to 2 and mix by pipetting up and down. Then add with a new pipette tip 10 µL from tube 2 to 3 and mix by pipetting up and down. Continue this series through to tube 9. Fill all samples in standard capillaries (see Note 19) and perform a capillary scan (button "Start CapScan" in NT Control) at 50% LED power to measure the fluorescence intensity at each concentration. Prepare a calibration curve with fluorescence intensity on the *y*- and dye concentration on the *x*-axis.
3. Determine the optimal concentration of the fluorescently labeled molecule. To this purpose, prepare a dilution series using the stock of labeled protein as in step 2. Fill the samples in standard capillaries and start the capillary scan with 50% LED power. If the fluorescence is much lower than expected compared to the calibration curve or not linear over the dilution series, the protein likely sticks to the reaction tube or pipette tips (see also step 4). In that case, add 0.05% Tween-20 or another detergent (see Figure 2A) and repeat the experiment. If the sample behaves well, adjust the concentration to be lower or at most in the order of the expected K_D, while still resulting in a fluorescence signal with high signal-to-noise (see Note 20 and 21).
4. Determine the optimal type of capillary coating to ensure a homogenous sample. To this purpose, load capillaries of each type (Monolith NT™ Standard, Hydrophobic, Hydrophilic (see Note 4) and Premium Treated) with working concentration of the labeled biomolecule determined in step 3 and perform a capillary scan. Inspect the shape of the fluorescence signal which reflects the distribution of the labeled molecule in a cross-section of the capillary. If a "U"- or "M"-shaped peak is observed instead of a smooth Gaussian-shaped fluorescence peak, the sample adsorbs to the capillary wall (Figure 2B). Also verify that no sticking occurs over time by running a second capillary scan ~15 minutes after the first one (see Figure 2C and Note 22). For further experiments, select capillaries with minimal or no sticking. In case of sticking in all capillary types, proceed to step 6 and optimize the assay buffer.
5. Use the capillary profiles to also judge the reproducibility of the fluorescence intensity from the four replicates, or from a binding experiment. Random variations larger than 10% can be caused by inaccurate pipetting or sticking to the walls of reaction tubes and pipette tips (Figure 2D). In that case, test whether addition of detergents like Tween-20, passivating agents like BSA, or higher salt concentrations in the assay buffer improve the results (see Note 23).
6. Check the thermophoresis signal for sample aggregation. To this purpose, start a thermophoresis measurement with the following settings: labeled molecule at working concentration; LED power adjusted to yield at least 200 fluorescence counts; 40% MST power; 30/5 seconds MST power on/off time. Aggregates, when present, will be transported in and out of the measurement volume, causing sharp increases and decreases in fluorescence over time and a bumpy appearance of the MST curve (Figure 2E). Make sure to use stocks and buffers that are free from aggregates or particulate matter, and adjust the assay buffer composition to prevent later aggregation (see Note 24).

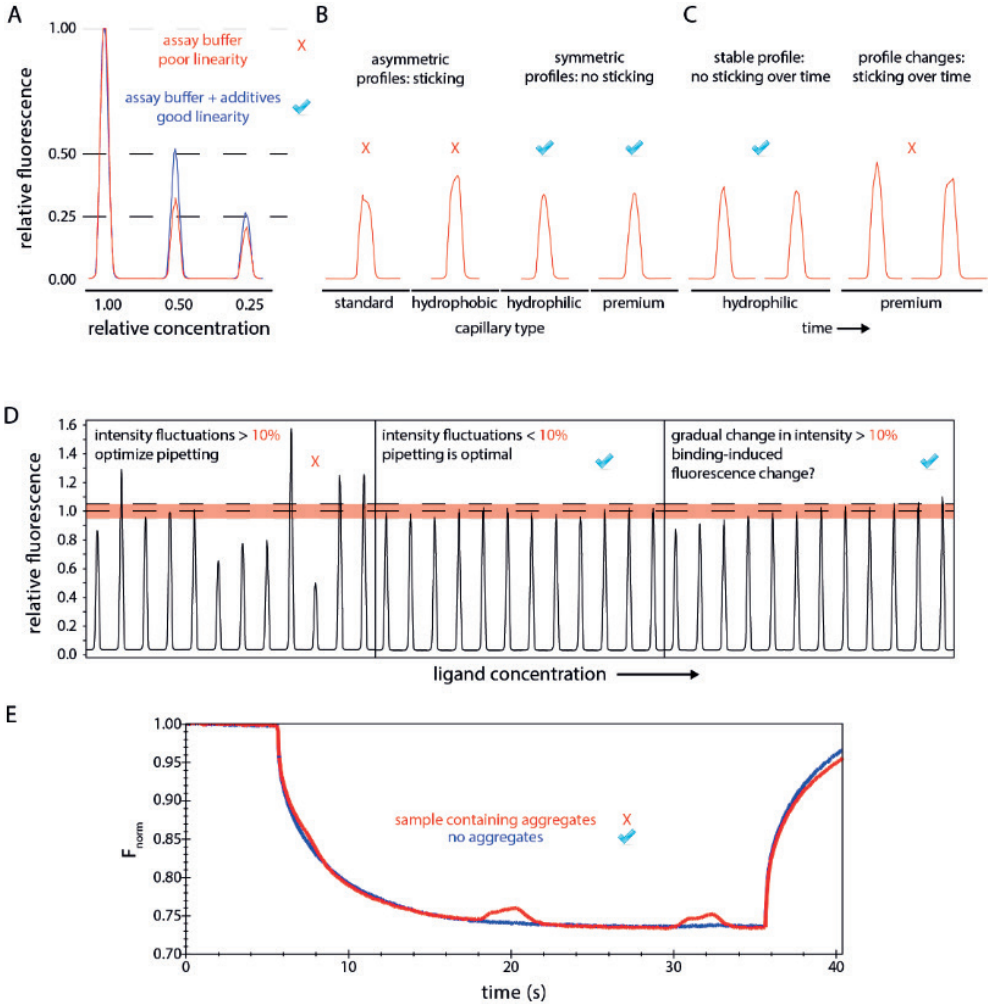

Figure 2. Optimization of assay conditions. (A) Capillary scans of a dilution series of the fluorescently labeled molecule. The addition of additives (0.5 mg/mL BSA and 0.05% Tween-20) prevents sticking to reaction tubes and leads to a consistent dilution series. **(B)** Capillary scans of different types of capillaries loaded with the same labeled molecule. Asymmetric peaks are a sign of adsorption to the capillary wall. **(C)** Time-dependent changes in the capillary scans for the same molecule. While both premium and hydrophilic coatings show no adsorption initially, only hydrophilic capillaries remain free of adsorption over time. **(D)** Capillary scans of a titration series of the same molecule. Addition of 0.5 mg/mL BSA and 0.05% Tween-20 together with diligent pipetting improves the reproducibility of the fluorescence intensity to within the required limits (compare left and middle panel). Gradual fluorescence intensity changes are indicative of a binding reaction and can be used for analysis (see Note 34). **(E)** Aggregates in the sample led to irregularly shaped MST-traces (red), which were prevented by spinning the sample for 20 minutes at 20,000 g and 4 °C to remove aggregates (Note 24) (blue). All data were acquired on NT-467-labeled $APLF^{FAD}$ and its interaction with core histone complexes (see Section 3.6).

3.3 Preparation of dilution series

To determine the dissociation constant (K_D) of a molecular interaction, a dilution series of up to 16 titration points is prepared, where the concentration of the fluorescent binding partner is kept constant and the concentration of the unlabeled binding partner is varied (see Notes 25 and 26).

1. Prepare 200 µL of the fluorescently labeled biomolecule (from step 3.1.10) in the optimized buffer with double the concentration of the final reaction to account for two-fold dilution with titrant (see Note 27). Here, and in subsequent steps, use small volume reaction tubes to avoid evaporation (e.g. 200 µL PCR tubes).
2. Prepare the titrant stock concentration to be 40-fold the expected K_D (see Note 28) in assay buffer (labeled tube 1) (see Note 29) and determine the concentration (see Note 30).
3. Prepare 15 tubes labeled 2 through 16 with 15 µL of the assay buffer. With a clean tip, transfer 15 µL from tube 1 to tube 2 and mix well by pipetting. Continue this serial dilution until tube 16 (see Note 31).
4. Transfer 10 µL from tubes 1-16 to new reaction tubes and add 10 µL of your fluorescently labeled sample stock to the tubes (see Note 32). Mix very well by pipetting up and down. After an adequate incubation time (typically 5 minutes, see Note 33), place the capillaries in the tubes to load the samples (see Note 19).

3.4 MST measurement

1. Load the capillaries of the previous step in the MST machine (see also Note 18) and perform a full MST measurement using the LED power setting determined earlier, and two consecutive measurements using 20% and 40% MST power (button "Start CapScan + MST Measurement") (see also Note 22).
2. Analyze the outcome of the measurement carefully to ensure the data is of sufficient quality. Inspect results of the capillary scan to see if there is ligand-induced sticking; inspect the reproducibility of the fluorescence intensity to see if the variation is larger than 10% (Figure 2D, see Note 34); inspect the MST-traces to see if there is ligand-induced aggregation (see Figure 2E). If any of these issues are observed, carefully reevaluate the previous steps. A new round of assay condition optimization, this time including the ligand, can help to solve these issues. When no issues are encountered, proceed to step 3.
3. Analyze the MST-derived binding curve in the MO Affinity Analysis software. If a transition is observed, estimate its amplitude. Estimate the noise from the scatter in the data points at the lowest concentration of ligand where no binding is expected. Minimum amplitude should be 5 units (5‰ normalized fluorescence intensity change) and minimum signal-to-noise should be 3. If either the amplitude or signal-to-noise is too low, increase the MST power to 60-80% (see Notes 35 and 36).
4. Once the final conditions have been established, perform the serial dilution (step 3.3.3 and 3.3.4) in triplicates each with two MST powers of the same dilution series. Next, proceed to data analysis (see 3.5).

3.5 MST DATA ANALYSIS

The manufacturer's MO Affinity Analysis software provides multiple options to extract a binding curve from the raw MST traces (see Note 37). The resulting binding curves can be fit directly in the software for a 1:1 binding model, or the data can be exported to be used in third party software. Here, we describe the default procedure using the instrument software, together with options for custom analysis (see Note 38).

1. In a new analysis set, click and drag the three replicates in a single experiment for a combined analysis.
2. If binding-induced changes in fluorescence intensity are observed, fit the binding curve using the "Initial Fluorescence" button (see also Note 34). Otherwise, proceed to step 3.
3. Extract replicate-averaged binding curves using the two default settings: (*i*) "Thermophoresis + T-Jump"; (*ii*) "Thermophoresis", and fit these using the thermodynamic model to extract the K_D (see Note 39). Compare the extracted values for consistency.
4. Use the "Temperature Jump" method to see if there is a binding-induced change in the fluorophore, which may hold structural information if the location of the fluorophore is known.
5. Export the data for further analysis, error estimation of fit parameters or fitting to custom binding models using e.g. MatLab (scripts available upon request to the corresponding author of the underlying publication of this chapter), Python, or the PALMIST program of Scheuermann *et al.* (20).

3.6 DESCRIPTION OF EXAMPLE

HISTONE BINDING BY HISTONE CHAPERONE APLF

Histone chaperones are involved in the assembly and disassembly of the nucleosome for DNA replication, transcription, and repair (21). Aprataxin and Polynucleotide kinase Like Factor (APLF) is a DNA repair protein with histone chaperone function (22). Here, we studied the interaction of the APLF acidic domain ($APLF^{AD}$) with histone complexes using MST. $APLF^{AD}$ was labeled with the manufacturer's red dye NT-647 according to section 3.1. Given the low labeling efficiency (~15%) and the expected high affinity, 25 nM of $APLF^{AD}$ was used with 100% LED power to obtain an optimal fluorescence intensity of 400 counts. The assay buffer was supplemented with both 0.5 mg/mL BSA and 0.05% Tween-20 and experiments were conducted in hydrophilic treated capillaries to prevent sticking to the reaction tubes and the capillaries (see Figure 2).

The MST data show that $APLF^{AD}$ binds with high and comparable affinities to both H2A-H2B and $(H3\text{-}H4)_2$, suggesting that APLF is a generic histone chaperone (Figure 3). Interestingly, the binding curves show in both cases two transitions, suggesting two separate binding events (see Note 40), one with affinity in the higher nanomolar range and one in the micromolar range. The data were fit to a sequential-binding site model using an in-house written MatLab script

with the Nelder-Mead simplex algorithm as minimization procedure. Errors in the best-fit parameters represent the 95% confidence interval based on statistical F-tests (20). The additional binding mode of histones to APLF^{AD} may be relevant for its chaperoning mechanism, promoting the retention of multiple copies of histone complexes.

These data demonstrate that MST can produce reproducible binding data for chromatin associated complexes in a convenient manner, using small amounts of materials, and minimalistic labeling approaches that do not interfere with the binding reaction. Furthermore, the sensitivity of the experiment due to its fluorescence detection based setup, might reveal in some cases additional binding modes with important functional implications which would otherwise remain hidden when using other techniques.

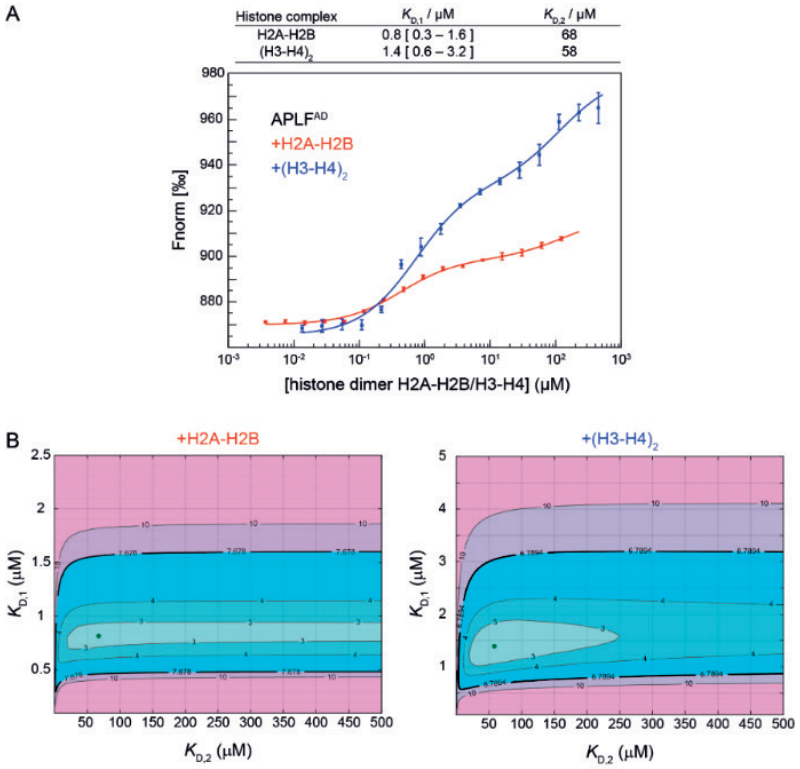

Figure 3. APLF^{AD} binds with similar affinities to H2A-H2B and (H3-H4)$_2$. (A) MST binding curves of H2A-H2B (red) or (H3-H4)$_2$ (blue) with fluorescently labeled APLF^{AD} (25 nM) in assay buffer (25 mM NaPi, pH 7.0, 300 mM NaCl, supplemented with 0.5 mg/mL BSA and 0.05% Tween-20), recorded at 25 °C, 20% MST and 100% LED power with 30/5 seconds laser-on/off time. The binding curve represents the average from 3 measurements with standard deviation. Best-fit values for the corresponding affinities and 95% confidence limits are listed in the table. **(B)** Plots showing the reduced χ^2-surface that expresses the quality of the fit in contour-mode as function of the high-affinity ($K_{D,1}$) and the low-affinity ($K_{D,2}$) dissociation constants for H2A-H2B (left) and (H3-H4)$_2$ (right) binding to APLF^{AD}. The best-fit values are indicated by a green dot. The 95% confidence critical value for the reduced χ^2 is indicated with a thick black line. Figure reproduced from Ref. (23) with permission from the authors.

4. NOTES

1. One is by no means restricted to use the manufacturer's fluorescent labeling kit. There are many commercially available fluorescent compounds that can be coupled to free amino or thiol groups. Make sure to use compounds compatible with the excitation and detection wavelengths of your instrument.
2. Assay buffer refers to the buffer of choice in which the interaction is investigated. The protein should be stable and well behaved in this buffer. Typical buffer conditions are 50 mM Tris-HCl pH 7.4, 150 mM NaCl, 10 mM $MgCl_2$, 0.05% Tween-20.
3. We limit the description of the method to the Monolith NT.115 instrument from NanoTemper Technologies (Munich, Germany). Instruments with either a higher fluorescence sensitivity, a setup to excite and detect intrinsic tryptophan fluorescence, or a high-throughput automated screening setup are also available.
4. Hydrophilic treated capillaries were used in this study, but these are no longer available. Premium capillaries are advised as replacement.
5. Higher stock concentrations are useful to have optimum flexibility to adjust exact assay buffer composition during optimization of the experimental conditions (see section 3.2) or in follow-up experiments.
6. In case no binding is detected with one binding partner fluorescently labeled, it is useful to try and test labeling the other binding partner.
7. Buffer exchange to labeling buffer (steps 2 and 3) can be skipped if the protein sample is purified directly into a suitable buffer (good buffers are HEPES, PBS, Na-Ac) with $6.5 < pH < 8.5$. Buffers should not contain reducing agents dithiothreitol (DTT) and β-mercaptoethanol (BME), since these substances significantly reduce labeling efficiency. Tris(2-carboxyethyl)phosphine (TCEP) can be used as reducing agent if required. Additionally, the buffer for NHS-labeling must be free of primary amines e.g. ammonium ions, Tris, glycine, ethanolamine, glutathione or imidazole. Buffers with protein impurities or protein carriers like bovine serum albumin (BSA) should not be used. If a labeling buffer is used other than the one supplied, dye concentrations required for optimum labeling efficiency may need to be re-established.
8. The dye can be used for a few hours after resuspending it according to the manufacturer's manual. For longer storage of stock solutions, dye may be frozen and aliquoted in DMSO under anhydrous conditions to prevent hydrolysis.
9. For some samples labeling efficiency may be increased by using a higher-fold excess of dye.
10. The reaction can be incubated in a drawer or cupboard, or wrapped in aluminum foil.
11. For optimal MST results, unreacted dye needs to be removed.
12. When using 200 μL labeling reaction, the volume must be adjusted to 500 μL after the sample has entered the bed by adding 300 μL assay buffer. If a scale-up or scale-down of the reaction is necessary, make sure the total volume loaded on the column is 500 μL. Ensure the whole labelling mix has entered the column bed before completing to 500 μL.
13. Use the early fractions that contain higher amounts of labeled protein. Depending on the assay buffer composition, later fractions might contain free dye. It can also be helpful to look at the thermophoresis signal and check for "bumps", which are indicative of aggregates in the sample (see Figure 2E).
14. If required, after fluorescent labeling, the protein can be concentrated using a device like an Amicon® Ultra Centrifugal Filter (Millipore).

15. The molar absorbance of the dye at 650 nm is 250,000 M^{-1} cm^{-1}. Protein absorption at 280 nm has to be adjusted according to $A_{protein} = A_{280} - 0.028 \cdot A_{650}$ due to absorption of the dye. Typically, the labeling ratio is between 0.5 and 1.1 (according to the manufacturer).
16. If the stored protein is to be used for a new interaction study, repetition of previous experiments can be conducted to assess the stability and quality of the sample.
17. The experimental temperature in the MST instrument can be set between 22 and 45 °C or left unspecified for room temperature. The temperature is best set to a defined value and reported, together with the used MST power.
18. After opening of the instrument's front door for sample insertion, close the door and wait until the set temperature is reached as shown on the instrument's display.
19. Both tube and capillary can be tilted to ease filling. To have air on both sides, the capillary may be inverted for one or two seconds after loading.
20. Typically, 5-100 nM of the fluorescently labeled molecule is sufficient to obtain optimal fluorescence, with intensity above 400 and below 1,500, with a minimum of 200. The LED power can be varied between 15% and 95% to achieve this. For very high-affinity interactions, use the lowest possible concentration in which you get 200 fluorescence counts with 95% LED power.
21. If the concentration of labeled molecule is on the order of the K_D, the dilution series (section 3.3) is better prepared linearly to optimally sample the binding curve, in which case the data is best plotted using a linear *x*-axis resulting in a hyperbole binding curve.
22. Capillary scans of each new titration should be performed at the start of the experiment to assess the quality of the samples and again at the end of the experiment to check for changes in the fluorescence peak shape and intensity that can occur over time.
23. Additives should be used at the lowest functional concentration possible as they may affect the binding.
24. Aggregates can be removed by centrifuging sample stocks (20 minutes, 20,000 g, 4 °C) and filter buffers through 0.22-0.45 µm filters. Detergents such as Tween-20 or Triton X-100 (0.01-0.1%) or changes in assay buffer conditions (different ionic strength or pH) can also help to prevent aggregation or binding-induced aggregation.
25. A control experiment can be conducted with an unrelated non-binding molecule or a binding-deficient mutant of the binding partner.
26. Do not use less than 10 titration points per experiment.
27. Using a two-fold serial dilution, which is easily performed with minimum source of error, optimally spaced data points along the sigmoidal binding curve are obtained (see also Note 21).
28. The "Concentration Finder" tool within the NT Control software can be used to simulate binding curves and determine the required titrant concentration ranges. In case the dissociation constant is unknown, a 3-5-fold dilution series starting from a high (~100 µM) concentration will allow the monitoring of binding events within a ligand concentration range of nM to µM. If a binding transition is observed, the titrant stock concentration and dilution series can be adjusted accordingly.
29. If the sample buffer is different from the assay buffer, adjust the composition of the buffers in order to obtain the same composition (e.g. DMSO, glycerol, salt, detergent, BSA *etc.*) by adding the components in the stock preparations to the final concentration needed.
30. As in any quantitative essay, it is essential to accurately determine protein concentrations, work with calibrated pipettes, and to perform precise and reproducible protein dilutions.

31. Change the pipet tip after each transfer or, alternatively, pre-wet the tip properly. For some pipettes it may be necessary to reset the pipetting volume after placing a new pipet tip.
32. After having obtained practical experience and confidence with the pipetting procedure, the pipetting volumes can be reduced to half to save material.
33. The incubation time is necessary to establish equilibrium which is determined by the binding kinetics of complex formation and dissociation. In sporadic cases with very high affinity and very low dissociation rates, equilibration may take hours to days (20). Equilibration can be verified by repeating a titration series after different incubation times, e.g. 1, 5, and 10 minutes.
34. A systematic ligand-dependent increase or decrease in fluorescence intensity may be caused by binding if the fluorophore is close to the binding site. To determine if this is the case, spin down the reaction tubes for 10 minutes at 15,000 g, remove 10 µL of supernatant and add this to 10 µL of denaturing buffer (4% sodium dodecyl sulfate (SDS), 40 mM DTT), then heat for 5 minutes at 95 °C, load the samples into capillaries and perform a capillary scan. If the fluorescence intensity is now constant within 10%, the effect was binding-induced. If the effect remains, sample may be lost due to aggregation and a new round of optimization has to be started.
35. Reduce the laser-on time at high MST powers to 15 seconds to reduce effects from sample-heating.
36. Compare Refs. (20), (24) and (25) for MST curves with a range of signal-to-noise ratios.
37. Sign and amplitude of the thermophoresis effect are typically not analyzed since they depend in a complex manner on the changes in conformation, size and charge.
38. The use of custom software permits more realistic determination of errors in fit parameters and flexibility in choosing binding models.
39. Avoid the use of the Hill equation since the reported EC50 values are protein concentration dependent and the fitted cooperativity coefficient may be larger than the number of binding sites.
40. In case multiple binding transitions are observed in an MST titration, it can be useful to confirm the result by using complementary techniques.

REFERENCES

1. Flores, J.K., Kariawasam, R., Gimenez, A.X., Helder, S., Cubeddu, L., Gamsjaeger, R. and Ataide, S.F. (2015) Biophysical Characterisation and Quantification of Nucleic Acid-Protein Interactions: EMSA, MST and SPR. *Curr Protein Pept Sci*, **16**, 727-734.
2. Oda, M. and Nakamura, H. (2000) Thermodynamic and kinetic analyses for understanding sequence-specific DNA recognition. *Genes Cells*, **5**, 319-326.
3. van Emmerik, C.L. and van Ingen, H. (2019) Unspinning chromatin: Revealing the dynamic nucleosome landscape by NMR. *Prog Nucl Magn Reson Spectrosc*, **110**, 1-19.
4. Ludwig, C., Staatsdruckerei, K.K.H.-u., Wien, K.A.d.W.i. and Braumüller. (1856) *Diffusion zwischen ungleich erwärmten Orten gleich zusammengesetzter Lösung.* Aus der K.K. Hof- und Staatsdruckerei, in Commission bei W. Braumüller, Buchhändler des K.K. Hofes und der K. Akademie der Wissenschaften.
5. Wienken, C.J., Baaske, P., Rothbauer, U., Braun, D. and Duhr, S. (2010) Protein-binding assays in biological liquids using microscale thermophoresis. *Nat Commun*, **1**, 100.
6. Duhr, S. and Braun, D. (2006) Why molecules move along a temperature gradient. *Proc Natl Acad Sci U S A*, **103**, 19678-19682.

7. Seidel, S.A., Dijkman, P.M., Lea, W.A., van den Bogaart, G., Jerabek-Willemsen, M., Lazic, A., Joseph, J.S., Srinivasan, P., Baaske, P., Simeonov, A. *et al.* (2013) Microscale thermophoresis quantifies biomolecular interactions under previously challenging conditions. *Methods*, **59**, 301-315.
8. Jerabek-Willemsen, M., André, T., Wanner, R., Roth, H.M., Duhr, S., Baaske, P. and Breitsprecher, D. (2014) MicroScale Thermophoresis: Interaction analysis and beyond. *Journal of Molecular Structure*, **1077**, 101-113.
9. Schubert, T., Pusch, M.C., Diermeier, S., Benes, V., Kremmer, E., Imhof, A. and Langst, G. (2012) Df31 protein and snoRNAs maintain accessible higher-order structures of chromatin. *Mol Cell*, **48**, 434-444.
10. Zillner, K., Filarsky, M., Rachow, K., Weinberger, M., Langst, G. and Nemeth, A. (2013) Large-scale organization of ribosomal DNA chromatin is regulated by Tip5. *Nucleic Acids Res*, **41**, 5251-5262.
11. Su, X.C., Wang, Y., Yagi, H., Shishmarev, D., Mason, C.E., Smith, P.J., Vandevenne, M., Dixon, N.E. and Otting, G. (2014) Bound or free: interaction of the C-terminal domain of Escherichia coli single-stranded DNA-binding protein (SSB) with the tetrameric core of SSB. *Biochemistry*, **53**, 1925-1934.
12. Silva, A.P., Ryan, D.P., Galanty, Y., Low, J.K., Vandevenne, M., Jackson, S.P. and Mackay, J.P. (2016) The N-terminal Region of Chromodomain Helicase DNA-binding Protein 4 (CHD4) Is Essential for Activity and Contains a High Mobility Group (HMG) Box-like-domain That Can Bind Poly(ADP-ribose). *J Biol Chem*, **291**, 924-938.
13. Yamagata, K. and Kobayashi, A. (2017) The cysteine-rich domain of TET2 binds preferentially to mono- and dimethylated histone H3K36. *J Biochem*, **161**, 327-330.
14. Zillner, K., Jerabek-Willemsen, M., Duhr, S., Braun, D., Langst, G. and Baaske, P. (2012) Microscale thermophoresis as a sensitive method to quantify protein: nucleic acid interactions in solution. *Methods Mol Biol*, **815**, 241-252.
15. Zhang, W., Duhr, S., Baaske, P. and Laue, E. (2014) Microscale thermophoresis for the assessment of nuclear protein-binding affinities. *Methods Mol Biol*, **1094**, 269-276.
16. Schubert, T. and Längst, G. (2015) Studying epigenetic interactions using MicroScale Thermophoresis (MST). *AIMS Biophysics*, **2**, 370-380.
17. Willhoft, O., McCormack, E.A., Aramayo, R.J., Bythell-Douglas, R., Ocloo, L., Zhang, X. and Wigley, D.B. (2017) Crosstalk within a functional INO80 complex dimer regulates nucleosome sliding. *Elife*, **6**.
18. Schrader, A., Gross, T., Thalhammer, V. and Langst, G. (2015) Characterization of Dnmt1 Binding and DNA Methylation on Nucleosomes and Nucleosomal Arrays. *PLoS One*, **10**, e0140076.
19. Zocco, M., Marasovic, M., Pisacane, P., Bilokapic, S. and Halic, M. (2016) The Chp1 chromodomain binds the H3K9me tail and the nucleosome core to assemble heterochromatin. *Cell Discov*, **2**, 16004.
20. Scheuermann, T.H., Padrick, S.B., Gardner, K.H. and Brautigam, C.A. (2016) On the acquisition and analysis of microscale thermophoresis data. *Anal Biochem*, **496**, 79-93.
21. Hammond, C.M., Stromme, C.B., Huang, H., Patel, D.J. and Groth, A. (2017) Histone chaperone networks shaping chromatin function. *Nat Rev Mol Cell Biol*, **18**, 141-158.
22. Mehrotra, P.V., Ahel, D., Ryan, D.P., Weston, R., Wiechens, N., Kraehenbuehl, R., Owen-Hughes, T. and Ahel, I. (2011) DNA repair factor APLF is a histone chaperone. *Mol Cell*, **41**, 46-55.
23. Corbeski, I., Dolinar, K., Wienk, H., Boelens, R. and van Ingen, H. (2018) DNA repair factor APLF acts as a H2A-H2B histone chaperone through binding its DNA interaction surface. *Nucleic Acids Res*, **46**, 7138-7152.
24. Allam, R., Scherbaum, C.R., Darisipudi, M.N., Mulay, S.R., Hagele, H., Lichtnekert, J., Hagemann, J.H., Rupanagudi, K.V., Ryu, M., Schwarzenberger, C. *et al.* (2012) Histones from dying renal cells aggravate kidney injury via TLR2 and TLR4. *J Am Soc Nephrol*, **23**, 1375-1388.
25. van der Berg, J.P., Madoori, P.K., Komarudin, A.G., Thunnissen, A.M. and Driessen, A.J. (2015) Binding of the Lactococcal Drug Dependent Transcriptional Regulator LmrR to Its Ligands and Responsive Promoter Regions. *PLoS One*, **10**, e0135467.


3

Chapter 3

DNA repair factor APLF acts as a H2A-H2B histone chaperone through binding its DNA interaction surface

Based on the published research article: Corbeski, I.[1], Dolinar, K.[1], Wienk, H.[1], Boelens, R.[1] and van Ingen, H.[1,2] (2018) DNA repair factor APLF acts as a H2A-H2B histone chaperone through binding its DNA interaction surface. *Nucleic Acids Res*, **46**, 7138-7152.

[1] NMR Spectroscopy, Bijvoet Center for Biomolecular Research, Utrecht University, The Netherlands.

[2] Macromolecular Biochemistry, Leiden Institute of Chemistry, Leiden University, The Netherlands.

ABSTRACT

Genome replication, transcription, and repair require the assembly/disassembly of the nucleosome. Histone chaperones are regulators of this process by preventing formation of nonnucleosomal histone-DNA complexes. Aprataxin and Polynucleotide kinase Like Factor (APLF) is a non-homologous end joining (NHEJ) DNA repair factor that possesses histone chaperone activity in its acidic domain ($APLF^{AD}$). Here, we studied the molecular basis of this activity using biochemical and structural methods. We find that $APLF^{AD}$ is intrinsically disordered and binds histone complexes $(H3\text{-}H4)_2$ and H2A-H2B specifically and with high affinity. $APLF^{AD}$ prevents unspecific complex formation between H2A-H2B and DNA in a chaperone assay, establishing for the first time its specific histone chaperone function for H2A-H2B. On the basis of a series of NMR studies, supported by mutational analysis, we show that the $APLF^{AD}$ histone binding domain (HBD) uses two aromatic side chains to anchor to the α1-α2-patches on both H2A and H2B, thereby covering most of their DNA-interaction surface. An additional binding site on both $APLF^{AD}$ and H2A-H2B may be involved in the handoff between APLF and DNA or other chaperones. Together, our data support the view that APLF provides not only a scaffold but also generic histone chaperone activity for the NHEJ complex.

INTRODUCTION

Replication, transcription, and repair of the genome are essential for cell division, growth, and maintenance of genome integrity (1-3). In order to carry out their function, dedicated molecular machineries have to be able to gain access to the DNA, perform their task, and subsequently restore a functional chromatin state. Thus, these processes are highly dependent on chromatin dynamics down to its smallest organizational level: the nucleosome. The nucleosome is characterized by 146 base pairs of DNA wrapped around a protein core of two histone H2A-H2B dimers and one $(H3\text{-}H4)_2$ tetramer (4). Assembly and disassembly of nucleosomes is coordinated by histone chaperones, a family of histone binding proteins (5,6). These chaperones prevent the formation of nonnucleosomal histone-DNA complexes, mediate histone variant exchange, and store histone complexes.

Aprataxin and Polynucleotide kinase Like Factor (APLF) is a DNA repair factor that facilitates repair of DNA single- and double-strand breaks (DSBs) (7-9). In non-homologous end joining (NHEJ) of DSBs (10,11), it provides a scaffold for the NHEJ complex (12,13), promotes the retention of specific NHEJ subunits at DSBs *in vivo*, and stimulates the rate of NHEJ repair (14). APLF is a 57 kDa protein composed of several distinct functional domains (Figure 1A). The N-terminal forkhead-associated (FHA) domain interacts with DNA repair proteins XRCC1 and the XRCC4/DNA Ligase IV complex (9,15). The central, mostly unstructured part of APLF contains Ser^{116}, which is phosphorylated in response to DNA damage (9,16), and a binding motif for DNA repair factor Ku (17). The C-terminal half of the protein contains two poly(ADP-ribose) (PAR) binding zinc (PBZ) domains (18-21). PAR is a post-translational modification attached rapidly and transiently at sites of DNA damage by ADP-ribosyltransferases (ARTs) (22,23). APLF is recruited to DNA damage sites via interaction of its PBZ domains with PAR and in a PAR-independent manner via interactions with XRCC1

and Ku (7-9,18). Recently, the C-terminal acidic domain of APLF was shown to harbor histone chaperone activity based on its capability to mediate chromatin assembly, to bind core histones, and to disassemble tetrasomes (24).

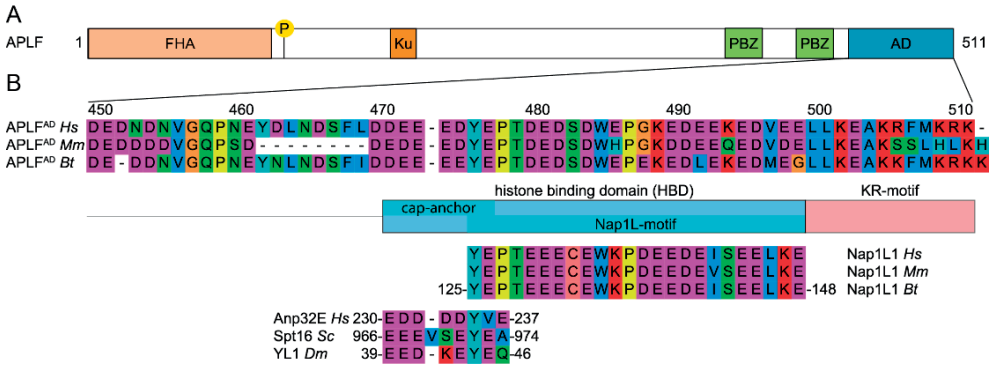

Figure 1. APLF contains an extended histone binding domain in its acidic domain. (A) Schematic representation of the APLF domain architecture. FHA = Forkhead associated domain, P = phosphorylation site Ser[116], Ku = Ku-binding motif, PBZ = Poly(ADP)ribose Binding Zinc finger, AD = acidic domain. (B) Sequence alignment of APLF^{AD}, motif analysis, and alignment with histone chaperones. APLF^{AD} shows conservation among species and with two motifs from histone chaperones: the NAP1L-motif present in Nap1-like proteins and the H2A-H2B binding cap-anchor motif of histone chaperones Anp32E, Spt16, and YL1. The amino acids are displayed by Seaview with color coding according to amino acid properties. Abbreviations: *Hs* = *Homo sapiens*; *Mm* = *Mus musculus*; *Bt* = *Bos taurus*; *Sc* = *Saccharomyces cerevisiae*; *Dm* = *Drosophila melanogaster*.

Here, we investigated the molecular basis of the histone chaperone function of the C-terminal APLF acidic domain, APLF^{AD}, using a combination of nuclear magnetic resonance (NMR) spectroscopy, crosslinking, microscale thermophoresis (MST), isothermal titration calorimetry (ITC), and a functional assay.

We show that APLF^{AD} is intrinsically disordered. It binds specifically and with high affinity to both $(H3\text{-}H4)_2$ and H2A-H2B histone complexes suggesting that it is a generic histone chaperone. Since the specificity and functionality of the H2A-H2B binding activity of APLF had not been addressed before, we characterized here in detail the molecular basis for the H2A-H2B binding of APLF^{AD}. The histone binding domain of APLF^{AD}, which contains two aromatic side chains, binds specifically to the region of H2A-H2B that interacts with DNA in the nucleosome. APLF^{AD} is shown to interfere with DNA binding to H2A-H2B, proving its H2A-H2B histone chaperone function. To rationalize these findings, we propose a novel double-anchor model in which two aromatic side chains anchor to the α1-α2-patches on H2A and H2B. Furthermore, we found evidence for a secondary binding mode involving the H2B αC-helix. Since this helix is an exposed feature on the surface of the nucleosome and many chaperone-histone complexes, this additional binding mode could represent a key step in the transfer of histone complexes from and to DNA or other chaperones. Collectively, our results suggest that APLF provides the NHEJ machinery with the capacity to bind and transfer histone complexes generically through an interaction mode that presents a novel variation in the recognition of the histone surface.

RESULTS

THE C-TERMINAL ACIDIC DOMAIN OF APLF IS CONSERVED AND UNSTRUCTURED

The APLF protein, including its C-terminal acidic domain, is highly conserved in a broad range of organisms (8,24). Further sequence analysis shows that the APLF acidic domain ($APLF^{AD}$, *Homo sapiens* (*Hs*) APLF residues 450-511) is homologous to various known histone chaperones in two partly overlapping regions (Figure 1B). The first region, residues 476-499, is conserved in the nucleosome assembly protein 1-like 1 (NAP1L1) protein, and this region has been shown to be important for interaction with histone proteins and DNA repair functionality (24). The second region is a negatively charged region (residues 471-477, starting just before the NAP1L1 motif) that aligns well with the conserved cap-anchor peptide motifs used by other histone chaperones for binding the H2A-H2B or H2A.Z-H2B histone dimer (34,38-42). The region of similarity with other chaperones is followed by a conserved positively charged C-terminal region, here termed KR-motif (with K/R as single-letter codes of amino acids lysine/arginine), which could have functional relevance. The presence of an extended, highly conserved region with homology to known histone chaperones suggests that the entire conserved region in APLF may be involved in histone binding. We therefore define residues 471-499 as the (putative) histone binding domain (HBD) of APLF.

The low complexity of the primary sequence and the sparsity of hydrophobic residues suggest that $APLF^{AD}$ is unstructured (43-46). To characterize the structural properties of $APLF^{AD}$ experimentally, we used NMR spectroscopy and recorded the fingerprint ^{1}H-^{15}N heteronuclear single quantum coherence (HSQC) NMR spectrum of free $APLF^{AD}$ (Figure 2A, and Supplementary Figure S1). All backbone amide protons resonate in a narrow spectral region between 7.8 and 8.7 ppm, indicating that $APLF^{AD}$ is mostly unstructured in solution. To allow more detailed analysis, the backbone chemical shifts were assigned and analyzed for secondary structure propensities using the program SSP (30). The entire domain, including the HBD, has a very low probability of being in either β-strand or α-helical conformation, implying that $APLF^{AD}$ is mostly unstructured (Figure 2B, upper panel). This is in agreement with a recent study that showed that full-length APLF is largely an intrinsically disordered protein (13). Noteworthy, the stretch of residues 496-506 at the C-terminal edge of the HBD shows a probability of up to ~40% of being in an α-helical conformation as found in our SSP analysis. Based on relaxation experiments by NMR spectroscopy, it is found that residues in this same stretch have significantly higher T_1/T_2 values compared to the rest of the acidic domain, which is indicative of reduced local flexibility and in agreement with transient formation of secondary structure (Figure 2B, lower panel).

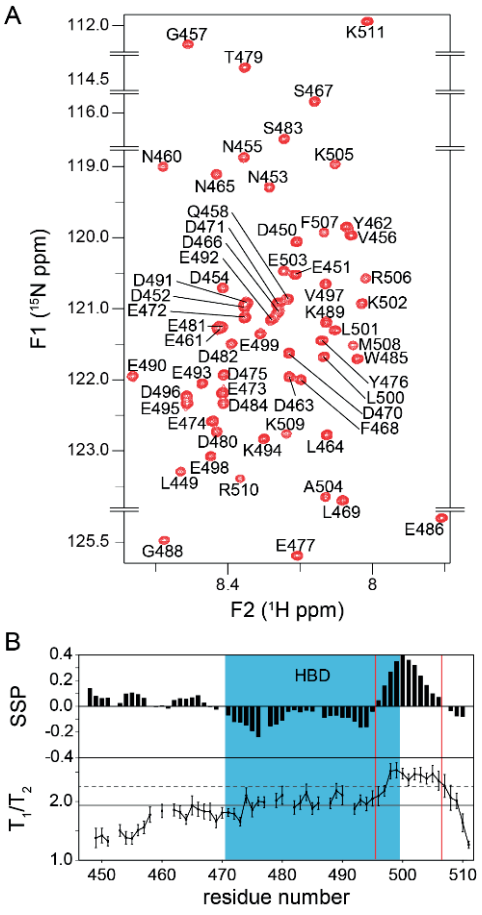

Figure 2. APLF^{AD} is an unstructured protein domain. (A) Zoomed ^{1}H-^{15}N HSQC spectrum of APLF^{AD} showing all backbone amide resonances with their assignments. Spectrum recorded at 22 °C, 25 mM NaPi, pH 6.6, 300 mM NaCl, 900 MHz ^{1}H Larmor frequency. (B) Secondary structure probabilities (SSPs) derived from NMR Cα and Cβ chemical shifts (upper panel) and experimental T_1/T_2 ratios from NMR relaxation measurements (lower panel) plotted against the sequence of APLF^{AD}. In the SSP diagram, negative and positive values indicate the probability of β-strand and α-helical conformation, respectively. In the T_1/T_2 plot, the solid (dashed) lines represent the average (average + one standard deviation) value. HBD is indicated in blue, the boundaries of the region with helical propensity are indicated with red lines.

APLF^{AD} INTERACTS WITH HIGH AFFINITY WITH HISTONES AND FORMS SPECIFIC COMPLEXES WITH H2A-H2B

In order to obtain the binding properties of APLF^{AD} and histone complexes, we studied their interactions by crosslinking, microscale thermophoresis (MST), and isothermal titration calorimetry (ITC) (Figure 3). All experiments were done at 300 mM salt in order to shield nonspecific interactions.

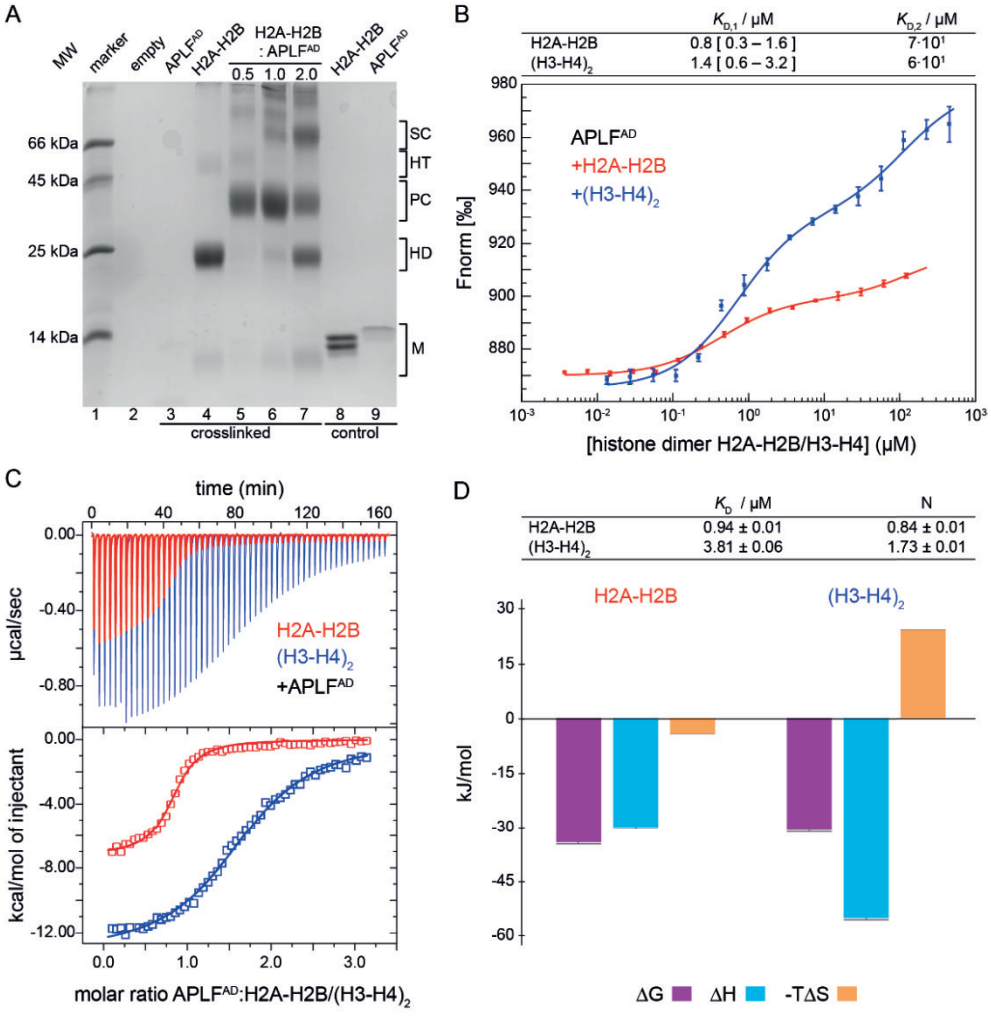

Figure 3. APLF^{AD} binds with high and similar affinities to H2A-H2B and (H3-H4)$_2$. (A) Sodium dodecyl sulfate polyacrylamide gel electrophoresis (SDS-PAGE) gel of room temperature crosslinking experiment of APLF^{AD}, H2A-H2B and their mixtures (molar ratios indicated on top of the gel). The molecular size regions for the histone and APLF^{AD} monomers are indicated (M), as well as regions for crosslinked histone dimers (HD), histone tetramers (HT), and histone-APLF^{AD} complexes: the primary and secondary complex (PC and SC). APLF^{AD} (7.7 kDa) migrates as a ~14 kDa protein (lane 9, control: non-crosslinked), presumably due to the acidic character of the protein. APLF^{AD} stains poorly, in particular in presence of the crosslinking agent (lane 3). (B) MST-derived binding curves of H2A-H2B (red) or (H3-H4)$_2$ (blue) titrated to fluorescently labeled APLF^{AD} at 25 °C. Data points are the average from three measurements, error bars are one standard deviation. Best-fit affinities using a sequential-binding model are listed in the table, the 95% confidence interval based on F-test is given in square brackets (see Supplementary Figure S2). Note that the concentration of (H3-H4)$_2$ is expressed in dimer units to allow direct comparison with H2A-H2B. (C) Calorimetric titration of APLF^{AD} to H2A-H2B (red) and (H3-H4)$_2$ (blue) via ITC at 25 °C. Experimental heat changes of injections of APLF^{AD} to H2A-H2B or (H3-H4)$_2$ are shown (upper panel) in red and blue, respectively. The resulting binding isotherms (lower panel) were fit to a one-set-of-sites binding mode. Best-fit values and fitting errors are shown in the table (D, top) together with the derived thermodynamic parameters (D, bottom). All data are obtained in 25 mM NaPi, pH 7.0, 300 mM NaCl.

The crosslinking agent dithiobis(succinimidyl-propionate) (DSP), which reacts with primary amine groups at the N-terminus of peptides and in lysine side chains, was used to trap complexes of APLF^{FAD} with histone complexes. While mixtures of $(H3\text{-}H4)_2$ and APLF^{FAD} precipitated (data not shown), mixtures of APLF^{FAD} and H2A-H2B were readily crosslinked (Figure 3A). In the absence of APLF^{FAD}, crosslinking of H2A-H2B yields dimers (~25 kDa) and a small population of $(H2A\text{-}H2B)_2$ tetramers (~50 kDa) (Figure 3A, lane 4), consistent with the ability of H2A-H2B to form transient tetramers (47). When APLF^{FAD} is titrated with H2A-H2B, a primary complex with an apparent molecular weight of ~40 kDa is formed, corresponding to one H2A-H2B dimer bound to one APLF^{FAD} (Figure 3A, lanes 5-7). In the presence of two-fold excess of H2A-H2B, additional bands corresponding to free H2A-H2B and secondary, higher-order complexes appear. The dominant band at ~70 kDa could correspond to one or two APLF^{FAD} bound to two H2A-H2B dimers (Figure 3A, lane 7).

Next, we set out to determine the affinity of binding between APLF^{FAD} and histone complexes using MST. Addition of H2A-H2B or $(H3\text{-}H4)_2$ to fluorescently labeled APLF^{FAD} resulted in clear changes in thermophoresis, reflecting binding of both types of histone complexes to the acidic domain (Figure 3B). Interestingly, in both cases two binding events were observed, one with a K_D in the sub-micromolar and one in the high micromolar range. This is consistent with the observation of a primary and a secondary complex formation in the crosslinking experiment described above that had the same overall titration setup, namely titration of histone complex to APLF^{FAD}. To extract the corresponding binding affinities, the data were fit to a sequential-binding model in which it was assumed that $(H3\text{-}H4)_2$, given its two-fold symmetry, presents two binding sites to APLF^{FAD}. The K_D values for the high-affinity binding events are 0.8 μM and 1.4 μM for H2A-H2B and $(H3\text{-}H4)_2$, respectively (Figure 3B and Supplementary Figure S2). For the secondary binding, the best-fit K_D value is ~50-fold higher, although it cannot be determined precisely because of lack of saturation (see Figure S2).

In order to determine the stoichiometry and thermodynamic parameters of binding, we investigated the binding between APLF^{FAD} and histones by ITC (Figure 3C). APLF^{FAD} binds to H2A-H2B with a K_D of 0.94 μM to form an enthalpically and entropically favorable complex (Figure 3D). APLF^{FAD} binds to $(H3\text{-}H4)_2$ with a K_D of 3.81 μM to form an enthalpically favorable but entropically unfavorable complex. The numbers of binding sites determined by ITC are ~0.8 and ~1.7 on H2A-H2B and $(H3\text{-}H4)_2$, respectively. This is consistent with one APLF^{FAD} binding to one H2A-H2B or H3-H4 dimer. The ITC-derived K_D value for H2A-H2B is very close to the high affinity binding value ($K_{D,1}$) obtained by MST, while the K_D value for $(H3\text{-}H4)_2$ is somewhat higher but close to the upper limit of the MST-derived $K_{D,1}$. Since high-affinity and high-enthalpy interactions dominate the ITC curve, no evidence for additional binding modes with lower affinity can be retrieved from the ITC experiments. Overall, MST and ITC data consistently show high-affinity interactions between APLF^{FAD} and both H2A-H2B and $(H3\text{-}H4)_2$ with low- to sub-micromolar dissociation constants, while crosslinking and MST data point to multiple binding modes at excess of histones.

H2A-H2B BINDS TO THE HBD OF APLF^{AD}

Since previous work had suggested that APLF preferentially chaperones $(H3\text{-}H4)_2$ and that the interaction with H2A-H2B is less salt-tolerant (24), we next asked whether the high-affinity interaction with H2A-H2B is specific or merely driven by unspecific electrostatic interactions. To determine the H2A-H2B interaction site on APLF^{AD}, we titrated unlabeled H2A-H2B dimers to ^{15}N-labeled APLF^{AD} and monitored spectral changes by NMR spectroscopy. Several APLF^{AD} backbone resonances show a change in peak intensity and/or a change in their chemical shift (chemical shift perturbation, CSP), indicating that these residues are involved in binding and/or undergo structural reorganization upon binding (Figure 4A). In contrast, the N-terminal part of APLF^{AD} up to residue number 468 is largely unaffected by the interaction (Figure 4B). Some of the affected resonances, such as of E477 and W485, disappear at low molar ratios of added histone dimer, reflecting a large exchange-induced line broadening (Figure 4A). This indicates that for these resonances the exchange between free and bound states is intermediate on the NMR chemical shift time scale, signifying a large chemical shift difference between these states. In a typical 1:1 binding model the bound-state resonances should be visible at the end of the titration, but most resonances in the stretch from D475 to E486 were not detected at high molar equivalents of H2A-H2B where APLF^{AD} should be fully bound. The increased size of the complex, in combination with residual exchange dynamics or additional dynamics in the bound states, may cause such loss of NMR signals. This has been demonstrated before for other unstructured histone chaperone domains binding to a histone complex (34,40,48). The overall pattern of observations is consistent with a low- to sub-micromolar affinity of APLF^{AD} for H2A-H2B.

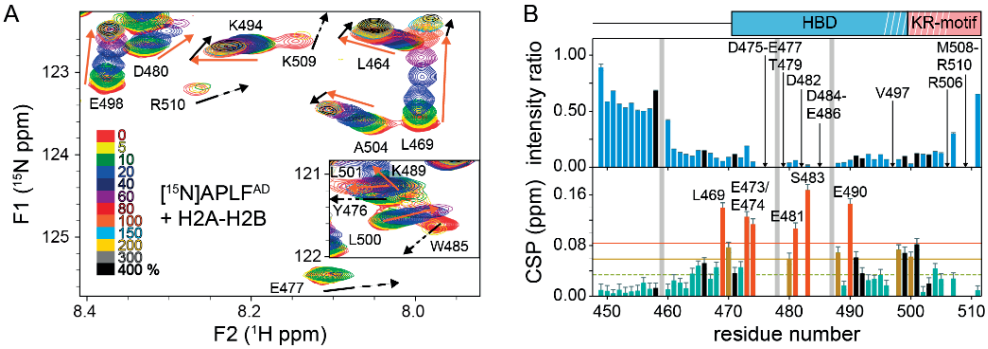

Figure 4. APLF^{AD} interacts with H2A-H2B through its HBD. (A) Zoomed region of overlaid ^{1}H-^{15}N transverse relaxation-optimized spectroscopy (TROSY) spectra of APLF^{AD} with increasing concentrations of H2A-H2B. The inset shows the region containing Y476 and W485 backbone resonances. Color coding indicated in the figure. Direction of peak shifts for disappearing resonances is indicated with dashed arrows. Peak shifts of selected resonances up to one (four) equivalents added are indicated with orange (black) arrows. Recorded at 900 MHz ^{1}H Larmor frequency at 35 °C in 25 mM NaPi buffer, pH 7.0 with 300 mM NaCl. (B) Analysis of APLF^{AD} ^{1}H-^{15}N peak intensity ratios (upper panel) and weighted average CSPs (lower panel) between H2A-H2B bound (4:1 molar ratio of H2A-H2B:APLF^{AD}) and free APLF^{AD}. Resonances that disappear during the titration are indicated by arrows and labeled. Resonances with CSPs more than 2 (1) standard deviation (SD) (orange (yellow) line) from the 10% trimmed mean (green dashed line) are highlighted in orange (yellow) and labeled. Position of the HBD and KR-motif are indicated above the plot, white stripes denote the helical region. Residues without titration data due to overlap or missing resonances are indicated with gray bars. Residues with strongly overlapped resonances in the bound state are indicated with black bars.

To map the H2A-H2B binding region on APLF^{FAD}, CSPs and peak intensity ratios were calculated from spectra without or with four molar equivalents of H2A-H2B (Figure 4B). Resonances corresponding to the central part of the putative HBD, residues D475 to E486, either show a substantial decrease in intensity or completely disappear. Resonances from adjacent residues near the termini of the HBD, including the C-terminal helical element, have low signal intensity and high CSPs. These data demonstrate that the primary region to interact with H2A-H2B is in fact the HBD of APLF^{FAD}. Importantly, this region also includes hydrophobic residues, in particular W485, which was previously found to be required for interaction with $(H3\text{-}H4)_2$ (24), and Y476 which is part of the cap-anchor motif (see Figure 1B). Additionally, several resonances display curved peak trajectories when adding more than one equivalent of histone dimer, see for instance L464, L469, K494 and A504 in Figure 4A. Together, our data indicate that the conserved HBD of APLF^{FAD} is responsible for a direct and high-affinity interaction with H2A-H2B, and that regions either N- or C-terminal to the HBD may play a role in secondary binding modes between APLF^{FAD} and H2A-H2B.

APLF^{AD} INTERACTS WITH THE DNA AND CHAPERONE BINDING REGION OF H2A-H2B

To further investigate the nature of the interaction between APLF^{FAD} and H2A-H2B, we mapped where the HBD contacts the H2A-H2B dimer. For this purpose, we titrated unlabeled APLF^{FAD} into the H2A-H2B dimer with either H2A or H2B ^{15}N-labeled ([^{15}N]H2A-H2B and H2A-[^{15}N]H2B, respectively) (Figure 5A,B). Backbone assignments of H2A and H2B in the H2A-H2B dimer were performed and transferred to assay conditions. Addition of APLF^{FAD} to [^{15}N]H2A-H2B causes significant CSPs for several residues (Figure 5A). Including resonances that disappear during the titration, such as R28, the affected residues cluster in and around the α1-helix and the L2-loop of H2A, which contain DNA binding residues (Figure 5C). In particular, the largest CSP is observed for R76, which anchors the L2-loop into the minor groove of DNA in the nucleosome (4,37). Additionally, the region around G27 and R28 is part of the α1-α2-patch formed by the α1-helix, L1-loop, and α2-helix, which is the contact point for DNA at the next superhelical location (Figure 5F).

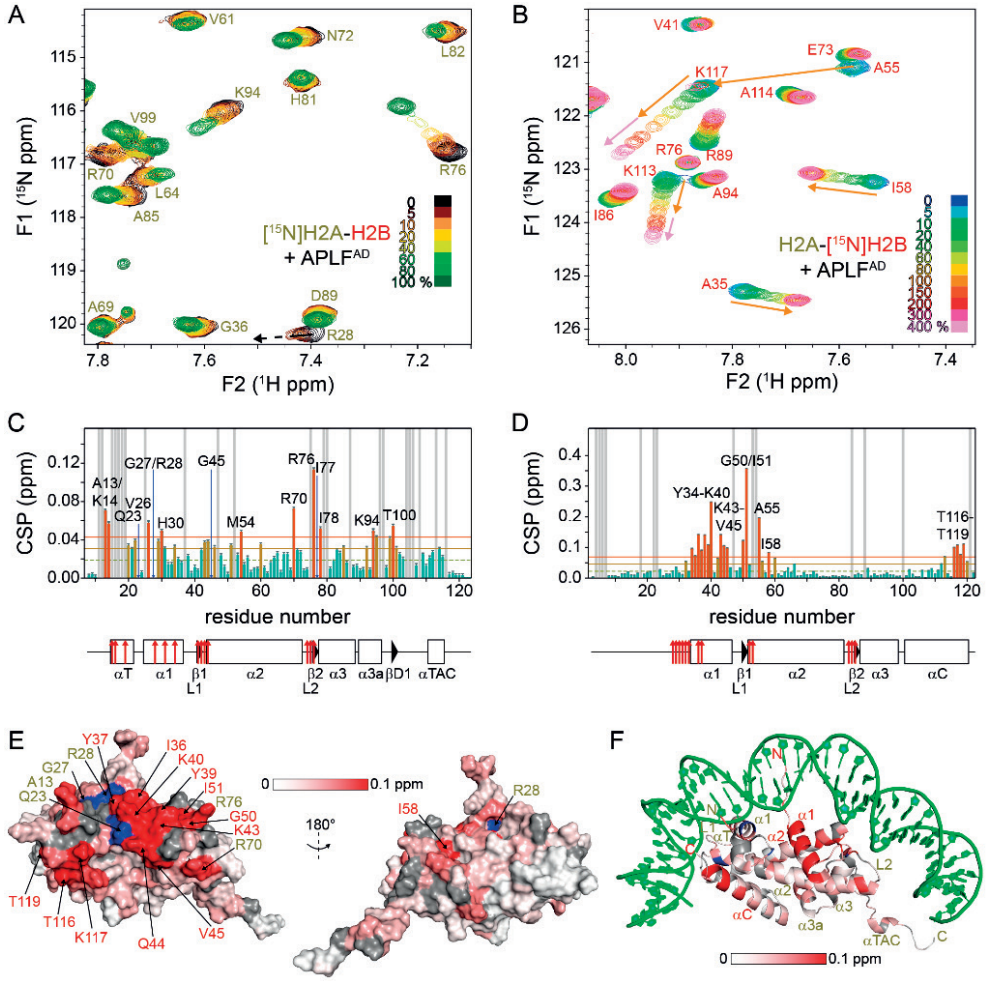

Figure 5. APLF^{AD} binds to the DNA and histone chaperone binding region of H2A-H2B. (A,B) Zoomed region of overlaid ^{1}H-^{15}N TROSY spectra of [^{15}N]H2A-H2B (A) and H2A-[^{15}N]H2B (B) with increasing concentrations of APLF^{AD}. Color coding of spectra is indicated in the figure. Data recorded at 850 MHz (A) or 750 MHz (B) ^{1}H Larmor frequency in 25 mM NaPi buffer, pH 7.0 with 300 mM NaCl, 35 °C. Direction of peak shifts for disappearing resonances is indicated with dashed arrows in (A). Peak shifts of selected resonances up to one (four) equivalents added are indicated with orange (pink) arrows in (B). (C,D) Weighted average CSP per residue in H2A (C) and H2B (D) upon addition of one molar equivalent of APLF^{AD}. Resonances that disappear during the titration are indicated by blue arrows and labeled in (C). Resonances with CSPs more than 2 (1) SD (orange (yellow) line) from the 10% trimmed mean (green dashed line) are highlighted in orange (yellow) and labeled. Residues without titration data due to overlap or missing resonances are indicated with gray bars. Secondary structure (SS) of H2A/H2B as in the nucleosome (PDB ID 2PYO) (37) indicated below the plot (line = loop, rectangle = α-helix, triangle = β-strand) with naming of SS-elements as in Ref. (49). Residues that interact with nucleosomal DNA (PDB ID 2PYO) are indicated by red arrows. (E,F) CSPs color coded on the surface (E) and cartoon (F) representation of H2A-H2B. H2A residues of which resonances disappear during the titration are colored blue and labeled. Surface residues with significant CSPs (more than 2 SD from the 10% trimmed mean, see panels C,D) are labelled in yellow (red) for H2A (H2B). Gray – residues without titration data; green – DNA.

In the titration experiment with H2A-[^{15}N]H2B, very pronounced CSPs were observed such as for A55, I58 and K117, shown in Figure 5B. Strikingly, the trajectories of the A55 and I58 resonances approach the bound state after addition of one molar equivalent APLF^{AD} whereas the K117 resonance shifts throughout the titration up to four equivalents. Together with kinked or curved CSP trajectories for several resonances (see Figures 6C,D and Supplementary Figure S3), these observations point to the presence of two binding sites on the H2A-H2B dimer, one with high affinity and a second with lower affinity. Using the CSPs observed up to one equivalent APLF^{AD} added, we identified the α1-α2-patch of H2B as the main binding region for APLF^{AD} (Figure 5D). This region was previously identified as chaperone binding region for H2A(.Z)-H2B chaperones Anp32E, Swr1, Spt16, and YL1 (34,38-41,50). In addition, the H2B αC-helix is also involved in the binding of APLF^{AD} as can be seen from the significant CSPs of H2B residues T116-T119 (Figure 5D). Using the CSPs between one and four added molar equivalents of APLF^{AD}, the secondary binding site can be mapped to the α3- and αC-helix of H2B, while no such rigorous conclusion can be drawn for H2A (Figure 6A). The most obvious indication of secondary binding in the titration data of [^{15}N]H2A-H2B is found for H2A G21, located close to the H2B αC-helix. The resonances of this residue display a curved peak trajectory, thus supporting the secondary binding to this site (Figure S3D,E). Interestingly, the H2B αC-helix is on the accessible surface of the nucleosome (Figure 6B).

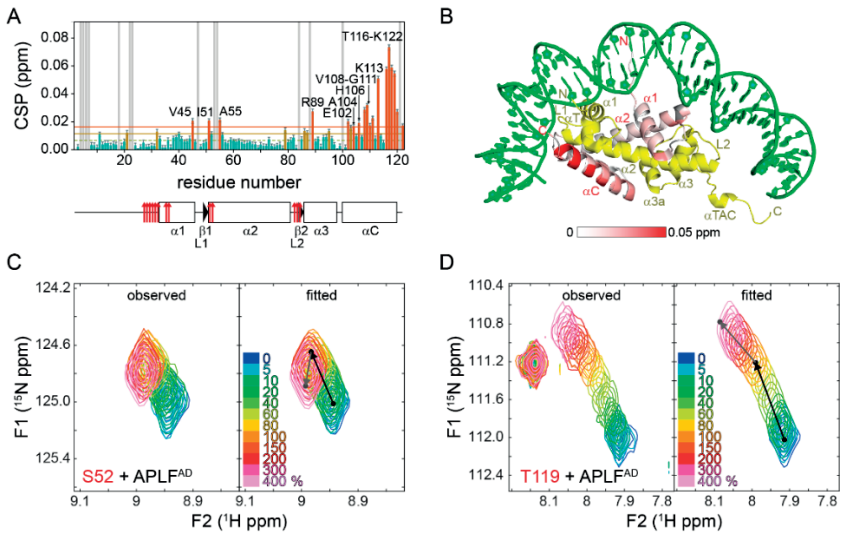

E

	K_D / μM	k_{off} / s^{-1}	N
primary binding	2.5 ± 0.1	5.7·10^2 ± 0.1·10^2	0.799 ± 0.003
secondary binding	97 ± 11	4·10^3 ± 2·10^3	1

Figure 6. The H2B α3- and αC-helices form a secondary binding site for APLF^{AD}. (A) Weighted average CSP per residue in H2B observed between one and four molar equivalents of APLF^{AD} added to H2A-H2B. Color coding, labeling of residues, and secondary structure plot as in Figure 5. (B) Observed CSPs color coded on the cartoon representation of H2A-H2B (PDB ID 2PYO). Color coding: yellow – H2A; gray – residues without titration data; green – DNA. (C,D) Observed and fitted 2D NMR lineshapes for two residues (C: S52 and D: T119) with pronounced kinked trajectories. Color coding of spectra is indicated in the figure. The black (gray) arrows indicate the displacements for the high (low) affinity interactions. (E) Table with best-fit values for binding parameters. N = number of binding sites.

To compare the affinities of the primary and secondary APLF^{AD} binding sites on H2A-H2B, the NMR lineshapes were quantitatively analyzed using the program TITAN (31). NMR lineshapes are very sensitive to the off-rate, k_{off}, and thus reasonably accurate K_D values can be determined even when the protein concentration exceeds the K_D. An excellent fit to the data was obtained using a sequential-binding model in which binding affinity to the primary binding site (formed by the chaperone-binding region and the H2A α1-α2-patch) is in the low micromolar range and ~40-fold higher than the affinity for the secondary site on the α3- and αC-helix of H2B (Figure 6E and Supplementary Figure S3). The difference in affinity can be attributed to a difference in dissociation rates (k_{off}), with best-fit values for the k_{off} of $6 \cdot 10^2$ s^{-1} and $4 \cdot 10^3$ s^{-1} for the high- and low-affinity interaction, respectively (Figure 6E). This translates to an average lifetime of 1.7 ms for APLF^{AD} bound to the primary interaction region. The highly dynamic nature of the complex underscores the important role of electrostatics in the interface.

We thus find that the negatively charged HBD of APLF^{AD} binds with high affinity to the DNA and chaperone-binding region of the H2A-H2B dimer. In addition, there is strong evidence for additional interaction modes between APLF^{AD} and H2A-H2B from the observed secondary binding sites on both APLF^{AD} and H2A-H2B.

A DOUBLE-ANCHOR MODEL FOR APLF^{AD} BINDING TO H2A-H2B

Having mapped the binding interfaces of APLF^{AD} and H2A-H2B, we sought to understand the interaction in more detail. Since APLF^{AD} is disordered and we have no detailed structural information on the bound-state conformation of APLF^{AD}, we decided to make use of homology to other known histone chaperones to build a structural model. In the procedure detailed below we make use of the following two assumptions.

First, we assume that the cap-anchor motif in APLF^{AD} binds to H2A-H2B in the same way as seen in recent structures of chaperone-histone complexes. These structures show that the aromatic anchor residue of this motif is buried in the H2B chaperone-binding region, while the cap residue forms a hydrogen bond to the N-terminus of the H2B α2-helix (34,38-41). This assumption is based on the conservation of the cap-anchor motif in APLF^{AD} (see Figure 1B) and the observation that this region (residues E473/Y476) as well as the chaperone-binding region in H2A-H2B (H2B residues Y34-I58) show the strongest effects in the NMR titrations (see Figure 4B and 5D).

Second, we assume that the bound-state conformation of the APLF^{HBD} resembles that of YL1. The structure of this chaperone bound to H2A.Z-H2B shows that YL1 binds through a cap-anchor interaction and a second aromatic side chain that interacts with the H2A α1-α2-patch (34,41). Similarly, the H2A-H2B binding region of APLF^{AD} contains two aromatic residues (Y476 and W485, see Figure 7A), and the H2A α1-α2-patch is involved in binding APLF^{AD} (Figure 5E). Notably, while in YL1 the aromatic anchors are spaced 14 residues apart, their separation in APLF^{AD} is only 9 residues (Figure 7A), illustrating the need for an atomistic model of the APLF^{HBD}-H2A-H2B complex to verify this assumption.

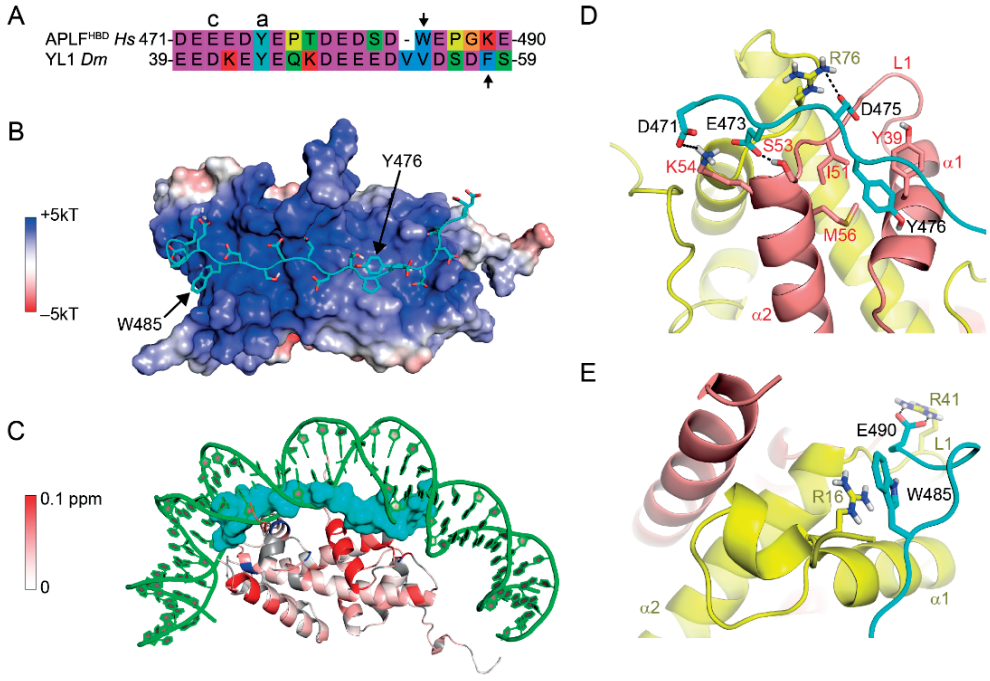

Figure 7. Structural model of APLF^{HBD} bound to H2A-H2B using two aromatic anchors. (A) Sequence alignment of APLF^{HBD} with YL1 used as template for modeling. Cap (c) and anchor (a) residues are indicated, second aromatic residue is indicated with an arrow. (B) Double-anchor model for APLF^{HBD} bound to H2A-H2B. APLF^{HBD} in cartoon representation with side chains shown as sticks. Electrostatic potential is color coded on the Van-der-Waals surface of H2A-H2B. (C) APLF^{HBD} (surface representation) binds to NMR-derived binding interface and interferes with DNA binding to H2A-H2B. Color coding of CSPs as in Figure 5. (D,E) Close-up views on the two aromatic anchor interactions. Cap-anchor bound to H2B chaperone-binding region in (D), second anchor bound to H2A α1-α2-patch in (E). APLF^{HBD} in cartoon representation with side chains shown as sticks. Selected residues and histone secondary structure elements are labeled. Hydrogen bonds indicated with dashes. Green – DNA; cyan – APLF; yellow – H2A; red – H2B.

To model the APLF^{HBD}-H2A-H2B complex, we thus first constructed a model of APLF^{HBD} based on the bound-state structure of histone chaperone YL1 using the program MODELLER (35) and the alignment in Figure 7A. The resulting APLF^{HBD} model was subsequently docked onto the structure of H2A-H2B using HADDOCK (36) driven only by distance restraints enforcing the cap-anchor binding motif. This procedure allows to verify whether both Y476 and W485 can simultaneously interact with H2A-H2B and allows validation using the NMR-derived binding interfaces.

The resulting model for the APLF^{HBD}-H2A-H2B complex shows that both aromatic residues are positioned close to the surface of H2A-H2B, connected by the negatively charged linker that runs over the positively charged surface of H2A-H2B (Figure 7B). The model has good physico-chemical properties, as indicated from excellent electrostatic match between the HBD and the dimer surface, the absence of clashes, and Ramachandran plot statistics (Supplementary Table S1). The HBD covers the H2A-H2B surface identified in the NMR titration studies and effectively

replaces the nucleosomal DNA (Figure 7C). Importantly, this structure shows that, despite different spacing compared to YL1, both aromatic residues can anchor to the dimer. The modeled cap-anchor interaction at the H2B α1-α2-patch is shown in Figure 7D. At the H2A α1-α2-patch, W485 of APLF is buried in the H2A patch with π-stacking to R16 in H2A, with additional stabilization from a salt bridge between APLF E490 and R41 in H2A (Figure 7E), although the precise details of this interaction depend strongly on the conformation of APLF^{HBD} submitted for docking (data not shown). In short, our model is in line with the experimental evidence and suggests a novel interaction mode between a histone chaperone and the H2A-H2B dimer with APLF^{FAD} binding the H2B hydrophobic pocket with a conserved tyrosine anchor and the H2A patch with a tryptophan anchor.

TWO AROMATIC ANCHORS IN APLF^{AD} ARE ESSENTIAL TO PREVENT AGGREGATION OF H2A-H2B-DNA COMPLEXES

To test our structural model of the APLF^{FAD}-H2A-H2B interaction and to validate its functional relevance, we assayed the histone chaperone activity of APLF^{FAD} *in vitro*. In absence of H3-H4, H2A-H2B binds in non-native manner to DNA, resulting in aggregation and precipitation at high concentrations of histone dimer (51). As a true histone chaperone, APLF^{FAD} should be able to prevent such incorrect histone-DNA interactions (52). We thus used a native polyacrylamide gel electrophoresis (PAGE) assay to detect the chaperone-mediated rescue of DNA precipitation (53). Control incubations of DNA with APLF^{FAD} wildtype (WT) or its mutants showed no effect, while incubation of DNA with H2A-H2B dimer led to loss of free DNA due to precipitation (Figure S4A), culminating in complete precipitation of DNA at a 15:1 H2A-H2B:DNA ratio (Figure 8A, lanes 2-3). However, when H2A-H2B was pre-incubated with different amounts of APLF^{FAD} WT, DNA precipitation was prevented and free DNA as well as soluble DNA complexes were observed (Figure 8A, lanes 4-6). Mutating the aromatic amino acids that we identified as key anchor residues in APLF^{FAD} according to our structural model reduces its ability to prevent histone-DNA aggregates. While in APLF^{FAD} Y476A chaperone activity is partially abolished (Figure 8A, lanes 7-9), the mutation W485A greatly reduces chaperone activity (Figure 8A, lanes 10-12), which is almost completely lost in the double mutant Y476A/W485A (Figure 8A, lanes 13-15). This reveals that APLF^{FAD} interferes with DNA binding to H2A-H2B and that the two aromatic side chains in the HBD of APLF^{FAD} are essential for chaperone function. These data imply that the interaction between APLF^{FAD} and H2A-H2B is specific and functional, thus strongly supporting the role of APLF^{FAD} as a domain with H2A-H2B chaperone function. In support of this result, we compared the affinities of H2A-H2B to the APLF^{FAD} mutants used in the chaperone assay by ITC. While the single mutants Y476A and W485A bound with slightly reduced affinities compared to WT APLF^{FAD} to H2A-H2B, no binding was detected for the double mutant Y476A/W485A (Figure 8B). This suggests that the linker region retains a high degree of flexibility such that the two anchors behave independently. Furthermore, whereas the binding of APLF^{FAD} WT and Y476A is mostly enthalpy driven, binding of W485A is entropy-driven. This suggests a higher conformational flexibility of the chaperone-histone complex with W485A, reducing its capability to screen the H2A-H2B DNA-binding surface, leaving it open for interaction with DNA.

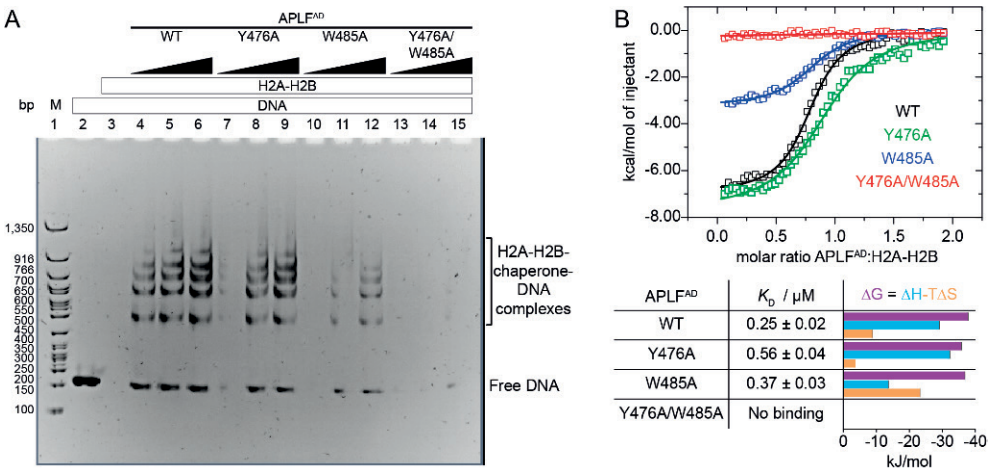

Figure 8. APLF^{AD} functions as histone chaperone and prevents H2A-H2B-mediated DNA precipitation. (A) Native PAGE analysis of 167 base pair (bp) DNA (1 µM) with the 601 nucleosome positioning sequence in presence or absence of APLF^{AD} WT or mutants and H2A-H2B. Chaperone assay performed at 37 °C. Lane 1: 50 bp DNA ladder (M). Lane 2: free DNA. Lane 3: DNA upon addition of 15 µM H2A-H2B. Lanes 4-15: DNA upon addition of 15 µM H2A-H2B preincubated with increasing concentrations (15, 45, or 90 µM) of APLF^{AD} WT, Y476A, W485A, or Y476A/W485A. (B) Calorimetric titration of APLF^{AD} WT or mutants to H2A-H2B via ITC at 25 °C. The resulting binding isotherms (upper panel) were fit to a one-set-of-sites binding mode. Best-fit values and fitting errors are shown in the table together with the derived thermodynamic parameters (lower panel). All data are obtained in 25 mM NaPi, pH 7.0, 300 mM NaCl.

Discussion

We describe here a detailed characterization of the interaction between the acidic domain of DNA repair factor APLF with core histone complexes to understand its histone chaperone activity. We have performed structural investigation on the recognition of H2A-H2B dimers and we present evidence that APLF can function as a true H2A-H2B chaperone. For this function, APLF makes use of a double-aromatic-anchor binding motif, a model supported by mutational analysis.

We find that APLF^{AD} binds comparably to both $(H3\text{-}H4)_2$ and H2A-H2B, implying that APLF is a generic histone chaperone without specificity for either type of histone complex. While Mehrotra *et al.* (Ref. (24)), who first characterized APLF as a histone chaperone, focused on the interaction with the H3-H4 tetramer, our data show consistently, quantitatively, and using a variety of techniques, that APLF^{AD} binds H2A-H2B with very similar affinity as $(H3\text{-}H4)_2$ (Figure 3). The NMR data indicate that the histone binding domain (HBD) binds generic elements of the histone fold in H2A-H2B, namely the α1-α2-patches of each histone that form contact points with nucleosomal DNA (Figure 5). Based on homology with YL1 and supported by mutational analysis, our structural model indicates that the APLF^{HBD} anchors to these patches via two aromatic anchors: W485 binds the H2A-patch (potentially via H2A R16) and Y476 binds the H2B-patch (most likely via H2B Y39). The unstructured nature of APLF^{AD} may

provide the HBD with the required conformational flexibility to adapt to the surfaces of either $(H3\text{-}H4)_2$ or H2A-H2B (54,55).

The double-anchor model of $APLF^{FAD}$ bound to H2A-H2B presented here constitutes a novel interaction mode that highlights adaptability in recognition of the H2A-H2B surface. Comparison of the model and the H2A.Z-H2B-YL1 structure suggests that the change in spacing between the two anchor residues (from 14 in YL1 to 9 residues in APLF) prevents anchor W485 in APLF from deep burial in the H2A-patch and instead forces it to form a different set of interactions.

Sequence analysis of histone chaperones Spt16, Pob3 and hNap1 (Nap1L1) shows that these also contain a second aromatic residue in their histone binding regions. Therefore, we hypothesize that the double-anchor interaction mode is also present in these H2A-H2B chaperones. The minimal binding domains (MBD) of both Spt16 and Pob3 contain a second aromatic residue, spaced 13 and 15 residues, respectively, C-terminal to the tyrosine H2B-patch anchor (39). While not present in the crystal structure of $Spt16^{MBD}$ with H2A-H2B, mutagenesis data show a strong contribution of this C-terminal region in the MBD to binding affinity. In case of hNap1, its C-terminal acidic domain (CTAD) has been shown to facilitate binding of two H2A-H2B dimers to the core of hNap1 (42). There are two cap-anchor motifs in the CTAD with their aromatic anchors spaced 23 residues apart. Since it was found that both motifs bind to one H2A-H2B dimer, it is likely that the CTAD is able to bind in a similar double-anchor mode as $APLF^{FAD}$. Differences in the spacer length and the identity of anchor and surrounding residues may account for differences in histone specificity.

We showed that $APLF^{FAD}$ binds both H2A-H2B dimers and H3-H4 tetramers with similar, low- to sub-micromolar affinities at high ionic strength, comparable to other chaperones under similar conditions. The results of our chaperone assay suggest that $APLF^{FAD}$ is able to compete with DNA to bind the H2A-H2B DNA-interaction surface. This is in line with thermodynamic studies indicating that the chaperone-histone binding affinity must be high enough to prevent nonnative histone-DNA complexes but low enough to allow handoff to the DNA when proper nucleosomal contacts are made (51,56). Thus, $APLF^{FAD}$ may promote proper nucleosome formation by preventing the formation of unspecific histone-DNA complexes.

In this regard, the additional weak interaction to the αC-helix of H2B, which is accessible in the nucleosome, could play a role in facilitating nucleosome assembly/disassembly or in the exchange of histone variants by providing a contact point compatible with DNA or chaperone binding (Figure 9A). In particular, $APLF^{FAD}$ is essential for the recruitment of macroH2A to sites of DNA damage and thus likely plays a role in the exchange of this variant (24,57). We speculate that the C-terminal KR-motif of APLF is involved in this interaction, based on the NMR data and the structural model showing that this region is closest to the H2B αC-helix. More investigation is needed to delineate the functional role of the secondary binding as well as its structural basis.

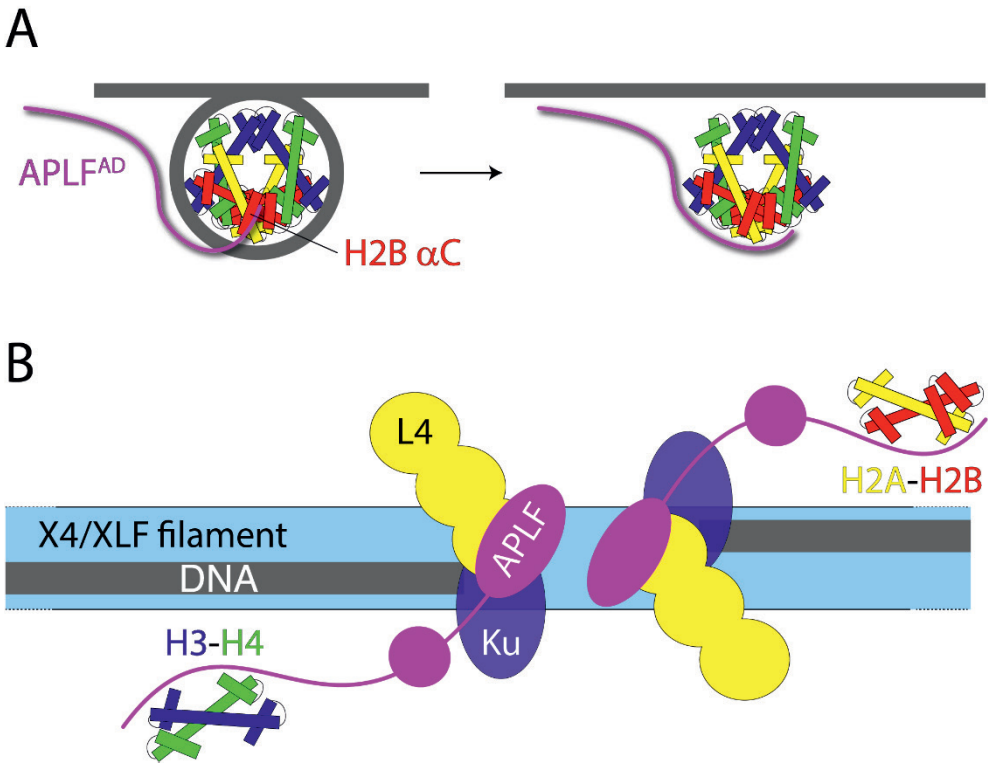

Figure 9. Schematic model of APLF chaperone function in NHEJ. (A) APLF binds to the nucleosome via its acidic domain to the H2B αC-helix. After nucleosome disassembly, a conformational rearrangement leads to APLF binding to the DNA binding surface of the histones to prevent nonnucleosomal interactions and store the core histones. (B) Schematic model of the NHEJ complex, based on Ref. (13) and this work. Broken DNA strands are held in place by the XRCC4 (X4)/XRCC4-like factor (XLF) protein filaments. The DNA ends are bound by Ku and DNA ligase IV (L4). APLF is bound to X4/L4 via its FHA domain at the DNA break site and stores core histone complexes for later reassembly of nucleosomes.

It was recently shown that full-length APLF scaffolds DNA repair factors in an extended and flexible DNA repair complex for non-homologous end joining (NHEJ) (13). NHEJ involves formation of long protein filaments on naked DNA to capture the broken DNA strands (58-60), requiring disassembly of nucleosomes. The presence of APLF at the DNA end-sites as in the model of Hammel *et al.* (13) suggests that APLF could function to temporarily store histone complexes and mediate their transfer to and from DNA or other chaperones at the break site (Figure 9B). After ligation, APLF may promote formation of a nucleosome to "seal" the repaired break. Overall, APLF could facilitate NHEJ with the required recognition of DNA damage, histone eviction, DNA repair, histone variant exchange and nucleosome assembly in one extended multi-protein DNA repair complex.

CONCLUSIONS

In conclusion, we show that the acidic domain of APLF is a histone chaperone that can bind both the histone H2A-H2B dimer and H3-H4 tetramer. We provide experimental proof for the chaperone activity for H2A-H2B and show that this can be rationalized by the screening of the DNA-binding surface by $APLF^{AD}$. $APLF^{AD}$ binds H2A-H2B through electrostatic interactions and two aromatic residues that form anchors to the α1-α2-patches on both histones. The recognition of these generic histone-fold elements combined with the unstructured nature of $APLF^{AD}$ suggests that APLF has the capability to temporarily store histone complexes at the DNA damage site for later nucleosome reassembly. Chaperone activity may be facilitated by the observed binding to the exposed H2B αC-helix as a key step in nucleosome (dis)assembly and histone transfer. Together, our study extends the assigned functions of APLF and underscores its important role in NHEJ. Finally, the case of the APLF acidic domain highlights that such domains are more than simple polyanionic unstructured polymers: their sequences encode specific recognition of the histone surface and may be tuned to provide the required specificity and affinity.

MATERIALS AND METHODS

PROTEIN EXPRESSION AND PURIFICATION

APLF^{AD} production

An APLF^{AD} expression plasmid was constructed according to the enzyme free cloning method for bacterial expression of proteins with an N-terminal histidine (His) and glutathione-S-transferase (GST) tag using a plasmid with the DNA sequence of human APLF as DNA template (25). The following primers were used:

5'-GCCGCGCGGCAGCCTGGATGAAGATAATGATAATGTTGGGCAAC-3' (LICFW)
+
5'-CTATTTTCTTTTCATAAACCTTTTTGCTTC-3' (RV)
and
5'-TGGATGAAGATAATGATAATGTTGGGCAAC-3' (FW)
+
5'-CAAGAAGAACCCCCTATTTTCTTTTCATAAACCTTTTTGCTTC-3' (LICRV)

and the pLIC-His-GST vector. Correct construction of the plasmid was verified by DNA sequencing. APLF^{AD} mutants were generated by site-directed mutagenesis on this vector and verified by sequencing.
APLF^{AD} was expressed as fusion protein with N-terminal His-GST tag in Rosetta2 (DE3) cells (Novagen). All media used contained ampicillin (100 mg/L) and chloramphenicol (34 mg/L). Colonies from a lysogeny broth (LB) agar plate were first grown in liquid LB at 37 °C. Cells from the LB culture were transferred to supplemented M9 minimal medium (MM) containing either $^{14}NH_4Cl$ and ^{12}C-glucose or $^{15}NH_4Cl$ and ^{13}C-glucose as the sources of nitrogen and carbon, respectively, and left to grow at 37 °C. Expression of recombinant protein was induced at OD_{600} 0.8 with 0.5 mM isopropyl β-D-1-thiogalactopyranoside (IPTG) and the culture was transferred to 30 °C. Cells were harvested 10-14.5 h after induction and frozen for storage. For purification, cells were resuspended in lysis buffer (50 mM Tris, pH 8.0, 150 mM NaCl, 5 mM β-mercaptoethanol (BME), 1 mM ethylenediaminetetraacetic acid (EDTA)) supplemented with 0.2 mM phenylmethylsulfonyl fluoride (PMSF) and in-house made protease inhibitor cocktail (PIC) (100 μM AEBSF, 0.3 μM aprotinin, 1 μM bestatin, 1 μM E-64, 10 μM leupeptin, 1 μM pepstatin A), then treated with lysozyme (Sigma-Aldrich) (2 mg per 1 g of wet cell pellet; 20 min on ice) and benzonase (Merck Millipore), frozen, thawed and sonicated. After insoluble cell material was removed by centrifugation (30 min, 35,000 g, 4 °C), His-GST-APLF^{AD} was purified using glutathione agarose beads (Sigma-Aldrich) preincubated in lysis buffer, and, after fusion protein binding, washed with lysis buffer. Bound fusion protein was eluted with 15 mM reduced glutathione (Sigma-Aldrich) in lysis buffer and cleaved with thrombin (Sigma-Aldrich) at room temperature, typically overnight. Cleavage was monitored using SDS-PAGE analysis and after complete cleavage, the protein mixture was dialyzed extensively against lysis buffer to remove glutathione and reapplied on glutathione agarose beads to remove GST. APLF^{AD} was further purified by anion exchange on a 5 ml HiTrap Q HP column (GE Healthcare Life Sciences) using ion exchange (IEX) low salt buffer (20 mM Tris, pH 7.5, 150 mM NaCl, 5 mM BME, 1 mM EDTA) and IEX high salt buffer (20 mM Tris, pH 7.5, 1 M NaCl, 5 mM BME, 1 mM

EDTA). Fractions with APLF^{FAD} were pooled and concentrated using a 3 kDa molecular weight cut-off (MWCO) Amicon Ultra Centrifugal Filter Unit (Merck Millipore) and elution buffer was exchanged to assay buffer (25 mM NaPi, pH 7.0, 300 mM NaCl). APLF^{FAD} was aliquoted, flash-frozen in liquid nitrogen and stored at -20 °C until further use.

Histone production

Histone proteins H2A, H2B, H3 and H4 from *Drosophila melanogaster* (*Dm*) were expressed in Rosetta2 (DE3) cells (Novagen) from a pET21b plasmid. All media contained ampicillin (100 mg/L) and chloramphenicol (34 mg/L). Colonies from an LB agar plate were first grown in LB at 37 °C. The cell culture was transferred to supplemented M9 minimal medium (MM) (unlabeled or containing $^{13}C_6D_7$-glucose, $^{15}NH_4Cl$, and D_2O for labeling) and grown at 37 °C. Expression of recombinant protein was induced at OD_{600} 0.6-0.8 with 0.5 mM IPTG. Cells with H4 were harvested 3 h after induction, cells with other histones 12.5 h after induction by centrifugation at 4,000 g for 20 min. Cells were resuspended in histone lysis buffer (50 mM Tris at pH 7.5, 100 mM NaCl, 5 mM BME, 1 mM EDTA) supplemented with 0.2 mM PMSF and in-house made PIC (as above), treated with lysozyme (as above), frozen, thawed and sonicated. First steps of purification – isolation and solubilization of histone inclusion bodies – were done according to the protocol described by Luger *et al.* (26). Solubilized histones were first purified on a gel filtration column HiLoad Superdex 75 pg (GE Healthcare Life Sciences) pre-equilibrated with histone gel filtration buffer (50 mM NaPi, pH 7.5, 150 mM NaCl, 5 mM BME, 1 mM EDTA, 7 M urea). Histone-containing fractions were pooled and loaded on a cation exchange chromatography column HiTrap SP HP (GE Healthcare Life Sciences) pre-equilibrated with histone gel filtration buffer. The same buffer was used to wash the column after loading. Histones were eluted with a linear gradient of NaCl (0.15 – 1 M), dialyzed against water, lyophilized, and stored at -20 °C.

PREPARATION OF HISTONE COMPLEXES

Lyophilized histone proteins were unfolded in unfolding buffer (50 mM Tris, pH 7.5, 100 mM NaCl, 10 mM dithiothreitol (DTT), 6 M guanidine hydrochloride) and mixed (H2A with H2B and H3 with H4) in equimolar ratios to a final protein concentration of 1 mg/ml. Refolding by dialysis and gel filtration of histone complexes were performed as described before for histone octamers (26). The gel filtration buffer was exchanged to assay buffer (see above) using a 3 and 10 kDa MWCO Amicon Ultra Centrifugal Filter Unit (Merck Millipore) for H2A-H2B and $(H3\text{-}H4)_2$, respectively. Protein samples were concentrated and used for experiments immediately or flash-frozen in liquid nitrogen and stored at -20 °C.

Crosslinking experiments

Crosslinking was performed using dithiobis(succinimidyl-propionate) (DSP). $APLF^{FAD}$ (5 µL of 40 µM) was mixed with H2A-H2B (5 µL of 20, 40 or 80 µM). Experiments on individual proteins were done by mixing $APLF^{FAD}$ (5 µL of 5 µM) or H2A-H2B (5 uL of 20 µM) with 5 µL of assay buffer. After 15 min of incubation at room temperature (RT), 1 µL of 1 mM DSP in dimethyl sulfoxide (DMSO) was added. Samples were crosslinked for 25 min at RT and then mixed with 4 µL of 4x non-reducing Laemmli sample buffer. After 15 min at RT, the samples were heated to 95 °C for 5 min and analyzed by non-reducing SDS-PAGE on a 14% polyacrylamide gel and stained with Coomassie Brilliant Blue G.

Microscale thermophoresis

For MST experiments, $APLF^{FAD}$ was labeled with a fluorescent tag (NT-647) on exposed lysine amino groups with the Monolith NT™ Protein Labeling Kit RED-NHS (NanoTemper Technologies) according to the supplied labeling protocol. NT-647-labeled $APLF^{FAD}$ was used at a concentration of 25 nM. Unlabeled H2A-H2B was titrated in 1:1 dilutions beginning at 118 µM. Unlabeled $(H3\text{-}H4)_2$ was titrated in 1:1 dilutions beginning at 217.5 µM (tetramer concentration). Optimization of experimental conditions is described in Ref. (27). Experiments were performed in assay buffer supplemented with 0.5 mg/ml bovine serum albumin (BSA) and 0.05% Tween-20 and measured in hydrophilic capillaries (NanoTemper Technologies). Three independent measurements were done on a NanoTemper Monolith NT.015 instrument at 25 °C, 20% MST and 100% LED power with 30/5 seconds laser-on/off time. Data were fit to a sequential-binding model using in-house MATLAB 2017a (The MathWorks, Inc.) scripts (available upon request to the corresponding author of the underlying publication of this chapter). Error bars were set to the standard deviation of each replicate point or to 0.5 Fnorm units at minimum. Errors in fit parameters were based on statistical F-test with 95% confidence interval (see Supplementary Figure S2).

Isothermal titration calorimetry

A calorimetric titration of $APLF^{FAD}$ to H2A-H2B or $(H3\text{-}H4)_2$ was performed using a MicroCal VP-ITC microcalorimeter (GE Healthcare) at 25 °C. Proteins were buffer exchanged exhaustively at 4 °C into assay buffer before use in the titration experiments. All solutions were degassed under vacuum for 5 min with gentle stirring immediately before use. For comparison between histone complexes (Figure 3C,D), H2A-H2B or $(H3\text{-}H4)_2$ was used in the sample cell at a concentration of 30 µM and titrated with 450 µM $APLF^{FAD}$ in the injection syringe. For mutational analysis (Figure 8B), binding of WT and mutant $APLF^{FAD}$ to H2A-H2B was measured using 10 µM H2A-H2B in the cell and 90 µM $APLF^{FAD}$ in the syringe. The H2A-H2B and $APLF^{FAD}$ cell and syringe components as well as the reaction mixes at the end of the titrations were analyzed by Tris-Tricine SDS-PAGE followed by coomassie staining as control of the integrity of the proteins and protein concentrations (Figure S4C). Binding isotherms were

generated by plotting the heat change of the binding reaction against the ratio of total concentration of $APLF^{FAD}$ to total concentration of H2A-H2B or $(H3\text{-}H4)_2$. The enthalpy of binding (ΔH, kcal mol^{-1}) was determined by integration of the injection peaks (5 μL) and correction for heats of dilution were determined from identical experiments without histone complexes. The entropy of binding (ΔS), the stoichiometry of binding (N), and the dissociation constant (K_D) were determined by fitting the resulting corrected binding isotherms by nonlinear least-squares analysis to a one-set-of-sites binding model using the Origin software (MicroCal, Inc.). Error in fit parameters are the standard errors derived from the regression analyses as reported by the software.

NMR EXPERIMENTS, BACKBONE ASSIGNMENTS AND TITRATION ANALYSIS

All NMR experiments were carried out on Bruker Avance III HD spectrometers. All NMR spectra were processed using Bruker TopSpin or NMRPipe (28) and analyzed using Sparky (29).

Samples of free $APLF^{FAD}$ typically contained 200-500 μM protein in buffer containing 25 mM NaPi, pH 7, 300 mM NaCl, 5% (v/v) D_2O, 0.02% NaN_3 and 1x PIC (cOmplete EDTA-free Protease Inhibitor Cocktail (Roche)). Experiments for backbone assignment of $APLF^{FAD}$ were performed on a spectrometer operating at 600 MHz ^1H Larmor frequency and equipped with a cryoprobe. Spectra were recorded on $[^{13}C/^{15}N]APLF^{FAD}$ at 300 K for optimal resolution. Relaxation experiments to measure ^{15}N-T_1 and -T_2 of free $APLF^{FAD}$ were performed at 750 MHz ^1H Larmor frequency on $[^{15}N]APLF^{FAD}$ at 298K.

Backbone resonances of $APLF^{FAD}$ were assigned to 94% completeness using 3D HNCO, HN(CA)CO, HNCACB, CBCA(CO)NH and HBHA(CO)NH spectra. The program SSP was used to analyze the secondary structure propensities based on the assigned Cα and Cβ chemical shifts (30).

Samples for assignment of H2B contained 500 μM H2A-$[U\text{-}^2H/^{13}C/^{15}N]$H2B in NMR assignment buffer (20 mM NaPi, pH 6.5, 50 mM NaCl, 5% D_2O, 0.02% NaN_3, 1x PIC). Backbone assignments were based on TROSY-based HNCACB, HN(CO)CACB, HNCA, HN(CO)CA, HNCB, HN(CO)CB, HNCO, and HN(CA)CO spectra, recorded at 900 MHz ^1H Larmor frequency at 308 K. Assignment of H2B backbone resonances was 94.1% complete. Assignments were transferred to assay conditions through a buffer titration. Assignment of H2A (96.1% complete) will be reported elsewhere (manuscript in preparation).

NMR titration of $[^{15}N]APLF^{FAD}$ with H2A-H2B was done at 900 MHz ^1H Larmor frequency at 308 K using sample containing 200 μM (at start) $[^{15}N]APLF^{FAD}$ in NMR titration buffer (25 mM NaPi, pH 7, 300 mM NaCl, 5% D_2O, 0.02% NaN_3, 1x PIC). ^1H-^{15}N TROSY spectra were measured for the free $APLF^{FAD}$ and after each addition of unlabeled H2A-H2B (12 points from 1:0 to 1:4 $APLF^{FAD}$:H2A-H2B).

H2A-H2B refolded with either ^{15}N-labeled H2A or $[^2H/^{13}C/^{15}N]$-labeled H2B was used at a concentration of 200 μM (at start) for NMR titration experiments with unlabeled $APLF^{FAD}$. Both $APLF^{FAD}$ and H2A-H2B samples were buffer exchanged to NMR titration buffer (as above). ^1H-^{15}N TROSY spectra were measured for the free H2A-H2B and after each addition of $APLF^{FAD}$ at 308 K. The two titrations consisted of 8 (12) points in the range of 1:0 and 1:1 (1:4)

molar ratio (H2A-H2B:APLF^{FAD}) on a 850 (750) MHz spectrometer with H2A(H2B)-labeled H2A-H2B.
Reported peak intensity ratios are corrected for differences in protein concentration (due to dilution) and number of scans. Residue-specific chemical shift perturbations (CSPs) were quantified from the perturbations in the ^{1}H ($\Delta\delta_H$) and ^{15}N ($\Delta\delta_N$) dimensions as the weighted average (composite) CSP in ppm:

$$CSP = \sqrt{\Delta\delta_H{}^2 + (\Delta\delta_N/6.51)^2}$$

2D NMR LINESHAPE ANALYSIS

2D NMR lineshape analysis of the H2A-[^{15}N]H2B NMR titration with APLF^{FAD} was done using the program TITAN (31). The experimental data were fit using a sequential-binding model. Fitting was done in three steps: (*i*) using residues that reported only on the high affinity interaction (A35, Y37, I38, K40, T49, G50, A55, I58, and N60) the parameters $K_{D,1}$, $k_{off,1}$, and n_1 of the high affinity binding event were determined using a simple 1:1 binding model with flexible binding stoichiometry; (*ii*) keeping these parameters fixed, data from residues that reported primarily on the second interaction (R89, V95, E102, H106, S109, G111, K113, K117, and S120) were fit to a sequential-binding model to extract the parameters $K_{D,2}$ and $k_{off,2}$ of the low-affinity binding event whilst fixing n_2 to 1; (*iii*) in the final step the thus obtained global parameters were kept fixed and the data for resonances with kinked trajectories that report on both binding events, such as S52 and T119 (see Figure 6C,D), were fit by optimizing the chemical shifts and line widths for the free and the two bound states. Error estimates for the fit-parameters were obtained using the bootstrap resampling of residuals procedure implemented in TITAN.

CHAPERONE ASSAY

A high-copy number plasmid containing 12 tandem repeats of a 167 base pair strong positioning DNA sequence (Widom's 601; (32,33)) was transformed into DH5α cells. The plasmid was purified using a Qiagen Plasmid Giga Kit. The 167-bp fragment was released from the vector by ScaI digestion and purified by anion exchange.
The ratio of H2A-H2B to DNA that caused complete precipitation was determined experimentally at a ratio of 15 molar equivalents of histone dimer to DNA (Figure S4A). Controls containing assay buffer or WT or mutant APLF^{FAD} at the concentration corresponding to the highest titration point of the assay were also carried out with DNA alone (Figure S4A). For the assay, histone dimer (final reaction concentration: 15 μM) was preincubated alone or with 1, 3 or 6 molar equivalents of APLF^{FAD} wildtype (WT) or its mutants. Binding of chaperone to histone was allowed to proceed at 37 °C for 15 min before the addition of DNA to a final concentration of 1 μM in a total reaction volume of 20 μL. Precipitation was carried out at 37 °C for 15 min before the addition of 5 μL native PAGE loading buffer (10 mM Tris-HCl, pH 7.5, 1 mM EDTA, 1 mM DTT, 0.1 mM PMSF, 0.1 mg/ml BSA, 25% sucrose, 0.1% bromophenol blue), removal of precipitates by centrifugation, and separation of the remaining soluble complexes on a 5% polyacrylamide gel run in 0.2 × TBE (17.8 mM Tris, 17.8 mM boric

acid, 0.4 mM EDTA) buffer at 4 °C. The gels were stained with DNA stain G (SERVA) before visualization using a Molecular Imager Gel Doc XR System (Bio-Rad). The histone dimer-APLF^{FAD} reaction mixes were analyzed by Tris-Tricine SDS-PAGE followed by coomassie staining as control of the integrity of the proteins and protein concentrations (Figure S4B).

Structural modeling

A structural model for APLF (residues 471-490) was built using the H2A.Z-H2B bound state of YL1 (residues 39-59, PDB ID 5CHL (34)) as template in the program MODELLER (http://salilab.org/modeller/; last accessed: May 17, 2018) (35). The sequences were aligned as in Figure 7A. This structure was used as input for docking to the H2A-H2B dimer using the program HADDOCK (36). Structure of the H2A-H2B dimer was taken from the *Dm.* nucleosome, PDB ID 2PYO (37). Docking was driven using unambiguous distance restraints to impose the cap-anchor interaction with the H2B chaperone region. These restraints were defined between side chain heavy atoms of E473/Y476 and heavy atoms of H2B Y39, I51, S52, K54 and M56 as average distance observed in the structures of histone chaperones Anp32E, Spt16, and YL1 bound to H2A(.Z)-H2B (PDB ID 4CAY, 4WNN, 5CHL (34,38,39)). No active or passive residues were defined, otherwise the default HADDOCK protocol was followed. Out of the 200 final water-refined structures, all but one clustered in a single cluster. The structure with lowest HADDOCK score was used for display. Validation statistics are reported in Table S1.

References

1. MacAlpine, D.M. and Almouzni, G. (2013) Chromatin and DNA replication. *Cold Spring Harb Perspect Biol*, **5**, a010207.
2. Li, B., Carey, M. and Workman, J.L. (2007) The role of chromatin during transcription. *Cell*, **128**, 707-719.
3. Papamichos-Chronakis, M. and Peterson, C.L. (2013) Chromatin and the genome integrity network. *Nat Rev Genet*, **14**, 62-75.
4. Luger, K., Mader, A.W., Richmond, R.K., Sargent, D.F. and Richmond, T.J. (1997) Crystal structure of the nucleosome core particle at 2.8 A resolution. *Nature*, **389**, 251-260.
5. Hammond, C.M., Stromme, C.B., Huang, H., Patel, D.J. and Groth, A. (2017) Histone chaperone networks shaping chromatin function. *Nat Rev Mol Cell Biol*, **18**, 141-158.
6. Mattiroli, F., D'Arcy, S. and Luger, K. (2015) The right place at the right time: chaperoning core histone variants. *EMBO Rep*, **16**, 1454-1466.
7. Bekker-Jensen, S., Fugger, K., Danielsen, J.R., Gromova, I., Sehested, M., Celis, J., Bartek, J., Lukas, J. and Mailand, N. (2007) Human Xip1 (C2orf13) is a novel regulator of cellular responses to DNA strand breaks. *J Biol Chem*, **282**, 19638-19643.
8. Iles, N., Rulten, S., El-Khamisy, S.F. and Caldecott, K.W. (2007) APLF (C2orf13) is a novel human protein involved in the cellular response to chromosomal DNA strand breaks. *Mol Cell Biol*, **27**, 3793-3803.
9. Macrae, C.J., McCulloch, R.D., Ylanko, J., Durocher, D. and Koch, C.A. (2008) APLF (C2orf13) facilitates nonhomologous end-joining and undergoes ATM-dependent hyperphosphorylation following ionizing radiation. *DNA Repair (Amst)*, **7**, 292-302.
10. Williams, G.J., Hammel, M., Radhakrishnan, S.K., Ramsden, D., Lees-Miller, S.P. and Tainer, J.A. (2014) Structural insights into NHEJ: building up an integrated picture of the dynamic DSB repair super complex, one component and interaction at a time. *DNA Repair (Amst)*, **17**, 110-120.
11. Radhakrishnan, S.K., Jette, N. and Lees-Miller, S.P. (2014) Non-homologous end joining: emerging themes and unanswered questions. *DNA Repair (Amst)*, **17**, 2-8.

12. Grundy, G.J., Rulten, S.L., Zeng, Z., Arribas-Bosacoma, R., Iles, N., Manley, K., Oliver, A. and Caldecott, K.W. (2013) APLF promotes the assembly and activity of non-homologous end joining protein complexes. *EMBO J*, **32**, 112-125.
13. Hammel, M., Yu, Y., Radhakrishnan, S.K., Chokshi, C., Tsai, M.S., Matsumoto, Y., Kuzdovich, M., Remesh, S.G., Fang, S., Tomkinson, A.E. *et al.* (2016) An Intrinsically Disordered APLF Links Ku, DNA-PKcs, and XRCC4-DNA Ligase IV in an Extended Flexible Non-homologous End Joining Complex. *J Biol Chem*, **291**, 26987-27006.
14. Rulten, S.L., Fisher, A.E., Robert, I., Zuma, M.C., Rouleau, M., Ju, L., Poirier, G., Reina-San-Martin, B. and Caldecott, K.W. (2011) PARP-3 and APLF function together to accelerate nonhomologous end-joining. *Mol Cell*, **41**, 33-45.
15. Ali, A.A., Jukes, R.M., Pearl, L.H. and Oliver, A.W. (2009) Specific recognition of a multiply phosphorylated motif in the DNA repair scaffold XRCC1 by the FHA domain of human PNK. *Nucleic Acids Res*, **37**, 1701-1712.
16. Fenton, A.L., Shirodkar, P., Macrae, C.J., Meng, L. and Koch, C.A. (2013) The PARP3- and ATM-dependent phosphorylation of APLF facilitates DNA double-strand break repair. *Nucleic Acids Res*, **41**, 4080-4092.
17. Shirodkar, P., Fenton, A.L., Meng, L. and Koch, C.A. (2013) Identification and functional characterization of a Ku-binding motif in aprataxin polynucleotide kinase/phosphatase-like factor (APLF). *J Biol Chem*, **288**, 19604-19613.
18. Rulten, S.L., Cortes-Ledesma, F., Guo, L., Iles, N.J. and Caldecott, K.W. (2008) APLF (C2orf13) is a novel component of poly(ADP-ribose) signaling in mammalian cells. *Mol Cell Biol*, **28**, 4620-4628.
19. Eustermann, S., Brockmann, C., Mehrotra, P.V., Yang, J.C., Loakes, D., West, S.C., Ahel, I. and Neuhaus, D. (2010) Solution structures of the two PBZ domains from human APLF and their interaction with poly(ADP-ribose). *Nat Struct Mol Biol*, **17**, 241-243.
20. Li, G.Y., McCulloch, R.D., Fenton, A.L., Cheung, M., Meng, L., Ikura, M. and Koch, C.A. (2010) Structure and identification of ADP-ribose recognition motifs of APLF and role in the DNA damage response. *Proc Natl Acad Sci U S A*, **107**, 9129-9134.
21. Ahel, I., Ahel, D., Matsusaka, T., Clark, A.J., Pines, J., Boulton, S.J. and West, S.C. (2008) Poly(ADP-ribose)-binding zinc finger motifs in DNA repair/checkpoint proteins. *Nature*, **451**, 81-85.
22. Wei, H. and Yu, X. (2016) Functions of PARylation in DNA Damage Repair Pathways. *Genomics Proteomics Bioinformatics*, **14**, 131-139.
23. Palazzo, L., Mikoc, A. and Ahel, I. (2017) ADP-ribosylation: new facets of an ancient modification. *FEBS J*.
24. Mehrotra, P.V., Ahel, D., Ryan, D.P., Weston, R., Wiechens, N., Kraehenbuehl, R., Owen-Hughes, T. and Ahel, I. (2011) DNA repair factor APLF is a histone chaperone. *Mol Cell*, **41**, 46-55.
25. de Jong, R.N., Daniels, M.A., Kaptein, R. and Folkers, G.E. (2006) Enzyme free cloning for high throughput gene cloning and expression. *J Struct Funct Genomics*, **7**, 109-118.
26. Luger, K., Rechsteiner, T.J. and Richmond, T.J. (1999) Preparation of nucleosome core particle from recombinant histones. *Methods Enzymol*, **304**, 3-19.
27. Corbeski, I., Horn, V., van der Valk, R.A., le Paige, U.B., Dame, R.T. and van Ingen, H. (2018) Microscale Thermophoresis Analysis of Chromatin Interactions. *Methods Mol Biol*, **1837**, 177-197.
28. Delaglio, F., Grzesiek, S., Vuister, G.W., Zhu, G., Pfeifer, J. and Bax, A. (1995) NMRPipe: a multidimensional spectral processing system based on UNIX pipes. *J Biomol NMR*, **6**, 277-293.
29. Lee, W., Tonelli, M. and Markley, J.L. (2015) NMRFAM-SPARKY: enhanced software for biomolecular NMR spectroscopy. *Bioinformatics*, **31**, 1325-1327.
30. Marsh, J.A., Singh, V.K., Jia, Z. and Forman-Kay, J.D. (2006) Sensitivity of secondary structure propensities to sequence differences between alpha- and gamma-synuclein: implications for fibrillation. *Protein Sci*, **15**, 2795-2804.
31. Waudby, C.A., Ramos, A., Cabrita, L.D. and Christodoulou, J. (2016) Two-Dimensional NMR Lineshape Analysis. *Sci Rep*, **6**, 24826.
32. Thastrom, A., Bingham, L.M. and Widom, J. (2004) Nucleosomal locations of dominant DNA sequence motifs for histone-DNA interactions and nucleosome positioning. *J Mol Biol*, **338**, 695-709.
33. Lowary, P.T. and Widom, J. (1998) New DNA sequence rules for high affinity binding to histone octamer and sequence-directed nucleosome positioning. *J Mol Biol*, **276**, 19-42.
34. Liang, X., Shan, S., Pan, L., Zhao, J., Ranjan, A., Wang, F., Zhang, Z., Huang, Y., Feng, H., Wei, D. *et al.* (2016) Structural basis of H2A.Z recognition by SRCAP chromatin-remodeling subunit YL1. *Nat Struct Mol Biol*, **23**, 317-323.
35. Webb, B. and Sali, A. (2016) Comparative Protein Structure Modeling Using MODELLER. *Curr Protoc Protein Sci*, **86**, 2 9 1-2 9 37.
36. van Zundert, G.C., Rodrigues, J.P., Trellet, M., Schmitz, C., Kastritis, P.L., Karaca, E., Melquiond, A.S., van Dijk, M., de Vries, S.J. and Bonvin, A.M. (2016) The HADDOCK2.2 Web Server: User-Friendly Integrative Modeling of Biomolecular Complexes. *J Mol Biol*, **428**, 720-725.

37. Clapier, C.R., Chakravarthy, S., Petosa, C., Fernandez-Tornero, C., Luger, K. and Muller, C.W. (2008) Structure of the Drosophila nucleosome core particle highlights evolutionary constraints on the H2A-H2B histone dimer. *Proteins*, **71**, 1-7.
38. Obri, A., Ouararhni, K., Papin, C., Diebold, M.L., Padmanabhan, K., Marek, M., Stoll, I., Roy, L., Reilly, P.T., Mak, T.W. *et al.* (2014) ANP32E is a histone chaperone that removes H2A.Z from chromatin. *Nature*, **505**, 648-653.
39. Kemble, D.J., McCullough, L.L., Whitby, F.G., Formosa, T. and Hill, C.P. (2015) FACT Disrupts Nucleosome Structure by Binding H2A-H2B with Conserved Peptide Motifs. *Mol Cell*, **60**, 294-306.
40. Hong, J., Feng, H., Wang, F., Ranjan, A., Chen, J., Jiang, J., Ghirlando, R., Xiao, T.S., Wu, C. and Bai, Y. (2014) The catalytic subunit of the SWR1 remodeler is a histone chaperone for the H2A.Z-H2B dimer. *Mol Cell*, **53**, 498-505.
41. Latrick, C.M., Marek, M., Ouararhni, K., Papin, C., Stoll, I., Ignatyeva, M., Obri, A., Ennifar, E., Dimitrov, S., Romier, C. *et al.* (2016) Molecular basis and specificity of H2A.Z-H2B recognition and deposition by the histone chaperone YL1. *Nat Struct Mol Biol*, **23**, 309-316.
42. Ohtomo, H., Akashi, S., Moriwaki, Y., Okuwaki, M., Osakabe, A., Nagata, K., Kurumizaka, H. and Nishimura, Y. (2016) C-terminal acidic domain of histone chaperone human NAP1 is an efficient binding assistant for histone H2A-H2B, but not H3-H4. *Genes Cells*, **21**, 252-263.
43. Romero, P., Obradovic, Z., Li, X., Garner, E.C., Brown, C.J. and Dunker, A.K. (2001) Sequence complexity of disordered protein. *Proteins*, **42**, 38-48.
44. Coeytaux, K. and Poupon, A. (2005) Prediction of unfolded segments in a protein sequence based on amino acid composition. *Bioinformatics*, **21**, 1891-1900.
45. Oldfield, C.J. and Dunker, A.K. (2014) Intrinsically disordered proteins and intrinsically disordered protein regions. *Annu Rev Biochem*, **83**, 553-584.
46. Wright, P.E. and Dyson, H.J. (2015) Intrinsically disordered proteins in cellular signalling and regulation. *Nat Rev Mol Cell Biol*, **16**, 18-29.
47. D'Arcy, S., Martin, K.W., Panchenko, T., Chen, X., Bergeron, S., Stargell, L.A., Black, B.E. and Luger, K. (2013) Chaperone Nap1 shields histone surfaces used in a nucleosome and can put H2A-H2B in an unconventional tetrameric form. *Mol Cell*, **51**, 662-677.
48. Zhou, Z., Feng, H., Hansen, D.F., Kato, H., Luk, E., Freedberg, D.I., Kay, L.E., Wu, C. and Bai, Y. (2008) NMR structure of chaperone Chz1 complexed with histones H2A.Z-H2B. *Nat Struct Mol Biol*, **15**, 868-869.
49. Chantalat, L., Nicholson, J.M., Lambert, S.J., Reid, A.J., Donovan, M.J., Reynolds, C.D., Wood, C.M. and Baldwin, J.P. (2003) Structure of the histone-core octamer in KCl/phosphate crystals at 2.15 A resolution. *Acta Crystallogr D Biol Crystallogr*, **59**, 1395-1407.
50. Moriwaki, Y., Yamane, T., Ohtomo, H., Ikeguchi, M., Kurita, J., Sato, M., Nagadoi, A., Shimojo, H. and Nishimura, Y. (2016) Solution structure of the isolated histone H2A-H2B heterodimer. *Sci Rep*, **6**, 24999.
51. Andrews, A.J., Chen, X., Zevin, A., Stargell, L.A. and Luger, K. (2010) The histone chaperone Nap1 promotes nucleosome assembly by eliminating nonnucleosomal histone DNA interactions. *Mol Cell*, **37**, 834-842.
52. Laskey, R.A., Honda, B.M., Mills, A.D. and Finch, J.T. (1978) Nucleosomes are assembled by an acidic protein which binds histones and transfers them to DNA. *Nature*, **275**, 416-420.
53. Hondele, M., Stuwe, T., Hassler, M., Halbach, F., Bowman, A., Zhang, E.T., Nijmeijer, B., Kotthoff, C., Rybin, V., Amlacher, S. *et al.* (2013) Structural basis of histone H2A-H2B recognition by the essential chaperone FACT. *Nature*, **499**, 111-114.
54. Liu, Z. and Huang, Y. (2014) Advantages of proteins being disordered. *Protein Sci*, **23**, 539-550.
55. Berlow, R.B., Dyson, H.J. and Wright, P.E. (2015) Functional advantages of dynamic protein disorder. *FEBS Lett*, **589**, 2433-2440.
56. Andrews, A.J., Downing, G., Brown, K., Park, Y.J. and Luger, K. (2008) A thermodynamic model for Nap1-histone interactions. *J Biol Chem*, **283**, 32412-32418.
57. Timinszky, G., Till, S., Hassa, P.O., Hothorn, M., Kustatscher, G., Nijmeijer, B., Colombelli, J., Altmeyer, M., Stelzer, E.H., Scheffzek, K. *et al.* (2009) A macrodomain-containing histone rearranges chromatin upon sensing PARP1 activation. *Nat Struct Mol Biol*, **16**, 923-929.
58. Hammel, M., Yu, Y., Fang, S., Lees-Miller, S.P. and Tainer, J.A. (2010) XLF regulates filament architecture of the XRCC4.ligase IV complex. *Structure*, **18**, 1431-1442.
59. Hammel, M., Rey, M., Yu, Y., Mani, R.S., Classen, S., Liu, M., Pique, M.E., Fang, S., Mahaney, B.L., Weinfeld, M. *et al.* (2011) XRCC4 protein interactions with XRCC4-like factor (XLF) create an extended grooved scaffold for DNA ligation and double strand break repair. *J Biol Chem*, **286**, 32638-32650.
60. Reid, D.A., Keegan, S., Leo-Macias, A., Watanabe, G., Strande, N.T., Chang, H.H., Oksuz, B.A., Fenyo, D., Lieber, M.R., Ramsden, D.A. *et al.* (2015) Organization and dynamics of the nonhomologous end-joining machinery during DNA double-strand break repair. *Proc Natl Acad Sci U S A*, **112**, E2575-2584.

SUPPORTING INFORMATION

Table S1. Structural quality of the APLF^{HBD}-H2A-H2B model[a].

	APLF^{HBD}	APLF^{HBD}-H2A-H2B
Ramachandran plot[b]	93/7/0/0 (77/23/0/0)	92/6/2/0 (92/7/2/0)
Number of clashes[c]	1 (3)	4[d] (9[d])

[a] Scores and statistics are reported for only the APLF^{HBD} chain and the full model for the lowest energy HADDOCK structure. Statistics for the top four structures are given between brackets.
[b] Percentage core/allowed/generously allowed/outliers, as reported by PROCHECK (1).
[c] Number of clashes > 0.4 Å, reported by MolProbity webserver (2).
[d] Intermolecular clashes only.

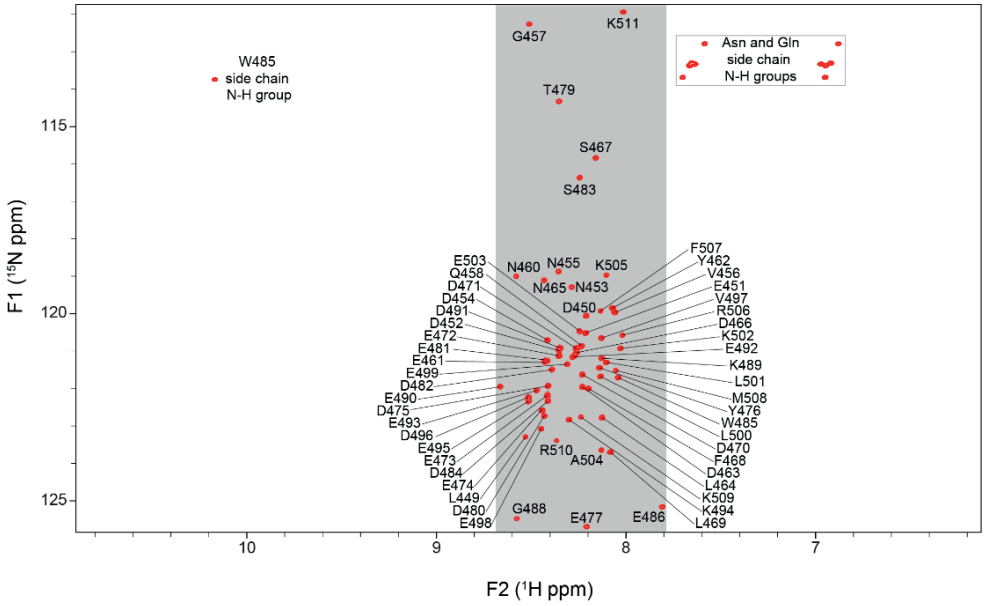

Figure S1. ^{1}H-^{15}N HSQC spectrum of APLF^{AD} showing all backbone and side chain amide resonances with their assignments. Spectrum recorded at 22 °C, 25 mM NaPi, pH 6.6, 300 mM NaCl, 900 MHz ^{1}H Larmor frequency. Assignments of the main-chain amide resonances are indicated by the single-letter amino acid code and residue number, asparagine/glutamine side chain amine resonances and side chain indole resonance of W485 are indicated. In total, 60 out of a possible 62 (^{1}H, ^{15}N) backbone cross-peaks are resolved with only the N-terminal 2 residues from the thrombin-cleavage site missing. All resolved backbone cross-peaks are in the spectral region indicated in gray.

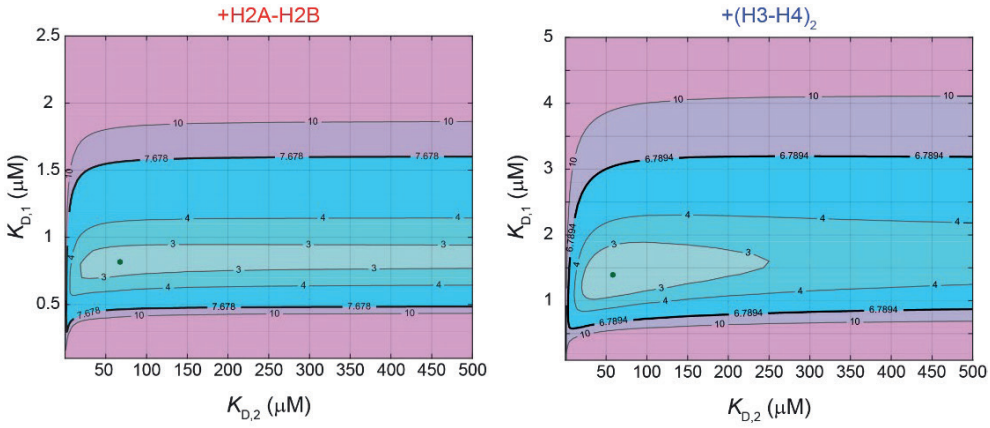

Figure S2. Error estimation in best-fit K_D values obtained from MST. MST-derived binding curves were fit to a sequential-binding model and quality of the fit was evaluated using the reduced χ^2. The plots show the reduced χ^2-surface in contour-mode as function of the high-affinity ($K_{D,1}$) and the low-affinity ($K_{D,2}$) dissociation constants for H2A-H2B (left) and $(H3\text{-}H4)_2$ (right) binding to $APLF^{FAD}$. The best-fit values are indicated by a green dot (H2A-H2B: 0.8/68 μM $K_{D,1}/K_{D,2}$ with reduced χ^2 2.7; H3-H4: 1.4/58 μM $K_{D,1}/K_{D,2}$ with reduced χ^2 2.4). The 95% confidence critical value of the reduced χ^2 is indicated with a thick black line.

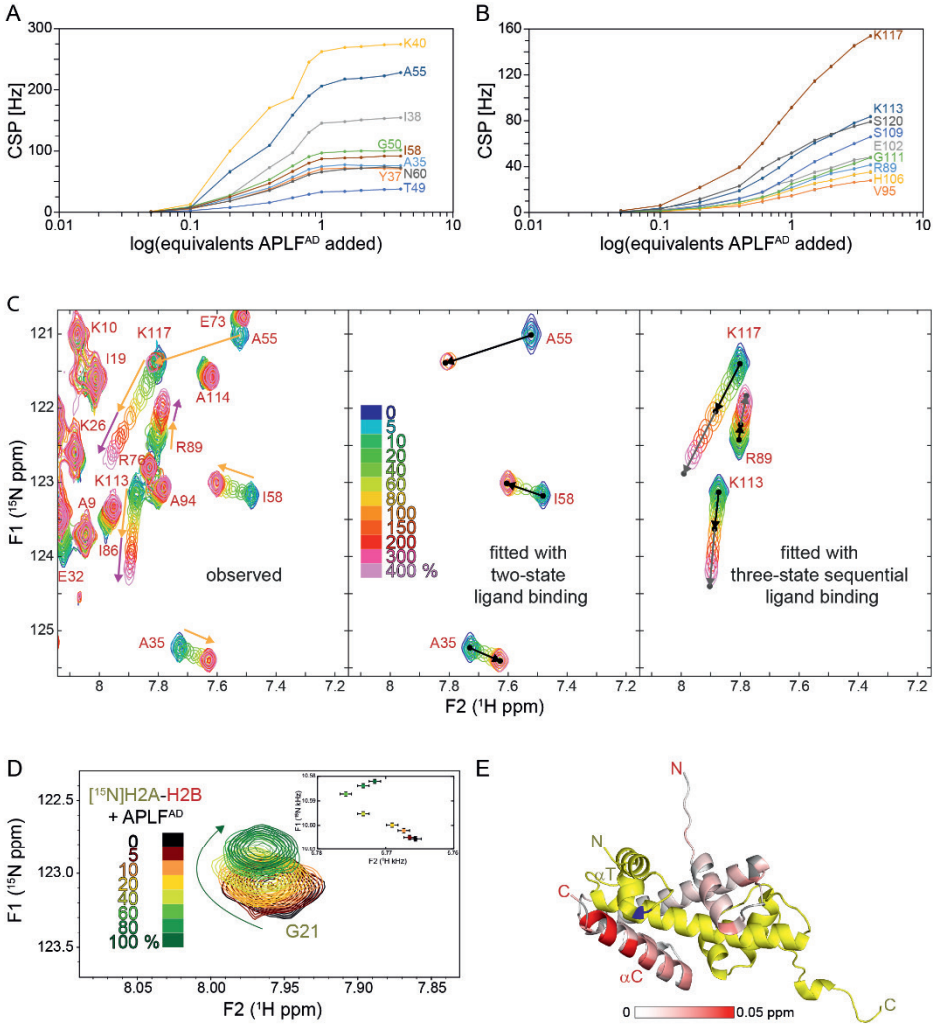

Figure S3. Confirmation of secondary binding to H2A-H2B. (A,B) CSP of H2B resonances selected for two-dimensional NMR lineshape analysis of the high (A) and the low (B) affinity binding site plotted against equivalents of APLF^{FAD} added. (C) Observed and fitted 2D NMR lineshapes for binding analysis. Zoomed region of overlaid ^{1}H-^{15}N TROSY spectra of H2A-[^{15}N]H2B (left panel) with increasing concentrations of APLF^{FAD}. Data recorded at 750 MHz ^{1}H Larmor frequency in 25 mM NaPi buffer, pH 7.0 with 300 mM NaCl, 35 °C. Peak shifts of selected resonances up to one (four) equivalents added are indicated with orange (pink) arrows. Results of two-dimensional lineshape analysis of the high (middle panel) and the low (right panel) affinity binding site for the titration of H2A-[^{15}N]H2B with APLF^{FAD}. The chemical shifts of free and 1st (2nd) bound states determined by the fitting procedure are marked by the black (gray) dots. The black (gray) arrows indicate the displacements for the high (low) affinity interactions. Color coding of spectra is indicated in the figure. (D) Zoomed H2A G21 region (note: peak is aliased) of overlaid ^{1}H-^{15}N TROSY spectra from the [^{15}N]H2A-H2B titration with APLF^{FAD} (see Figure 5). Color coding of spectra is indicated in the figure. Data recorded at 850 MHz ^{1}H Larmor frequency in 25 mM NaPi buffer, pH 7.0 with 300 mM NaCl, 35 °C. Direction and curvature of the peak shift is indicated with a green arrow. Inset: Plot showing the peak displacement of H2A G21; black bars – standard deviation. (E) Residue H2A G21 (blue) is located close to the H2B αC-helix. Observed CSPs from the titration of H2A-[^{15}N]H2B between one and four molar equivalents of APLF^{FAD} added color coded on the cartoon representation of H2A-H2B (PDB ID 2PYO; yellow – H2A; gray – residues without titration data) with labeling of relevant secondary structure elements (see Figure 6).

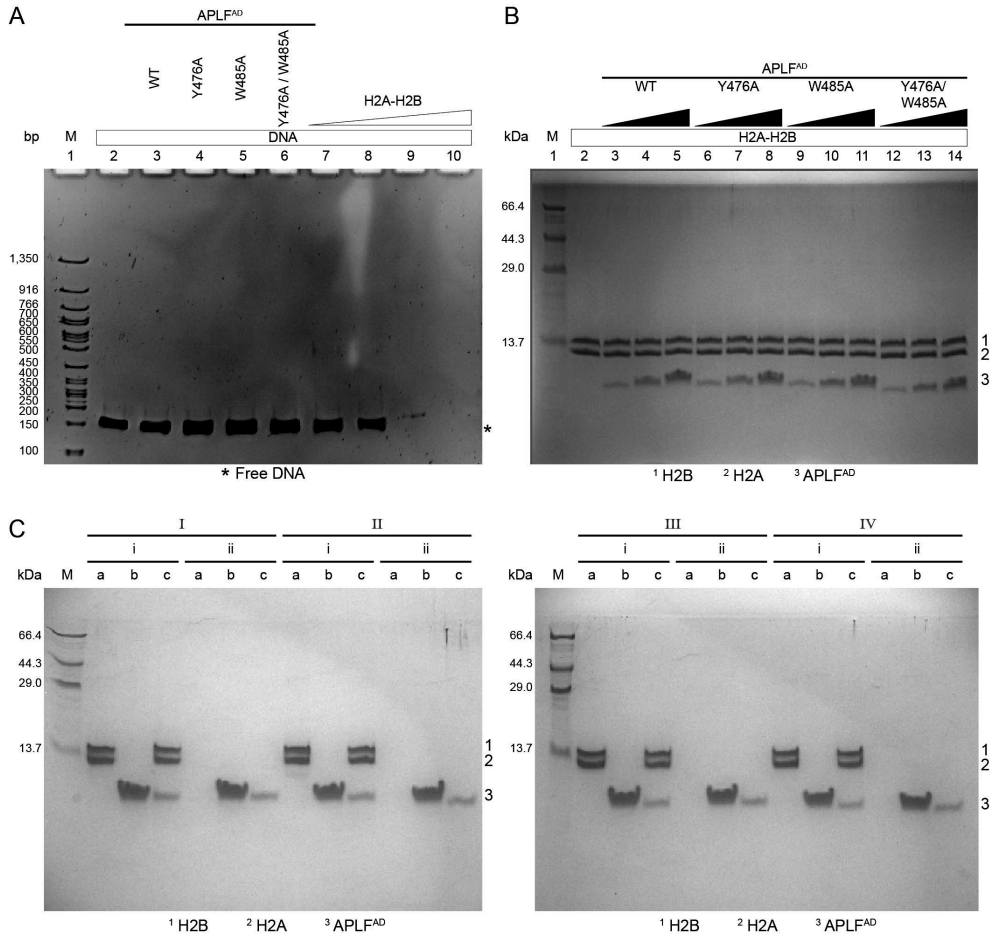

Figure S4. Quality control of chaperone assay and ITC experiments. (A) Native PAGE analysis of 167 base pair (bp) DNA (1 μM) with the 601 nucleosome positioning sequence in presence or absence of APLF^{AD} WT or mutants, and H2A-H2B. Lane 1: 50 bp DNA ladder (M). Lane 2: free DNA. Lanes 3-6: DNA upon addition of 90 μM APLF^{AD} WT and mutants, showing no effect. Lanes 7-10: DNA upon addition of 6, 9, 12, and 15 μM H2A-H2B, showing loss of free DNA due to precipitation. (B) Tris-Tricine SDS-PAGE analysis of protein mixes used in the chaperone assay (see Figure 8A). Lane 1: Protein molecular weight marker (M). Lane 2: H2A-H2B. Lanes 3-14: H2A-H2B with increasing concentrations (1, 3, and 6 molar equivalents) of APLF^{AD} WT, Y476A, W485A, and Y476A/ W485A. (C) Tris-Tricine SDS-PAGE analysis of protein mixes used in the ITC experiments of H2A-H2B with WT or mutant APLF^{AD} (see Figure 8B). I, II, III, and IV stand for the reactions with APLF^{AD} WT, Y476A, W485A, and Y476A/W485A, respectively. i and ii stand for the reactions of H2A-H2B with APLF^{AD} and control experiments without H2A-H2B, respectively. a, b, and c stand for the component in the cell, the syringe, and the reaction mixture at the end of the titration, respectively. M: Protein molecular weight marker.

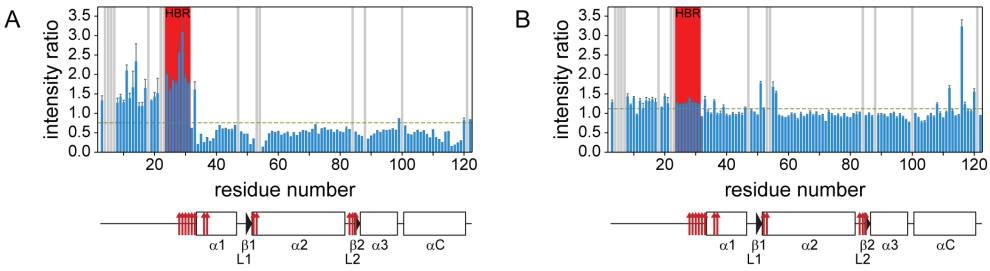

Figure S5. Primary APLF^{FAD} binding to H2A-H2B causes changes in H2B N-terminal tail. Recorded at 750 MHz ^{1}H Larmor frequency, 35 °C, 25 mM NaPi buffer, pH 7.0, 300 mM NaCl. Analysis of H2B ^{1}H-^{15}N peak intensity ratios between free H2A-H2B and after addition of one molar equivalent of APLF^{FAD} (A) or between one and four molar equivalents of APLF^{FAD} added (B). The 10% trimmed mean is indicated with a green dashed line. Secondary structure (SS) of H2B as in the nucleosome and residues interacting with nucleosomal DNA (PDB ID 2PYO) (3)) indicated below the plot (line = loop, rectangle = α-helix, triangle = β-strand, red arrows = DNA interaction sites) with naming of SS-elements as in Ref. (4). Position of H2B repression (HBR) domain indicated with a red bar (5,6). Residues without titration data due to overlap or missing resonances indicated with gray bars.

SUPPLEMENTARY REFERENCES

1. Laskowski, R.A., MacArthur, M.W., Moss, D.S. and Thornton, J.M. (1993) PROCHECK - a program to check the stereochemical quality of protein structures. *J Appl Cryst*, **26**, 283-291.
2. Davis, I.W., Leaver-Fay, A., Chen, V.B., Block, J.N., Kapral, G.J., Wang, X., Murray, L.W., Arendall, W.B., 3rd, Snoeyink, J., Richardson, J.S. *et al.* (2007) MolProbity: all-atom contacts and structure validation for proteins and nucleic acids. *Nucleic Acids Res*, **35**, W375-383.
3. Clapier, C.R., Chakravarthy, S., Petosa, C., Fernandez-Tornero, C., Luger, K. and Muller, C.W. (2008) Structure of the Drosophila nucleosome core particle highlights evolutionary constraints on the H2A-H2B histone dimer. *Proteins*, **71**, 1-7.
4. Chantalat, L., Nicholson, J.M., Lambert, S.J., Reid, A.J., Donovan, M.J., Reynolds, C.D., Wood, C.M. and Baldwin, J.P. (2003) Structure of the histone-core octamer in KCl/phosphate crystals at 2.15 A resolution. *Acta Crystallogr D Biol Crystallogr*, **59**, 1395-1407.
5. Parra, M.A., Kerr, D., Fahy, D., Pouchnik, D.J. and Wyrick, J.J. (2006) Deciphering the roles of the histone H2B N-terminal domain in genome-wide transcription. *Mol Cell Biol*, **26**, 3842-3852.
6. Mao, P., Kyriss, M.N., Hodges, A.J., Duan, M., Morris, R.T., Lavine, M.D., Topping, T.B., Gloss, L.M. and Wyrick, J.J. (2016) A basic domain in the histone H2B N-terminal tail is important for nucleosome assembly by FACT. *Nucleic Acids Res*, **44**, 9142-9152.


4

Chapter 4

A chaperone that assembles the histone octamer to promote its deposition onto DNA

Based on the manuscript: Corbeski, I.[1], Graewert, M.A.[2], Fasci, D.[3], Wiegant, W.[4], Vreeken, K.[4], Mattiroli, F.[5], Wienk, H.[1], Svergun, D.I.[2], Heck, A.J.R.[3], Van Attikum, H.[4], Boelens, R.[1], van Ingen, H.[1] (2019) A chaperone that assembles the histone octamer to promote its deposition onto DNA. *In preparation*.

[1] NMR Spectroscopy, Bijvoet Center for Biomolecular Research, Utrecht University, The Netherlands.

[2] European Molecular Biology Laboratory (EMBL), Hamburg Outstation, DESY, Hamburg, Germany.

[3] Biomolecular Mass Spectrometry and Proteomics, Bijvoet Center for Biomolecular Research and Utrecht Institute for Pharmaceutical Sciences, Utrecht University, The Netherlands.

[4] Department of Human Genetics, Leiden University Medical Center, The Netherlands.

[5] Hubrecht Institute, Utrecht, The Netherlands.

ABSTRACT

Genomic DNA forms chromatin with the nucleosome, consisting of a histone octamer that is encircled by 146 base pairs of double-stranded DNA, as repeating unit. The histone octamer consists of two copies of each histone H2A, H2B, H3 and H4. The mechanism of nucleosome assembly *in vivo* is unclear.

Here, we report a structural model based on an integrative approach of a histone chaperone-bound histone octamer. This complex, that we call the "chaperonosome", is capable of promoting histone deposition onto DNA through a mechanism that is dependent on aromatic residues in the chaperone. We show that two copies of the histone chaperone acidic domain of DNA repair factor APLF ($APLF^{AD}$), which is disordered free in solution, can bind the histone octamer to compete with major DNA interactions of the histones. $APLF^{AD}$ has two distinct binding sites specific for each of the histone dimers H2A-H2B and H3-H4, and both contain aromatic amino acid residues that bind to the α1-α2-patches of H2A, H2B, and H3 as the key determinants of the interaction and of histone chaperone function. Small-angle X-ray scattering of the complex formed by $APLF^{AD}$, H2A-H2B and H3-H4, in combination with biochemical and biophysical data, including nuclear magnetic resonance spectroscopy and mass spectrometry, support an underlying chaperone-mediated assembly of the histone octamer for its possible deposition mechanism onto DNA. These results provide insights for understanding the mechanism of nucleosome assembly.

INTRODUCTION

The replication, transcription, and repair of DNA are essential for cell division, growth, and genome stability (1-3). Molecular machineries have to access the DNA to perform their tasks and subsequently restore the chromatin state (4,5). These processes are dependent on the dynamics of the nucleosome, the repeating unit of chromatin, characterized by approximately 146 base pairs of DNA wrapped around a histone octamer of two H2A-H2B dimers and one $(H3\text{-}H4)_2$ tetramer (6). In its role as the principal packaging element of chromatin in eukaryotes, the nucleosome is the primary determinant of DNA accessibility.

Nucleosome assembly and disassembly are coordinated by histone binding proteins called histone chaperones (7-9). They prevent incorrect histone-DNA and promote nucleosomal interactions, mediate histone variant exchange, and store histone proteins (10-13). The common feature of histone chaperones is their shielding of histone surfaces that functionally interact with other histones and DNA in the nucleosome. An entire histone chaperone network supports histone dynamics across different cellular processes that depend on chromatin dynamics (14). Several structures of histone chaperones alone and in complex with histones have helped to elucidate the structural basis of histone chaperone specificity for the type of histone complex (H2A-H2B or H3-H4), the recognition of histone variant specific motifs, the binding of H3-H4 as dimer or tetramer, as well as histone transport (15). Many histone chaperones rely on intrinsically disordered and/or highly acidic domains for their chaperone function (16). In some cases it has been shown that such chaperones involve in fuzzy complexes that are primarily electrostatically driven (17,18). Yet, little is known about the individual steps and possible

intermediate complexes formed by which histones are exchanged between chaperones or deposited onto DNA. Furthermore, the mechanistic details and structural determinants of how histone chaperones promote the organized assembly of nucleosomes are unknown (19).

In the classical paradigm of their function, histone chaperones are thought to promote nucleosome assembly by maintaining a very low free histone pool to eliminate competing, nonnucleosomal histone-DNA interactions (20,21).

Histone chaperones regulate accessibility to the genome during the processes of DNA transcription, replication and repair (22,23). In DNA repair, the chaperones involved allow to incorporate histone variants to promote the process and to reassemble chromatin as signal for DNA damage checkpoint recovery (24-26). In non-homologous end joining (NHEJ) repair of DNA double-strand breaks, histones are evicted from DNA and the NHEJ machinery is assembled at the break site. The scaffold for this complex is the protein Aprataxin and Polynucleotide kinase Like Factor (APLF) (27-43). Its disordered C-terminal acidic domain ($APLF^{AD}$) harbors histone chaperone activity, and deletions of this chaperone domain have been shown to impair cell survival after DNA damage (44,45).

Here, we use a range of biochemical, biophysical and structural methods to show that $APLF^{AD}$ can simultaneously bind to H2A-H2B and H3-H4 and form stable complexes with histone octamers. We show by nuclear magnetic resonance spectroscopy and mutational analysis that $APLF^{AD}$ has distinct histone binding motifs for H2A-H2B and H3-H4, each containing two aromatic side chains that are crucial for binding and chaperone activity. Together with small-angle X-ray scattering and mass spectrometry studies, our findings strongly support a structural model of the histone octamer-$APLF^{AD}$ complex in which the aromatic side chains of $APLF^{AD}$ anchor simultaneously to the α1-α2-patches of the helical histone fold of H2A, H2B, and H3 in the histone octamer which are key histone interaction sites for DNA in the nucleosome. $APLF^{AD}$ assembles the histones in their octameric organization as in the nucleosome. Hence, we call the $APLF^{AD}$-bound histone octamer complex the "chaperonosome".

$APLF^{AD}$ interferes with DNA binding to the histone octamer and promotes histone deposition onto DNA in a chaperone assay. This supports a function of $APLF^{AD}$ as histone chaperone for the histone octamer. Our results support a new paradigm in which histone chaperones can promote nucleosome assembly by pre-assembling the histone octamer in its nucleosomal arrangement.

RESULTS

$APLF^{AD}$ INTERACTS WITH THE HISTONE OCTAMER TO FORM A SPECIFIC HIGH-AFFINITY COMPLEX

We recently reported that $APLF^{AD}$ can bind H2A-H2B and H3-H4 with high affinity (45). This raises the possibility that $APLF^{AD}$ can also bind both histone complexes simultaneously. To test this, a stoichiometric mixture of H2A-H2B and H3-H4 corresponding

to the histone octamer (referred to here as a histone octamer mix) was incubated with $APLF^{FAD}$ and subjected to analytical gel filtration, isothermal titration calorimetry (ITC), and native mass spectrometry (MS). Analytical gel filtrations of mixtures of $APLF^{FAD}$ with either H2A-H2B or H3-H4 show formation of a higher molecular weight complex as expected (Figure 1A, upper and middle panel). While the histone octamer mix alone elutes as two separate species corresponding to H2A-H2B and $(H3\text{-}H4)_2$, one defined peak is obtained in the presence of $APLF^{FAD}$ with significantly increased apparent molecular weight than either H2A-H2B-$APLF^{FAD}$ or $(H3\text{-}H4)_2$-$APLF^{FAD}$ (Figure 1A, bottom panel). Careful titration experiments, monitored by analytical gel filtration, suggest that the complex includes two equivalents of $APLF^{FAD}$ per histone octamer (Supplementary Figure S1).

In order to firmly establish the composition of the complexes and the stoichiometry of the constituents involved, we subjected the various histone-$APLF^{FAD}$ complexes to native MS. $APLF^{FAD}$ binds to H2A-H2B to form a 35 kDa H2A-H2B-$APLF^{FAD}$ complex and to $(H3\text{-}H4)_2$ to form a 69 kDa $(H3\text{-}H4)_2$-$(APLF^{FAD})_2$ complex (Figure 1B, (i) and (ii)). Interestingly, the minor fraction of free H3-H4 is detected as $(H3\text{-}H4)_2$ tetramers whereas H3-H4 alone appears exclusively as dimers under the native MS conditions (Supplementary Figure S2) (46). Whereas the histone octamer is not detected in native MS in the absence of chaperone, in the presence of $APLF^{FAD}$ several high molecular weight complexes are obtained (Supplementary Figure S2). Titration of $APLF^{FAD}$ to the histone octamer mix shows that the minimal size of this complex corresponds to histone octamer-$(APLF^{FAD})_2$ (Figure 1B, (iii)), while at higher $APLF^{FAD}$:histone octamer ratios up to four copies of $APLF^{FAD}$ are bound through an interaction that as stable at varying ionic strengths in the native MS samples (Supplementary Figures S2-S4).

In order to confirm the stoichiometry and determine thermodynamic parameters of binding, we investigated the interaction between $APLF^{FAD}$ and the histone octamer mix by ITC and compared it with its binding to either H2A-H2B or H3-H4 (Figure 1C,D). $APLF^{FAD}$ binds the histone octamer with a K_D of 150 nM to form an enthalpically favorable but entropically unfavorable complex. The isolated H2A-H2B or H3-H4 complexes are bound with slightly lower affinities, corresponding to K_D values of 250 nM and 550 nM for H2A-H2B and H3-H4, respectively. These values are consistent with our previous investigation (45), except for a slightly lower K_D for H3-H4 which we ascribe to a lower protein concentration used here (Supplementary Figure S5). The enthalpy of binding of $APLF^{FAD}$ to the histone octamer is more than twice the combined binding enthalpies for H2A-H2B and H3-H4, suggesting that new histone-histone contacts are formed when bound by $APLF^{FAD}$ (Figure 1D and Supplementary Figure S6). This synergistic binding effect is accompanied by a strong entropic loss from the combination of at least five individual subunits forming one complex.

The number of $APLF^{FAD}$ binding sites on H2A-H2B and $(H3\text{-}H4)_2$ is ~1 and ~2, respectively, which is consistent with one $APLF^{FAD}$ binding to one H2A-H2B or H3-H4 dimer (Figure 1D). For the histone octamer, the stoichiometry of binding is ~2:1 $APLF^{FAD}$:octamer. These data are consistent with the results obtained from native MS. Evidence for higher order complexes cannot be retrieved from the ITC curves, although their presence may be masked by the major high-affinity and high-enthalpy interactions. Overall, analytical gel filtration, native MS and ITC data consistently demonstrate that $APLF^{FAD}$ can bind all four histones simultaneously to form a stable and high-affinity complex.

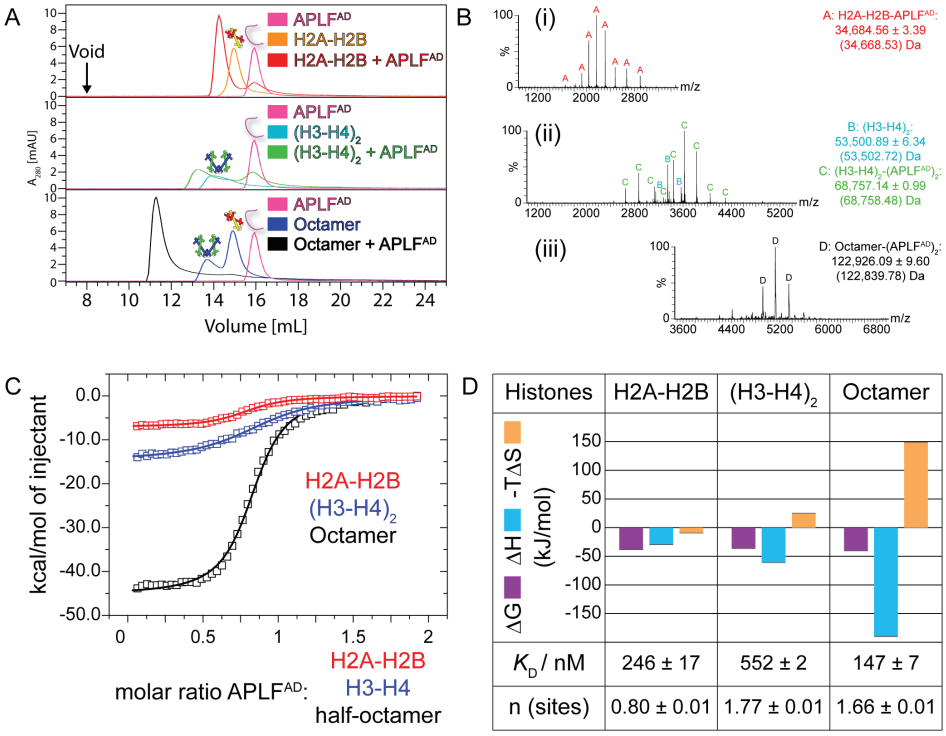

Figure 1. APLF^{AD} can bind all four histones simultaneously to form a stable and high-affinity complex. (A) Analytical gel filtration assay of histone complexes in absence and presence of APLF^{AD}. (B) Native mass spectra of the histone-APLF^{AD} complexes. The relative signal intensity (RSI) is plotted against the mass-to-charge ratio (m/z) with peak annotation and experimental (theoretical in brackets) molecular weights of the identified species. (C) ITC of APLF^{AD} to H2A-H2B, H3-H4 or histone octamer mix at 25 °C. The resulting binding isotherms were fit to a one-set-of-sites binding mode. (D) ITC derived best-fit values and fitting errors are shown in the table, the derived thermodynamic parameters in the histogram. Experiments were performed in 25 mM NaPi, pH 7.0, 300 mM NaCl.

H3-H4 BINDS TO A SECOND DOUBLE-AROMATIC ANCHOR MOTIF IN APLF^{AD}

Both ITC and native MS analysis show that one APLF^{AD} binds per H2A-H2B or H3-H4 dimer, yet, two APLF^{AD} bind the octamer which corresponds to 0.5 APLF^{AD} per histone dimer. This can be reconciled with APLF^{AD} binding H2A-H2B and H3-H4 through distinct binding interfaces. Previously, we used nuclear magnetic resonance (NMR) spectroscopy to map the binding site for H2A-H2B within the histone binding domain (HBD) spanning residues 471-499 of APLF^{AD} (HBD$^{471-499}$) (45). To delineate also the APLF^{AD} binding interface for H3-H4, we titrated unlabeled H3-H4 to ^{15}N-labeled APLF^{AD} and monitored spectral changes by NMR spectroscopy (Figure 2A). This titration was conducted in 600 mM salt to reduce nonspecific interactions because we observed complete precipitation of the complex in a titration conducted in 300 mM salt (Supplementary Figure S7). Several APLF^{AD} backbone amide resonances show significant chemical shift perturbations (CSPs), indicating that these

residues are involved in binding and/or undergo structural changes upon binding, while other signals, such as of Y462 and F468, disappear already at low molar ratios of added H3-H4 (Figure 2A). The latter reflects a large chemical exchange-induced line broadening, even further aggravated by line broadening due to formation of a large 69 kDa complex (see Figure 1B). These effects, possibly in combination with residual exchange or conformational dynamics in the bound state, may cause the loss of the NMR signal intensities, as we also reported for the H2A-H2B binding of [^{15}N]APLF^{FAD} (45). The overall pattern of spectral changes is consistent with the sub-micromolar affinity of APLF^{FAD} for H3-H4 that we measured (see Figure 1D).

We mapped the H3-H4 binding site on APLF^{FAD} by comparing peak intensity ratios and CSPs from APLF^{FAD} spectra in its free state and after the addition of one molar equivalent of H3-H4 (Figure 2B). Resonances corresponding to a continuous stretch of residues N460-E474 completely disappear, indicating this region to be the core interaction site. In contrast, residues N-terminal and directly C-terminal to this region are mostly unaffected by the interaction. Resonances from the C-terminal helical element and KR-motif (residues 496-511) have low signal intensity combined with high CSPs indicating these are additionally involved in the interaction. Comparison of the NMR spectra of APLF^{FAD} in its free state and in complex with either H2A-H2B or H3-H4 confirms that different sets of APLF^{FAD} resonances are perturbed in the two complexes (Figure 2C). A plot of the APLF^{FAD} peak intensity ratios between the H2A-H2B or H3-H4 bound and the free state of APLF^{FAD} shows that the primary H3-H4 binding region is N-terminal and directly adjacent with only partial overlap to the previously defined HBD$^{471-499}$, namely residues 460-474 (Figure 2D). Interestingly, the NMR signal of W485, which was previously shown by us to be important for H2A-H2B binding and chaperone activity (45), and by others to be important for the interaction with H3-H4 (44), is not strongly affected during the titration with H3-H4 but disappears in the titration with H2A-H2B (Supplementary Figure S8). Furthermore, the ^{1}H-^{15}N NMR spectral region of the Asn/Gln side chain NH groups shows the disappearance of resonances in the H3-H4 but not in the H2A-H2B bound state indicating that one or several Asn/Gln of APLF^{FAD} are strongly involved in H3-H4 but not in H2A-H2B binding (Supplementary Figure S8). In APLF^{FAD}, the only Asn/Gln can be found between residues N453-N465, which is part of the primary H3-H4 binding region. These data demonstrate that the primary region of APLF^{FAD} to interact with H3-H4 is adjacent to the region we previously defined (HBD$^{471-499}$).

Full analysis of the NMR titration data indicates that the conserved part HBD$^{471-499}$ of APLF^{FAD}, that interacts with H2A-H2B, is extended by residues 460-470 containing a motif that is responsible for the direct and high-affinity interaction with H3-H4, and that the full HBD of APLF^{FAD} comprises residues 460-499 with adjacent H3-H4 and H2A-H2B binding regions.

We previously showed that two aromatic residues of APLF^{FAD} (Y476 and W485) are critical for imposing a functional H2A-H2B binding mode (45). Strikingly, the H3-H4 binding region includes two aromatic residues, Y462 and F468, that are particularly affected in the NMR titration (see Figure 2A,B). The segment of APLF^{FAD} that contains these residues aligns well with the binding motifs of the known H3-H4 histone chaperones UBN1 and MCM2 (Figure 2E) (47,48). Their motifs contain a conserved tyrosine, the so-called "tyrosine-key", which is buried in the deep surface pocket formed by the α1-α2-patch of H3 in the chaperone-histone complex (49). In the APLF^{FAD} binding site for H3-H4, the well-conserved tyrosine residue Y462 could be the tyrosine-key. The UBN1 interaction with H3-H4 is further aided by a second aromatic anchor residue (F138) that is also present in the H3-H4 binding region of APLF^{FAD} (F468, Figure 2E).

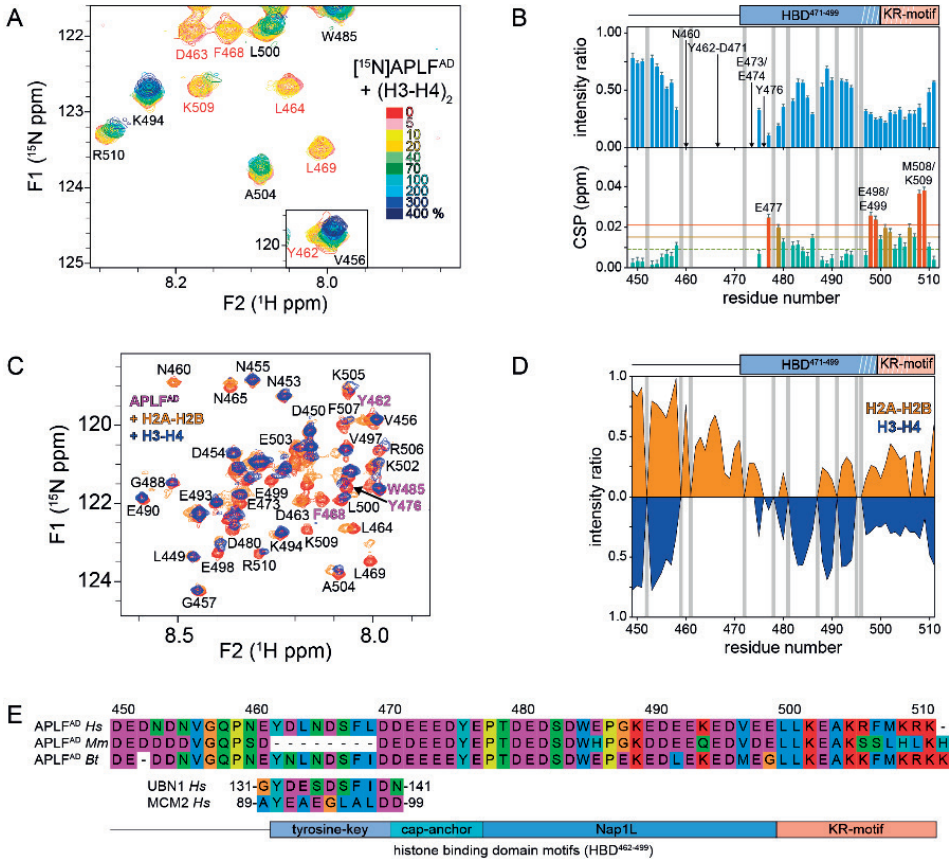

Figure 2. APLF^{AD} interacts with H3-H4 through an extension of its HBD. (A) Zoomed region of overlaid ^{1}H-^{15}N heteronuclear single quantum coherence (HSQC) spectra of APLF^{AD} with increasing concentrations of H3-H4. The inset shows the region containing the Y462 backbone resonance. Color coding indicated in the figure. Residues with disappeared resonances at the end of the titration are labeled red. Recorded at 900 MHz ^{1}H Larmor frequency at 25 °C in 25 mM NaPi buffer, pH 7.0 with 600 mM NaCl, 20 µM APLF^{AD}. (B) Analysis of APLF^{AD} ^{1}H-^{15}N peak intensity ratios (upper panel) and weighted average CSPs (lower panel) between H3-H4 bound (1:1 molar ratio of H3-H4:APLF^{AD}) and free APLF^{AD}. Resonances that disappear during the titration are indicated by arrows and labeled. Resonances with CSPs more than 2 (1) standard deviation (SD) (orange (yellow) line) from the 10% trimmed mean (green dashed line) are highlighted in orange (yellow) and labeled. Position of the HBD and KR-motif are indicated above the plot, white stripes denote the helical region. Residues without titration data due to overlap or missing resonances are indicated with gray bars. (C) Overlaid ^{1}H-^{15}N HSQC spectra of APLF^{AD} (red), and APLF^{AD} in complex with H2A-H2B (orange) or H3-H4 (blue). (D) Plot showing the APLF^{AD} peak intensity ratios between its free and H2A-H2B (orange) or H3-H4 (blue) bound state. (E) Sequence alignment of APLF^{AD}, motif analysis, and alignment with the H3-H4 binding tyrosine-key of histone chaperones UBN1 and MCM2. The amino acids are displayed with color coding according to amino acid properties. Abbreviations: *Hs* = *Homo sapiens*; *Mm* = *Mus musculus*; *Bt* = *Bos taurus*.

To test whether the APLF^{AD} residues Y462 and F468 are crucial for H3-H4 binding, we compared the affinities of H3-H4 to the APLF^{AD} aromatic anchor alanine mutants by ITC. Whereas Y462A binds with ~4-fold reduced affinity and F468A with slightly reduced affinity compared to WT APLF^{AD} to H3-H4, a ~10-fold reduced affinity is detected for the double mutant Y462A/F468A (double-anchor 1 mutant (DA1mut)) (Figure 3A,B). In comparison,

mutating the two aromatic residues of APLF^{AD} that are critical for imposing a functional H2A-H2B binding mode, Y476 and W485 (Y476A/W485A, double-anchor 2 mutant (DA2mut)), does not have such a strong effect on H3-H4 binding (Supplementary Figure S9).

To also map the interaction site for APLF^{AD} on the H3-H4 surface, we optimized the NMR spectral qualities of the H3-H4 dimer. A series of mutants and conditions were assayed to have H3-H4 in a purely dimeric state to minimize the size of the complex for NMR. Most successful results were obtained using wildtype [^{15}N]H3-H4 at pH 5, conditions under which the H3-H4 secondary structure remains well-preserved (50). Under these conditions, addition of the unlabeled synthetic peptide APLF$^{459-474}$, representing the primary H3-H4 binding motif as found in the NMR titration (see Figure 2B), results in CSPs and loss of peak intensity that clearly indicate the presence of a specific binding site on the H3-H4 surface (Figure 3C and Supplementary Figure S10). Based on a preliminary NMR amide backbone assignment of H3, we identified CSPs and loss of peak intensities for resonances corresponding to residues F84, S86, and S87, which are situated in the α1-α2-patch of H3 (Figure 3D,E).

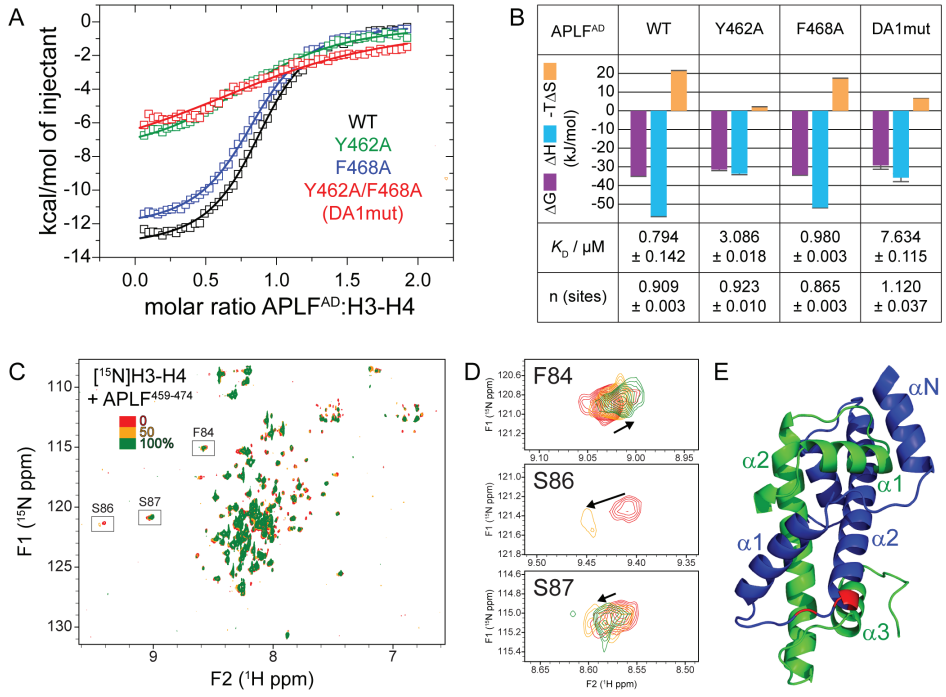

Figure 3. APLF^{AD} interacts with the α1-α2-patch of H3 through a tyrosine-key motif. (A) ITC of APLF^{AD} WT or mutants to H3-H4 at 25 °C. The resulting binding isotherms were fit to a one-set-of-sites binding mode. (B) ITC best-fit values and fitting errors together with the derived thermodynamic parameters. All data were obtained in 25 mM NaPi, pH 7.0, 300 mM NaCl. (C) Overlaid ^{1}H-^{15}N transverse relaxation-optimized spectroscopy (TROSY) spectra of [^{15}N]H3-H4 with increasing concentrations of the synthetic peptide corresponding to APLF$^{459-474}$. Color coding indicated in the figure. Positions of selected residues are marked by a rectangle and labeled. (D) Overlaid ^{1}H-^{15}N TROSY spectral regions of selected H3 residues marked in (C). Color coding as in (C). Peak shift directions are marked with arrows. (E) Selected residues from (D) labeled red on the cartoon representation of H3-H4 (PDB ID 2PYO). Blue: H3; green: H4. Secondary structural elements are labeled.

Combined, our data support an interaction mode between APLF^{FAD} and H3-H4 where APLF^{FAD} binds the H3 α1-α2-patch using two aromatic anchor residues in a binding interface that is distinct from the H2A-H2B binding site. This strengthens the hypothesis that one APLF^{FAD} monomer can bind a half-octamer that is formed by H2A-H2B and H3-H4 in the histone octamer complex.

STRUCTURAL CHARACTERIZATION OF THE OCTAMER-APLF^{AD} COMPLEX

To get more structural insights into the interaction of APLF^{FAD} with the histone octamer, we used small-angle X-ray scattering (SAXS) and crosslinking MS and tested the relevance of the aromatic anchors for binding the histone octamer. SAXS data obtained from batch measurements of the histone octamer mix yield a radius of gyration (R_g) of 3.5 nm with a molecular weight (MW) estimate of 87-99 kDa (Supplementary Table S1). These values are close to the ones expected for a histone octamer in solution and as it occurs in the nucleosome (MW (theoretical) = 107 kDa, R_g (literature) = 3.25-3.30 nm (51,52)). Importantly, when subjecting this sample to size exclusion chromatography coupled SAXS (SEC-SAXS) scattering curves of two distinct peaks were obtained, corresponding to the individual histone complexes (data not shown). In contrast, the octamer-APLF^{FAD} complex eluted as a single peak from the column in SEC-SAXS, and dilution negligibly affected the scattering curves (data not shown). The batch mode curves show increased scattering of the octamer-APLF^{FAD} complex at low scattering values compared to the histone octamer mix alone indicating an increase in overall size of the complex (Figure 4A). Analysis of the scattering curves indicates that the octamer-APLF^{FAD} complex has an R_g of 4 nm and a molecular weight of 122-152 kDa (Supplementary Table S1), similar to the native MS determined and theoretical mass for the minimal complex of 123 kDa. Further analyses indicates a slight tendency for oligomerization at higher concentrations of the complex (Supplementary Figure S11 and Table S1). Kratky plot analysis suggests that the octamer-APLF^{FAD} complex has the same conformation as the histone octamer and the pair-distance distribution function suggests that the complex is slightly more extended than the histone octamer alone (Figure 4B,C). Overall, the data is consistent with ~2 APLF^{FAD} binding per histone octamer assembled into a predominantly globular structure.

A crosslinking MS analysis of similar preparations as for SAXS, using disuccinimidyl sulfoxide (DSSO, which imposes a 28 Å protein backbone Cα-Cα distance constraint) as crosslinking agent, reveal many close contacts, mostly between the abundant and highly reactive lysines that are present in the flexible histone tails. In our analysis, however, we focused on the crosslinks between the lysines that can be localized to the structured histone fold regions. Since the SAXS data indicate that the octameric histone mixture in absence and with APLF^{FAD} resembles a histone octamer in its overall shape, the crosslinks were compared to the structure of the native histone octamer as it occurs in the nucleosome. Crosslinks were categorized into three classes depending on their solvent-accessible surface distance (SASD) (53) in the native histone octamer complex: (i) those that are consistent with this structure (SASD ≤ 28 Å), (ii) that could be compatible when allowing for some "breathing" of the complex (28 Å < SASD ≤ 32 Å), and (iii) that are incompatible (SASD > 32 Å). For the histone octamer mixture without APLF^{FAD}, approximately 40% of the crosslinks are consistent with the structure while about

50% of the crosslinks are incompatible with SASD values of even up to 80 Å (Figure 4D,E). The remaining 10% of crosslinks belong to category (ii). This indicates that under the assay conditions the histone dimers interact to a large extent in an unspecific manner. Addition of increasing amounts of APLF^{AD} results in a drastic reduction of the unspecific while retaining the native dimer-dimer contacts as in the histone octamer and this effect is dependent on the presence of the aromatic anchor residues. Addition of all the APLF^{AD} Y462A/F468A mutant (DA1mut, mutation in the H3-H4 binding region), the Y476A/W485A mutant (DA2mut, mutation in the H2A-H2B binding region), or the Y462A/F468A/Y476A/W485A mutant (quadruple anchor mutant (QAmut)) results in a large increase in non-native histone-histone contacts (Figure 4E). Together with the SAXS data these results strongly suggest that H2A-H2B and H3-H4 are associated in their native octameric organization in the histone octamer-APLF^{AD} complex and that this binding mode depends on the presence of the aromatic anchor residues.

In conclusion, the SAXS data unambiguously demonstrate that in solution the histone octamer-APLF^{AD} complex has overall dimensions compatible with the formation of a native histone octamer. This is consistent with the native MS data showing the formation of the histone octamer complex and the native histone-histone contacts observed in the presence of APLF^{AD}.

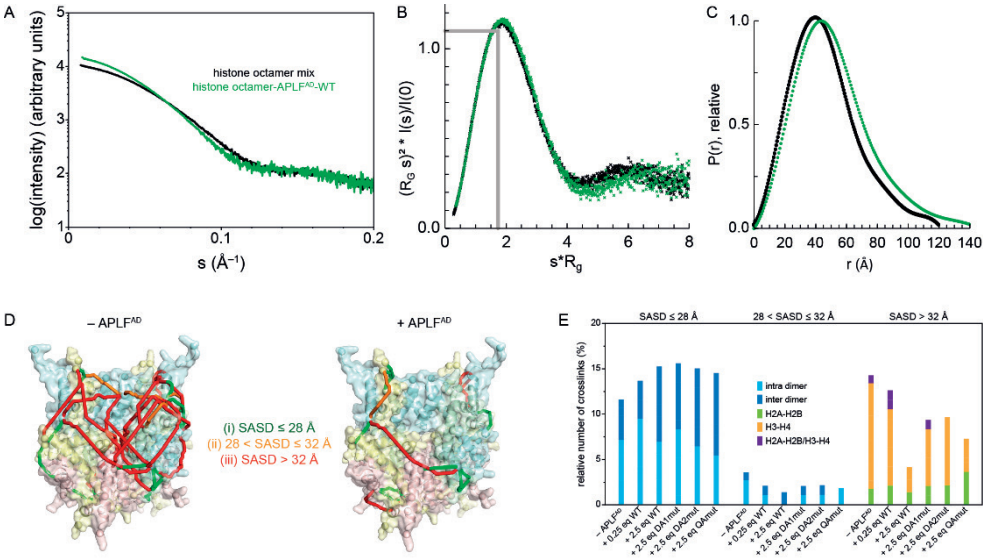

Figure 4. APLF^{AD} stabilizes the histone octamer arrangement. (A) Batch mode SAXS data for histone octamer mix (black) and histone octamer-APLF^{AD} complex (green). (B) Dimensionless Kratky plot indicates that the two complexes are slightly elongated. The reference point in gray indicates where most globular compact particles have a maximum. (C) Normalized pair-distance distribution function shows that histone octamer-APLF^{AD} is slightly larger than histone octamer alone. (D) The solvent accessible surface distance (SASD) for the crosslinks involving the histone core are shown as spheres with color coding of the three SASD categories on the surface representation of the histone octamer structure as in the nucleosome (PDB ID 2PYO) (paleyellow: H2A, lightpink: H2B, lightblue: H3, palegreen: H4). (E) Plotted relative number of crosslinks of the three SASD categories for the different histone octamer mix preparations without and with APLF^{AD} WT or mutants.

STRUCTURAL MODEL OF THE HISTONE OCTAMER-APLF^{AD} COMPLEX

We next aimed to obtain an atomic model for the histone octamer-APLF^{AD} complex combining the binding data from NMR, SAXS and crosslinking MS in an integrative modeling approach using HADDOCK (54). We focus here on the minimal complex formed by one histone octamer and two APLF^{AD} as demonstrated by native MS and supported by SAXS and ITC. Based on the globular shape of the complex as indicated by SAXS and the high degree of correspondence between the observed crosslinks and the native octamer structure, we assume that the histones are organized in their nucleosomal octameric configuration and that the structure of the histone octamer is a valid starting point for modeling. Since APLF^{AD} is fully disordered in solution and we have no detailed structural information on the conformation of APLF^{AD} in the bound state, we made use of the sequence homology of the double-aromatic anchor motifs of APLF^{AD} to other histone chaperones for which structural information is available to build our structural model. We previously modeled the complex between H2A-H2B and its APLF^{AD} interaction region (APLF$^{471-490}$) using NMR and mutational data (45). Here, we extended this model by including the H3-H4 interaction motif (APLF$^{460-470}$) identified in our NMR titration of [^{15}N]APLF^{AD} with H3-H4 (see Figure 2B). Since this part of the sequence aligns well with the two aromatic residues in the histone binding motif of histone chaperone UBN1 (see Figure 2E), we used this structure as a template for modeling of the bound-state conformation of the H3-H4 binding region of APLF^{AD}. The structural model of APLF$^{460-490}$ was docked to the histone octamer structure guided by the experimentally supported interaction data: we enforced the interaction of Y462 and F468 to H3 to mimic the tyrosine-key motif seen in UBN1 as supported by the NMR titration data (see Figures 2 and 3), and we enforced the interaction of Y476 and W485 to the H2A-H2B α1-α2-patches as described previously (45).

The resulting solutions cluster in one group. All solutions show that the four aromatic residues of APLF^{AD} are appropriately spaced to allow a simultaneous interaction of the tyrosine-key and cap-anchor motifs with H3-H4 and H2A-H2B, respectively (Figure 5A). The APLF^{AD} backbone has reasonable backbone angles in this conformation as judged from the Ramachandran plot quality and the interface has overall proper physio-chemical properties (Supplementary Table S2). The interface between APLF^{AD} and the histones is formed by extensive electrostatic contacts, next to the hydrophobic aromatic anchor interactions (Figure 5B). Importantly, the model shows that the aromatic anchors of one APLF^{AD} can simultaneously bind to the α1-α2-patches of H3, H2A, and H2B in the histone octamer (Figure 5C,D). The interface between the two bound APLF^{AD} molecules and the histones largely overlaps with the DNA binding surface of the histone octamer (Figure 5E). Overall, our data-driven model suggests that APLF^{AD} may act to substitute the DNA and organize the histone octamer as in the nucleosome. Hence, we refer to this structure as the "chaperonosome".

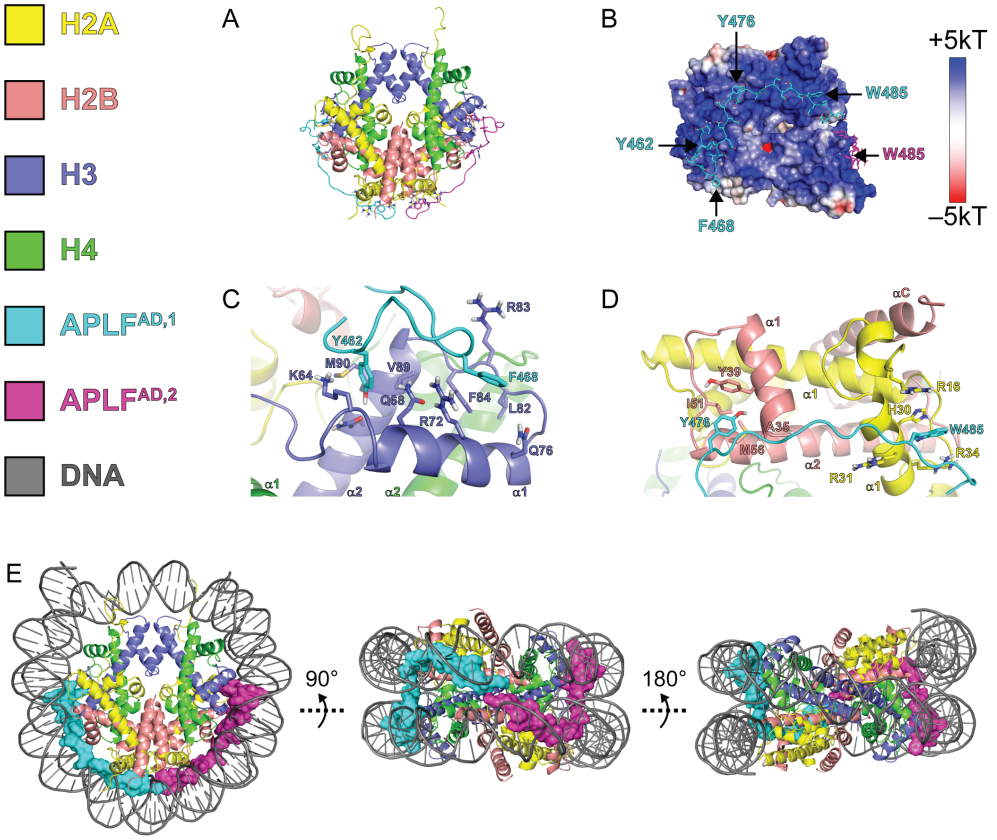

Figure 5. Structural model of APLF$^{460-490}$ bound to the histone octamer using four aromatic anchors. (A) Quadruple-anchor model for two copies of APLF$^{460-490}$ bound to the histone octamer. APLF$^{460-490}$ and histones in cartoon representation. APLF$^{460-490}$ aromatic anchor side chains as well as interacting histone residues shown as sticks. (B) APLF$^{460-490}$ in cartoon representation with side chains shown as sticks. Electrostatic potential is color coded on the Van-der-Waals surface of the histone octamer. (C,D) Close-up views on the aromatic anchor interactions. Double-anchor 1 (DA1) bound to H3 α1-α2-patch (C), and double-anchor 2 (DA2) bound to H2A-H2B α1-α2-patches (D). APLF$^{460-490}$ in cartoon representation with side chains shown as sticks. Selected residues and histone secondary structure elements are labeled. (E) APLF$^{460-490}$ (surface representation) interferes with DNA binding to the histones. DNA taken from PDB ID 1KX5.

FOUR AROMATIC ANCHORS OF APLF^{AD} ARE ESSENTIAL FOR CHAPERONE ACTIVITY

To test our structural model of the histone octamer-APLF^{AD} complex and to validate its functional relevance, we assayed the histone octamer chaperone activity of APLF^{AD} *in vitro*. In the absence of a histone chaperone and at close to physiological salt concentration, the histone octamer binds in non-native manner to DNA, resulting in aggregation and precipitation at high molar excess of histones (21). As a genuine histone chaperone, APLF^{AD} should be able to prevent incorrect histone-DNA interactions and promote nucleosome formation (7). We

thus used a native polyacrylamide gel electrophoresis (PAGE) assay to detect the chaperone-mediated rescue of DNA precipitation and nucleosome assembly (45,55). As a control, incubation of a 167 bp DNA fragment with histone octamer leads to loss of free DNA due to precipitation, culminating in almost complete precipitation of DNA at a 2.05:1 histone octamer:DNA ratio (Figure 6A, lanes 2-3). However, when the histone octamer is pre-incubated with different amounts of APLF^{FAD} WT, DNA precipitation is prevented and soluble histone-DNA complexes are observed, of which the major species, running between the 450 and 500 bp marker bands, could correspond to the nucleosome (Figure 6A, lanes 1 and 4-6). This suggests that APLF^{FAD} can function as histone chaperone by competing with DNA for binding to the histone octamer, thereby preventing aggregation and promoting histone deposition onto DNA. Mutations of the aromatic amino acids that we identified as key anchor residues in APLF^{FAD} according to our structural model reduce its histone chaperone activity. While in the APLF^{FAD} Y462A/F468A double-anchor mutant (DA1mut) chaperone activity is partially abolished (Figure 6A, lanes 7-9), the double-anchor mutation Y476A/W485A (DA2mut) greatly reduces chaperone activity (Figure 6A, lanes 10-12), which is almost completely abolished in the quadruple anchor mutant Y462A/F468A/Y476A/W485A (QAmut) (Figure 6A, lanes 13-15).

To further evaluate the impact of the aromatic anchors on binding, we investigated the interaction of the APLF^{FAD} mutants with the histone octamer mix by native MS and ITC. Strikingly, native MS experiments of the mutants show that they can form a complex with the histone octamer as WT APLF^{FAD} and ITC shows that they bind the histone octamer with slightly reduced affinities (Figure 6B-D). However, the reduced binding enthalpies of the mutants clearly show the involvement of these aromatic anchor residues in direct contacts of APLF^{FAD} with the histones. With these major binding residues missing in the mutants, the interaction between APLF^{FAD} and the histone octamer likely relies predominantly on electrostatics. In such a charge-mediated interaction in the absence of the aromatic anchor residues, however, specific histone-APLF^{FAD} interactions are reduced making APLF^{FAD} unable to effectively compete with DNA binding as well as leading to more non-native histone-histone contacts which could be captured in the crosslinking MS experiments (see Figure 4E).

The combined results reveal that APLF^{FAD} interferes with DNA binding to the histone octamer and that the four aromatic side chains in the HBD of APLF^{FAD} are essential for chaperone function. Strikingly, since the quadruple mutant is capable of binding the histone octamer, its lack of chaperone activity suggests that without the specific aromatic anchors APLF^{FAD} lacks the capability to bind the histone DNA-binding surface, leaving it open for interaction with DNA. These data imply that the interaction between APLF^{FAD} and the octamer is specific and functional, thus strongly supporting the role of APLF^{FAD} as a domain with histone octamer chaperone function.

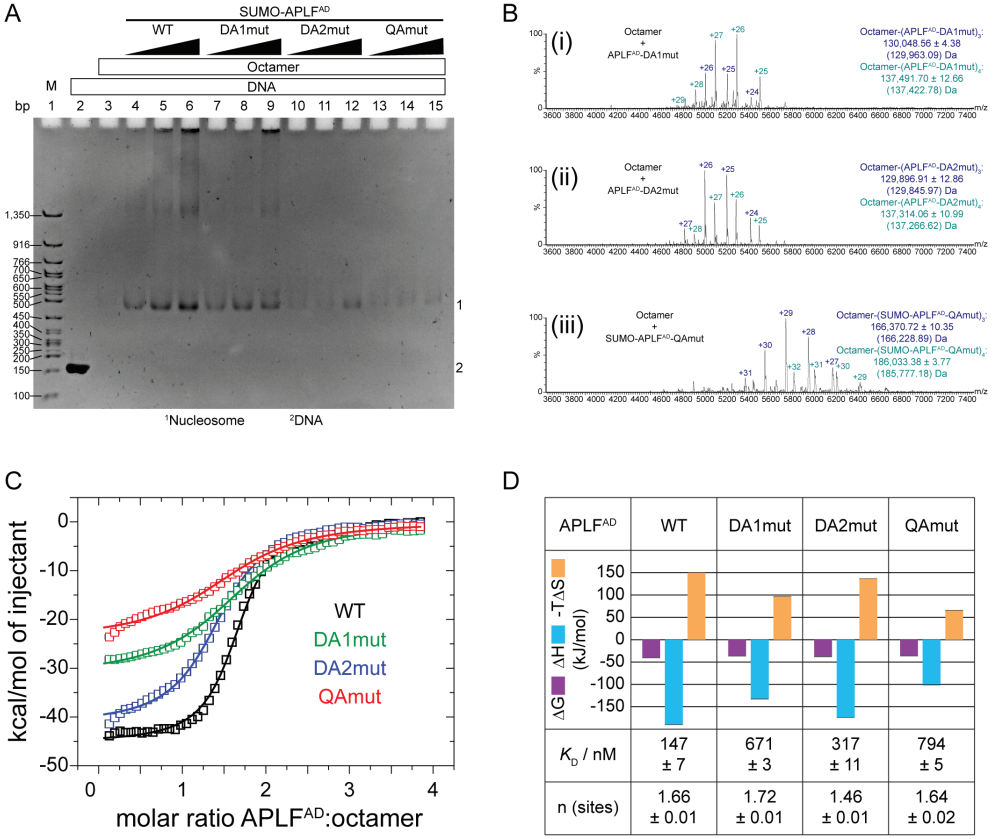

Figure 6. APLF^{AD} functions as histone chaperone to assemble the nucleosome. (A) Native PAGE analysis of 167 base pair (bp) DNA (1 µM) with the 601 nucleosome positioning sequence in presence or absence of APLF^{AD} WT or mutants and histone octamer. All APLF^{AD} were with N-terminally fused SUMO which was shown in the WT version to bind as APLF^{AD} without fusion (Supplementary Figure S12). Chaperone assay performed at RT. Lane 1: 50 bp DNA ladder (M). Lane 2: free DNA. Lane 3: DNA upon addition of 2.05 µM octamer. Lanes 4-15: DNA upon addition of 2.05 µM octamer pre-incubated with increasing concentrations (25-, 50-, or 100-fold) of APLF^{AD} WT or mutants. (B) Native mass spectra of mixtures of histone octamer and APLF^{AD} aromatic anchor mutants showing same type of complex formation as with WT APLF^{AD} with up to 4 APLF^{AD} bound (see Supplementary Figure S3). APLF^{AD}-QAmut was with N-terminally fused SUMO for the purpose of concentration determination by absorbance at 280 nm. The relative signal intensity (RSI) is plotted against the mass-to-charge ratio (m/z). Charge states are given for each signal. Experimental (theoretical in brackets) molecular weights of the identified species are listed. Samples were in 300 mM ammonium acetate, pH 7.5. (C) Calorimetric titration of APLF^{AD} WT or mutants to histone octamer mix via ITC at 25 °C. APLF^{AD}-QAmut was with N-terminally fused SUMO for the purpose of concentration determination by absorbance at 280 nm. The resulting binding isotherms (upper panel) were fit to a one-set-of-sites binding mode. Best-fit values and fitting errors are shown in the table together with the derived thermodynamic parameters. All data were obtained in 25 mM NaPi, pH 7.0, 300 mM NaCl. (D) ITC best-fit values and fitting errors together with the derived thermodynamic parameters.

THE ROLE OF THE KR-MOTIF IN THE CHAPERONOSOME

APLF^{FAD} contains six lysines of which four are in the KR-motif (residues 500-511), which is together with two arginines a positively charged segment of the otherwise acidic APLF C-terminal domain (theoretical pI = 11.17 for the KR-motif, theoretical pI = 3.87 for APLF^{FAD}). The NMR titrations of [^{15}N]APLF^{FAD} with both H2A-H2B and H3-H4 at high salt concentration show spectral changes, disappearance of resonances and high CSPs for residues in the KR-motif (see Figure 2 and Supplementary Figures S8). To test for direct interaction with the histone octamer, we measured binding of the APLF^{FAD} deletion mutant without KR-motif (mutant APLF^{FAD}-Δ) for binding to the histone octamer via ITC (Figure 7A,B). APLF^{FAD}-Δ binds the histone octamer similar to APLF^{FAD} WT. However, combining this deletion with APLF^{FAD} mutants containing the H2A-H2B binding deficiency mutation Y476A/W485A in APLF^{FAD}-DA2mut and -QAmut, APLF^{FAD}-DA2mutΔ and -QAmutΔ, leads to a decreased enthalpy and affinity of binding. In contrast, no additional effect on histone octamer binding is observed for the H3-H4 binding site mutant APLF^{FAD}-DA1mut when combined with the KR-deletion (APLF^{FAD}-DA1mutΔ), confirmed by a similar outcome for binding H3-H4 alone (Supplementary Figure S13). As support of these results, the native mass spectrum of APLF^{FAD}-QAmutΔ shows that, other than the histone octamer-APLF^{FAD} complexes, histone hexamer-APLF^{FAD} complexes are formed in which one H2A-H2B dimer is lost from the histone octamer (Supplementary Figure S14). Furthermore, in the crosslinking MS data, for which we assume that the compositions of the complexes are as revealed by native MS, intermolecular crosslinks in the minimal histone octamer-(APLF^{FAD})$_2$ complex are found between the APLF^{FAD} KR-motif and the H2B αC-helix (Supplementary Figure S15). Crosslinks with H3-H4 are only found in histone-octamer-(APLF^{FAD})$_{3/4}$, but not in the minimal complex. These results indicate that in the minimal histone octamer-(APLF^{FAD})$_2$ complex the KR-motif is not involved in binding H3-H4 but H2A-H2B, in particular H2B. The crosslinks in the histone octamer-(APLF^{FAD})$_{3/4}$ complex could come from the additional bound APLF^{FAD} molecules. Histone-APLF^{FAD} crosslinks in histone octamer-(APLF^{FAD})$_{3/4}$ are also present in the double-anchor mutants suggesting that the KR-motif can interact with the histone octamer independently from the aromatic anchors. In particular, several crosslinks between the KR-motif of APLF^{FAD} and the H2B αC-helix are found. This suggests a secondary binding close to the H2B αC-helix. This fits with our previously demonstrated NMR titration of H2A-[^{15}N]H2B with APLF^{FAD} which revealed that the region around the H2B αC-helix is a binding site for a secondary, weaker interaction with APLF^{FAD} (45), which we support here with a similar NMR titration with [^{15}N]H2A-H2B and APLF^{FAD} (Supplementary Figure S16).

SAXS data suggest a slightly reduced overall size for the histone octamer-APLF^{FAD}-Δ complex as can be judged from the reduced scattering at low *s* values compared to the complex with APLF^{FAD} WT (Figure 7C). Importantly, an ab-initio-model using the SAXS data demonstrates that the histone octamer-APLF^{FAD}-Δ complex has overall dimensions compatible with the formation of a globular complex in the shape of the native histone octamer (Figure 7C, inset, and Supplementary Table S3). Kratky plot analysis and the pair-distance distribution function also indicate that the octamer-APLF^{FAD}-Δ complex is more compact than the complex with APLF^{FAD} WT (Figure 7D,E and Supplementary Table S3).

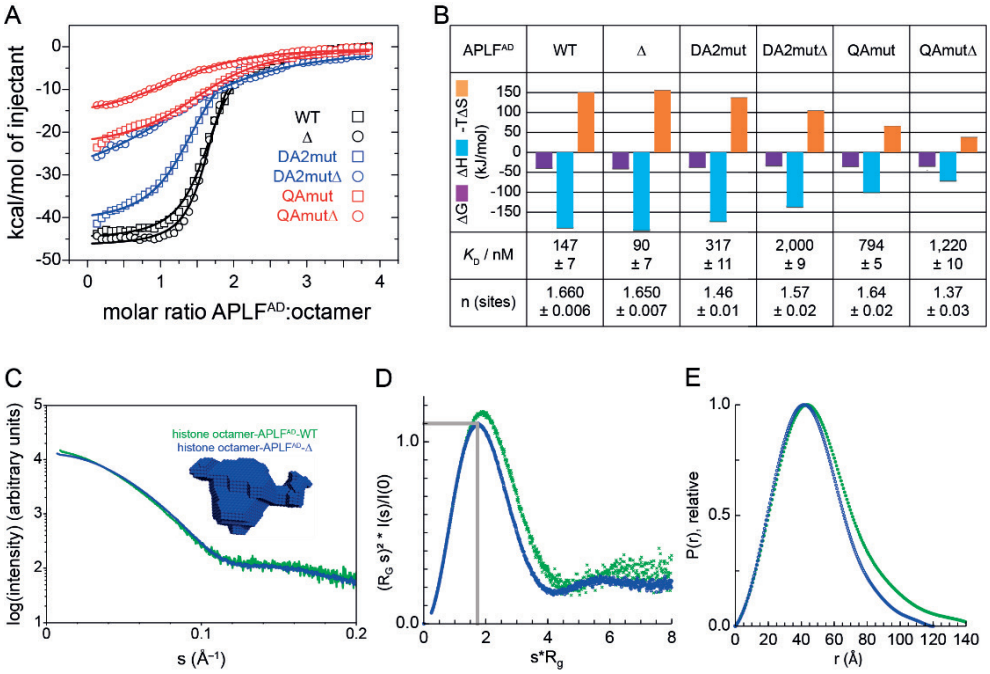

Figure 7. The APLF^{AD} KR-motif is involved in histone octamer binding. (A) Calorimetric titration of APLF^{AD} WT or mutants to histone octamer via ITC at 25 °C. APLF^{AD}-QAmut and -QAmutΔ were with N-terminally fused SUMO for the purpose of concentration determination by absorbance at 280 nm. The resulting binding isotherms were fit to a one-set-of-sites binding mode. All data were obtained in 25 mM NaPi, pH 7.0, 300 mM NaCl. (B) ITC best-fit values and fitting errors together with the derived thermodynamic parameters. (C) Batch mode SAXS data for histone octamer-APLF^{AD} WT (green) and histone octamer-APLF^{AD}-Δ (blue) with ab-initio bead model. (D) Dimensionless Kratky plot indicates that the histone octamer-APLF^{AD}-Δ is more compact than histone octamer-APLF^{AD} WT. The reference point in gray indicates where most globular compact particles have a maximum. (E) Normalized pair-distance distribution function shows that histone octamer-APLF^{AD}-Δ has a globular shape and is more compact than histone octamer-APLF^{AD} WT.

Taken together, the results suggest that the KR-motif contributes to histone octamer binding, and forms part of the binding interface for H2A-H2B within the histone octamer. Thus, we wanted to see whether APLF^{AD} could bind simultaneously to H3-H4 and H2A-H2B using the aromatic anchors and to the H2B αC-helix using the KR-motif. Hence, we extended the APLF model (residues 460-490) to include the KR-motif. We modeled the structure of the KR-motif in the conformation of Chz1, an intrinsically disordered histone chaperone that also binds the H2B αC-helix and for which structural information is available from its complex with H2A.Z-H2B (56,57). As restraints for this motif, we used the two intermolecular crosslinks between APLF^{AD} and the histones found in the crosslinking MS experiment of the minimal histone octamer-(APLF^{AD})$_2$ complex. Additionally, we enforced the aromatic anchor interactions and docked APLF$^{460-511}$ on the histone octamer (Figure 8 and Supplementary Table S4). Interestingly, the model demonstrates that the KR-motif can bind the distal H2A-H2B dimer, suggesting that APLF^{AD} not only can bind H2A-H2B and H3-H4 but could also stabilize their octameric arrangement (Figure 8A,B). Furthermore, the model indicates that intermolecular

contacts can be formed between the two bound APLF^{FAD} molecules in this conformation which could further stabilize the complex (Figure 8C). These possible stabilizing interactions are supported by a crosslinking MS analysis of histone octamer complexes with KR-motif deletion mutants of APLF^{FAD} which show increased non-native histone-histone contacts compared to the histone octamer-APLF^{FAD} WT complex (Supplementary Figure S17). Finally, the model shows how APLF^{FAD} could interfere with DNA binding to the histone octamer but also bind to a histone site that is exposed in the nucleosome (Figure 8D).

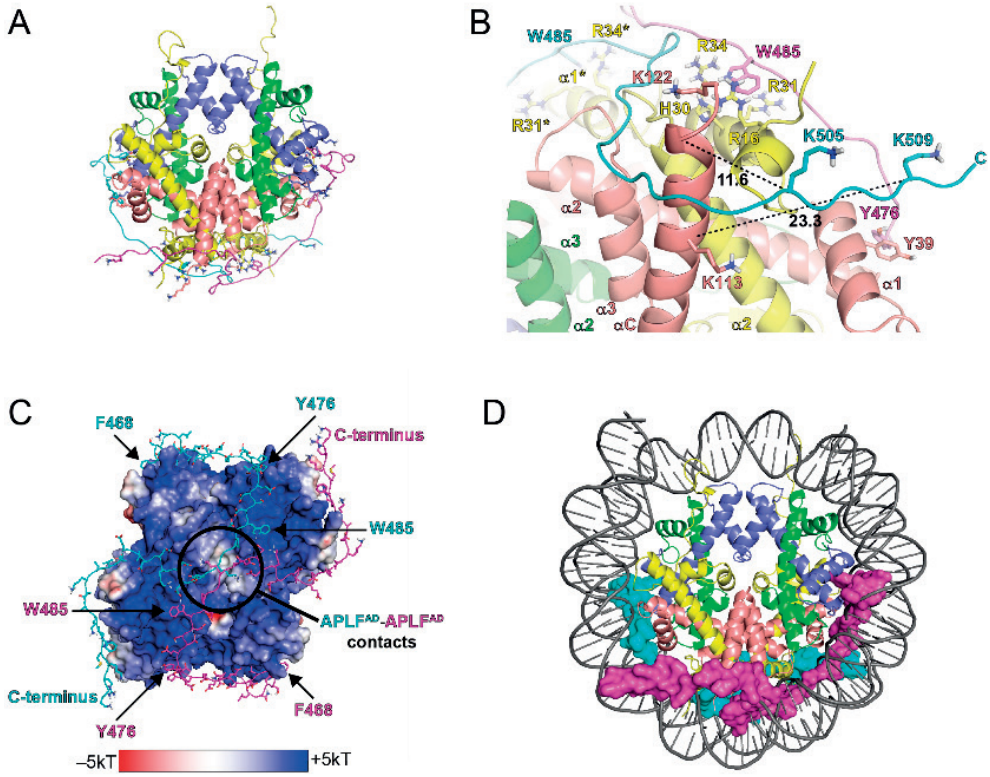

Figure 8. Structural model of APLF$^{460-511}$ bound to the histone octamer with the KR-motif bound to the distal dimer. (A) Model for two copies of APLF$^{460-511}$ bound to the histone octamer. APLF$^{460-511}$ in cartoon representation with its aromatic anchor side chains as well as interacting histone residues shown as sticks. Lysines forming crosslink pairs are shown as sticks. (B) Close-up view on the lysine crosslink pairs. Crosslinked lysines are indicated by dashed lines between their Cα atoms with distance labels in Å. APLF$^{460-511}$ in cartoon representation with side chains shown as sticks. Selected residues and histone secondary structure elements are labeled. An asterisk indicates the symmetry-related histone. (C) APLF$^{460-511}$ in cartoon representation with side chains shown as sticks. Electrostatic potential is color coded on the Van-der-Waals surface of the histone octamer. (D) APLF$^{460-511}$ (surface representation) interferes with DNA binding to the histones. DNA taken from PDB ID 1KX5.

DISCUSSION

We describe here a detailed characterization of the interaction between the acidic domain of DNA repair factor APLF (APLF^{AD}) and different histone complexes to get more insight into its histone chaperone activity. We performed biophysical, mutational, and structural investigations on the recognition of the histone octamer and our results strongly suggest that APLF^{AD} is a true histone octamer chaperone with possible nucleosome assembly function. For this, APLF^{AD} makes use of a quadruple-aromatic-anchor binding motif, a model that is supported by mutational analysis.

Our data show consistently, quantitatively, and using a variety of techniques, that APLF^{AD} can bind simultaneously to both H2A-H2B and H3-H4 to form a specific, high-affinity complex. The NMR data indicate that the APLF^{AD} histone binding domain (HBD) uses distinct regions to bind the two different types of histone complexes. Each of these regions contains two aromatic residues embedded within a predominantly acidic sequence. Mutation of these aromatic residues impairs histone binding, both in the context of the individual histone complexes, H2A-H2B and H3-H4, as well as for the histone octamer. While in the APLF^{AD} H2A-H2B binding region the aromatic residues Y476/W485 are strictly required for H2A-H2B binding, Y462 and F468 in the H3-H4 binding region are not strictly required for H3-H4 binding indicating the importance of electrostatic interactions to support this interaction. Similarly, in the context of the histone octamer mixture the mutation of the aromatic residues impairs but does not abrogate complex formation. Strikingly, despite complex formation these residues are indispensable for chaperone activity, indicating that they are crucial for imposing a specific and functional binding mode.

The stoichiometry of the histone octamer-APLF^{AD} complex corresponds to two APLF^{AD} molecules bound to one histone octamer as evidenced by native MS and supported by analytical gel filtrations, SAXS and ITC. At higher APLF^{AD} concentrations, additional APLF^{AD} molecules can associate to this minimal complex as shown by both native MS and SAXS. While this means that under the conditions of the chaperone activity assay such higher order complexes can also be formed, our mutational analysis clearly highlights the essential role of the aromatic anchor residues, suggesting the minimal octamer-(APLF^{AD})$_2$ complex as the functional unit that we call the chaperonosome. Importantly, the SAXS data unambiguously demonstrate that in solution the histone octamer-APLF^{AD} complex has overall dimensions compatible with the formation of a histone octamer. This is consistent with the native MS data showing the formation of the histone octamer and the native histone-histone crosslinks observed in crosslinking MS of the histone octamer-APLF^{AD} complex.

The presented structural model rationalizes the chaperone activity of APLF^{AD} by illustrating how the placement of the aromatic anchors within the acidic domain optimally fits with the α1-α2-patches of H2A, H2B, and H3 of the H2A-H2B and H3-H4 dimers within the histone octamer. These regions form contact points with nucleosomal DNA. Upon specific binding to the DNA binding surface, APLF^{AD} prevents, by competition, non-native histone-DNA interactions. Our data further suggest that the APLF^{AD} C-terminal KR-motif could interact with the distal H2A-H2B dimer within the minimal chaperonosome complex. Mechanistically, this interaction may be in part responsible for stabilization of the histone octamer arrangement, and could explain how APLF^{AD} can capture the octamer in its near-native conformation. Given the basic character of the KR-motif, an intriguing idea is that it could also interact with DNA. To

this end, an NMR titration of [^{15}N]APLF^{FAD} with 167 bp 601-DNA was carried out to test for binding (Supplementary Figure 18). However, no spectral changes were visible and titration analysis revealed only very small effects of binding on APLF^{FAD} backbone resonances suggesting there could be a slight tendency for the KR-motif to weakly interact with DNA alone. But in the context of the chaperonosome it could be involved in fuzzy interactions mediating contacts between histones and DNA.

The structural model of the chaperonosome in combination with all data presented further provides a plausible mechanism for octamer deposition onto DNA. In the absence of APLF^{FAD}, predominantly nonspecific histone-DNA complexes are formed because the specific complexes involve only a subset of all potential histone-DNA interactions (Figure 9, left part). But APLF^{FAD} may guide nucleosome assembly in a direct fashion by presenting the histones in the correct organization and orientation (Figure 9, right part). In our model, two copies of APLF^{FAD} wrap around the histone octamer. This interaction is stabilized by the APLF^{FAD} aromatic anchors interacting with the α1-α2-patches on H2A, H2B and H3 leaving the one of H4 free for interaction with DNA. By increasing the likelihood of specific interactions between the histone octamer and the DNA, APLF^{FAD} skews the reaction kinetics towards nucleosome formation. APLF^{FAD} is involved in a transient complex with the histone octamer and the DNA. The formation of this transient ternary complex prevents nonspecific histone-DNA interactions and causes an apparent decrease in activation energy for nucleosome formation, favoring it over the nonspecific histone-DNA interaction path. Once the first contact between the DNA and the histone octamer-APLF^{FAD} complex is formed, the DNA can outcompete APLF^{FAD} by having higher affinity for binding to the other histone-DNA interaction sites (in the order) of H3, H2A, and finally H2B. The DNA displaces APLF^{FAD} as it wraps around the histone octamer to form the nucleosome (Figure 9). While ternary chaperone-histone-DNA complexes have not been observed directly, as expected by their transient nature, they can be inferred from experimental indications. In the native PAGE gel of the chaperone assay (see Figure 6A), a reaction band is visible at the height of the 1,350 bp marker band. This reaction band increases in intensity with higher APLF^{FAD} concentrations. Hence, it could represent a low populated ternary APLF^{FAD}-histone-DNA complex of one of the intermediates of the nucleosome assembly reaction. Such an intermediate has also been suggested from similar experimental observations for histone chaperones FACT and CAF1 (58-62).

The quadruple-aromatic anchor model of APLF^{FAD} bound to the histone octamer presented here constitutes a novel interaction mode that highlights adaptability in recognition of the histone surface by combination of distinct histone binding motifs in APLF^{FAD}. The unstructured nature of APLF^{FAD} may provide the HBD with the required conformational flexibility to adapt to the histone surfaces (63,64). Our chaperone assay together with the structure of the APLF^{FAD} bound histone octamer suggests that APLF^{FAD} can bind the histone octamer and promote its deposition onto DNA. Further validation by a micrococcal nuclease (MNase) assay is needed to proof that the DNA band formed between the 450-500 bp marker bands in the chaperone assay is indeed the nucleosome. To support the tyrosine-key binding of APLF^{FAD} to H3-H4, a mutational analysis can be performed to confirm the binding site on H3-H4. Furthermore, since it was shown that APLF^{FAD} is essential for cell survival upon DNA damage and that this is associated with impaired DNA repair by NHEJ, it would be interesting to find out the *in vivo* importance of the aromatic residues identified here to be essential for histone binding and chaperone activity and relate this to DNA repair. Collectively, our results suggest that APLF^{FAD} provides the NHEJ machinery with the capacity to store the histone octamer during the DNA repair process and deposit it on the repaired DNA to reassemble the nucleosome.

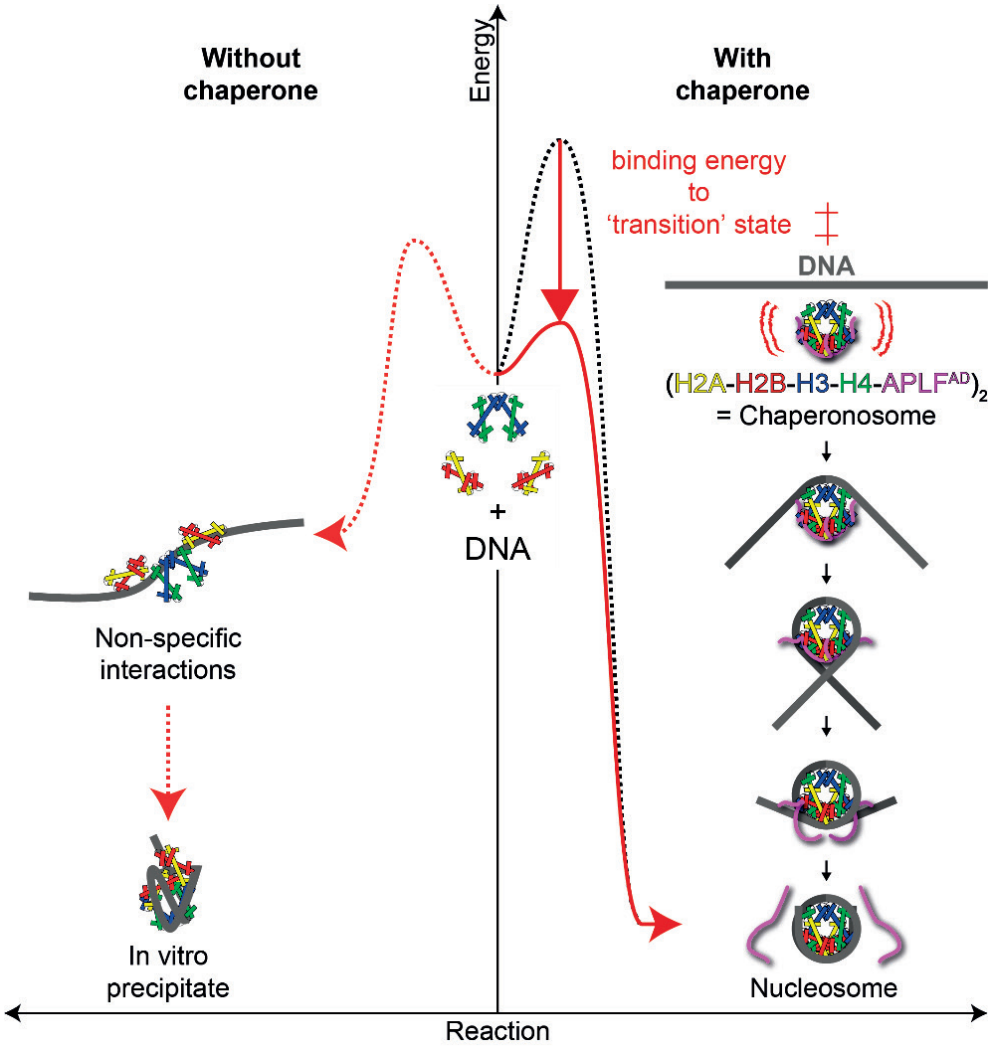

Figure 9. Free-energy reaction diagram of histone chaperone function and nucleosome assembly mechanism. Free-energy is plotted along the histone-DNA interaction coordinate. Reaction is postulated to go through a "transition state" of highest free-energy (‡) before forming the product. The transition state represents a kinetic barrier for the reaction. Left: In the absence of a histone chaperone under physiological conditions: 1. hydrophobic histone-histone interactions cannot overcome the repulsion of their positive charges, 2. nonspecific histone-DNA interactions are favored over nucleosomal interactions. Right: The chaperone binds to form a "transition state" that is competent to directly deposit histones onto DNA (19). This state might be a conformationally activated histone complex, like the histone octamer, that is primed to form nucleosomal DNA contacts. In the presence of a histone chaperone: 1. nonspecific histone-DNA interactions are efficiently competed by more stable histone chaperone-histone interactions, 2. negative charges of the histone chaperone neutralize positive charges of the histones making hydrophobic histone-histone interactions favorable. The "chaperonosome" (histone chaperone-bound histone octamer) is: 1. a stabilized "transition state" compensated for high loss of entropy concurrent with nucleosome assembly through a high enthalpy interaction, 2. able to directly deposit the histone octamer in a nuclesomal arrangement. Note that stable intermediates and additional transition states that could form on the nucleosome assembly path are omitted for simplicity.

CONCLUSIONS

Here, we show that the acidic domain of DNA repair factor APLF (APLF^{AD}) is a histone chaperone that can bind the histone octamer. We provide experimental proof for the APLF^{AD} histone chaperone activity for the histone octamer and show that this can be rationalized by the binding to the DNA-binding surface of the histones by APLF^{AD} and structural organization of the histone octamer with controlled stoichiometry. APLF^{AD} binds the histone octamer through electrostatic interactions and four aromatic residues that form anchors to the α1-α2-patches of H2A, H2B, and H3. The recognition of these generic histone-fold elements combined with the unstructured nature of its acidic domain suggests that APLF has the capability to temporarily store histone complexes at a DNA damage site and that this may subsequently promote nucleosome assembly to seal the repaired DNA. Our study extends the assigned functions of APLF that may be relevant for NHEJ DNA repair. Finally, since until now it has been assumed that histone chaperones function to prevent non-functional histone-DNA interactions and promote correct ones by reducing the pool of free histones, our findings represent a paradigm shift in this regard by showing that the histone deposition process depends on a controlled pre-assembly of the histone octamer for a possible stepwise deposition mechanism onto DNA to form the nucleosome.

MATERIALS AND METHODS

PROTEIN AND 601-DNA EXPRESSION AND PURIFICATION

APLF^{AD} production

APLF^{AD} for all NMR titrations as well as ITC experiments of H3-H4 for comparison between APLF^{AD} WT, Y476A, W485A, and Y476A/W485A was expressed and purified using a pLIC_His-GST-TCS-APLF^{AD} plasmid that upon induction expresses a fusion protein with an N-terminal histidine (His) and glutathione-S-transferase (GST) tag and thrombin cleavage site (TCS) as previously described (45).

For all other experiments the TCS was either replaced by tobacco etch virus protease cleavage site (TEVPCS) using site-directed mutagenesis to yield the construct pLIC_His-GST-TEVPCS-APLF^{AD}, or APLF^{AD} was cloned with N-terminal SUMO-tag into pET29b to yield the construct pET29b_SUMO-APLF^{AD} containing a His-tag and TEVPCS N-terminal to SUMO. Mutations were introduced using site-directed mutagenesis. Correct construction of plasmids and mutagenesis was verified by DNA sequencing.

APLF^{AD} (or SUMO-APLF^{AD}) was expressed in BL21 Rosetta2 (DE3) cells (Novagen). All media used contained ampicillin (100 mg/L) (for pLIC_His-GST-TCS-APLF^{AD} constructs) or kanamycin (30 mg/L) (for pET29b_SUMO-APLF^{AD} constructs), and chloramphenicol (34 mg/L). Colonies from a lysogeny broth (LB) agar plate were first grown in liquid LB at 37 °C. Cells from the LB culture were transferred to supplemented M9 minimal medium (MM) containing $^{14}NH_4Cl$ ($^{15}NH_4Cl$ for NMR titration experiments) and glucose as the sources of nitrogen and carbon, respectively, and left to grow at 37 °C. Expression of recombinant protein was induced at OD_{600} 0.8 with 0.5 mM isopropyl β-D-1-thiogalactopyranoside (IPTG) and the culture was transferred to 30 °C. Cells were harvested 5-14.5 h after induction and frozen for storage. For purification, cells were thawed and resuspended in lysis buffer (50 mM Tris, pH 8.0, 150 mM NaCl, 5 mM β-mercaptoethanol (BME), 20 mM imidazole) supplemented with 0.2 mM phenylmethylsulfonyl fluoride (PMSF) and in-house made protease inhibitor cocktail (PIC) (100 μM AEBSF, 0.3 μM aprotinin, 1 μM bestatin, 1 μM E-64, 10 μM leupeptin, 1 μM pepstatin A), then treated with lysozyme (Sigma-Aldrich) and benzonase (Merck Millipore), frozen, thawed and sonicated. After insoluble cell material was removed by centrifugation, His-GST-APLF^{AD} (or His-SUMO-APLF^{AD}) was purified using a 5 ml HisTrap FF column (GE Healthcare Life Sciences), pre-equilibrated in lysis buffer, and, after fusion protein binding, washed with lysis buffer. Bound fusion protein was eluted with a gradient of 20-500 mM imidazole in lysis buffer and cleaved with TEVP (in-house made) at room temperature, typically overnight. Cleavage was monitored using SDS-PAGE analysis and after complete cleavage, APLF^{AD} (or SUMO-APLF^{AD}) was further purified by anion exchange on a 5 ml HiTrap Q HP column (GE Healthcare Life Sciences) using ion exchange (IEX) low salt buffer (20 mM Tris, pH 7.5, 150 mM NaCl, 5 mM BME, 1 mM EDTA) and IEX high salt buffer (20 mM Tris, pH 7.5, 1 M NaCl, 5 mM BME, 1 mM EDTA). Elution fractions containing APLF^{AD} (or SUMO-APLF^{AD}) were pooled, supplemented with $MgCl_2$ (1.1 mM final concentration), and applied on a 5 ml HisTrap FF column (GE Healthcare Life Sciences) to remove His-tagged protein. Fractions with APLF^{AD} (or SUMO-APLF^{AD}) were pooled, buffer-exchanged to assay buffer

(25 mM NaPi, pH 7.0, 300 mM NaCl) using a 3 kDa (or 10 kDa) molecular weight cut-off (MWCO) Amicon Ultra Centrifugal Filter Unit (Merck Millipore), and used directly or aliquoted, flash-frozen in liquid nitrogen and stored at -20 °C until further use.

Histone production

Histones were expressed and purified as previously described with some changes (45). Histones H2A, H2B, H3 and H4 from *Drosophila melanogaster* were expressed in BL21 Rosetta2 (DE3) cells (Novagen) from pET21b plasmids. All media contained ampicillin (100 mg/L) and chloramphenicol (34 mg/L). Colonies from an LB agar plate were first grown in LB at 37 °C. The cell culture was transferred to supplemented M9 MM (either unlabeled with $^{14}NH_4Cl$ and $^{12}C_6$-glucose or containing $^{13}C_6D_7$-glucose, $^{15}NH_4Cl$, and D_2O for stable isotope labeling) and grown at 37 °C. Expression of recombinant protein was induced at OD_{600} 0.6-1.6 with 0.5 mM IPTG. Cells were harvested after 3-12.5 h by centrifugation and frozen for storage. Cells were resuspended in histone lysis buffer (50 mM Tris at pH 7.5, 100 mM NaCl, 5 mM BME, 1 mM EDTA) supplemented with 0.2 mM PMSF and in-house made PIC (as above), treated with lysozyme, frozen, thawed and sonicated. The first steps of purification - isolation and solubilization of histone inclusion bodies - were done according to the protocol described by Luger *et al.* (65). Solubilized histones were first purified on a gel filtration column HiLoad Superdex 75 pg (GE Healthcare Life Sciences) pre-equilibrated with histone gel filtration buffer (HGFB) with low or high salt (50 mM NaPi, pH 7.5, 0.15 (HGFB150) or 1 M NaCl (HGFB1000), 5 mM BME, 1 mM EDTA, 7 M urea). Histone containing fractions were pooled (and, if HGFB1000 was used, diluted with HGFB without salt (HGFB0) to a final NaCl concentration of 0.15 M) and first purified by anion exchange to remove nucleic acids on a 5 ml HiTrap Q HP column (GE Healthcare Life Sciences) followed by cation exchange on a 5 ml HiTrap SP HP column (GE Healthcare Life Sciences), both pre-equilibrated with HGFB150. The same buffer was used to wash the column after loading. Histones were eluted with a linear gradient of NaCl (0.15 - 1 M) in HGFB. Histone fractions were either dialyzed against water and lyophilized prior to storage, or supplemented with 1 mM lysine (final concentration) and stored directly at -20 °C.

601-DNA production

A high-copy number plasmid containing 12 tandem repeats of a 167 base pair strong positioning DNA sequence (Widom's 601; (66,67)) was transformed into DH5α cells. The plasmid was purified using a QIAGEN Plasmid Giga Kit. The 167-bp fragment was released from the vector by ScaI (Thermo Fisher Scientific) digestion and purified by anion exchange.

PREPARATION OF HISTONE COMPLEXES

Histones were refolded as previously described with some changes (45). Histone proteins were unfolded (if stored lyophilized) or buffer exchanged (if stored directly after IEX)

using a 3 kDa molecular weight cut-off (MWCO) Amicon Ultra Centrifugal Filter Unit (Merck Millipore) in unfolding buffer (50 mM Tris, pH 7.5, 100 mM NaCl, 10 mM dithiothreitol (DTT), 6 M guanidine hydrochloride) and mixed (H2A + H2B for histone dimer H2A-H2B, H3 + H4 for histone tetramer $(H3\text{-}H4)_2$, and H2A + H2B + H3 + H4 for histone octamer) in equimolar ratios to a final protein concentration of 1 mg/ml. Refolding by dialysis and gel filtration of histone complexes were performed as described for histone octamers by Luger *et al.* (65). The gel filtration buffer was exchanged to assay buffer (see above) using a 10 kDa MWCO Amicon Ultra Centrifugal Filter Unit (Merck Millipore). Complexes were aliquoted, flash frozen in liquid nitrogen and stored at -20 °C.

Analytical gel filtrations

Histone complexes and $APLF^{FAD}$ alone or mixtures thereof in assay buffer at the ratios indicated in the figures were incubated for 30 min on ice, centrifuged to remove aggregates and loaded on a Superdex 200 Increase 10/300 GL column (GE Healthcare Life Sciences) equilibrated in assay buffer and run at room temperature.

Crosslinking mass-spectrometry

Samples for crosslinking

1. Histone complexes in assay buffer.
2. $APLF^{FAD}$ in assay buffer.
3. Histone Octamer-$APLF^{FAD}$ (WT, saturated): histone octamer mix and $APLF^{FAD}$ were mixed in assay buffer at a ratio of 1:2.5 octamer:$APLF^{FAD}$ and purified on a Superdex 200 Increase 10/300 GL column (GE Healthcare Life Sciences) equilibrated in assay buffer and run at room temperature.
4. H2A-H2B-$APLF^{FAD}$: H2A-H2B and $APLF^{FAD}$ were mixed in assay buffer at a ratio of 1:2.5 H2A-H2B:$APLF^{FAD}$ and purified on a Superdex 200 Increase 10/300 GL column (GE Healthcare Life Sciences) equilibrated in assay buffer and run at room temperature.
5. H3-H4-$APLF^{FAD}$ (WT, peptide, and mutant), octamer-$APLF^{FAD}$ (WT, minimal complex), octamer-$APLF^{FAD}$mut (mutants): histone complexes and $APLF^{FAD}$ were mixed in assay buffer at a ratio of 1:2 for $(H3\text{-}H4)_2$:$APLF^{FAD}$ (WT, peptide, and mutant), 1:0.25 for octamer:$APLF^{FAD}$ (WT, minimal complex), and 1:2.5 for octamer:$APLF^{FAD}$mut (mutants).

Crosslinking conditions

Each sample (4 µL per reaction of 20 µM samples (concentration of purified complex or of the histones in mixtures) in assay buffer) was diluted to 10 µM in 50 mM HEPES pH 7.5 and crosslinked for 15 minutes at room temperature with 500 µM disuccinimidyl sulfoxide

(DSSO). The reaction was quenched with 1 M Tris pH 7.5 (50 mM final concentration). The crosslinking reaction was performed three times per sample.

Proteolytic digestion

Each sample was supplemented with urea to 8 M, reduced by addition of DTT at a final concentration of 10 mM for 1 hour at room temperature, and alkylated for 0.5 hours at room temperature in the dark by addition of iodoacetamide at a final concentration of 50 mM. The samples were digested in two rounds. In the first round, the samples were digested with Lys-C at an enzyme-to-protein ratio of 1:50 (w/w) at 30 °C for 3 hours. In the final round the samples were diluted four times in 50 mM AmBic and further digested with trypsin at an enzyme-to-protein ratio of 1:100 (w/w) at 37 °C for 16 hours. The digested samples were desalted using homemade C18 stage tips, dried and stored at -80 °C until further use.

Mass spectrometry

The samples were analyzed by LC-MS/MS using an Agilent 1290 Infinity System (Agilent Technologies) in combination with an Orbitrap Fusion Lumos (Thermo Scientific). Reverse phase chromatography was carried out using a 100-µm inner diameter 2-cm trap column (packed in-house with ReproSil-Pur C18-AQ, 3 µm) coupled to a 75-µm inner diameter 50 cm analytical column (packed in-house with Poroshell 120 EC-C18, 2.7 µm) (Agilent Technologies). Mobile-phase solvent A consisted of 0.1% formic acid in water, and mobile-phase solvent B consisted of 0.1% formic acid in 80% acetonitrile. A 120 minutes gradient was used, and start and end percentage buffer B were adjusted to maximize sample separation.

MS acquisition was performed using the MS2_MS3 strategy:

- the MS1 scan was recorded in Orbitrap at a resolution of 60,000.
- the selected precursors were fragmented in MS2 with CID and the crosslinker signature peaks recorded at a resolution of 30,000.
- The fragments displaying the mass difference specific for DSSO were further fragmented in a MS3 scan in the ion trap (IT) (68).

Data analysis

Proteome Discoverer 2.2 was used for data analysis with the XlinkX nodes integrated. The processing workflow was set up with the following nodes. The built-in nodes "Spectrum Files" and "Spectrum Selector" were used to extract the MS2 scans together with a precise precursor m/z and charge. To extract precursor intensity information we added the built-in node "Minora feature detection". The following crosslinking workflow consists of the following nodes. The "XlinkX Detect" node performs diagnostic peak detection specific for the used labile crosslinker DSSO. For this node the acquisition strategy "MS2_MS3" was specified. The following "XlinkX Filter" nodes only filters out all MS2 scans for which no diagnostic peak set

was detected. The remaining MS2 scans were identified with the dedicated crosslink peptide search engine "XlinkX Search" node, for which the following settings were used: database obtained from bottom up analysis of the samples, protease Trypsin (Full), 2 allowed missed cleavages, precursor mass tolerance of 10 ppm, fragment mass tolerance of 20 ppm, carbamidomethyl on C as static modification, oxidation on M as variable modification, where appropriate acetylation or ubiquitination on K were also set as variable modification. The results from the search were FDR corrected to 1% using the "XlinkX Validator" node, which utilizes a specific set of crosslink peptide spectral features and machine learning to define the cutoff as developed for peptide spectral matches in Percolator. Finally, in the "Crosslink Consensus" node the individual crosslink spectral matches were grouped in those cases where they represent the same peptide sequence and modification state. General workflows were provided with the Proteome Discoverer installed as common templates.

NATIVE MASS SPECTROMETRY

Samples for native mass spectrometry

1. Histone complexes in assay buffer.
2. APLF^{FAD} in assay buffer.
3. Octamer-APLF^{FAD} (WT, saturated): histone octamer mix and APLF^{FAD} were mixed in assay buffer at a ratio of 1:2.5 octamer:APLF^{FAD} and purified on a Superdex 200 Increase 10/300 GL column (GE Healthcare Life Sciences) equilibrated in assay buffer and run at room temperature.
4. Octamer-APLF^{FAD} (WT, saturated, ionic strength titration): histone octamer mix and APLF^{FAD} were mixed in assay buffer at a ratio of 1:2.5 octamer:APLF^{FAD} and purified on a HiLoad 16/600 Superdex 200 pg column (GE Healthcare Life Sciences) equilibrated in assay buffer and run at 4 °C.
5. H2A-H2B-APLF^{FAD}: H2A-H2B and APLF^{FAD} were mixed in assay buffer at a ratio of 1:2.5 H2A-H2B:APLF^{FAD} and purified on a Superdex 200 Increase 10/300 GL column (GE Healthcare Life Sciences) equilibrated in assay buffer and run at room temperature.
6. H3-H4-APLF^{FAD} (WT, peptide, and mutant), octamer-APLF^{FAD} (WT, titration with APLF^{FAD}), octamer-APLF^{FAD}mut (mutants): histone complexes and APLF^{FAD} were mixed in assay buffer at a ratio of 1:2 for $(H3\text{-}H4)_2$:APLF^{FAD} (WT, peptide, and mutant), 1:0.25 to 1:3 for octamer:APLF^{FAD} (WT, titration with APLF^{FAD}), and 1:2.5 for octamer:APLF^{FAD}mut (mutants)

Native mass spectrometry conditions

20 μL of each sample (20 μM concentration of purified complex or of the histones in mixtures with APLF^{FAD} in assay buffer) were buffer exchanged into 50-600 mM ammonium acetate, pH 7.5 using 3 kDa MWCO Amicon Ultra Centrifugal Filter Units (Merck Millipore). After buffer exchange the volume of each sample was ~40 μL. The samples were then measured at the Exactive Plus EMR.

ISOTHERMAL TITRATION CALORIMETRY

Calorimetric titrations of $APLF^{FAD}$ to H2A-H2B were performed in Ref. (45). A calorimetric titration of $APLF^{FAD}$ to $(H3\text{-}H4)_2$ or histone octamer mix was performed using a MicroCal VP-ITC microcalorimeter (Malvern Panalytical) at 25 °C. All proteins were buffer exchanged exhaustively using Amicon Ultra Centrifugal Filter Units (Merck Millipore) at 4 °C into assay buffer before use in the titration experiments. All solutions were degassed under vacuum for 5 minutes with gentle stirring immediately before use. For comparison between histone complexes, 5 μM $(H3\text{-}H4)_2$ or histone octamer was used in the sample cell and titrated with 90 μM $APLF^{FAD}$ in the injection syringe. For binding comparison between $(H3\text{-}H4)_2$ and $APLF^{FAD}$ WT, Y476A, W485A, or Y476A/W485A, 5 μM $(H3\text{-}H4)_2$ in the cell was titrated with 90 μM $APLF^{FAD}$ in the syringe. For all other mutational analyses, 10 μM $(H3\text{-}H4)_2$ (5 μM histone octamer) in the cell was titrated with 180 μM (90 μM) $APLF^{FAD}$ (WT or mutant) in the syringe. Binding isotherms were generated by plotting the heat change of the binding reaction against the ratio of total concentration of $APLF^{FAD}$ to total concentration of H3-H4 or histone octamer. The enthalpy of binding (ΔH, kcal mol^{-1}) was determined by integration of the injection peaks (5 μL) and correction for heats of dilution were determined from identical experiments without histone complexes. The entropy of binding (ΔS), the stoichiometry of binding (N), and the dissociation constant (K_D) were determined by fitting the resulting corrected binding isotherms by nonlinear least-squares analysis to a one set of sites binding model using the Origin software (MicroCal, Inc.). Errors in fit parameters are the standard errors derived from the regression analyses as reported by the software.

NMR EXPERIMENTS, BACKBONE ASSIGNMENTS AND TITRATION ANALYSIS

All NMR experiments were carried out on Bruker Avance III HD spectrometers. NMR spectra were processed using Bruker TopSpin and analyzed using Sparky (69). NMR titrations of $APLF^{FAD}$ with histone complexes at high salt were done at 900 MHz ^1H Larmor frequency at 298 K using sample containing 20 μM [^{15}N]$APLF^{FAD}$ in 25 mM NaPi, pH 7.0, 600 mM NaCl, 5% D_2O, 1x cOmplete EDTA-free Protease Inhibitor Cocktail (Roche). ^1H-^{15}N HSQC spectra were measured for the free $APLF^{FAD}$ and for its mixtures with unlabeled histone complexes (14 points from 1:0 to 1:2 for H2A-H2B or $(H3\text{-}H4)_2$). NMR titration of $APLF^{FAD}$ with H3-H4 at low salt was done at 900 MHz ^1H Larmor frequency at 308 K using sample containing 100 μM [^{15}N]$APLF^{FAD}$ at start in NMR titration buffer (25 mM NaPi, pH 7, 300 mM NaCl, 5% D_2O, 0.02% NaN_3, 1x cOmplete EDTA-free Protease Inhibitor Cocktail (Roche)). ^1H-^{15}N HSQC spectra were measured for the free $APLF^{FAD}$ and after each addition of unlabeled H3-H4 (5 points from 1:0 to 1:0.8 for H3-H4).
NMR titration of $APLF^{FAD}$ with 601-DNA was done at 750 MHz ^1H Larmor frequency at 298 K using sample containing 20 μM [^{15}N]$APLF^{FAD}$ at start in NMR titration buffer. ^1H-^{15}N HSQC spectra were measured for the free $APLF^{FAD}$ and after each addition of unlabeled 601-DNA (8 points from 1:0 to 1:1 for 601-DNA).
H2A-H2B refolded with [^2H/^{13}C/^{15}N]-labeled H2A and unlabeled H2B was used for NMR titration experiments with unlabeled $APLF^{FAD}$. Both $APLF^{FAD}$ and H2A-H2B samples were

buffer exchanged to NMR titration buffer (as above). ^{1}H-^{15}N TROSY spectra were measured for the free H2A-H2B (200 μM at start) and after each addition of $APLF^{FAD}$ at 308 K. The titration consisted of 12 points in the range of 1:0 and 4:1 molar ratio $APLF^{FAD}$:H2A-H2B on a 750 MHz spectrometer.
Reported peak intensity ratios are corrected for differences in protein concentration (due to dilution) and number of scans. Residue-specific chemical shift perturbations (CSPs) were quantified from the perturbations in the ^{1}H ($\Delta\delta_H$) and ^{15}N ($\Delta\delta_N$) dimensions as the weighted average (composite) CSP in ppm:

$$CSP = \sqrt{\Delta\delta_H{}^2 + (\Delta\delta_N/6.51)^2}.$$

Samples for assignment of H3 contained 325 μM [U-^{2}H/^{13}C/^{15}N]H3-H4 in NMR assignment buffer (290 mM acetic acid, pH 3.8, 1 mM EDTA, 5 mM BME, 5% D_2O, 0.02% NaN_3, 1x cOmplete EDTA-free Protease Inhibitor Cocktail (Roche)). Backbone assignments were based on TROSY-based HNCA, HN(CO)CA, HNCB, and HN(CO)CB spectra, recorded at 900 MHz ^{1}H Larmor frequency at 298 K. Available assignments were tentatively transferred to NMR titration conditions (H3-H4 NMR interaction buffer: 50 mM acetic acid, pH 5, 1 mM EDTA, 5 mM BME, 5% D_2O, 0.02% NaN_3, 1x cOmplete EDTA-free Protease Inhibitor Cocktail (Roche), at 308 K). A peptide corresponding to $APLF^{459-474}$ (sequence: PNEYDLNDSFLDDEEE) was ordered from Biomatik as TFA salt with N-terminal acetylation, C-terminal amidation and >95% purity. The peptide was dissolved in assay buffer supplemented with 1 mM EDTA and 5 mM BME. For an NMR interaction study to map the binding site on H3, 20 μM [U-^{2}H/^{13}C/^{15}N]H3-H4 was incubated with 0, 10, or 20 μM peptide in assay buffer supplemented with 1 mM EDTA and 5 mM BME for 30 minutes on ice and subsequently buffer exchanged to H3-H4 NMR interaction buffer using a 10 kDa molecular weight cut-off (MWCO) Amicon Ultra Centrifugal Filter Unit (Merck Millipore). ^{1}H-^{15}N TROSY spectra of these samples were measured on a 900 MHz spectrometer.

CHAPERONE ASSAY

The ratio of histone octamer to DNA that caused almost complete precipitation was determined experimentally at a ratio of 2.05 molar equivalents of histone octamer to DNA. For the assay, histone octamer (final reaction concentration: 2.05 μM) was pre-incubated alone or with 25, 50 or 100 molar equivalents of $APLF^{FAD}$ wildtype (WT) or mutants. Binding of chaperone to histone was allowed to proceed at room temperature (RT) for 15 min before the addition of DNA to a final concentration of 1 μM in a total reaction volume of 20 μl. Precipitation took place at RT for 1 h before the addition of 5 μl native PAGE loading buffer (10 mM Tris-HCl, pH 7.5, 1 mM EDTA, 1 mM DTT, 0.1 mM PMSF, 0.1 mg/ml BSA, 25% sucrose, 0.1% bromophenol blue), removal of precipitates by centrifugation, and separation of the remaining soluble complexes on a pre-equilibrated 5% polyacrylamide gel run in 0.2x TBE (17.8 mM Tris, 17.8 mM boric acid, 0.4 mM EDTA) buffer at 4 °C. The gel was stained with DNA stain G (SERVA) before visualization using a Molecular Imager Gel Doc XR System (Bio-Rad).

SMALL-ANGLE X-RAY SCATTERING (SAXS)

Samples for SAXS were prepared as follows in SAXS buffer (25 mM NaPi, pH 7.0, 300 mM NaCl, 3% v/v glycerol, 1 mM DTT):

1. Histone complexes buffer exchanged into SAXS buffer.
2. APLF^{FAD} buffer exchanged into SAXS buffer.
3. Octamer-APLF^{FAD} (WT, saturated): histone octamer mix and APLF^{FAD} were mixed in assay buffer at a ratio of 1:2.5 octamer:APLF^{FAD} and purified on a HiLoad 16/600 Superdex 200 pg column (GE Healthcare Life Sciences) equilibrated in SAXS buffer and run at 4 °C.
4. Octamer-APLF^{FAD} (WT, minimal complex): histone octamer mix and APLF^{FAD} in assay buffer were mixed at a ratio of 1:0.5 octamer:APLF^{FAD} and purified on a HiLoad 16/600 Superdex 200 pg column (GE Healthcare Life Sciences) equilibrated in SAXS buffer and run at 4 °C and fractions of the elution peak corresponding to the complex were pooled, concentrated and purified again.
5. Octamer-APLF^{FAD}-Δ (KR-motif deletion mutant): histone octamer mix and APLF^{FAD}-Δ were mixed at a ratio of 1:2.5 octamer:APLF^{FAD}-Δ and purified on a HiLoad 16/600 Superdex 200 pg column (GE Healthcare Life Sciences) equilibrated in SAXS buffer and run at 4 °C.

Synchrotron radiation X-ray scattering data from the various complexes in SEC-SAXS and standard batch mode were collected at the EMBL P12 beamline of the storage ring PETRA III (DESY, Hamburg, Germany) (70). Images were collected using a photon counting Pilatus-6M detector at a sample to detector distance of 3.1 m and a wavelength (λ) of 0.12 nm covering the range of momentum transfer (s) $0.15 < s < 5$ nm^{-1}; with $s=4\pi\sin\theta/\lambda$, where 2θ is the scattering angle. A continuous flow cell capillary was used to reduce radiation damage. The latter was monitored by collecting 20 successive 50 ms exposures, comparing the frames, and discarding those displaying significant alterations.

The data were normalized to the intensity of the transmitted beam and radially averaged; the scattering of pure buffer was used for background subtraction and the difference curves were scaled for solute concentration. The forward scattering $I(0)$, the radius of gyration (R_g) along with the probability distribution of the particle distances $P(r)$ and the maximal dimension (D_{max}) were computed using the automated SAXS data analysis pipeline SASFLOW (71) and various tools as implemented in ATSAS 2.8 package (72).

The molecular masses (MM) were evaluated by comparison of the forward scattering with that from reference solutions of bovine serum albumin. In addition, various concentration-independent methods were applied utilizing empirical relationships between MM and several structural parameters obtained directly from the data (73).

The *ab initio* bead modeling was performed using 10 independent runs of *DAMMIF* (74), from this the most probable model was selected for further analysis by *DAMAVER* (75).

CRYSOL (76) was used to calculate the scattering profile from the atomic model described here and to compare with the experimental data.

To quantitatively characterize mixtures of different oligomeric species, the program OLIGOMER (77) was used, which fits the observed experimental data by a weighted combination of the theoretical scattering curves (form factors) from different quaternary structures.

The experimental data and models will be deposited in SASBDB (78) with the accession codes: to be determined.

STRUCTURAL MODELING

Structural models for $APLF^{AD}$ (residues 460-490 and 460-511) were built by using the H3-H4 bound state of UBN1 (residues 130-142, PDB ID 4ZBJ (47)) and the H2A-H2B bound state of $APLF^{AD}$ (residues 471-490, modeled in Ref. (45), based on YL1 residues 39-59, PDB ID 5CHL (79)) for the model of $APLF^{460-490}$, and additionally, for $APLF^{460-511}$, the H2A.Z-H2B bound state of Chz1 (residues 16-35, PDB ID 2JSS (57)), as templates in the program MODELLER (http://salilab.org/modeller/) (80). These structures were used as input for docking to the histone octamer using the program HADDOCK (54). Structure of the histone octamer was taken from the *Dm.* nucleosome, PDB ID 2PYO (81). Docking was driven using unambiguous distance restraints to impose the anchor interactions of APLF residues Y476 and W485 with H2A-H2B as described in Ref. (45) and the anchor interactions of APLF residues Y462 and F468 with H3. Restraints were defined between ring heavy atoms of Y462 and heavy atoms of H3 K64, I89, G90, and Q93 as average distances observed for the corresponding tyrosine-keys in the structures of histone chaperones DAXX, UBN1, and MCM2 bound to H3-H4 (PDB ID 4HGA, 4ZBJ, and 5BNV (47,48,82)). The F468 restraints were defined between the center of F468 and heavy atoms of H3 R72, Q76, L82, R83, and F84 as observed for the corresponding phenylalanine in the structure of histone chaperone UBN1 bound to H3-H4 (PDB ID 4ZBJ (47)). For $APLF^{460-511}$, also distance restraints were used based on crosslinking data for the minimal octamer-$APLF^{AD}$ complex between APLF lysine residues 505 and 509 and H2B lysine residues 122 and 113, respectively. No active or passive residues were defined. The following semi-flexible segments were chosen for both $APLF^{460-490}$ and $APLF^{460-511}$: 460-464, 466-470, 474-478, and 483-487. The following fully-flexible segments were chosen for $APLF^{460-490}$: 465-465, 471-473, 479-482, and 488-490. The following fully-flexible segments were chosen for $APLF^{460-511}$: 465-465, 471-473, 479-482, and 488-511. In each case, the docking was done in two steps: a first molecule of either $APLF^{460-490}$ or $APLF^{460-511}$ was docked and the resulting structure was used for docking of a second molecule of either $APLF^{460-490}$ or $APLF^{460-511}$ by using the same restraints for both APLF moieties and by applying non-crystallographic symmetry restraints between them. Out of the 200 final water-refined structures, all clustered in a single cluster. The structure with lowest HADDOCK score was used for display. Validation statistics are reported in Tables S2 and S4.

REFERENCES

1. MacAlpine, D.M. and Almouzni, G. (2013) Chromatin and DNA replication. *Cold Spring Harb Perspect Biol*, **5**, a010207.
2. Li, B., Carey, M. and Workman, J.L. (2007) The role of chromatin during transcription. *Cell*, **128**, 707-719.
3. Papamichos-Chronakis, M. and Peterson, C.L. (2013) Chromatin and the genome integrity network. *Nat Rev Genet*, **14**, 62-75.
4. Smerdon, M.J. (1991) DNA repair and the role of chromatin structure. *Curr Opin Cell Biol*, **3**, 422-428.
5. Soria, G., Polo, S.E. and Almouzni, G. (2012) Prime, repair, restore: the active role of chromatin in the DNA damage response. *Mol Cell*, **46**, 722-734.
6. Luger, K., Mader, A.W., Richmond, R.K., Sargent, D.F. and Richmond, T.J. (1997) Crystal structure of the nucleosome core particle at 2.8 A resolution. *Nature*, **389**, 251-260.
7. Laskey, R.A., Honda, B.M., Mills, A.D. and Finch, J.T. (1978) Nucleosomes are assembled by an acidic protein which binds histones and transfers them to DNA. *Nature*, **275**, 416-420.
8. Akey, C.W. and Luger, K. (2003) Histone chaperones and nucleosome assembly. *Current Opinion in Structural Biology*, **13**, 6-14.
9. Eitoku, M., Sato, L., Senda, T. and Horikoshi, M. (2008) Histone chaperones: 30 years from isolation to elucidation of the mechanisms of nucleosome assembly and disassembly. *Cell Mol Life Sci*, **65**, 414-444.
10. Loyola, A. and Almouzni, G. (2004) Histone chaperones, a supporting role in the limelight. *Biochim Biophys Acta*, **1677**, 3-11.
11. De Koning, L., Corpet, A., Haber, J.E. and Almouzni, G. (2007) Histone chaperones: an escort network regulating histone traffic. *Nat Struct Mol Biol*, **14**, 997-1007.
12. Park, Y.J. and Luger, K. (2008) Histone chaperones in nucleosome eviction and histone exchange. *Curr Opin Struct Biol*, **18**, 282-289.
13. Mattiroli, F., D'Arcy, S. and Luger, K. (2015) The right place at the right time: chaperoning core histone variants. *EMBO Rep*, **16**, 1454-1466.
14. Hammond, C.M., Stromme, C.B., Huang, H., Patel, D.J. and Groth, A. (2017) Histone chaperone networks shaping chromatin function. *Nat Rev Mol Cell Biol*, **18**, 141-158.
15. Das, C., Tyler, J.K. and Churchill, M.E. (2010) The histone shuffle: histone chaperones in an energetic dance. *Trends Biochem Sci*, **35**, 476-489.
16. Warren, C. and Shechter, D. (2017) Fly Fishing for Histones: Catch and Release by Histone Chaperone Intrinsically Disordered Regions and Acidic Stretches. *J Mol Biol*, **429**, 2401-2426.
17. Borgia, A., Borgia, M.B., Bugge, K., Kissling, V.M., Heidarsson, P.O., Fernandes, C.B., Sottini, A., Soranno, A., Buholzer, K.J., Nettels, D. *et al.* (2018) Extreme disorder in an ultrahigh-affinity protein complex. *Nature*, **555**, 61-66.
18. Ivic, N., Potocnjak, M., Solis-Mezarino, V., Herzog, F., Bilokapic, S. and Halic, M. (2019) Fuzzy Interactions Form and Shape the Histone Transport Complex. *Mol Cell*.
19. Elsasser, S.J. and D'Arcy, S. (2013) Towards a mechanism for histone chaperones. *Biochim Biophys Acta*, **1819**, 211-221.
20. Andrews, A.J., Downing, G., Brown, K., Park, Y.J. and Luger, K. (2008) A thermodynamic model for Nap1-histone interactions. *J Biol Chem*, **283**, 32412-32418.
21. Andrews, A.J., Chen, X., Zevin, A., Stargell, L.A. and Luger, K. (2010) The histone chaperone Nap1 promotes nucleosome assembly by eliminating nonnucleosomal histone DNA interactions. *Mol Cell*, **37**, 834-842.
22. Ransom, M., Dennehey, B.K. and Tyler, J.K. (2010) Chaperoning histones during DNA replication and repair. *Cell*, **140**, 183-195.
23. Burgess, R.J. and Zhang, Z. (2013) Histone chaperones in nucleosome assembly and human disease. *Nat Struct Mol Biol*, **20**, 14-22.
24. Chen, C.C., Carson, J.J., Feser, J., Tamburini, B., Zabaronick, S., Linger, J. and Tyler, J.K. (2008) Acetylated lysine 56 on histone H3 drives chromatin assembly after repair and signals for the completion of repair. *Cell*, **134**, 231-243.
25. Kim, J.A. and Haber, J.E. (2009) Chromatin assembly factors Asf1 and CAF-1 have overlapping roles in deactivating the DNA damage checkpoint when DNA repair is complete. *Proc Natl Acad Sci U S A*, **106**, 1151-1156.
26. Piquet, S., Le Parc, F., Bai, S.K., Chevallier, O., Adam, S. and Polo, S.E. (2018) The Histone Chaperone FACT Coordinates H2A.X-Dependent Signaling and Repair of DNA Damage. *Mol Cell*, **72**, 888-901 e887.
27. Bekker-Jensen, S., Fugger, K., Danielsen, J.R., Gromova, I., Sehested, M., Celis, J., Bartek, J., Lukas, J. and Mailand, N. (2007) Human Xip1 (C2orf13) is a novel regulator of cellular responses to DNA strand breaks. *J Biol Chem*, **282**, 19638-19643.

28. Iles, N., Rulten, S., El-Khamisy, S.F. and Caldecott, K.W. (2007) APLF (C2orf13) is a novel human protein involved in the cellular response to chromosomal DNA strand breaks. *Mol Cell Biol*, **27**, 3793-3803.
29. Macrae, C.J., McCulloch, R.D., Ylanko, J., Durocher, D. and Koch, C.A. (2008) APLF (C2orf13) facilitates nonhomologous end-joining and undergoes ATM-dependent hyperphosphorylation following ionizing radiation. *DNA Repair (Amst)*, **7**, 292-302.
30. Rulten, S.L., Fisher, A.E., Robert, I., Zuma, M.C., Rouleau, M., Ju, L., Poirier, G., Reina-San-Martin, B. and Caldecott, K.W. (2011) PARP-3 and APLF function together to accelerate nonhomologous end-joining. *Mol Cell*, **41**, 33-45.
31. Fenton, A.L., Shirodkar, P., Macrae, C.J., Meng, L. and Koch, C.A. (2013) The PARP3- and ATM-dependent phosphorylation of APLF facilitates DNA double-strand break repair. *Nucleic Acids Res*, **41**, 4080-4092.
32. Grundy, G.J., Rulten, S.L., Zeng, Z., Arribas-Bosacoma, R., Iles, N., Manley, K., Oliver, A. and Caldecott, K.W. (2013) APLF promotes the assembly and activity of non-homologous end joining protein complexes. *EMBO J*, **32**, 112-125.
33. Williams, G.J., Hammel, M., Radhakrishnan, S.K., Ramsden, D., Lees-Miller, S.P. and Tainer, J.A. (2014) Structural insights into NHEJ: building up an integrated picture of the dynamic DSB repair super complex, one component and interaction at a time. *DNA Repair (Amst)*, **17**, 110-120.
34. Kanno, S., Kuzuoka, H., Sasao, S., Hong, Z., Lan, L., Nakajima, S. and Yasui, A. (2007) A novel human AP endonuclease with conserved zinc-finger-like motifs involved in DNA strand break responses. *EMBO J*, **26**, 2094-2103.
35. Rulten, S.L., Cortes-Ledesma, F., Guo, L., Iles, N.J. and Caldecott, K.W. (2008) APLF (C2orf13) is a novel component of poly(ADP-ribose) signaling in mammalian cells. *Mol Cell Biol*, **28**, 4620-4628.
36. Ahel, I., Ahel, D., Matsusaka, T., Clark, A.J., Pines, J., Boulton, S.J. and West, S.C. (2008) Poly(ADP-ribose)-binding zinc finger motifs in DNA repair/checkpoint proteins. *Nature*, **451**, 81-85.
37. Li, G.Y., McCulloch, R.D., Fenton, A.L., Cheung, M., Meng, L., Ikura, M. and Koch, C.A. (2010) Structure and identification of ADP-ribose recognition motifs of APLF and role in the DNA damage response. *Proc Natl Acad Sci U S A*, **107**, 9129-9134.
38. Eustermann, S., Brockmann, C., Mehrotra, P.V., Yang, J.C., Loakes, D., West, S.C., Ahel, I. and Neuhaus, D. (2010) Solution structures of the two PBZ domains from human APLF and their interaction with poly(ADP-ribose). *Nat Struct Mol Biol*, **17**, 241-243.
39. Shirodkar, P., Fenton, A.L., Meng, L. and Koch, C.A. (2013) Identification and functional characterization of a Ku-binding motif in aprataxin polynucleotide kinase/phosphatase-like factor (APLF). *J Biol Chem*, **288**, 19604-19613.
40. Cherry, A.L., Nott, T.J., Kelly, G., Rulten, S.L., Caldecott, K.W. and Smerdon, S.J. (2015) Versatility in phospho-dependent molecular recognition of the XRCC1 and XRCC4 DNA-damage scaffolds by aprataxin-family FHA domains. *DNA Repair (Amst)*, **35**, 116-125.
41. Hammel, M., Yu, Y., Radhakrishnan, S.K., Chokshi, C., Tsai, M.S., Matsumoto, Y., Kuzdovich, M., Remesh, S.G., Fang, S., Tomkinson, A.E. *et al.* (2016) An Intrinsically Disordered APLF Links Ku, DNA-PKcs, and XRCC4-DNA Ligase IV in an Extended Flexible Non-homologous End Joining Complex. *J Biol Chem*, **291**, 26987-27006.
42. Kim, K., Pedersen, L.C., Kirby, T.W., DeRose, E.F. and London, R.E. (2017) Characterization of the APLF FHA-XRCC1 phosphopeptide interaction and its structural and functional implications. *Nucleic Acids Res*, **45**, 12374-12387.
43. Nemoz, C., Ropars, V., Frit, P., Gontier, A., Drevet, P., Yu, J., Guerois, R., Pitois, A., Comte, A., Delteil, C. *et al.* (2018) XLF and APLF bind Ku80 at two remote sites to ensure DNA repair by non-homologous end joining. *Nat Struct Mol Biol*, **25**, 971-980.
44. Mehrotra, P.V., Ahel, D., Ryan, D.P., Weston, R., Wiechens, N., Kraehenbuehl, R., Owen-Hughes, T. and Ahel, I. (2011) DNA repair factor APLF is a histone chaperone. *Mol Cell*, **41**, 46-55.
45. Corbeski, I., Dolinar, K., Wienk, H., Boelens, R. and van Ingen, H. (2018) DNA repair factor APLF acts as a H2A-H2B histone chaperone through binding its DNA interaction surface. *Nucleic Acids Res*, **46**, 7138-7152.
46. Bich, C., Baer, S., Jecklin, M.C. and Zenobi, R. (2010) Probing the hydrophobic effect of noncovalent complexes by mass spectrometry. *J Am Soc Mass Spectrom*, **21**, 286-289.
47. Ricketts, M.D., Frederick, B., Hoff, H., Tang, Y., Schultz, D.C., Singh Rai, T., Grazia Vizioli, M., Adams, P.D. and Marmorstein, R. (2015) Ubinuclein-1 confers histone H3.3-specific-binding by the HIRA histone chaperone complex. *Nat Commun*, **6**, 7711.
48. Huang, H., Stromme, C.B., Saredi, G., Hodl, M., Strandsby, A., Gonzalez-Aguilera, C., Chen, S., Groth, A. and Patel, D.J. (2015) A unique binding mode enables MCM2 to chaperone histones H3-H4 at replication forks. *Nat Struct Mol Biol*, **22**, 618-626.
49. Ricketts, M.D., Han, J., Szurgot, M.R. and Marmorstein, R. (2019) Molecular basis for chromatin assembly and modification by multiprotein complexes. *Protein Sci*, **28**, 329-343.
50. Karantza, V., Freire, E. and Moudrianakis, E.N. (1996) Thermodynamic studies of the core histones: pH and ionic strength effects on the stability of the (H3-H4)/(H3-H4)2 system. *Biochemistry*, **35**, 2037-2046.

51. Wood, M.J., Yau, P., Imai, B.S., Goldberg, M.W., Lambert, S.J., Fowler, A.G., Baldwin, J.P., Godfrey, J.E., Moudrianakis, E.N., Koch, M.H. *et al.* (1991) Neutron and x-ray scatter studies of the histone octamer and amino and carboxyl domain trimmed octamers. *J Biol Chem*, **266**, 5696-5702.
52. Lambert, S., Muyldermans, S., Baldwin, J., Kilner, J., Ibel, K. and Wijns, L. (1991) Neutron scattering studies of chromatosomes. *Biochem Biophys Res Commun*, **179**, 810-816.
53. Matthew Allen Bullock, J., Schwab, J., Thalassinos, K. and Topf, M. (2016) The Importance of Non-accessible Crosslinks and Solvent Accessible Surface Distance in Modeling Proteins with Restraints From Crosslinking Mass Spectrometry. *Mol Cell Proteomics*, **15**, 2491-2500.
54. van Zundert, G.C., Rodrigues, J.P., Trellet, M., Schmitz, C., Kastritis, P.L., Karaca, E., Melquiond, A.S., van Dijk, M., de Vries, S.J. and Bonvin, A.M. (2016) The HADDOCK2.2 Web Server: User-Friendly Integrative Modeling of Biomolecular Complexes. *J Mol Biol*, **428**, 720-725.
55. Hondele, M., Stuwe, T., Hassler, M., Halbach, F., Bowman, A., Zhang, E.T., Nijmeijer, B., Kotthoff, C., Rybin, V., Amlacher, S. *et al.* (2013) Structural basis of histone H2A-H2B recognition by the essential chaperone FACT. *Nature*, **499**, 111-114.
56. Luk, E., Vu, N.D., Patteson, K., Mizuguchi, G., Wu, W.H., Ranjan, A., Backus, J., Sen, S., Lewis, M., Bai, Y. *et al.* (2007) Chz1, a nuclear chaperone for histone H2AZ. *Mol Cell*, **25**, 357-368.
57. Zhou, Z., Feng, H., Hansen, D.F., Kato, H., Luk, E., Freedberg, D.I., Kay, L.E., Wu, C. and Bai, Y. (2008) NMR structure of chaperone Chz1 complexed with histones H2A.Z-H2B. *Nat Struct Mol Biol*, **15**, 868-869.
58. Tsunaka, Y., Fujiwara, Y., Oyama, T., Hirose, S. and Morikawa, K. (2016) Integrated molecular mechanism directing nucleosome reorganization by human FACT. *Genes Dev*, **30**, 673-686.
59. Mattiroli, F., Gu, Y., Yadav, T., Balsbaugh, J.L., Harris, M.R., Findlay, E.S., Liu, Y., Radebaugh, C.A., Stargell, L.A., Ahn, N.G. *et al.* (2017) DNA-mediated association of two histone-bound complexes of yeast Chromatin Assembly Factor-1 (CAF-1) drives tetrasome assembly in the wake of DNA replication. *Elife*, **6**.
60. Sauer, P.V., Timm, J., Liu, D., Sitbon, D., Boeri-Erba, E., Velours, C., Mucke, N., Langowski, J., Ochsenbein, F., Almouzni, G. *et al.* (2017) Insights into the molecular architecture and histone H3-H4 deposition mechanism of yeast Chromatin assembly factor 1. *Elife*, **6**.
61. Zheng, S., Crickard, J.B., Srikanth, A. and Reese, J.C. (2013) A Highly Conserved Region within H2B Is Important for FACT To Act on Nucleosomes. *Molecular and Cellular Biology*, **34**, 303-314.
62. Wang, T., Liu, Y., Edwards, G., Krzizike, D., Scherman, H. and Luger, K. (2018) The histone chaperone FACT modulates nucleosome structure by tethering its components. *Life Science Alliance*, **1**.
63. Liu, Z. and Huang, Y. (2014) Advantages of proteins being disordered. *Protein Sci*, **23**, 539-550.
64. Berlow, R.B., Dyson, H.J. and Wright, P.E. (2015) Functional advantages of dynamic protein disorder. *FEBS Lett*, **589**, 2433-2440.
65. Luger, K., Rechsteiner, T.J. and Richmond, T.J. (1999) Preparation of nucleosome core particle from recombinant histones. *Methods Enzymol*, **304**, 3-19.
66. Thastrom, A., Bingham, L.M. and Widom, J. (2004) Nucleosomal locations of dominant DNA sequence motifs for histone-DNA interactions and nucleosome positioning. *J Mol Biol*, **338**, 695-709.
67. Lowary, P.T. and Widom, J. (1998) New DNA sequence rules for high affinity binding to histone octamer and sequence-directed nucleosome positioning. *J Mol Biol*, **276**, 19-42.
68. Liu, F., Lossl, P., Scheltema, R., Viner, R. and Heck, A.J.R. (2017) Optimized fragmentation schemes and data analysis strategies for proteome-wide cross-link identification. *Nat Commun*, **8**, 15473.
69. Lee, W., Tonelli, M. and Markley, J.L. (2015) NMRFAM-SPARKY: enhanced software for biomolecular NMR spectroscopy. *Bioinformatics*, **31**, 1325-1327.
70. Blanchet, C.E., Spilotros, A., Schwemmer, F., Graewert, M.A., Kikhney, A., Jeffries, C.M., Franke, D., Mark, D., Zengerle, R., Cipriani, F. *et al.* (2015) Versatile sample environments and automation for biological solution X-ray scattering experiments at the P12 beamline (PETRA III, DESY). *J Appl Crystallogr*, **48**, 431-443.
71. Franke, D., Kikhney, A.G. and Svergun, D.I. (2012) Automated acquisition and analysis of small angle X-ray scattering data. *Nuclear Instruments and Methods in Physics Research Section A: Accelerators, Spectrometers, Detectors and Associated Equipment*, **689**, 52-59.
72. Franke, D., Petoukhov, M.V., Konarev, P.V., Panjkovich, A., Tuukkanen, A., Mertens, H.D.T., Kikhney, A.G., Hajizadeh, N.R., Franklin, J.M., Jeffries, C.M. *et al.* (2017) ATSAS 2.8: a comprehensive data analysis suite for small-angle scattering from macromolecular solutions. *J Appl Crystallogr*, **50**, 1212-1225.
73. Hajizadeh, N.R., Franke, D., Jeffries, C.M. and Svergun, D.I. (2018) Consensus Bayesian assessment of protein molecular mass from solution X-ray scattering data. *Sci Rep*, **8**, 7204.
74. Franke, D. and Svergun, D.I. (2009) DAMMIF, a program for rapid ab-initio shape determination in small-angle scattering. *J Appl Crystallogr*, **42**, 342-346.
75. Volkov, V.V. and Svergun, D.I. (2003) Uniqueness of ab initio shape determination in small-angle scattering. *Journal of Applied Crystallography*, **36**, 860-864.
76. Svergun, D., Barberato, C. and Koch, M.H.J. (1995) CRYSOL - a Program to Evaluate X-ray Solution Scattering of Biological Macromolecules from Atomic Coordinates. *Journal of Applied Crystallography*, **28**, 768-773.

77. Konarev, P.V., Volkov, V.V., Sokolova, A.V., Koch, M.H.J. and Svergun, D.I. (2003) PRIMUS: a Windows PC-based system for small-angle scattering data analysis. *Journal of Applied Crystallography*, **36**, 1277-1282.
78. Valentini, E., Kikhney, A.G., Previtali, G., Jeffries, C.M. and Svergun, D.I. (2015) SASBDB, a repository for biological small-angle scattering data. *Nucleic Acids Res*, **43**, D357-363.
79. Liang, X., Shan, S., Pan, L., Zhao, J., Ranjan, A., Wang, F., Zhang, Z., Huang, Y., Feng, H., Wei, D. *et al.* (2016) Structural basis of H2A.Z recognition by SRCAP chromatin-remodeling subunit YL1. *Nat Struct Mol Biol*, **23**, 317-323.
80. Webb, B. and Sali, A. (2016) Comparative Protein Structure Modeling Using MODELLER. *Curr Protoc Protein Sci*, **86**, 2 9 1-2 9 37.
81. Clapier, C.R., Chakravarthy, S., Petosa, C., Fernandez-Tornero, C., Luger, K. and Muller, C.W. (2008) Structure of the Drosophila nucleosome core particle highlights evolutionary constraints on the H2A-H2B histone dimer. *Proteins*, **71**, 1-7.
82. Elsasser, S.J., Huang, H., Lewis, P.W., Chin, J.W., Allis, C.D. and Patel, D.J. (2012) DAXX envelops a histone H3.3-H4 dimer for H3.3-specific recognition. *Nature*, **491**, 560-565.

SUPPORTING INFORMATION

Table S1. SAXS data summary of histone octamer mix and octamer-APLF^{AD} WT complex.

Sample	R_g[a] [nm]	D_{max}[b] [nm]	MM_{exp}[c] [kDa]	MW_{th}[d] [kDa]
Histone octamer mix	3.51	10.5	91.20 (87.00-99.20)	107.06
Octamer-APLF^{AD} WT (@ 1.7 mg/ml)	3.96	14.6	130.90 (121.50-151.50)	122.49
Octamer-APLF^{AD} WT (@ 4.8 mg/ml)	4.00	13.6	146.80 (142.00-176.00)	122.49

[a] Radius of gyration.
[b] Maximum interatomic distance.
[c] Experimental molecular mass with range given in brackets.
[d] Theoretical molecular weight based on protein sequence.

Table S2. Structural quality of the histone octamer-APLF$^{460-490}$ model[a].

	APLF$^{460-490}$	Octamer-APLF$^{460-490}$
Ramachandran analysis[b]	100/72/0	99/93/1
Number of clashes[c]	2	14[d]

[a] Scores are reported for only the APLF$^{460-490}$ chain and the full model for the lowest energy HADDOCK structure.
[b] Percentage Ramachandran allowed/favored/outliers, as reported by MolProbity webserver (3).
[c] Number of clashes > 0.4 Å, as reported by MolProbity webserver (3).
[d] Intermolecular clashes only.

Table S3. SAXS data summary of histone octamer-APLF^{FAD} WT and -APLF^{FAD}-Δ complexes.

Sample	R_g[a] [nm]	D_{max}[b] [nm]	MM_{exp}[c] [kDa]	MW_{th}[d] [kDa]
Octamer-APLF^{FAD} WT	3.96	14.6	130.90 (121.50-151.50)	122.49
Octamer-APLF^{FAD}-Δ	3.50	10.5	113.65 (102.90-121.40)	117.05

[a] Radius of gyration.
[b] Maximum interatomic distance.
[c] Experimental molecular mass with range given in brackets.
[d] Theoretical molecular weight based on protein sequence.

Table S4. Structural quality of the histone octamer-APLF$^{460-511}$ model[a].

	APLF$^{460-511}$	Octamer-APLF$^{460-511}$
Ramachandran analysis[b]	98/80/2	99/93/1
Number of clashes[c]	3	15[d]

[a] Scores are reported for only the APLF$^{460-511}$ chain and the full model for the lowest energy HADDOCK structure.
[b] Percentage Ramachandran allowed/favored/outliers, as reported by MolProbity webserver (3).
[c] Number of clashes > 0.4 Å, as reported by MolProbity webserver (3).
[d] Intermolecular clashes only.

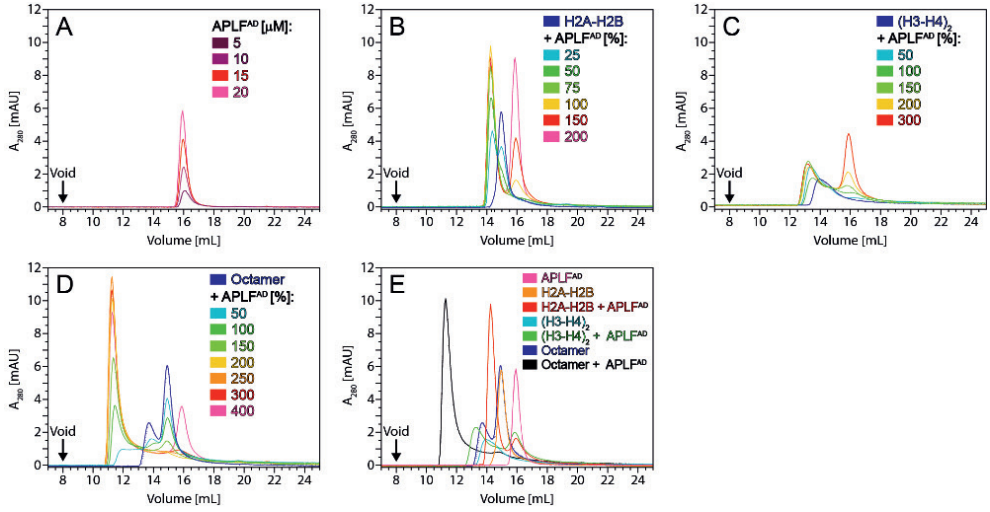

Figure S1. Analytical gel filtration assay of APLF^{FAD}, histone complexes and their mixtures. (A) APLF^{FAD} alone at different concentrations does not form higher molecular weight species. (B) H2A-H2B alone elutes as dimer and forms one specific higher molecular weight complex upon addition of APLF^{FAD}. (C) (H3-H4)$_2$ alone elutes in a peak broadened towards lower molecular weight species, most likely due to an equilibrium with H3-H4 dimers under the experimental conditions, and forms one specific higher molecular weight complex upon addition of APLF^{FAD}. (D) The histone octamer mix elutes in two peaks corresponding to H2A-H2B and (H3-H4)$_2$ and forms one specific higher molecular weight complex upon addition of APLF^{FAD}. (E) Overlay of chromatograms taken from A-D for direct comparison of the individual components and their complexes. Experiments were performed in 25 mM NaPi, pH 7.0, 300 mM NaCl, at room temperature.

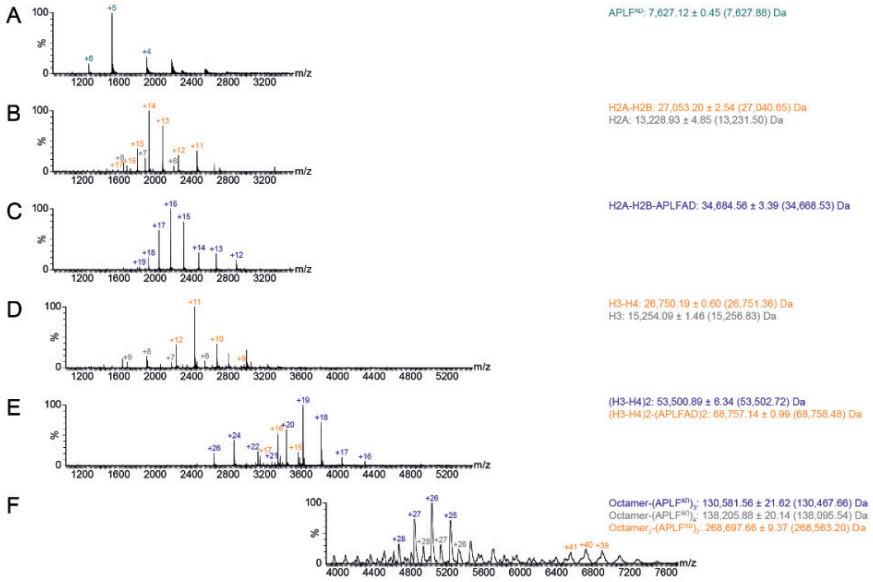

Figure S2. Native mass spectra of APLF^{AD}, histones and their complexes. APLF^{AD} (A), H2A-H2B (B) and H3-H4 (D) alone. H3-H4 is a dimer under these conditions. H2A-H2B-APLF^{AD} (C) and (H3-H4)$_2$-(APLF^{AD})$_2$ (E) complexes as in Figure 1 upper and middle panel, respectively, with charge states. (F) Histone octamer-APLF^{AD} preparation containing different complexes. All samples were in 50 mM ammonium acetate, pH 7.5.

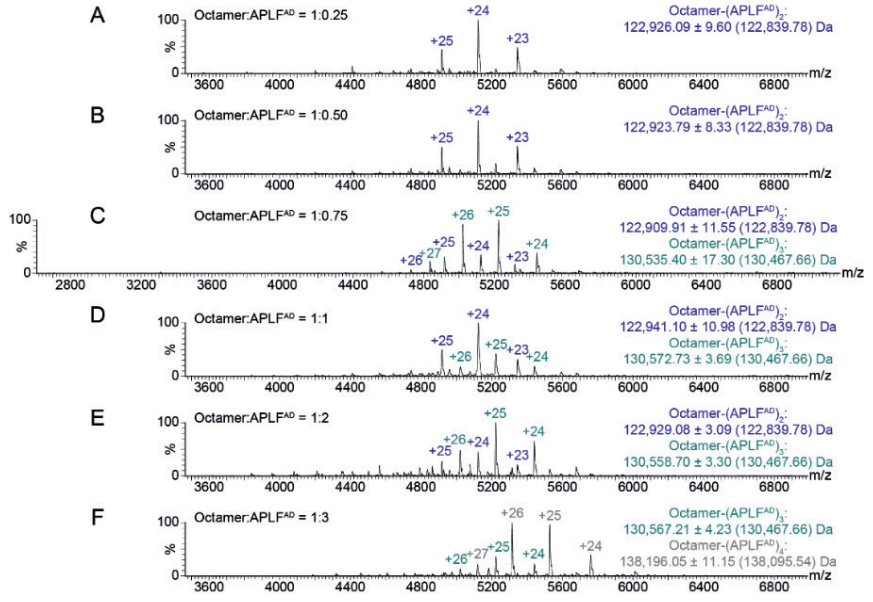

Figure S3. Native mass spectra of histone octamer mixes with different concentrations of APLF^{AD}. At 25-50% APLF^{AD} (A,B) the minimal complex is the only detectable species. With increasing concentrations (C-F), a 3rd (C-E) and 4th (F) molecule of APLF^{AD} associate with the octamer. All samples were in 300 mM ammonium acetate, pH 7.5.

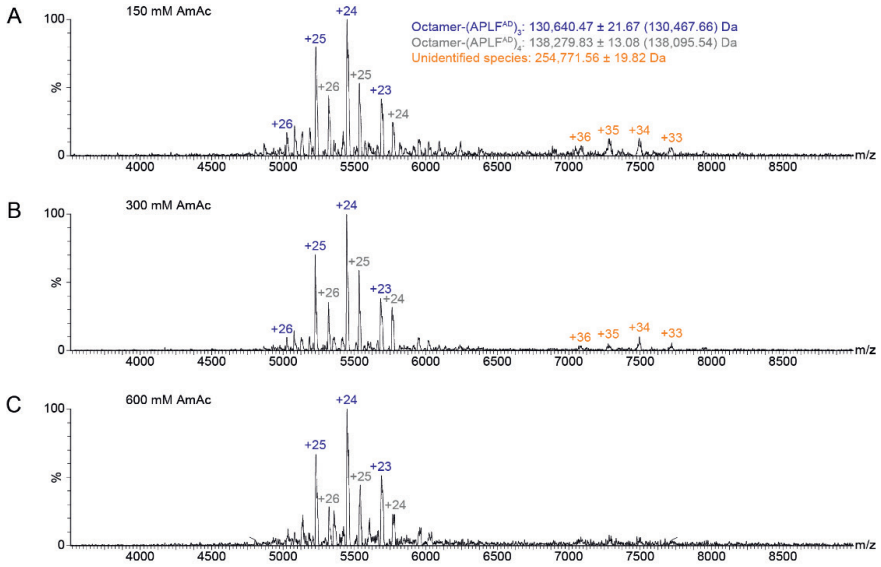

Figure S4. Native mass spectra of octamer-APLF^{AD} complex at different ionic strengths show stable association of 3rd and 4th APLF^{AD} molecules. Samples were in the ammonium acetate (AmAc) ionic strengths indicated for each panel at pH 7.5.

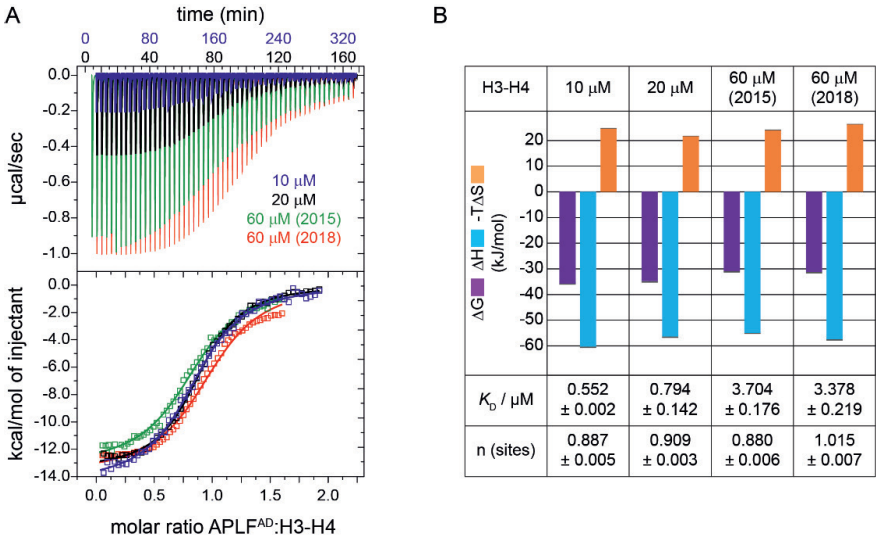

Figure S5. ITC of APLF^{AD} to H3-H4 showing the effect of different histone concentrations on the determined K_D and consistency of preparations and experimental setups. (A) ITC titration curves including raw data of experiments with different histone concentrations and done at different time points (year in brackets). For the experiment with 10 µM H3-H4 a longer injection time interval was used (blue upper x-axis). The resulting binding isotherms were fit to a one-set-of-sites binding mode. (B) ITC derived best-fit values and fitting errors are shown in the table, the derived thermodynamic parameters in the histogram. Experiments were performed in 25 mM NaPi, pH 7.0, 300 mM NaCl, at 25 °C.

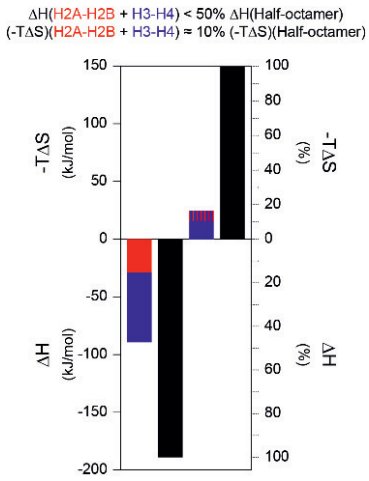

Figure S6. Disproportionate enthalpy and entropy loss upon octamer-APLF^{AD} binding. Comparison of thermodynamics of APLF^{AD} binding individually to H2A-H2B (red) or H3-H4 (blue) and the histone half-octamer (H2A-H2B-H3-H4) (black). The added enthalpies of binding (lower part of the histogram) of H2A-H2B and H3-H4 are less than 50% of the enthalpy of binding of the half-octamer indicating a synergistic binding effect and the formation of additional histone-histone contacts in the complex with APLF^{AD}. The added entropies of binding (upper part of the histogram) of H2A-H2B (dashed to indicate a reversed sign) and H3-H4 are less than 10% of the entropy of binding of the half-octamer indicating complex formation.

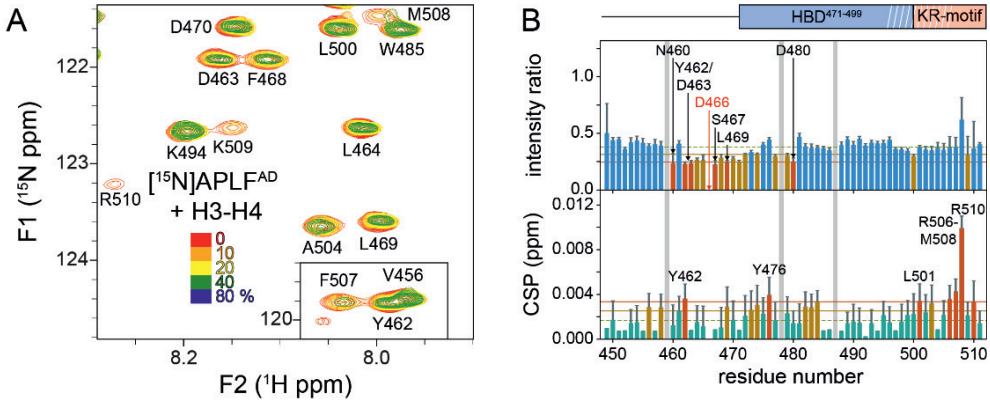

Figure S7. APLF^{AD} interacts strongly with H3-H4 at low salt concentration. (A) Zoomed region of overlaid ^{1}H-^{15}N TROSY spectra of APLF^{AD} with increasing concentrations of H3-H4. The inset shows the region containing the Y462 backbone resonance. Color coding indicated in the figure. At 80% histone complex added, signal intensities dropped below the shown contour levels and at even higher histone concentrations signals completely disappeared due to protein precipitation. Recorded at 900 MHz ^{1}H Larmor frequency at 35 °C in 25 mM NaPi buffer, pH 7.0 with 300 mM NaCl, 100 µM APLF^{AD} at start. (B) Analysis of APLF^{AD} ^{1}H-^{15}N peak intensity ratios (upper panel) and weighted average CSPs (lower panel) after adding 40% H3-H4. Resonances with intensity ratios less than 2 (1) standard deviation (SD) (orange (yellow) line) from the 10% trimmed mean (green dashed line) are highlighted in orange (yellow), indicated with black arrows and labeled. Resonances that disappeared during the titration are indicated by red arrows and labels. Resonances with CSPs more than 2 (1) standard deviation (SD) (orange (yellow) line) from the 10% trimmed mean (green dashed line) are highlighted in orange (yellow) and labeled. Position of the HBD and KR-motif are indicated above the plots, white stripes denote the helical region. Residues without titration data due to overlap or missing resonances are indicated with gray bars.

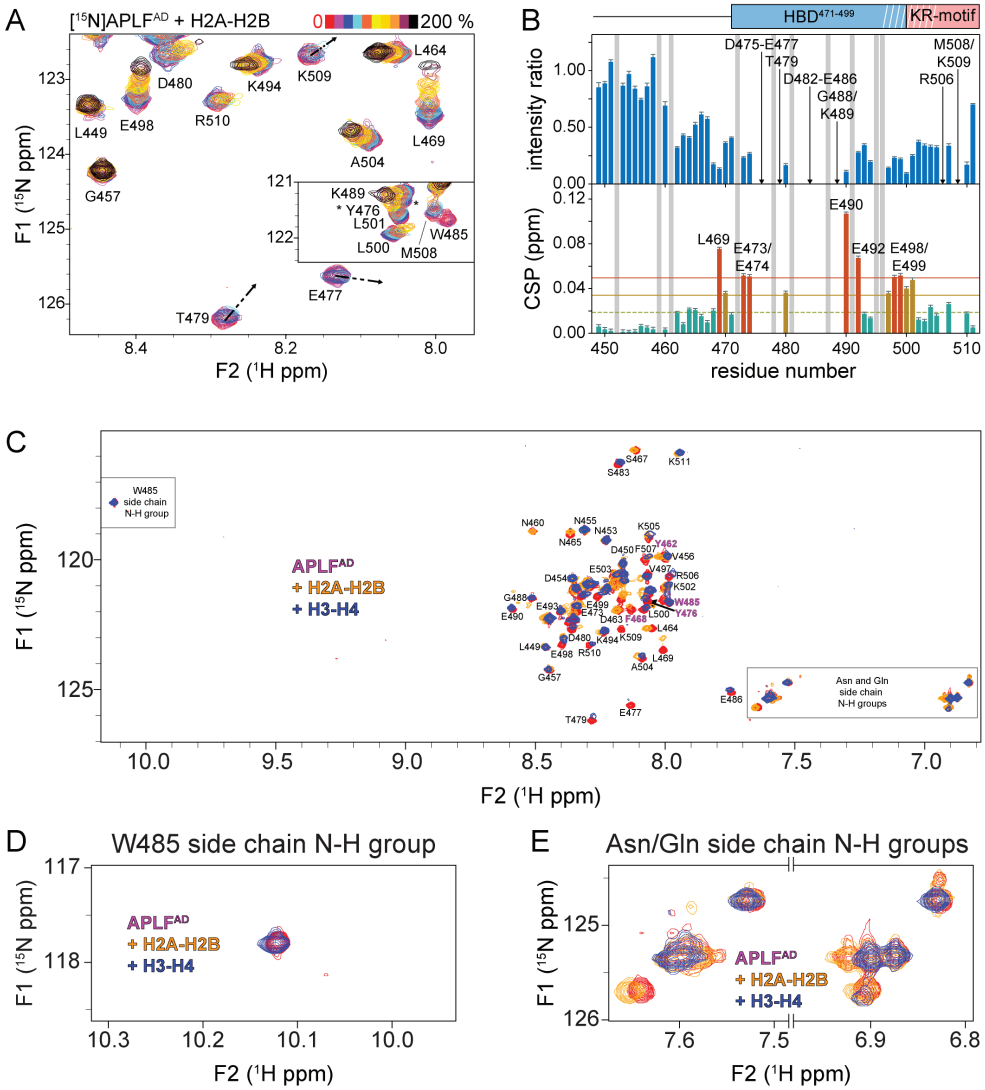

Figure S8. APLF^{AD} interacts with H2A-H2B and H3-H4 through different binding sites. (A,B) APLF^{AD} interacts with H2A-H2B through its HBD also at high salt. (A) Zoomed region of overlaid ^{1}H-^{15}N HSQC spectra of APLF^{AD} with increasing concentrations of H2A-H2B. The inset shows the region containing the Y476 and W485 backbone resonances. Color coding indicated on top. Direction of peak shifts for disappearing resonances is indicated with arrows. Recorded at 900 MHz ^{1}H Larmor frequency at 25 °C in 25 mM NaPi buffer, pH 7.0 with 600 mM NaCl, 20 µM APLF^{AD}. (B) Analysis of APLF^{AD} ^{1}H-^{15}N peak intensity ratios (upper panel) and weighted average CSPs (lower panel) between H2A-H2B bound (2:1 molar ratio of H2A-H2B:APLF^{AD}) and free APLF^{AD}. Resonances that disappear during the titration are indicated by arrows and labeled. Resonances with CSPs more than 2 (1) standard deviation (SD) (orange (yellow) line) from the 10% trimmed mean (green dashed line) are highlighted in orange (yellow). Position of the HBD and KR-motif indicated above the plot, white stripes denote the helical region. Residues without titration data due to overlap or missing resonances are indicated with gray bars. (C) Overlaid ^{1}H-^{15}N HSQC spectra of APLF^{AD} (red), and APLF^{AD} in complex with H2A-H2B (orange) or H3-H4 (blue) with selected resonances labeled. The aromatic anchor residues are labeled magenta. Rectangles with labels indicate side chain amine resonances (note: peaks are aliased). (D) As (C), zoomed region of the W485 side chain amine group. (E) As (C), zoomed region of the Asn/Gln side chain amine groups.

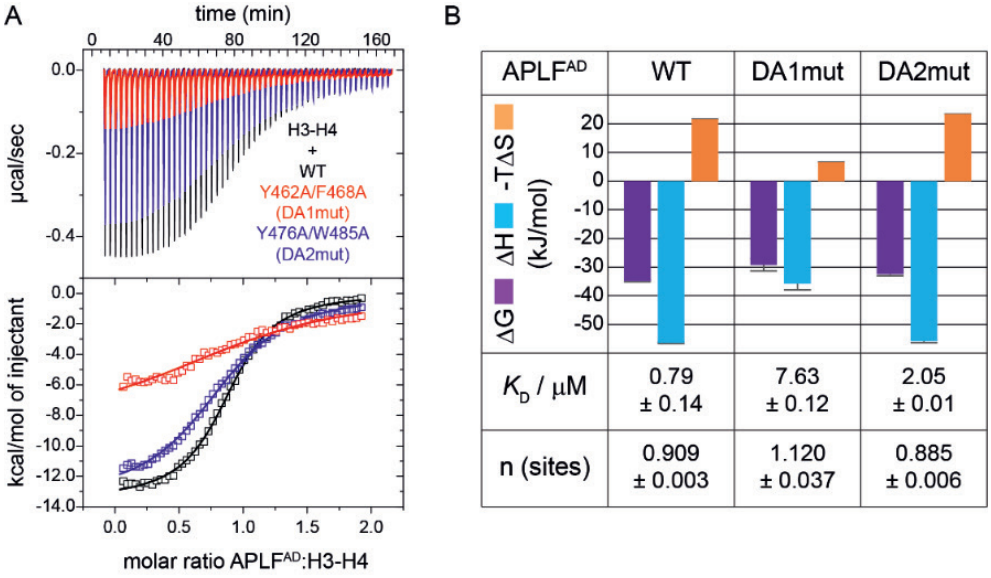

Figure S9. APLF^{AD} interacts with H3-H4 mainly through its Y462/F468 double-aromatic anchor. (A) ITC of APLF^{AD} WT or double-aromatic anchor mutants to H3-H4. The resulting binding isotherms were fit to a one-set-of-sites binding mode. (B) ITC best-fit values and fitting errors together with the derived thermodynamic parameters. All data were obtained in 25 mM NaPi, pH 7.0, 300 mM NaCl, at 25 °C.

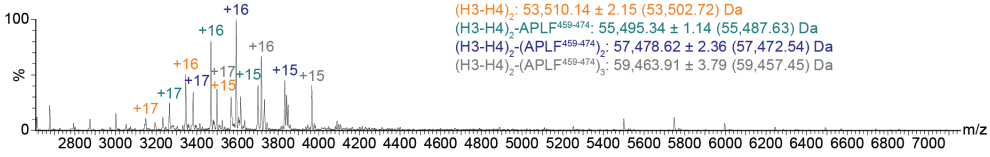

Figure S10. Native mass spectrum of a mixture of H3-H4 with the synthetic peptide APLF$^{459-474}$ shows complex formation. The expected $(H3\text{-}H4)_2$-$(APLF^{459-474})_2$ is formed as the most abundant complex (based on RSI). Sample was in 300 mM ammonium acetate, pH 7.5.

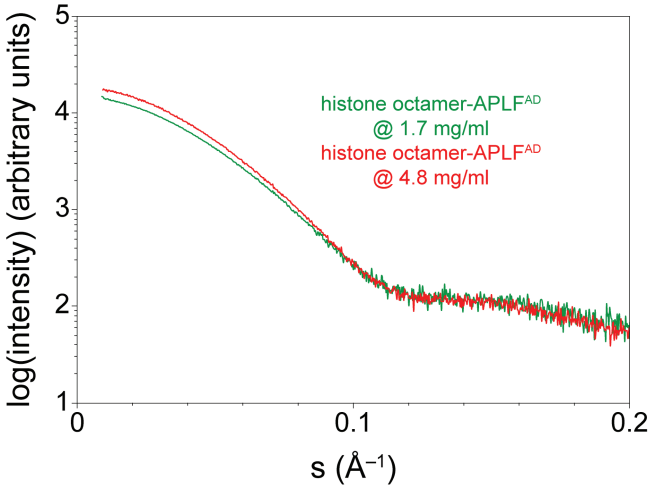

Figure S11. Batch mode SAXS data for histone octamer-APLF^{AD} WT. A slight tendency for oligomerization at higher concentrations (4.8 mg/ml, red) is indicated by higher intensity at low *s* values compared to a lower concentration (1.7 mg/ml, green).

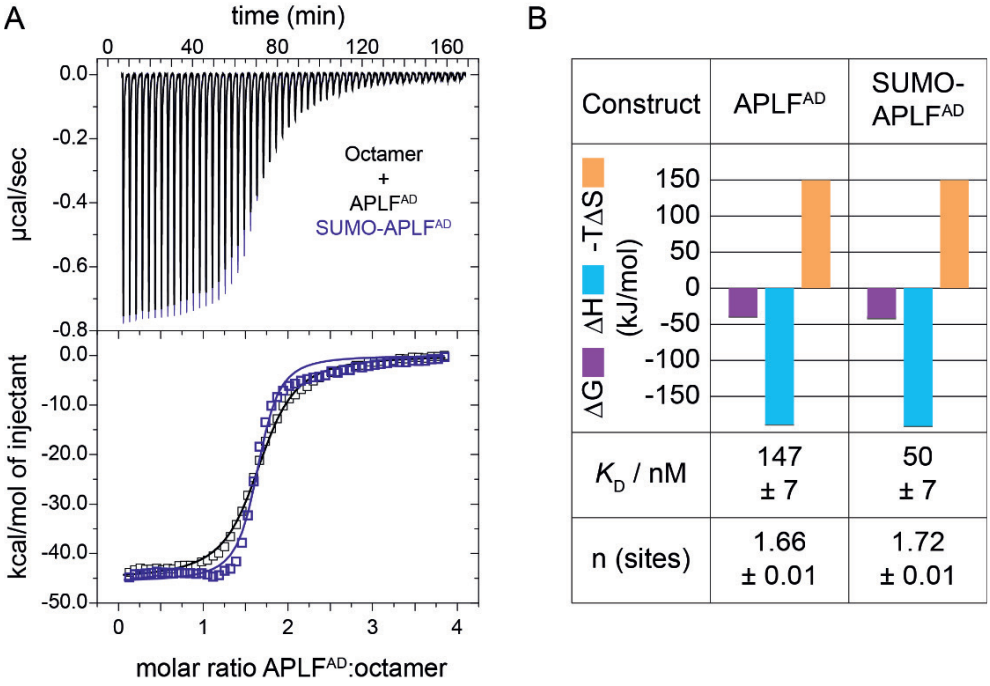

Figure S12. ITC of APLF^{AD} showing similar binding with and without SUMO fusion. (A) ITC titration curves including raw data of experiments with different APLF^{AD} constructs. The resulting binding isotherms were fit to a one-set-of-sites binding mode. (B) ITC derived best-fit values and fitting errors are shown in the table, the derived thermodynamic parameters in the histogram. Experiments were performed in 25 mM NaPi, pH 7.0, 300 mM NaCl, at 25 °C.

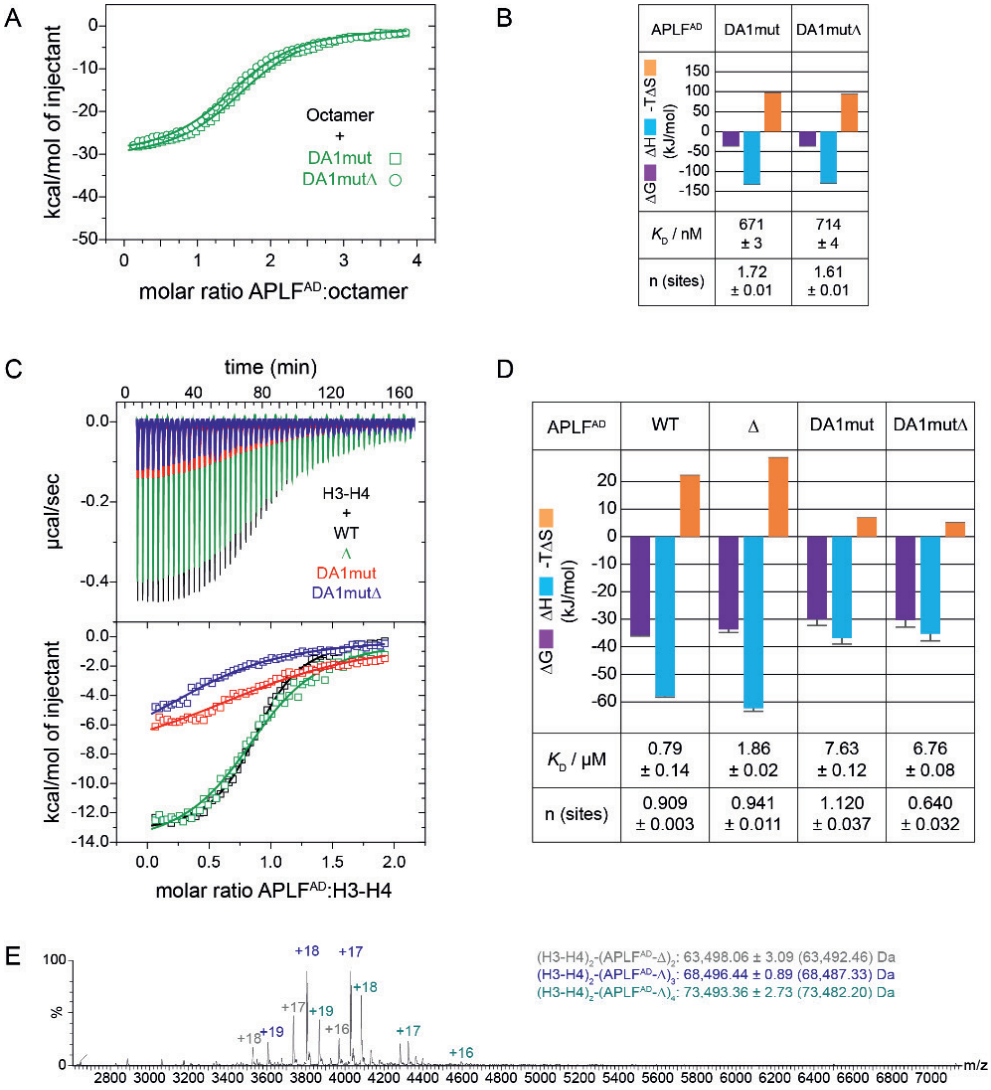

Figure S13. The APLF^{AD} KR-motif is not strongly involved in H3-H4 binding. (A) Calorimetric titration of APLF^{AD} WT or mutants to histone octamer via ITC. The resulting binding isotherms were fit to a one-set-of-sites binding mode. All data were obtained in 25 mM NaPi, pH 7.0, 300 mM NaCl, at 25 °C. (B) ITC best-fit values and fitting errors together with the derived thermodynamic parameters. When combining the alanine mutations of the double-aromatic anchor residues in the tyrosine-key motif of APLF^{AD} that binds H3-H4 with the KR-motif deletion (DA1mutΔ), only small changes occurred in the thermodynamic parameters of binding compared to the double-aromatic anchor mutant alone (DA1mut). (C) Calorimetric titration of APLF^{AD} WT or mutants to H3-H4 via ITC. The resulting binding isotherms were fit to a one-set-of-sites binding mode. All data were obtained in 25 mM NaPi, pH 7.0, 300 mM NaCl, at 25 °C. (D) ITC best-fit values and fitting errors together with the derived thermodynamic parameters. (E) Native mass spectrum of a mixture of H3-H4 with APLF^{AD}-Δ shows complex formation. Sample was in 300 mM ammonium acetate, pH 7.5. Interestingly, up to three molecules of APLF^{AD}-Δ can associate with the H3-H4 tetramer in contrast to APLF^{AD} WT which forms (H3-H4)$_2$-(APLF^{AD})$_2$.

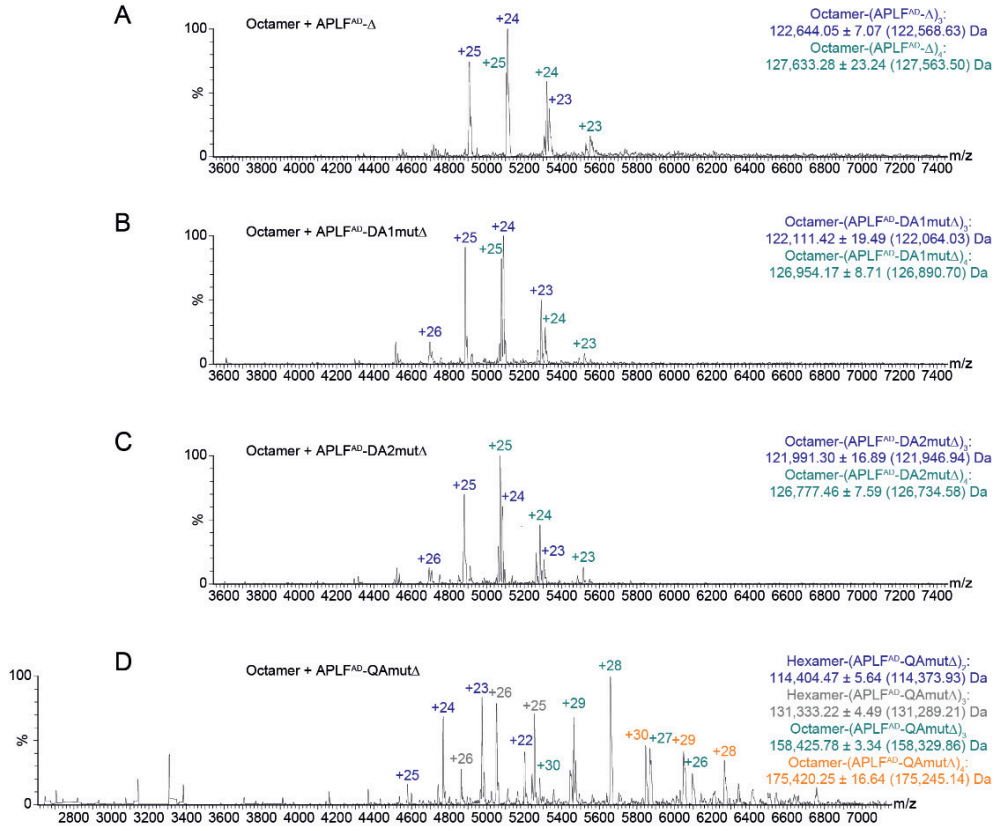

Figure S14. Native mass spectra of mixtures of histone octamer and APLF^{AD} aromatic anchor mutants with KR-motif deletions. Same type of complexes are formed as with WT APLF^{AD} with up to 4 APLF^{AD} bound. Other than histone octamer, also histone hexamers missing one H2A-H2B dimer are found in complex with APLF^{AD}-QAmutΔ. APLF^{AD}-QAmutΔ was with N-terminally fused SUMO for the purpose of concentration determination by absorbance at 280 nm. The relative signal intensity (RSI) is plotted against the mass-to-charge ratio (m/z). Charge states are given for each signal. Experimental (theoretical in brackets) molecular weights of the identified species are listed. Samples were in 300 mM ammonium acetate, pH 7.5.

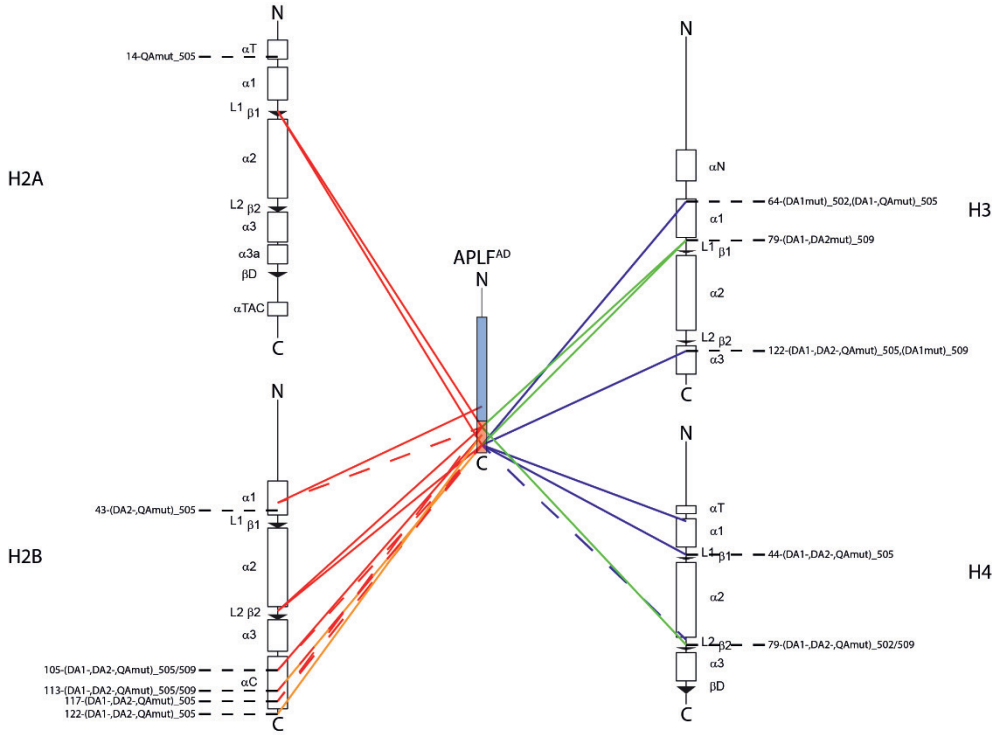

Figure S15. Histone-APLF^{AD} crosslinks identified in complexes. Secondary structure (SS) and binding motifs indicated for histones and APLF^{AD}, respectively, from N = N-terminus to C = C-terminus. SS-elements of histones as in the nucleosome (PDB ID 2PYO) (1) (line = loop, rectangle = α-helix, triangle = β-strand) with naming as in Ref. (2). APLF^{AD} motifs: lightblue = histone binding domain, lightred = KR-motif. Lines of different colors connect crosslinked residues: red = histone-APLF^{AD} crosslinks in H2A-H2B-APLF^{AD}, red dashed = histone-APLF^{AD} crosslinks in H2A-H2B-APLF^{AD} also present in histone octamer-APLF^{AD}, orange = histone-APLF^{AD} crosslinks in the minimal histone octamer-(APLF^{AD})$_2$ complex, blue = histone-APLF^{AD} crosslinks in H3-H4-APLF^{AD}, blue dashed = histone-APLF^{AD} crosslinks in H3-H4-APLF^{AD} also present in histone octamer-APLF^{AD}, green = histone-APLF^{AD} crosslinks in histone octamer-APLF^{AD}. Black annotations: crosslinks in histone octamer-APLF^{AD} with sequence numbering of the histone lysine involved followed by the APLF^{AD} mutation and residue number of the APLF^{AD} lysine involved. In agreement with our structural model, the crosslinks indicate spatial proximity between the KR-motif and the H2B αC-helix. One crosslink to H4 is common to H3-H4 alone and the histone octamer. In contrast, all H2B-APLF^{AD} crosslinks present in histone octamer-APLF^{AD} are also present in H2A-H2B-APLF^{AD}. Some of the crosslinks between APLF^{AD} and the histone octamer are also present in the double-anchor mutants indicating that the KR-motif can interact with the histone octamer independently from the aromatic anchors that are important for the chaperone function. Furthermore, there are also crosslinks present between APLF^{AD} mutants and the histone octamer that are not present in APLF^{AD} WT. In the crosslinking MS analysis of the histone octamer structure we showed that the aromatic anchors are important to stabilize the histone octamer. Hence, when the anchors are mutated, the histone octamer structure is perturbed and other sets of crosslinks between APLF^{AD} and the histone octamer can occur.

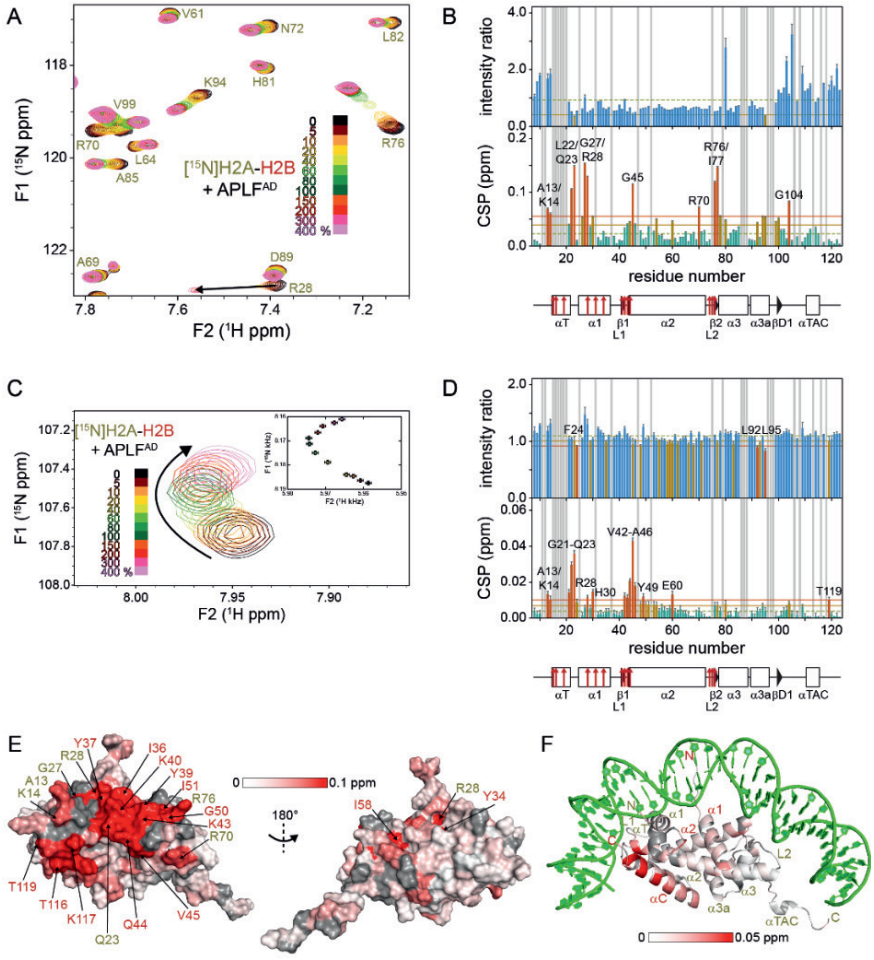

Figure S16. APLF^{FAD} binds to the α1-α2-patch of H2A. (A) Zoomed region of overlaid ^{1}H-^{15}N TROSY spectra of [^{15}N]H2A-H2B with increasing concentrations of APLF^{FAD}. Color coding of spectra is indicated in the figure. Data recorded at 750 MHz ^{1}H Larmor frequency in 25 mM NaPi buffer, pH 7.0 with 300 mM NaCl, at 35 °C. Peak shifts of selected resonances are indicated with arrows. (B) Analysis of H2A ^{1}H-^{15}N peak intensity ratios (upper panel) and weighted average CSPs (lower panel) between APLF^{FAD} bound (4:1 molar ratio of APLF^{FAD}:H2A-H2B) and free H2A-H2B. Resonances with intensity ratios less than 2 (1) standard deviation (SD) (orange (yellow) line) from the 10% trimmed mean (green dashed line) are highlighted in orange (yellow). Resonances with CSPs more than 2 (1) SD (orange (yellow) line) from the 10% trimmed mean (green dashed line) are highlighted in orange (yellow) and labeled. Residues without titration data due to overlap or missing resonances are indicated with gray bars. Secondary structure (SS) of H2A as in the nucleosome (PDB ID 2PYO) (1)) indicated below the plot (line = loop, rectangle = α-helix, triangle = β-strand) with naming of SS-elements as in Ref. (2). Residues that interact with nucleosomal DNA (PDB ID 2PYO) (1)) are indicated by red arrows. (C) Zoomed H2A G21 region of overlaid ^{1}H-^{15}N TROSY spectra as in (A). Direction and curvature of the peak shift is indicated with a green arrow. Inset: Plot showing the peak displacement of H2A G21; black bars – standard deviation. (D) Analysis of H2A ^{1}H-^{15}N peak intensity ratios (upper panel) and weighted average CSPs (lower panel) between one and four molar equivalents of APLF^{FAD} added to H2A-H2B. Color coding, labeling of residues, and secondary structure plot as in (A). (E) CSPs color coded on the surface representation of H2A-H2B between the unbound and bound state after addition of four molar equivalents of APLF^{FAD}. Surface residues with significant CSPs (more than 2 SD from the 10% trimmed mean) are labelled in yellow (red) for H2A (H2B). (F) CSPs color coded on the cartoon representation of H2A-H2B between one and four molar equivalents of APLF^{FAD} added. Gray – residues without titration data; green – DNA; with labeling of relevant secondary structure elements.

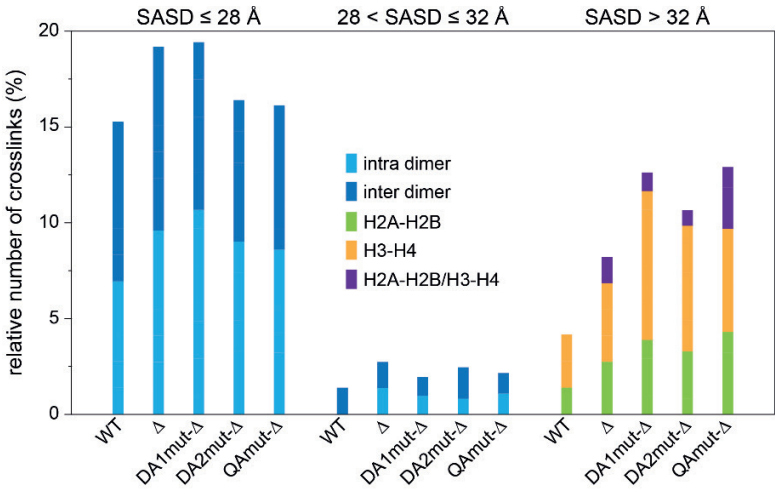

Figure S17. The KR-motif of APLF^{AD} contributes to stabilizing the histone octamer arrangement. Plotted number of crosslinks of the three SASD categories for the different histone octamer mix preparations without and with APLF^{AD} WT or mutants.

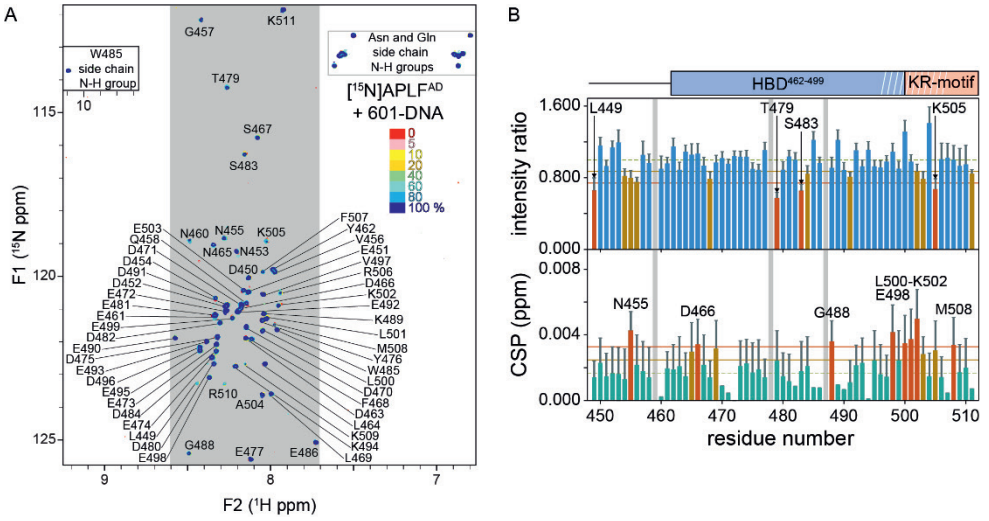

Figure S18. APLF^{AD} interacts only weakly with DNA. (A) ^{1}H-^{15}N HSQC spectra of APLF^{AD} with increasing concentrations of 167 bp 601-DNA. Color coding indicated in the figure. Recorded at 750 MHz ^{1}H Larmor frequency at 25 °C in 25 mM NaPi buffer, pH 7.0 with 300 mM NaCl. Assignments of the main-chain amide resonances are indicated by the single-letter amino acid code and residue number, asparagine/glutamine side chain amine resonances and side chain indole resonance of W485 are indicated. (B) Analysis of APLF^{AD} ^{1}H-^{15}N peak intensity ratios (upper panel) and weighted average CSPs (lower panel) between DNA bound (1:1 molar ratio of DNA:APLF^{AD}) and free APLF^{AD}. Resonances with intensity ratios less than 2 (1) standard deviation (SD) (orange (yellow) line) from the 10% trimmed mean (green dashed line) are highlighted in orange (yellow), indicated with black arrows and labeled. Resonances with CSPs more than 2 (1) standard deviation (SD) (orange (yellow) line) from the 10% trimmed mean (green dashed line) are highlighted in orange (yellow) and labeled. Position of the HBD and KR-motifs are indicated above the plot, white stripes denote the helical region. Residues without titration data due to overlap or missing resonances are indicated with gray bars.

SUPPLEMENTARY REFERENCES

1. Clapier, C.R., Chakravarthy, S., Petosa, C., Fernandez-Tornero, C., Luger, K. and Muller, C.W. (2008) Structure of the Drosophila nucleosome core particle highlights evolutionary constraints on the H2A-H2B histone dimer. *Proteins*, **71**, 1-7.
2. Chantalat, L., Nicholson, J.M., Lambert, S.J., Reid, A.J., Donovan, M.J., Reynolds, C.D., Wood, C.M. and Baldwin, J.P. (2003) Structure of the histone-core octamer in KCl/phosphate crystals at 2.15 A resolution. *Acta Crystallogr D Biol Crystallogr*, **59**, 1395-1407.
3. Davis, I.W., Leaver-Fay, A., Chen, V.B., Block, J.N., Kapral, G.J., Wang, X., Murray, L.W., Arendall, W.B., 3rd, Snoeyink, J., Richardson, J.S. *et al.* (2007) MolProbity: all-atom contacts and structure validation for proteins and nucleic acids. *Nucleic Acids Res*, **35**, W375-383.


5

Chapter 5

General Discussion, Conclusions & Perspectives

In this thesis, I describe in detail the characterization of the histone chaperone function of Aprataxin and Polynucleotide kinase Like Factor (APLF) which is a DNA repair factor involved in DNA double-strand break (DSB) repair by non-homologous end joining (NHEJ). In particular, the investigations were conducted using the intrinsically disordered C-terminal acidic domain of APLF ($APLF^{AD}$) which harbors the chaperone activity. My key finding is a detailed model of the complex of $APLF^{AD}$ with the histone octamer that explains the histone chaperone function of APLF. In this complex, two copies of $APLF^{AD}$ bind to and stabilize the histone octamer, partially replacing the DNA from the nucleosome to form a complex that we term the "chaperonosome". That is achieved through the interaction of well-positioned aromatic residues in $APLF^{AD}$ that anchor to specific sites on the surface of the histone octamer. These interactions are key for the chaperone function of APLF and its nucleosome assembly mechanism.

Below, I detail the implications of the chaperonosome model I developed.

HYDROPHOBIC OVER ELECTROSTATIC INTERACTIONS

As highly charged proteins, abundant electrostatic interactions between histone chaperones and histones are commonplace. Also in $APLF^{AD}$ electrostatic interactions contribute to binding affinity. However, I showed in **Chapters 3 and 4** that for $APLF^{AD}$, aromatic residues are the key determinants of specific and functional interactions with histones. Others have also found that for a different histone chaperone, nucleoplasmin, with completely different structural properties and function than $APLF^{AD}$, the non-electrostatic contribution to its binding affinity for histones is larger than the electrostatic one (1). The aromatic anchor interactions help to place the negative charges of $APLF^{AD}$ in a position where they can neutralize most of the positive charges of the histone fold domains. This allows the histones to assemble as histone octamer, to which two molecules of $APLF^{AD}$ are bound to compete with nucleosomal DNA interactions during the nucleosome assembly process.

THE ROLE OF INTRINSIC DISORDER IN THE CHAPERONOSOME

In **Chapter 3** we characterized $APLF^{AD}$ as a highly negatively charged, intrinsically disordered protein (IDP) domain. Yet, the defining feature of the chaperonosome model is that $APLF^{AD}$ wraps around the histone octamer and interacts specifically with both the H2A-H2B and H3-H4 subunits, as described in **Chapter 4**. Crucially, these specific interactions between aromatic residues in $APLF^{AD}$ and the histones are required for a functional binding mode. Such a dominant role for specific interactions may at first glance be surprising for an IDP. However, the IDP nature of $APLF^{AD}$ may make it ideally suited for its histone chaperone function. IDPs have been suggested to help cells to increase complexity (2), and may carry distinct advantages for protein function (3), which we recapitulate here and see how they apply to $APLF^{AD}$:

(i) Reduction of protein size with same binding interface area: IDPs can form interface areas that would require a structured protein two to three times the size (4). APLF^{FAD} consists of 62 residues of which only 20 (residues 471-490) are needed to cover the DNA binding surface of H2A-H2B as shown in our structural model in **Chapter 3**. In contrast, histone chaperone Nap1 covers the same surface of H2A-H2B and requires for this a dimer of 284 residues each (5).

(ii) Overcoming steric restrictions of binding: as a flexible IDP, APLF^{FAD} can wrap around the histone octamer and form a complementary binding interface in a way that would be difficult for a well-structured protein.

(iii) Allowing transient, high-enthalpy interactions: the entropic cost of IDP binding can help to enable transient binding while still allowing for many enthalpic interactions to ensure specificity. APLF^{FAD} has to bind the histone octamer specifically, yet, be able to transfer it to DNA or other chaperones, necessitating a dynamic interaction.

(iv) Increased binding rate: IDPs often have low complexity sequences that, when charged, can accelerate the on-rate for complex formation. The on-rate for APLF^{FAD} binding to H2A-H2B is ~10^8 M^{-1} s^{-1} based on our NMR titration analysis in **Chapter 3**, similar to the rate that has also been found for chaperone Chz1 binding to H2A.Z-H2B (6), and faster than diffusion limit for neutral molecules of this size (~10^5-10^6 M^{-1} s^{-1}) (7,8), showing the additional effect of attractive electrostatic interactions for association.

(v) Preventing aggregation: the low-complexity sequence in APLF^{FAD} has low hydrophobicity and high (negative) net charge which prevents its own aggregation and makes it an effective chaperone for histones to prevent their aggregation with DNA.

(vi) Facilitating post-translational modifications (PTMs): the overall accessibility of residues in an IDP can increase installation of PTMs which may well allow regulation of APLF function. No PTMs are known for APLF^{FAD} but APLF can be phosphorylated in its middle domain, which is also disordered, on serine residue 116 in response to DNA damage (9,10).

(vii) Enable flexible linking between rigid structures: the N-terminal structured FHA and mostly disordered middle domain of APLF have been shown to link the components of NHEJ in an extended and flexible complex (11), to which a histone binding and chaperone function is linked in APLF^{FAD}.

(viii) Resistance to denaturation: as APLF^{FAD} is unstructured it cannot lose its function due to unfolding.

(ix) Sequence diversity: the primary sequence space available for structured proteins is smaller than that for IDPs (12). Remarkably, in APLF^{FAD}, two similarly unstructured regions of different sequence have specificity for H2A-H2B and H3-H4, respectively (**Chapter 4**).

A potential disadvantage of IDPs in biomolecular recognition is that they are prone to engage in promiscuous molecular interactions which could drive pathological changes upon overexpression and lead to various diseases (13). To suppress the harmful effects of IDPs, their availability is tightly regulated (14). It was shown that enhanced expression of APLF is associated with breast cancer (15). Hence, it can be assumed that the availability of (active) APLF is most likely tightly regulated for its involvement in NHEJ DNA repair of DSBs (16,17) on one or more levels of protein regulation which spans gene transcription, processing and

degradation of mRNA, and protein synthesis, localization, modification and degradation (18). In particular, APLF undergoes hyperphosphorylation of serine residue 116 upon DNA damage and this modification facilitates efficient DSB repair (9,10). Furthermore, since APLF contains intrinsically disordered regions, one could imagine that intramolecular interactions are possible between the different parts or domains of APLF to mask functional sites which could be set free by binding of the other repair factors or the histones upon DNA damage. Such functionally important intramolecular interactions have been described for nucleoplasmin as a control mechanism for histone binding and release (19).

LIMITATIONS IN THE CHAPERONOSOME STRUCTURE

The chaperonosome model is based on the histone octamer structure as it occurs free in solution in 2 M KCl (20), or equivalently, when wrapped by DNA in the form of the nucleosome (21). Individual histone subunits, the H2A-H2B dimers and $(H3\text{-}H4)_2$ tetramer, have structural elements that fold in the context of the histone octamer. In particular, the H2A docking domain folds upon interaction with H3-H4 and locks the H3 αN-helix in position between the entry/exit and dyad DNA turns which is stabilized by the DNA in the nucleosome (21). The H3 αN-helix is otherwise structurally heterogeneous in H3-H4 (21-23). Our data do not allow to experimentally verify that the H2A docking domain and the H3 αN-helix interact in the chaperonosome in the same way as in the histone octamer or the nucleosome. The ITC data clearly show a disproportional enthalpy of binding upon chaperonosome formation compared to the individual interactions of $APLF^{FAD}$ with H2A-H2B or H3-H4. This is compelling evidence for the formation of histone-histone contacts in the chaperonosome. The crosslinking mass spectrometry analyses of the histone octamer complexes with $APLF^{FAD}$ WT and its mutants indicate that the histone-histone contacts formed are as in the histone octamer in the nucleosome. Therefore, at this moment, I can conclude that $APLF^{FAD}$-mediated histone octamer assembly is a prerequisite for deposition of the histone octamer onto DNA.

Our data in **Chapter 3** have indicated a propensity of $APLF^{FAD}$ to engage in an additional, secondary binding mode with H2A-H2B, which involves the H2B αC-helix. This interaction may be crucial for the function of the chaperonosome, but as of yet, no unambiguous interpretation of this interaction can be made. The NMR titrations of H2A-H2B showed significant CSPs upon addition of molar excess of $APLF^{FAD}$ for resonances of H2A E60 and H2B E102 which are part of the nearby H2A-H2B acidic patch (**Chapter 4**, supplementary data). Since the H2A-H2B acidic patch is a target site for several binding factors of the nucleosome through a double-arginine anchor motif (24-32), it is especially interesting to note that $APLF^{FAD}$ also contains two arginines (R506/R510) in its KR-motif and that the resonance of $APLF^{FAD}$ R506 disappears in the NMR titration of $APLF^{FAD}$ with H2A-H2B (**Chapter 3**). In addition, at molar excess of $APLF^{FAD}$ to histone octamer, crosslinks between the $APLF^{FAD}$ KR-motif and the chaperonosome occur in this region (**Chapter 4**, supplementary data). These data suggest the possibility of a secondary interaction between the KR-motif and the H2A-H2B acidic patch. Alternatively, the nearby H2B-H4 cleft, formed by the H2B-H4 four-helix bundle, another known interaction site for nucleosome binding factors (31,33), may be the secondary binding site of $APLF^{FAD}$. Independent of the exact location, this additional interaction provides

a mechanism in which one APLF^{FAD} molecule may bind to both H2A-H2B dimers of the histone octamer and thus may be key for the stabilization of the histone octamer organization.

Finally, the histone tails are a functional part of the histones (34) and have recently been linked to histone chaperone function (35,36). In particular, the so-called H2B repression (HBR) domain in the H2B tail was shown to be important for nucleosome assembly by histone chaperone FACT (37,38). Interestingly, in the NMR titration of H2A-[^{15}N]H2B with APLF^{FAD}, peak intensities of resonances of H2B tail residues, including the corresponding HBR domain, increase upon addition of APLF^{FAD} (**Chapter 3**, supplementary data). It could be that there is an interaction between the H2B tail and the histone fold domain which is competed off by binding of APLF^{FAD}. Hence, next to the assembly of the histone octamer, one other possible contribution of APLF^{FAD} binding could be the change in conformation or flexibility of the H2B tail to prime H2A-H2B for deposition onto DNA.

THE CHAPERONOSOME MECHANISM

Nucleosome assembly is generally thought to involve deposition of $(H3\text{-}H4)_2$ to form a tetrasome followed by the deposition of two H2A-H2B dimers to form the nucleosome (39). Furthermore, histone chaperones are thought to promote nucleosome assembly not by delivering histones, but through disfavoring nonnucleosomal interactions (40). Our results yielded persuasive evidence to indicate that APLF^{FAD} may act in a very different manner. In particular:

(i) Histone octamer binding suggests its complete deposition onto DNA, rather than a stepwise deposition. This represents a new paradigm since histones are found as H2A-H2B and H3-H4 pairs and histone chaperones usually bind and have preferential affinity to one of these pairs.

(ii) The chaperonosome model shows that the DNA binding sites of H2A-H2B are covered by APLF^{FAD} while the DNA binding site of H3-H4 that interacts with DNA close to the nucleosomal dyad is exposed (**Chapter 4**). In this way, H3-H4 can contact the DNA first to form a complex that can be seen as a tetrasome to which $(H2A\text{-}H2B\text{-}APLF^{FAD})_2$ is bound. Upon formation of this intermediate, the DNA can wrap around the histone octamer while competing off APLF^{FAD}.

(iii) The slightly different "affinity windows" for H2A-H2B (K_D ~250 nM, higher affinity) and H3-H4 (K_D ~550 nM, lower affinity) (**Chapter 4**) may translate to higher off-rates for the H3-H4 binding site in APLF^{FAD} compared to the H2A-H2B binding site, under the assumption that the on-rates are the same. This may then favor sequential invasion by the DNA to replace APLF^{FAD}. Since the DNA will be bound to the central, exposed dyad region first, such sequential wrapping is also favored from simple steric considerations. To further elucidate the mechanism, one could investigate the rate of DNA wrapping around the histone octamer once the first contact with the chaperonosome is established. Furthermore, one could investigate whether the DNA actively displaces APLF^{FAD} or wrapping occurs after dissociation of APLF^{FAD} from the histones.

(iv) APLF^{FAD}-DA1mut, with a weakened binding to H3-H4, is the most active mutant in the native PAGE chaperone assay (**Chapter 4**). This can be explained by the fact that this mutant can bind H2A-H2B and thereby keep H3-H4 associated with it to deposit the histone octamer in a controlled manner, albeit with slightly lower efficiency than APLF^{FAD} WT. But APLF^{FAD}-DA2mut and -QAmut, which are deficient in binding and chaperoning H2A-H2B alone, have a much lower activity, indicating that chaperoning of H2A-H2B is a crucial last step to "seal" the histone octamer during the nucleosome assembly process and prevent non-native interactions with H2A-H2B that would lead to precipitation. With APLF^{FAD}-DA2mut and -QAmut, no tetrasomes were detected, probably because the excess H2A-H2B makes them unstable or interacts with them unspecifically which leads to precipitation. Also for histone chaperone Nap1 it was suggested that nucleosome assembly is promoted by disfavoring nonnucleosomal interactions between H2A-H2B dimers and DNA (40).

(v) Furthermore, a thermodynamic nucleosome assembly mechanism has been proposed based on studies of Nap1 function (40-42) (Figure 1). It is proposed that Nap1 binds the histones and lowers their free energy below that of nonspecific histone-DNA complexes thereby promoting nucleosome assembly which lowers the free energy even further (43). But APLF^{FAD} does not have a high enough affinity for the histones to lower their energy below that of nonspecific histone-DNA complexes (**Chapter 4**). Furthermore, the APLF^{FAD} aromatic anchor mutants bind the histones with similar affinities as APLF^{FAD} WT which means that their lower chaperone activity cannot be explained due to a change in thermodynamics of binding. Hence, in our model in **Chapter 4** we show that APLF^{FAD} guides nucleosome assembly in a more directed fashion by presenting the histones in their octameric nucleosomal configuration in the form of the chaperonosome which is involved in a transient chaperone-histone-DNA complex that is resolved by DNA wrapping and displacement of APLF^{FAD}. Additionally, APLF^{FAD} also prevents nonspecific histone-DNA interactions in the chaperonosome and skews the reaction kinetics towards nucleosome assembly by increasing the likelihood of specific interactions between the histone octamer and DNA. Hence, the formation of a transient ternary complex causes an apparent decrease in activation energy towards nucleosome assembly, favoring it over nonspecific histone-DNA interactions with a high activation energy barrier.

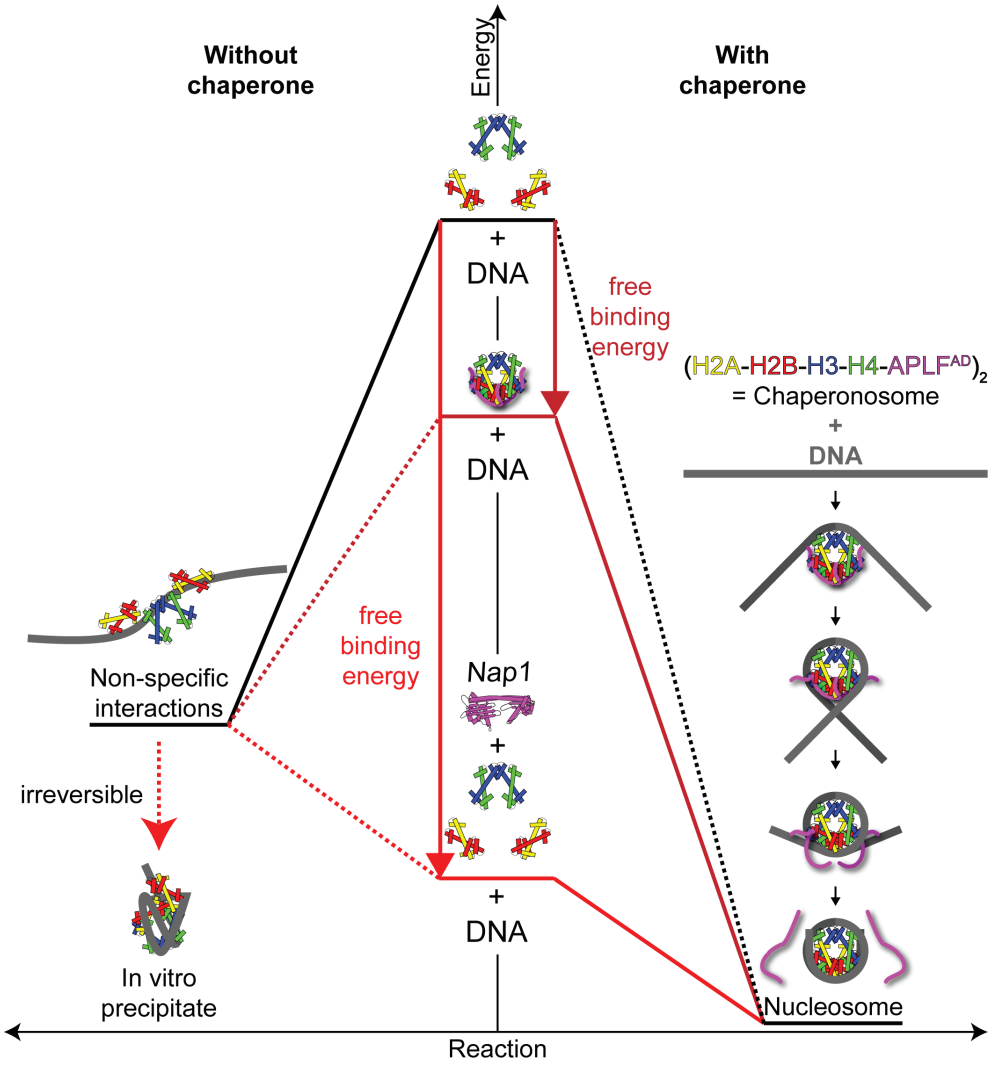

Figure 1. Thermodynamic model of histone chaperone function illustrated as free-energy reaction diagram (43). The change in free-energy is plotted along the reaction coordinate of histones and DNA (middle) towards precipitate (left) or nucleosome (right). The black route shows that in the absence of a histone chaperone, nonspecific interactions of histones with DNA are favored (solid black line) because of irreversible precipitation over nucleosome formation which requires histones and DNA to encounter in a non-random orientation (dashed black line). The dark red route shows that APLF^{FAD} binding of histones lowers the free-energy only little and nonspecific histone interactions with DNA (dotted dark red line) are almost equally favorable as nucleosome formation (solid dark red line). The light red route shows that histone chaperone Nap1 binds histones with a free-energy similar to the nucleosome so that nonspecific histone interactions with DNA would lead to an increase in free-energy (dotted light red line), thus favoring nucleosome formation (solid light red line). In conclusion, such a thermodynamic model can explain the histone chaperone function of Nap1 but not of APLF^{FAD}. Note that stable intermediates and additional energy levels that could form on the reaction path are omitted for simplicity.

The nucleosome disassembly reaction most likely goes via the same steps in the reverse direction of the nucleosome assembly reaction. However, in the case of APLF^{AD} with its lower affinity for histones in comparison to DNA (40), nucleosome disassembly would be a thermodynamic uphill reaction and hence more difficult. Any changes that weaken the nucleosome structure can be a target for a histone chaperone to aid in nucleosome disassembly (32,44-49). APLF^{AD} would most likely need the assistance of other factors like chromatin remodelers, other chaperones or DNA repair factors to weaken histone-DNA interactions at the break site. One such factor could be the histone chaperone nucleolin which can promote nucleosome remodeling (50). It also promotes histone eviction during NHEJ and leads to recruitment of the NHEJ factor XRCC4 (51). This could be a direct link to the NHEJ complex in which XRCC4 is involved with APLF as scaffold (11).

IMPORTANCE OF ENTHALPY-ENTROPY COMPENSATION

The ITC study with the different aromatic anchor mutants of APLF^{AD} showed decreased enthalpy of binding, because of the missing interactions of the aromatic anchors, but overall highly similar affinities compared to APLF^{AD} WT (**Chapter 4**). This indicates that complex formation of APLF^{AD} with the histone octamer is accompanied by strong enthalpy-entropy compensation (EEC) (52). In the complex of the histone octamer with APLF^{AD} WT, entropy is greatly reduced, while in the histone octamer complexes with the APLF^{AD} aromatic anchor mutants, more of the entropy is retained. Such EEC of macromolecular interactions means that for tighter contacts leading to higher specificity and more negative enthalpy, the increased reduction in conformational entropy allows to maintain a reasonable dissociation rate of the complex. In a comparative study it was found that EEC was more complete for disordered than for ordered protein complexes (53). By enabling many routes to the same change in free energy, EEC could also give IDPs broad binding specificities (52). For APLF^{AD}, EEC may thus be the essential thermodynamic basis of its function as histone chaperone, simultaneously acting in storage of the histone octamer, histone exchange, and controlled nucleosome assembly.

Another explanation is that a large proportion of the EEC comes from changes in solvation which give the same effect as conformational changes because of a link between the amount of bound water and protein flexibility (54,55). From the analysis and interpretation of two NMR studies that derived binding entropy changes as conformational entropy changes (56,57), it was concluded that the more rigid the complex, the more water is immobilized and increasing flexibility results in immobilization of less water (54). The high-resolution nucleosome structures have revealed that solvent molecules and ions contribute to the NCP structure by mediating about half of all histone-DNA contacts (58,59). This could also have important implications for chromatin remodeling and nucleosome assembly by histone chaperones with an accompanying effect of EEC through changes in flexibility and solvation of the components.

FUNCTION AND MODULARITY OF THE CHAPERONOSOME

The chaperonosome is a modular protein assembly of the histone octamer bound by APLF^{FAD} that could fulfill the following functions:

(i) maintain the right stoichiometry between histone pairs at the DNA damage site,

(ii) shield functional histone surfaces from nonspecific association with DNA during the DNA repair process,

(iii) exchange histone pairs,

(iv) assembly of the histones in their nucleosomal octameric organization, and finally,

(v) deposition of the histones back onto the DNA to seal the repaired site and signal for repair completion.

As a modular unit, I hypothesize that one of the two APLF^{FAD} molecules in the chaperonosome could be replaced by another chaperone, for instance one that is specific for a histone variant. Furthermore, the APLF^{FAD}-chaperonosome could be complemented by a chaperone that binds to the periphery of H3-H4 close to the nucleosomal dyad to shield also this free histone DNA binding surface.

In the same way as the nucleosome is a modular protein-DNA and the histone octamer is a modular protein assembly, the intrinsically disordered APLF^{FAD} can be seen as a modular histone binding and chaperone platform. In the histone octamer, a modular assembly of histone dimers is linked in a stable yet flexible manner to form a basic protein core with evenly spaced DNA-binding sites which bind to ~30 bp of DNA each (60). APLF^{FAD} is a modular assembly of aromatic anchors and flexible binding motifs that bind to roughly one functional histone site each and are linked in a stable yet flexible manner to another binding module. This modularity allows APLF^{FAD} to bind either type of histone complex, dimers, tetramers, hexamers, and octamers by using one, two, three, or all four aromatic anchors with or without the KR-motif or the KR-motif alone. In this way, APLF^{FAD} can be the modular histone chaperone match for the modular histone octamer protein assembly.

THE FOLDING CHAPERONE LINK

Molecular chaperones are proteins that prevent unspecific interactions of their clients. This is the case for histone chaperones as it is for folding chaperones. Histone chaperones are a class of proteins responsible for: (i) binding of the basic histones, (ii) shielding them from nonspecific interactions with DNA and other factors, (iii) their nuclear import, and (iv) facilitating their deposition onto DNA either by directly transferring them to DNA or by handing them over to other chaperones (61-64). A folding chaperone is a protein that associates with a target protein and prevents its misfolding, thereby avoiding the production of inactive or aggregated forms. For folding chaperones this translates to a class of proteins responsible for:

(i) binding of (partially) unfolded proteins, (ii) shielding them from nonspecific intra- and intermolecular interactions, (iii) insertion of proteins into the membrane or import into cellular compartments, and (iv) facilitating protein folding.

Folding chaperones can be divided into three categories: (i) ATP-dependent chaperones, which use ATP hydrolysis to induce conformational changes in the chaperone and promote correct protein folding, (ii) ATP-independent chaperones, which bind to (partially) unfolded proteins to prevent aggregation and pass them on to ATP-dependent chaperones for folding (65), and (iii) chaperones that help to fold proteins while bound to them without ATP hydrolysis. In this last scenario, the client protein folds while the chaperone continuously but passively interacts with it (66-69). It was proposed that such a simple mechanism could be evolutionarily ancient and serve a primitive folding function under situations of cellular stress under which the cell can be depleted of energy (66). This mechanism fits very well with the proposed nucleosome assembly mechanism mediated by APLF^{FAD} (**Chapter 4**). Similar to the latter category of folding chaperones, APLF^{FAD} utilizes favorable electrostatic surfaces to allow flexible binding to intermediates, and hydrophobic surfaces to specifically recognize the histone substrates. The mechanism for folding chaperone assisted protein folding can thus be drawn in the same way as APLF^{FAD} assisted nucleosome assembly (Figure 2). In this Figure 2, I show how a hypothetical folding chaperone binds an unfolded protein substrate thereby preventing its misfolding and aggregation. Instead, chaperone binding stabilizes the folding transition state from which the protein can fold while bound to the chaperone.

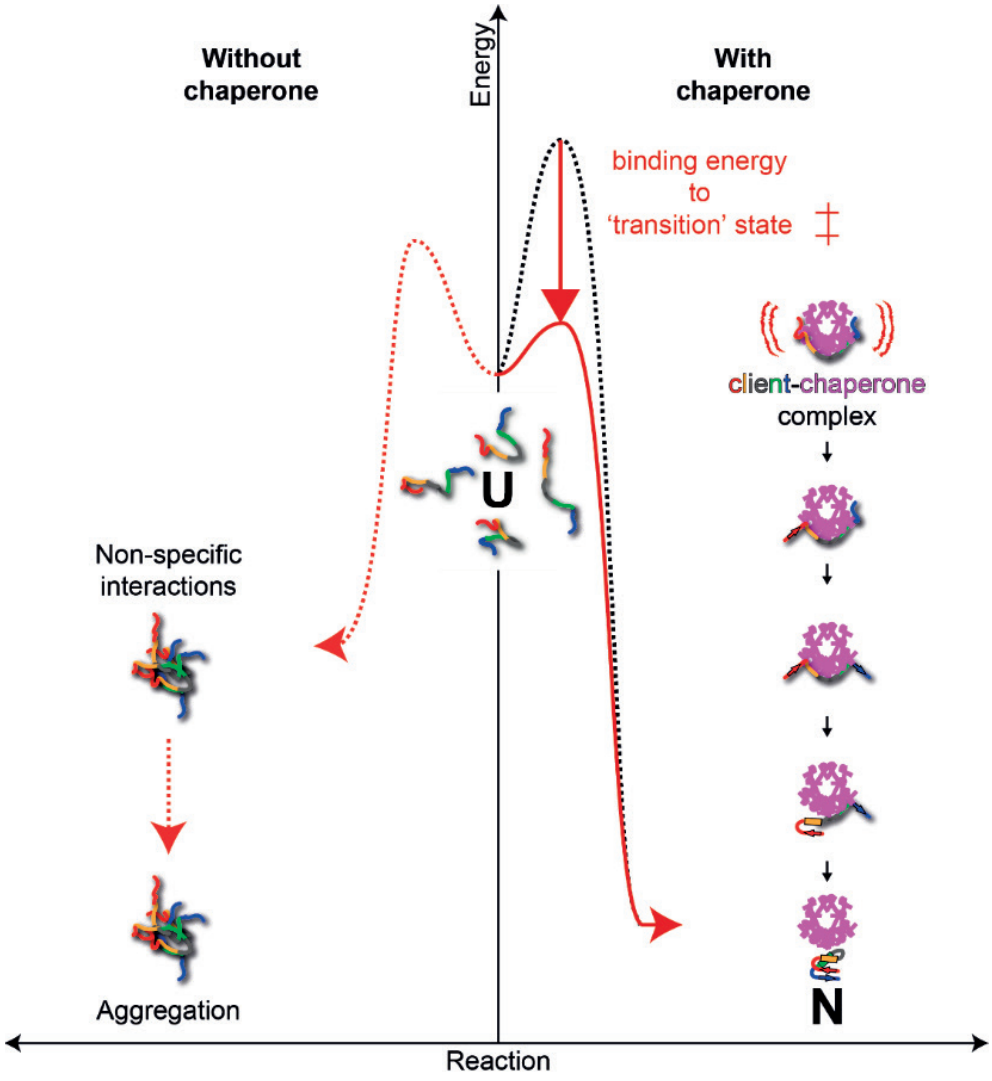

Figure 2. Schematic diagram of a protein folding while bound to a chaperone. Simplified two-stage folding from an unfolded state (U, middle) to a native state (N, bottom right). The unfolded state is an ensemble of unfolded conformations. These can form nonspecific contacts which can lead to aggregation in the absence of a chaperone (left). A chaperone can prevent nonspecific interactions by binding to reactive sites of the unfolded protein (right). Interactions with the chaperone stabilize the folding transition state from which the protein can fold through forming native contacts until the different protein components (single residues or secondary structure elements represented by different colors) displace themselves through intramolecular interactions from the chaperone. Note that stable intermediates and additional transition states that could form on the folding path are omitted for simplicity.

HISTONE TRANSFER IN OTHER CHAPERONES

Historically, histone chaperone activity is measured by the ability to mediate the formation of the nucleosome (or of an intermediate thereof) *in vitro*, whereas *in vivo* chaperones can be restricted to handling histones at earlier stages in the chaperone network and only a few histone chaperones are recognized as actual deposition factors (70). The general activity of the chaperone is thus the guided transfer of histones. We postulate that APLF^{FAD} mediates transfer of the histone octamer to the DNA according to the mechanism outlined above. What general functional properties are required to mediate histone transfer remains unclear. Especially, in the case of structured histone chaperones the question arises how they can release the histones in a specific manner to hand them over to other chaperones or deposit them onto DNA. There are several possibilities:

(i) Through kinetics: Depending on the binding kinetics, the histones will be released at some point and captured by another chaperone or DNA. This is thought to be the mechanism of action for the assembly chaperones Nap1 and CAF-1 that bind to DNA binding surfaces of the histones (5,71). In the case of CAF-1, deposition onto DNA is facilitated by direct DNA binding through its winged helix domain. Similarly, histone transfer to another chaperone could be assisted by an interaction between the chaperones.

(ii) Through distinct histone binding interfaces and co-chaperone binding: Histone chaperones generally shield functional surfaces of histones without fully encasing the histone fold. The combination of multiple histone chaperones therefore has the potential to form a more complete shield around the histones as part of a co-chaperone complex. While one chaperone shields one histone binding site, another chaperone can bind to another and by release of the one chaperone the histones are transferred to the other. Thus, which histone surface is protected by a chaperone gives a strong clue for the step in the assembly it is involved in (72). This is clearly illustrated in the case of Asf1 that shields the tetramerization interface of H3-H4, leaving the DNA binding surface exposed (73,74). Thereby, Asf1 can mediate histone transfer to chaperones MCM2, UBN1, and CAF-1, which shield the DNA and/or H2A-H2B binding interfaces of H3-H4 (23,71,75,76).

(iii) Through conformational changes: A conformational change that is encoded in the protein sequence of the chaperone can set free a certain binding interface of the histone for binding by another chaperone or DNA. A candidate for this could be DAXX which is almost completely disordered in its free state but folds upon binding H3.3-H4 (77).

(iv) Through PTMs of the histone or chaperone that could weaken their interaction and promote histone release: At the same time a modification of the histone or another chaperone could promote binding by that other chaperone or to DNA. Asf1 phosphorylation promotes histone binding and interaction with downstream chaperones to ensure efficient histone supply during DNA replication (78,79). Hyperphosphorylation of H2A-H2B-loaded nucleoplasmin induces dissociation of linker histones from nearby chromatin to replace the bound H2A-H2B on nucleoplasmin for deposition onto DNA (1). This scenario can also be turned around: a modification of the histone could lead to altered interaction with the chaperone, dissociation and binding of another histone. This is probably just the tip of the iceberg, and histone chaperone PTMs are likely to emerge as an important means to regulate histone eviction, handover, and deposition.

(v) Through IDRs: A structured histone binding domain of a chaperone could hand over the histones through intra- or intermolecular transfer to an IDR from which the mechanism of histone exchange can go about as in the proposed nucleosome assembly mechanism for APLF^{AD} (**Chapter 4**). Candidates for this are Nap1 and nucleoplasmin which contain intrinsically disordered acidic domains (19,80).

ROLE OF THE CHAPERONOSOME IN DNA REPAIR

Since APLF forms a scaffold for the NHEJ repair complex, its histone chaperone activity is likely to be functionally relevant for the repair process (Figure 3). In this Figure 3, I show how APLF^{AD} could capture the histone octamer after its eviction from the DNA to form the chaperonosome. This could have the function to prevent the histone octamer from unspecific binding to DNA, exchange of histones, and, after repair completion, promotion of nucleosome assembly to seal the site as signal for repair completion and chromatin compaction.

The fate of both parental and newly deposited histones is critical for the chromatin state. Mobilizing parental histones away from the damage site and depositing them back onto the repaired DNA could thus contribute to restoring the initial chromatin organization. In addition to histone recycling, re-establishing the original chromatin landscape would require active removal of DNA damage-induced histone PTMs and transmission of parental marks to newly synthesized histones. The APLF-chaperonosome could serve as a template for enzymes that can recognize the modification on the parental histones and copy it to new histones and thereby establish the pre-damage chromatin state for epigenome maintenance.

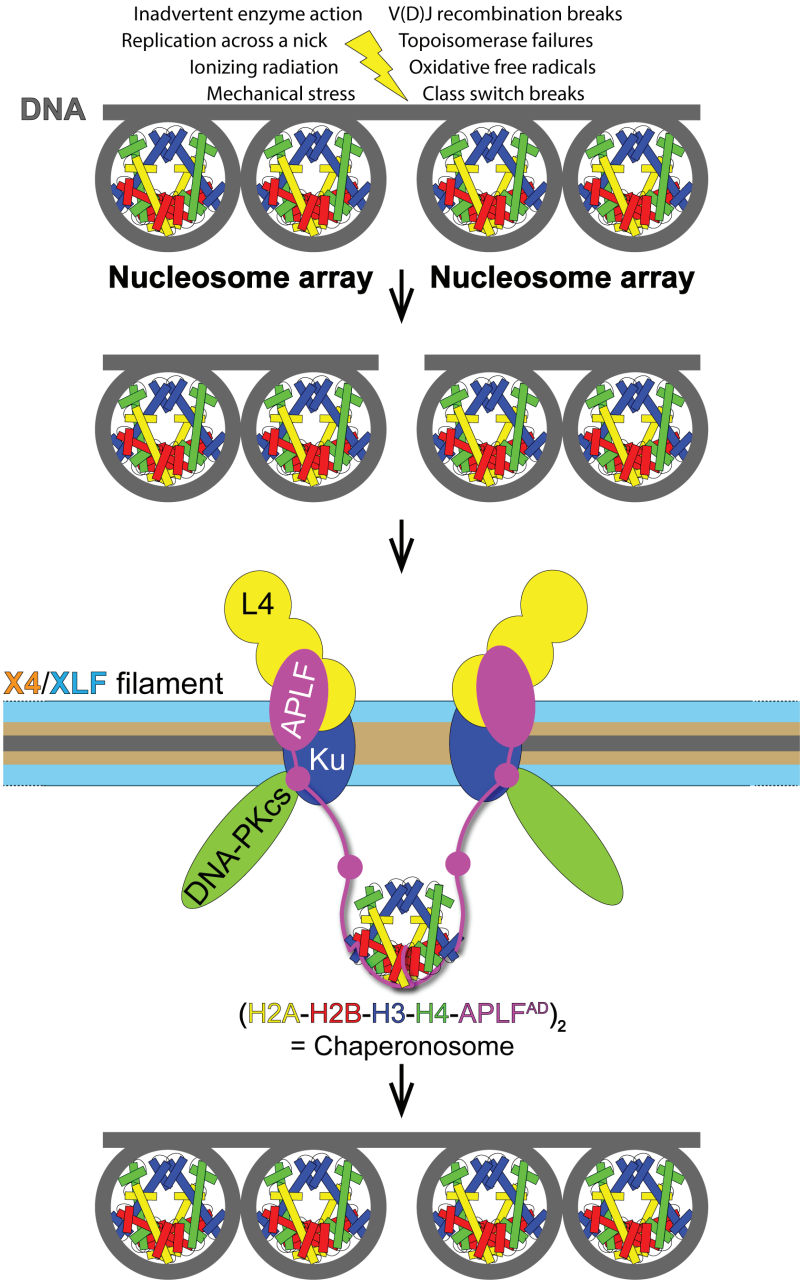

Figure 3. The architecture of DSB repair by NHEJ with the chaperonosome. APLF links through its N-terminal FHA and mostly intrinsically disordered middle domain the DNA repair factors in an extended and flexible NHEJ complex while its C-terminal APLF^{AD} keeps the histones as histone octamer away from the break site during the repair process. After the DNA is repaired, the histone octamer can be deposited onto the DNA in a nucleosome assembly reaction through the proposed chaperonosome mechanism to seal the break site.

Since APLF^{FAD} also recognizes generic elements of H2A-H2B and H3-H4, it could also chaperone histone variants thereof. In NHEJ, H3 variant H3.3 displays increased incorporation at sites of DNA damage which is assisted by the chromatin remodeler CHD2 (81). This remodeler could be assisted by APLF. While the histone chaperone function of APLF has been linked to H2A variant macroH2A1.1, it is of yet unclear what the functional relevance of this interaction is (82). APLF has been shown to recruit the macrodomain of macroH2A1.1 to DNA damage sites. However, while macroH2A1.1 associates with damaged chromatin in a Poly(ADP-ribose) (PAR)-dependent manner, proper incorporation into nucleosomes has not been shown (82-84). Thus, this variant does not behave like a bona-fide histone protein but rather like a chromatin associated factor.

FUTURE PERSPECTIVES

The full complexity of the histone chaperone story has not been elucidated, yet. While histones represent some of the most conserved proteins in eukaryotes, histone chaperones have so far emerged as a large and diverse family of proteins in terms of sequence, fold and interaction mode. Even for individual chaperones there may be functional differences between species, such as for APLF^{FAD}. In particular, the H3-H4 binding region in APLF^{FAD} which is present in human and bovine, is missing for example in mouse, which could mean the chaperonosome is species-specific or the H3-H4 chaperone function of APLF is complemented by another chaperone in mouse.

A key question emerging from this thesis is whether other histone chaperones could also functionally bind the histone octamer. FACT has been shown to be capable of binding all four histones simultaneously, but functionally interacts with histone hexamers rather than octamers (49). Nucleoplasmin, which can form a decamer of a single histone chaperone subunit, has been hypothesized to bind five histone octamers docked around its core, in which the same H3-H4 binding site as in the APLF^{FAD}-chaperonosome is exposed for a possible first contact point with DNA in nucleosome assembly (85). Interestingly, the histone binding motif of nucleoplasmin's disordered domain contains aromatic residues that could function as anchors in histone binding and chaperoning (19). However, there are different and partially contradicting models for the nucleoplasmin interaction with histones and future studies will have to shed more light on this to determine if it can really bind histone octamers (1,85-89).

The histone chaperone family likely holds more surprises other than the chaperonosome in the form of chaperones with unique capabilities. For instance, it would be interesting to find out whether there are specific linker histone chaperones that can remove or deposit the linker histones, either in DNA repair where it forms a barrier to the damage site, or in other processes. Likewise, one could imagine the existence of histone chaperones that control the interactions of the histone tails as part of nucleosome assembly. The large number of possible PTMs on the histone tails could function as switches to specifically turn their interactions with chaperones on or off. Another exciting class of histone chaperones could depend on RNA for their function, as was shown for yeast chaperone Hif1p (90). How such histone chaperones make use of RNA as cofactor in the chaperone mechanism and how broadly RNA impacts chaperone function are intriguing open questions.

The emphasis in the chaperone field is very much on their impact in the nucleosome assembly pathway. Yet, just like there is a chromatin assembly factor one could imagine there to be also a chromatin disassembly factor. It would be interesting to find such factors and further investigate the process of nucleosome disassembly.

Interaction of DNA with the histone octamer surface is relatively stable (91,92). But the stability varies depending on the distance of the histone-DNA interaction from the DNA entry/exit site along the DNA axis (93). The time constant of local nucleosomal DNA unwrapping varies from minutes near the nucleosome (pseudo)dyad axis to milliseconds near the nucleosomal DNA entry/exit site, reflecting a probability of histone site exposure that varies over several orders of magnitude along the DNA (94,95). Chromatin remodelers may exploit the intrinsic instability of nucleosomal DNA to dramatically enhance the rate of histone site exposure (96-99). Opening of the nucleosome at its edge would free histone binding sites for histone chaperones which have been implicated in histone eviction and deposition during enzyme passage through nucleosomal DNA (100-102). Hence, it is an intriguing idea that histone chaperones work together with chromatin remodelers in nucleosome (dis)assembly and histone exchange (103,104). It would be interesting to investigate their relationships and the mechanisms involved.

Finally, the chaperonesome that I identified and characterized in this thesis, is a modular and dynamic complex in which the DNA from the nucleosome is (partially) replaced by histone chaperones. In this complex the histone octamer can contain canonical histones and histone variants. Furthermore, several chaperone molecules can be bound to the histone octamer, which represents the possibility of specific recognition of the chaperonosome, its binding, modification, and processing. Future challenges will be to incorporate the chaperonosome in the picture of chromatin biology, find interaction partners that specifically recognize it and function on it just like the writers, readers, erasers, and remodelers of the nucleosome. But I would like to add a "c" here as a branding for the chaperonosome (Figure 4). cWriters: enzymes that specifically recognize and bind the chaperonosome, which occurs only at a very specific portion of the time in the life of a cell, and modify it for signaling a certain chromatin state. cReaders: proteins that recognize and specifically bind the (un)modified chaperonosome and catalyze a downstream reaction. cErasers: enzymes that come into action once the chaperonosome has fulfilled its function, remove the modification that was added to it and signal for the end of the reaction. cRemodelers: proteins that specifically recognize the chaperonosome and remodel it by catalyzing the exchange of one of the components for another, for instance a canonical histone for a histone variant to form a hybrid octamer that can then be deposited onto DNA to form a hybrid nucleosome.

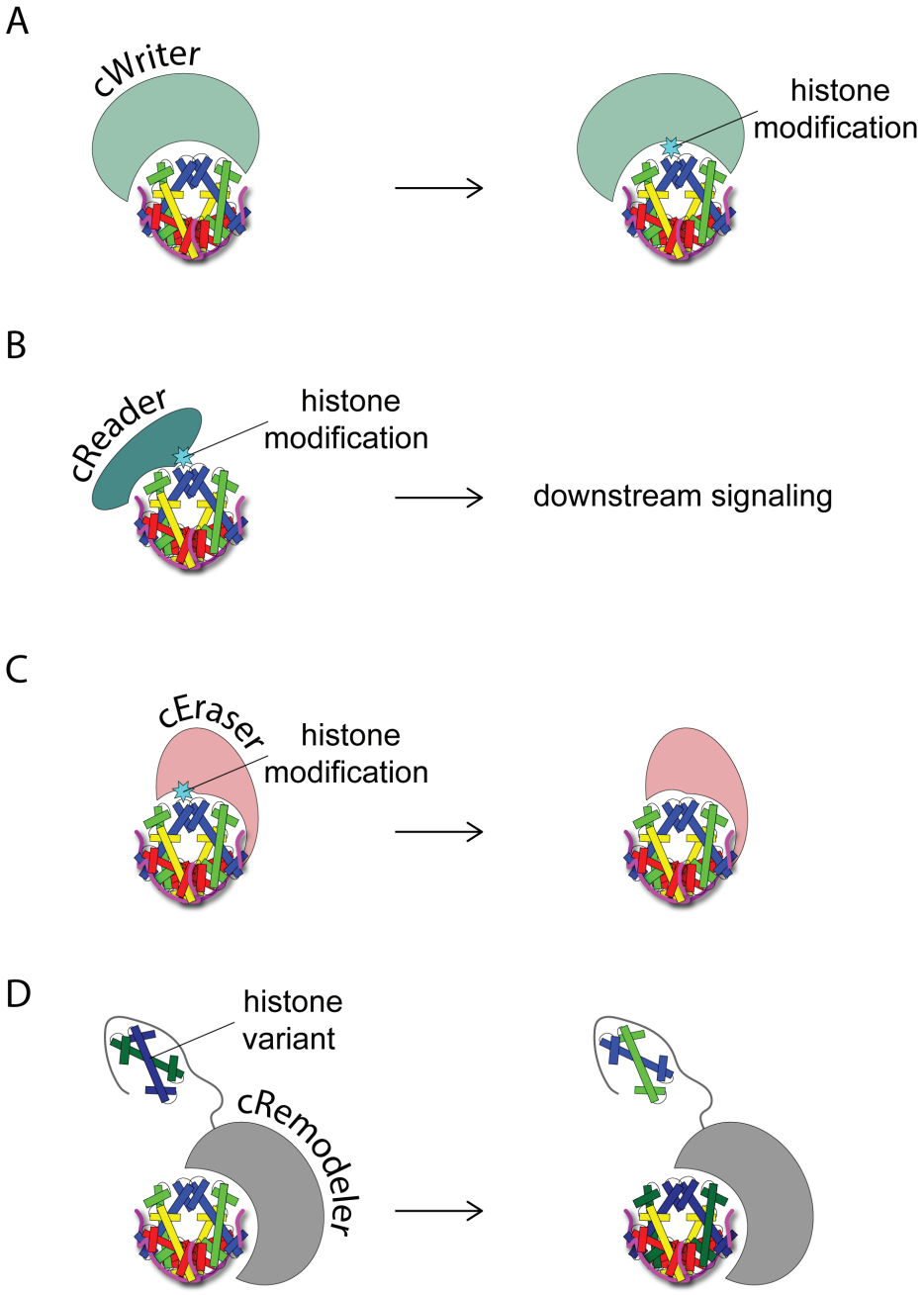

Figure 4. A future perspective for chaperonosome research. (A) cWriters: enzymes that recognize and bind the chaperonosome and modify it through, for example, post-translationally modifying a histone. (B) cReaders: proteins that recognize and bind an (un)modified chaperonosome to induce for example a downstream signaling reaction. (C) cErasers: enzymes that recognize and bind a modified chaperonosome to remove the modification to, for example, stop a signaling reaction. (D) cRemodelers: proteins that recognize and bind the chaperonosome and remodel it by, for example, exchanging canonical for variant histones.

REFERENCES

1. Taneva, S.G., Banuelos, S., Falces, J., Arregi, I., Muga, A., Konarev, P.V., Svergun, D.I., Velazquez-Campoy, A. and Urbaneja, M.A. (2009) A mechanism for histone chaperoning activity of nucleoplasmin: thermodynamic and structural models. *J Mol Biol*, **393**, 448-463.
2. Schlessinger, A., Schaefer, C., Vicedo, E., Schmidberger, M., Punta, M. and Rost, B. (2011) Protein disorder--a breakthrough invention of evolution? *Curr Opin Struct Biol*, **21**, 412-418.
3. Liu, Z. and Huang, Y. (2014) Advantages of proteins being disordered. *Protein Sci*, **23**, 539-550.
4. Gunasekaran, K., Tsai, C.J., Kumar, S., Zanuy, D. and Nussinov, R. (2003) Extended disordered proteins: targeting function with less scaffold. *Trends Biochem Sci*, **28**, 81-85.
5. Aguilar-Gurrieri, C., Larabi, A., Vinayachandran, V., Patel, N.A., Yen, K., Reja, R., Ebong, I.O., Schoehn, G., Robinson, C.V., Pugh, B.F. *et al.* (2016) Structural evidence for Nap1-dependent H2A-H2B deposition and nucleosome assembly. *EMBO J*, **35**, 1465-1482.
6. Hansen, D.F., Zhou, Z., Feng, H., Jenkins, L.M.M., Bai, Y. and Kay, L.E. (2009) Binding Kinetics of Histone Chaperone Chz1 and Variant Histone H2A.Z-H2B by Relaxation Dispersion NMR Spectroscopy. *Journal of Molecular Biology*, **387**, 1-9.
7. Schlosshauer, M. and Baker, D. (2004) Realistic protein-protein association rates from a simple diffusional model neglecting long-range interactions, free energy barriers, and landscape ruggedness. *Protein Sci*, **13**, 1660-1669.
8. Alsallaq, R. and Zhou, H.X. (2007) Prediction of protein-protein association rates from a transition-state theory. *Structure*, **15**, 215-224.
9. Macrae, C.J., McCulloch, R.D., Ylanko, J., Durocher, D. and Koch, C.A. (2008) APLF (C2orf13) facilitates nonhomologous end-joining and undergoes ATM-dependent hyperphosphorylation following ionizing radiation. *DNA Repair (Amst)*, **7**, 292-302.
10. Fenton, A.L., Shirodkar, P., Macrae, C.J., Meng, L. and Koch, C.A. (2013) The PARP3- and ATM-dependent phosphorylation of APLF facilitates DNA double-strand break repair. *Nucleic Acids Res*, **41**, 4080-4092.
11. Hammel, M., Yu, Y., Radhakrishnan, S.K., Chokshi, C., Tsai, M.S., Matsumoto, Y., Kuzdovich, M., Remesh, S.G., Fang, S., Tomkinson, A.E. *et al.* (2016) An Intrinsically Disordered APLF Links Ku, DNA-PKcs, and XRCC4-DNA Ligase IV in an Extended Flexible Non-homologous End Joining Complex. *J Biol Chem*, **291**, 26987-27006.
12. Uversky, V.N. (2013) Unusual biophysics of intrinsically disordered proteins. *Biochim Biophys Acta*, **1834**, 932-951.
13. Vavouri, T., Semple, J.I., Garcia-Verdugo, R. and Lehner, B. (2009) Intrinsic protein disorder and interaction promiscuity are widely associated with dosage sensitivity. *Cell*, **138**, 198-208.
14. Gsponer, J., Futschik, M.E., Teichmann, S.A. and Babu, M.M. (2008) Tight regulation of unstructured proteins: from transcript synthesis to protein degradation. *Science*, **322**, 1365-1368.
15. Majumder, A., Syed, K.M., Mukherjee, A., Lankadasari, M.B., Azeez, J.M., Sreeja, S., Harikumar, K.B., Pillai, M.R. and Dutta, D. (2018) Enhanced expression of histone chaperone APLF associate with breast cancer. *Mol Cancer*, **17**, 76.
16. Bekker-Jensen, S., Fugger, K., Danielsen, J.R., Gromova, I., Sehested, M., Celis, J., Bartek, J., Lukas, J. and Mailand, N. (2007) Human Xip1 (C2orf13) is a novel regulator of cellular responses to DNA strand breaks. *J Biol Chem*, **282**, 19638-19643.
17. Iles, N., Rulten, S., El-Khamisy, S.F. and Caldecott, K.W. (2007) APLF (C2orf13) is a novel human protein involved in the cellular response to chromosomal DNA strand breaks. *Mol Cell Biol*, **27**, 3793-3803.
18. Vogel, C. and Marcotte, E.M. (2012) Insights into the regulation of protein abundance from proteomic and transcriptomic analyses. *Nat Rev Genet*, **13**, 227-232.
19. Warren, C., Matsui, T., Karp, J.M., Onikubo, T., Cahill, S., Brenowitz, M., Cowburn, D., Girvin, M. and Shechter, D. (2017) Dynamic intramolecular regulation of the histone chaperone nucleoplasmin controls histone binding and release. *Nat Commun*, **8**, 2215.
20. Chantalat, L., Nicholson, J.M., Lambert, S.J., Reid, A.J., Donovan, M.J., Reynolds, C.D., Wood, C.M. and Baldwin, J.P. (2003) Structure of the histone-core octamer in KCl/phosphate crystals at 2.15 A resolution. *Acta Crystallogr D Biol Crystallogr*, **59**, 1395-1407.
21. Luger, K., Mader, A.W., Richmond, R.K., Sargent, D.F. and Richmond, T.J. (1997) Crystal structure of the nucleosome core particle at 2.8 A resolution. *Nature*, **389**, 251-260.
22. Bowman, A., Ward, R., El-Mkami, H., Owen-Hughes, T. and Norman, D.G. (2010) Probing the (H3-H4)2 histone tetramer structure using pulsed EPR spectroscopy combined with site-directed spin labelling. *Nucleic Acids Res*, **38**, 695-707.
23. Huang, H., Stromme, C.B., Saredi, G., Hodl, M., Strandsby, A., Gonzalez-Aguilera, C., Chen, S., Groth, A. and Patel, D.J. (2015) A unique binding mode enables MCM2 to chaperone histones H3-H4 at replication forks. *Nat Struct Mol Biol*, **22**, 618-626.

24. Barbera, A.J., Chodaparambil, J.V., Kelley-Clarke, B., Joukov, V., Walter, J.C., Luger, K. and Kaye, K.M. (2006) The nucleosomal surface as a docking station for Kaposi's sarcoma herpesvirus LANA. *Science*, **311**, 856-861.
25. Kato, H., Jiang, J., Zhou, B.R., Rozendaal, M., Feng, H., Ghirlando, R., Xiao, T.S., Straight, A.F. and Bai, Y. (2013) A conserved mechanism for centromeric nucleosome recognition by centromere protein CENP-C. *Science*, **340**, 1110-1113.
26. Makde, R.D., England, J.R., Yennawar, H.P. and Tan, S. (2010) Structure of RCC1 chromatin factor bound to the nucleosome core particle. *Nature*, **467**, 562-566.
27. McGinty, R.K., Henrici, R.C. and Tan, S. (2014) Crystal structure of the PRC1 ubiquitylation module bound to the nucleosome. *Nature*, **514**, 591-596.
28. Yang, D., Fang, Q., Wang, M., Ren, R., Wang, H., He, M., Sun, Y., Yang, N. and Xu, R.M. (2013) Nalpha-acetylated Sir3 stabilizes the conformation of a nucleosome-binding loop in the BAH domain. *Nat Struct Mol Biol*, **20**, 1116-1118.
29. Kato, H., van Ingen, H., Zhou, B.R., Feng, H., Bustin, M., Kay, L.E. and Bai, Y. (2011) Architecture of the high mobility group nucleosomal protein 2-nucleosome complex as revealed by methyl-based NMR. *Proc Natl Acad Sci U S A*, **108**, 12283-12288.
30. Kalashnikova, A.A., Porter-Goff, M.E., Muthurajan, U.M., Luger, K. and Hansen, J.C. (2013) The role of the nucleosome acidic patch in modulating higher order chromatin structure. *J R Soc Interface*, **10**, 20121022.
31. Wilson, M.D., Benlekbir, S., Fradet-Turcotte, A., Sherker, A., Julien, J.P., McEwan, A., Noordermeer, S.M., Sicheri, F., Rubinstein, J.L. and Durocher, D. (2016) The structural basis of modified nucleosome recognition by 53BP1. *Nature*, **536**, 100-103.
32. Zhou, K., Gaullier, G. and Luger, K. (2019) Nucleosome structure and dynamics are coming of age. *Nat Struct Mol Biol*, **26**, 3-13.
33. Armache, K.J., Garlick, J.D., Canzio, D., Narlikar, G.J. and Kingston, R.E. (2011) Structural basis of silencing: Sir3 BAH domain in complex with a nucleosome at 3.0 A resolution. *Science*, **334**, 977-982.
34. Biswas, S. and Rao, C.M. (2018) Epigenetic tools (The Writers, The Readers and The Erasers) and their implications in cancer therapy. *Eur J Pharmacol*, **837**, 8-24.
35. Borgia, A., Borgia, M.B., Bugge, K., Kissling, V.M., Heidarsson, P.O., Fernandes, C.B., Sottini, A., Soranno, A., Buholzer, K.J., Nettels, D. *et al.* (2018) Extreme disorder in an ultrahigh-affinity protein complex. *Nature*, **555**, 61-66.
36. Hansen, J.C., Lu, X., Ross, E.D. and Woody, R.W. (2006) Intrinsic protein disorder, amino acid composition, and histone terminal domains. *J Biol Chem*, **281**, 1853-1856.
37. Mao, P., Kyriss, M.N., Hodges, A.J., Duan, M., Morris, R.T., Lavine, M.D., Topping, T.B., Gloss, L.M. and Wyrick, J.J. (2016) A basic domain in the histone H2B N-terminal tail is important for nucleosome assembly by FACT. *Nucleic Acids Res*, **44**, 9142-9152.
38. Parra, M.A., Kerr, D., Fahy, D., Pouchnik, D.J. and Wyrick, J.J. (2006) Deciphering the roles of the histone H2B N-terminal domain in genome-wide transcription. *Mol Cell Biol*, **26**, 3842-3852.
39. Smith, S. and Stillman, B. (1991) Stepwise assembly of chromatin during DNA replication in vitro. *EMBO J*, **10**, 971-980.
40. Andrews, A.J., Chen, X., Zevin, A., Stargell, L.A. and Luger, K. (2010) The histone chaperone Nap1 promotes nucleosome assembly by eliminating nonnucleosomal histone DNA interactions. *Mol Cell*, **37**, 834-842.
41. Mazurkiewicz, J., Kepert, J.F. and Rippe, K. (2006) On the mechanism of nucleosome assembly by histone chaperone NAP1. *J Biol Chem*, **281**, 16462-16472.
42. Andrews, A.J., Downing, G., Brown, K., Park, Y.J. and Luger, K. (2008) A thermodynamic model for Nap1-histone interactions. *J Biol Chem*, **283**, 32412-32418.
43. Elsasser, S.J. and D'Arcy, S. (2013) Towards a mechanism for histone chaperones. *Biochim Biophys Acta*, **1819**, 211-221.
44. Chaires, J.B. (1983) Daunomycin inhibits the B leads to Z transition in poly d(G-C). *Nucleic Acids Res*, **11**, 8485-8494.
45. Guschin, D., Chandler, S. and Wolffe, A.P. (1998) Asymmetric linker histone association directs the asymmetric rearrangement of core histone interactions in a positioned nucleosome containing a thyroid hormone response element. *Biochemistry*, **37**, 8629-8636.
46. Lee, K.M. and Hayes, J.J. (1998) Linker DNA and H1-dependent reorganization of histone-DNA interactions within the nucleosome. *Biochemistry*, **37**, 8622-8628.
47. Ikura, T., Tashiro, S., Kakino, A., Shima, H., Jacob, N., Amunugama, R., Yoder, K., Izumi, S., Kuraoka, I., Tanaka, K. *et al.* (2007) DNA damage-dependent acetylation and ubiquitination of H2AX enhances chromatin dynamics. *Mol Cell Biol*, **27**, 7028-7040.
48. Heo, K., Kim, H., Choi, S.H., Choi, J., Kim, K., Gu, J., Lieber, M.R., Yang, A.S. and An, W. (2008) FACT-mediated exchange of histone variant H2AX regulated by phosphorylation of H2AX and ADP-ribosylation of Spt16. *Mol Cell*, **30**, 86-97.
49. Tsunaka, Y., Fujiwara, Y., Oyama, T., Hirose, S. and Morikawa, K. (2016) Integrated molecular mechanism directing nucleosome reorganization by human FACT. *Genes Dev*, **30**, 673-686.

50. Angelov, D., Bondarenko, V.A., Almagro, S., Menoni, H., Mongelard, F., Hans, F., Mietton, F., Studitsky, V.M., Hamiche, A., Dimitrov, S. *et al.* (2006) Nucleolin is a histone chaperone with FACT-like activity and assists remodeling of nucleosomes. *EMBO J*, **25**, 1669-1679.
51. Goldstein, M., Derheimer, F.A., Tait-Mulder, J. and Kastan, M.B. (2013) Nucleolin mediates nucleosome disruption critical for DNA double-strand break repair. *Proc Natl Acad Sci U S A*, **110**, 16874-16879.
52. Fox, J.M., Zhao, M., Fink, M.J., Kang, K. and Whitesides, G.M. (2018) The Molecular Origin of Enthalpy/Entropy Compensation in Biomolecular Recognition. *Annu Rev Biophys*, **47**, 223-250.
53. Huang, Y. and Liu, Z. (2013) Do intrinsically disordered proteins possess high specificity in protein-protein interactions? *Chemistry*, **19**, 4462-4467.
54. Dragan, A.I., Read, C.M. and Crane-Robinson, C. (2017) Enthalpy-entropy compensation: the role of solvation. *Eur Biophys J*, **46**, 301-308.
55. Lumry, R. and Rajender, S. (1970) Enthalpy-entropy compensation phenomena in water solutions of proteins and small molecules: a ubiquitous property of water. *Biopolymers*, **9**, 1125-1227.
56. Frederick, K.K., Marlow, M.S., Valentine, K.G. and Wand, A.J. (2007) Conformational entropy in molecular recognition by proteins. *Nature*, **448**, 325-329.
57. Tzeng, S.R. and Kalodimos, C.G. (2012) Protein activity regulation by conformational entropy. *Nature*, **488**, 236-240.
58. Davey, C.A., Sargent, D.F., Luger, K., Maeder, A.W. and Richmond, T.J. (2002) Solvent mediated interactions in the structure of the nucleosome core particle at 1.9 a resolution. *J Mol Biol*, **319**, 1097-1113.
59. Davey, C.A. and Richmond, T.J. (2002) DNA-dependent divalent cation binding in the nucleosome core particle. *Proc Natl Acad Sci U S A*, **99**, 11169-11174.
60. Luger, K. and Richmond, T.J. (1998) DNA binding within the nucleosome core. *Curr Opin Struct Biol*, **8**, 33-40.
61. Liu, W.H. and Churchill, M.E. (2012) Histone transfer among chaperones. *Biochem Soc Trans*, **40**, 357-363.
62. Burgess, R.J. and Zhang, Z. (2013) Histone chaperones in nucleosome assembly and human disease. *Nat Struct Mol Biol*, **20**, 14-22.
63. Li, Q., Burgess, R. and Zhang, Z. (2013) All roads lead to chromatin: multiple pathways for histone deposition. *Biochim Biophys Acta*, **1819**, 238-246.
64. Park, Y.J. and Luger, K. (2008) Histone chaperones in nucleosome eviction and histone exchange. *Curr Opin Struct Biol*, **18**, 282-289.
65. Beissinger, M. and Buchner, J. (1998) How chaperones fold proteins. *Biol Chem*, **379**, 245-259.
66. Horowitz, S., Koldewey, P., Stull, F. and Bardwell, J.C. (2018) Folding while bound to chaperones. *Curr Opin Struct Biol*, **48**, 1-5.
67. Corrales, F.J. and Fersht, A.R. (1995) The folding of GroEL-bound barnase as a model for chaperonin-mediated protein folding. *Proc Natl Acad Sci U S A*, **92**, 5326-5330.
68. Stenberg, G. and Fersht, A.R. (1997) Folding of barnase in the presence of the molecular chaperone SecB. *J Mol Biol*, **274**, 268-275.
69. Stull, F., Koldewey, P., Humes, J.R., Radford, S.E. and Bardwell, J.C.A. (2016) Substrate protein folds while it is bound to the ATP-independent chaperone Spy. *Nat Struct Mol Biol*, **23**, 53-58.
70. Hammond, C.M., Stromme, C.B., Huang, H., Patel, D.J. and Groth, A. (2017) Histone chaperone networks shaping chromatin function. *Nat Rev Mol Cell Biol*, **18**, 141-158.
71. Mattiroli, F., Gu, Y., Yadav, T., Balsbaugh, J.L., Harris, M.R., Findlay, E.S., Liu, Y., Radebaugh, C.A., Stargell, L.A., Ahn, N.G. *et al.* (2017) DNA-mediated association of two histone-bound complexes of yeast Chromatin Assembly Factor-1 (CAF-1) drives tetrasome assembly in the wake of DNA replication. *Elife*, **6**.
72. Sauer, P.V., Gu, Y., Liu, W.H., Mattiroli, F., Panne, D., Luger, K. and Churchill, M.E. (2018) Mechanistic insights into histone deposition and nucleosome assembly by the chromatin assembly factor-1. *Nucleic Acids Res*, **46**, 9907-9917.
73. English, C.M., Adkins, M.W., Carson, J.J., Churchill, M.E. and Tyler, J.K. (2006) Structural basis for the histone chaperone activity of Asf1. *Cell*, **127**, 495-508.
74. Natsume, R., Eitoku, M., Akai, Y., Sano, N., Horikoshi, M. and Senda, T. (2007) Structure and function of the histone chaperone CIA/ASF1 complexed with histones H3 and H4. *Nature*, **446**, 338-341.
75. Wang, H., Wang, M., Yang, N. and Xu, R.-M. (2015) Structure of the quaternary complex of histone H3-H4 heterodimer with chaperone ASF1 and the replicative helicase subunit MCM2. *Protein & Cell*, **6**, 693-697.
76. Ricketts, M.D., Frederick, B., Hoff, H., Tang, Y., Schultz, D.C., Singh Rai, T., Grazia Vizioli, M., Adams, P.D. and Marmorstein, R. (2015) Ubinuclein-1 confers histone H3.3-specific-binding by the HIRA histone chaperone complex. *Nat Commun*, **6**, 7711.
77. DeNizio, J.E., Elsasser, S.J. and Black, B.E. (2014) DAXX co-folds with H3.3/H4 using high local stability conferred by the H3.3 variant recognition residues. *Nucleic Acids Res*, **42**, 4318-4331.
78. Sillje, H.H. and Nigg, E.A. (2001) Identification of human Asf1 chromatin assembly factors as substrates of Tousled-like kinases. *Curr Biol*, **11**, 1068-1073.

79. Klimovskaia, I.M., Young, C., Stromme, C.B., Menard, P., Jasencakova, Z., Mejlvang, J., Ask, K., Ploug, M., Nielsen, M.L., Jensen, O.N. *et al.* (2014) Tousled-like kinases phosphorylate Asf1 to promote histone supply during DNA replication. *Nat Commun*, **5**, 3394.
80. Ohtomo, H., Akashi, S., Moriwaki, Y., Okuwaki, M., Osakabe, A., Nagata, K., Kurumizaka, H. and Nishimura, Y. (2016) C-terminal acidic domain of histone chaperone human NAP1 is an efficient binding assistant for histone H2A-H2B, but not H3-H4. *Genes Cells*, **21**, 252-263.
81. Luijsterburg, M.S., de Krijger, I., Wiegant, W.W., Shah, R.G., Smeenk, G., de Groot, A.J.L., Pines, A., Vertegaal, A.C.O., Jacobs, J.J.L., Shah, G.M. *et al.* (2016) PARP1 Links CHD2-Mediated Chromatin Expansion and H3.3 Deposition to DNA Repair by Non-homologous End-Joining. *Mol Cell*, **61**, 547-562.
82. Mehrotra, P.V., Ahel, D., Ryan, D.P., Weston, R., Wiechens, N., Kraehenbuehl, R., Owen-Hughes, T. and Ahel, I. (2011) DNA repair factor APLF is a histone chaperone. *Mol Cell*, **41**, 46-55.
83. Timinszky, G., Till, S., Hassa, P.O., Hothorn, M., Kustatscher, G., Nijmeijer, B., Colombelli, J., Altmeyer, M., Stelzer, E.H., Scheffzek, K. *et al.* (2009) A macrodomain-containing histone rearranges chromatin upon sensing PARP1 activation. *Nat Struct Mol Biol*, **16**, 923-929.
84. Karras, G.I., Kustatscher, G., Buhecha, H.R., Allen, M.D., Pugieux, C., Sait, F., Bycroft, M. and Ladurner, A.G. (2005) The macro domain is an ADP-ribose binding module. *EMBO J*, **24**, 1911-1920.
85. Dutta, S., Akey, I.V., Dingwall, C., Hartman, K.L., Laue, T., Nolte, R.T., Head, J.F. and Akey, C.W. (2001) The crystal structure of nucleoplasmin-core: implications for histone binding and nucleosome assembly. *Mol Cell*, **8**, 841-853.
86. Namboodiri, V.M., Dutta, S., Akey, I.V., Head, J.F. and Akey, C.W. (2003) The crystal structure of Drosophila NLP-core provides insight into pentamer formation and histone binding. *Structure*, **11**, 175-186.
87. Arnan, C., Saperas, N., Prieto, C., Chiva, M. and Ausio, J. (2003) Interaction of nucleoplasmin with core histones. *J Biol Chem*, **278**, 31319-31324.
88. Platonova, O., Akey, I.V., Head, J.F. and Akey, C.W. (2011) Crystal structure and function of human nucleoplasmin (npm2): a histone chaperone in oocytes and embryos. *Biochemistry*, **50**, 8078-8089.
89. Ramos, I., Fernandez-Rivero, N., Arranz, R., Aloria, K., Finn, R., Arizmendi, J.M., Ausio, J., Valpuesta, J.M., Muga, A. and Prado, A. (2014) The intrinsically disordered distal face of nucleoplasmin recognizes distinct oligomerization states of histones. *Nucleic Acids Res*, **42**, 1311-1325.
90. Knapp, A.R., Wang, H. and Parthun, M.R. (2014) The yeast histone chaperone hif1p functions with RNA in nucleosome assembly. *PLoS One*, **9**, e100299.
91. Arents, G. and Moudrianakis, E.N. (1995) The histone fold: a ubiquitous architectural motif utilized in DNA compaction and protein dimerization. *Proc Natl Acad Sci U S A*, **92**, 11170-11174.
92. Moudrianakis, E.N. and Arents, G. (1993) Structure of the histone octamer core of the nucleosome and its potential interactions with DNA. *Cold Spring Harb Symp Quant Biol*, **58**, 273-279.
93. Anderson, J.D. and Widom, J. (2000) Sequence and position-dependence of the equilibrium accessibility of nucleosomal DNA target sites. *J Mol Biol*, **296**, 979-987.
94. Tims, H.S., Gurunathan, K., Levitus, M. and Widom, J. (2011) Dynamics of nucleosome invasion by DNA binding proteins. *J Mol Biol*, **411**, 430-448.
95. Bilokapic, S., Strauss, M. and Halic, M. (2018) Histone octamer rearranges to adapt to DNA unwrapping. *Nat Struct Mol Biol*, **25**, 101-108.
96. Aalfs, J.D. and Kingston, R.E. (2000) What does 'chromatin remodeling' mean? *Trends Biochem Sci*, **25**, 548-555.
97. Fry, C.J. and Peterson, C.L. (2001) Chromatin remodeling enzymes: who's on first? *Curr Biol*, **11**, R185-197.
98. Logie, C. and Peterson, C.L. (1997) Catalytic activity of the yeast SWI/SNF complex on reconstituted nucleosome arrays. *EMBO J*, **16**, 6772-6782.
99. Logie, C., Tse, C., Hansen, J.C. and Peterson, C.L. (1999) The core histone N-terminal domains are required for multiple rounds of catalytic chromatin remodeling by the SWI/SNF and RSC complexes. *Biochemistry*, **38**, 2514-2522.
100. Kireeva, M.L., Walter, W., Tchernajenko, V., Bondarenko, V., Kashlev, M. and Studitsky, V.M. (2002) Nucleosome Remodeling Induced by RNA Polymerase II. *Molecular Cell*, **9**, 541-552.
101. Belotserkovskaya, R., Oh, S., Bondarenko, V.A., Orphanides, G., Studitsky, V.M. and Reinberg, D. (2003) FACT facilitates transcription-dependent nucleosome alteration. *Science*, **301**, 1090-1093.
102. Hansen, J.C. (2002) Conformational dynamics of the chromatin fiber in solution: determinants, mechanisms, and functions. *Annu Rev Biophys Biomol Struct*, **31**, 361-392.
103. Chen, H., Li, B. and Workman, J.L. (1994) A histone-binding protein, nucleoplasmin, stimulates transcription factor binding to nucleosomes and factor-induced nucleosome disassembly. *EMBO J*, **13**, 380-390.
104. Owen-Hughes, T. and Workman, J.L. (1996) Remodeling the chromatin structure of a nucleosome array by transcription factor-targeted trans-displacement of histones. *EMBO J*, **15**, 4702-4712.

Summary

At any time in the nucleus of a eukaryotic cell, chromatin, the protein-DNA supercomplex that harbors the genome, undergoes various processes to meet the needs of the cell during its life cycle. These processes serve to regulate the replication, transcription, or repair of the DNA and are as such dependent on the dynamics of the nucleosome, the fundamental repeating unit of chromatin. A nucleosome is assembled from a protein core of histone proteins around which DNA is wrapped. However, for nuclear processes in which the DNA serves as template for proteins, DNA has to be (partially) unwrapped in a process called nucleosome disassembly. Nucleosome assembly and disassembly are dependent on a family of proteins called histone chaperones. These chaperones bind and manage the histone proteins for all chromatin processes. One of these processes is repair of DNA double-strand breaks (DSBs), a common type of DNA damage in eukaryotic cells. The major pathway for DSB repair in human cells is non-homologous end joining (NHEJ). The NHEJ DNA repair factor Aprataxin and Polynucleotide kinase Like Factor (APLF) was shown to harbor histone chaperone function in its C-terminal acidic domain ($APLF^{AD}$).

The topic of this dissertation is the characterization of the histone chaperone function of $APLF^{AD}$. A multidisciplinary approach is used to better understand how this histone chaperone functions, from histone binding to nucleosome assembly. The aim is to provide a better understanding of NHEJ DNA repair and the mechanism of nucleosome assembly.

Chapter 1 provides a general introduction to the basic terms and principles that are key to this thesis, starting with a structural description of the histone proteins. The four core histones H2A, H2B, H3, and H4 are small highly basic proteins that form the dimers and tetramers H2A-H2B and $(H3\text{-}H4)_2$, respectively. Two H2A-H2B and one $(H3\text{-}H4)_2$ assemble into a histone octamer to form the protein core of the nucleosome, the fundamental repeating unit of chromatin. After a brief account of nucleosome structure, an overview of the structure and function of histone chaperone proteins is given. These proteins bind to histones, prevent unintended interactions with DNA or other factors, help to control histone supply and, crucially, facilitate the ordered and stepwise assembly of nucleosomes. The chaperone that is central to this thesis is the DNA repair factor APLF. Its function as a scaffold protein for the NHEJ complex is described, ending with a discussion on the possible role of its histone chaperone activity in the unstructured C-terminal tail ($APLF^{AD}$).

Chapter 2 describes a detailed protocol for the use of microscale thermophoresis (MST) to study histone-protein interactions, with special emphasis on the interaction of $APLF^{AD}$ with core histones H2A-H2B and H3-H4. Motivated by the small material consumption, sensitivity, speed and ease of the MST experiment, we focus on obtaining reproducible, high-quality binding data. Key steps in the design, strategies to detect and overcome assay issues, the step-by-step optimization of experimental conditions, as well as the execution and analysis of the experiments are discussed and illustrated on the experimental data. The MST derived binding curves show that $APLF^{AD}$ binds with high and comparable affinities to both H2A-H2B and $(H3\text{-}H4)_2$, suggesting $APLF^{AD}$ is a generic histone chaperone domain. Two transitions are observed in each case, suggesting the presence of two separate binding events, which may be relevant for the chaperoning mechanism of $APLF^{AD}$.

In **Chapter 3**, we investigated the molecular basis of the histone chaperone function of APLF^{FAD} for H2A-H2B based on MST, nuclear magnetic resonance (NMR) spectroscopy, crosslinking, isothermal titration calorimetry (ITC), and a functional chaperone assay. We show that APLF^{FAD} is intrinsically disordered and binds specifically and with high affinity to both H2A-H2B and H3-H4. APLF^{FAD} binds H2A-H2B through an acidic histone binding domain (HBD) containing two aromatic residues that contact two patches on H2A-H2B. Based on our data, we propose a structural model in which APLF^{FAD} binds H2A-H2B through electrostatic interactions and uses the aromatic side chains to anchor specifically to the DNA-interaction surface of the histones. In a chaperone assay, APLF^{FAD} is shown to prevent unspecific complex formation between H2A-H2B and DNA in a manner that depends on the aromatic anchors. Furthermore, we found evidence for a secondary binding mode involving the H2B αC-helix, an exposed feature on the nucleosome surface. This additional binding mode could represent a key step in the transfer of histone complexes from and to DNA and other chaperones. Our results suggest that APLF has the capability to temporarily store histone complexes at the DNA damage site for later nucleosome reassembly.

The presence of a distinct binding site for H3-H4 within APLF^{FAD} is reported in **Chapter 4**. As for the H2A-H2B binding domain, this region contains two aromatic residues that, in this case, bind to the α1-α2-patch of H3. We show using a variety of techniques that two APLF^{FAD} molecules can bind simultaneously to H2A-H2B and H3-H4 to form stable complexes with histone octamers. Through data-driven docking, we show that the four aromatic residues are appropiately spaced to engage simultaneously to the α1-α2-patches of H2A, H2B, and H3, holding the histones in their native nucleosomal configuration while at the same time allowing for extensive electrostatic interactions with the DNA binding surface of the histone octamer. We call this APLF^{FAD}-bound histone octamer complex the "chaperonosome". As shown in a chaperone assay, APLF^{FAD} promotes deposition of the histone octamer onto DNA through a mechanism that is dependent on the aromatic anchors. The structural model of the APLF^{FAD}-histone complex and mutational analysis strongly suggests a logical mechanism for this chaperone activity: the DNA first contacts a free DNA binding site on H4 within the chaperonosome followed by wrapping of the DNA around the histone octamer as it displaces the two APLF^{FAD} molecules. APLF may thus endow the NHEJ DNA repair complex with the capability to both temporarily store the histone octamer and subsequently promote nucleosome assembly to seal the repaired DNA. These findings highlight that histone deposition can depend on a controlled pre-assembly and transfer of the complete histone octamer rather than a stepwise transfer of histone sub-complexes.

Chapter 5 gives a general discussion based on the major result of this thesis which is the formation of the histone octamer complex by APLF^{FAD}, the "chaperonosome" structural model, as well as an "octamer preassembly"-based model for nucleosome assembly. We underscore the functional importance of the aromatic anchors in imposing a functional binding mode and contrast this to the nonspecific electrostatic interaction. We discuss the advantages of protein disorder for formation of the chaperonosome. The limitations of the structural model are discussed with particular focus on a possible role for the KR-motif in APLF^{FAD} to mediate the secondary binding interaction to the histones. This motif may bind to the H2A-H2B acidic patch or the H2B-H4 cleft, thereby contributing to the stabilization of the histone octamer. We detail the chaperonosome based assembly mechanism and stress the role of enthalpy-entropy compensation in allowing ordered nucleosome assembly. After pointing out the shared modular nature of the chaperonosome, nucleosome, and histone octamer, histone transfer and

nucleosome assembly mechanisms of other histone chaperones are discussed. Following drawing parallels to protein folding, we incorporate the chaperonosome in a model of the NHEJ DNA repair complex for the binding, storing, and deposition of the histone octamer onto DNA in the process. Finally, we make propositions for implementing the chaperonosome for future studies on chromatin.

In summary, this thesis presents a detailed characterization of the histone chaperone function of APLF^{AD} resulting in a model of a histone chaperone-bound histone octamer complex that we call "chaperonosome", and that explains the mechanism of nucleosome assembly by APLF. With a multidisciplinary approach we developed a sophisticated nucleosome assembly mechanism centered around pre-assembly of the histone octamer and its transfer onto DNA. These findings open up a number of possibilities for future research on histone chaperone function in health and disease. Therefore, I conclude that for histone chaperone research

"… this is not the end. It is not even the beginning of the end. But it is, perhaps, the end of the beginning."

(Winston Churchill in his speech *The Bright Gleam of Victory* on November 10, 1942, in the Mansion House, London, United Kingdom)*.

* Winston S. Churchill, The End of the Beginning, Cassell and Company Ltd, London, 1943.

Samenvatting

In de eukaryote celkern is chromatine, het eiwit-DNA-supercomplex dat het genoom herbergt, voortdurend bezig de cel te ondersteunen tijdens zijn deling, groei en instandhouding van de genetische informatie. De processen die verantwoordelijk zijn voor DNA-replicatie, transcriptie en reparatie zijn direct afhankelijk van de dynamiek van het nucleosoom, de fundamentele repeterende eenheid van chromatine. Een nucleosoom bestaat uit een kern van histoneiwitten waar DNA zich omheen wikkelt. Echter tijdens transcriptie, waarbij de genetische code afgelezen wordt, moet DNA (gedeeltelijk) ontwonden worden in een proces dat nucleosoom-demontage wordt genoemd. Verantwoordelijk voor de nucleosoom-assemblage en -demontage is een familie van eiwitten die histon-chaperonnes worden genoemd. Deze chaperonnes binden en begeleiden de histoneiwitten tijdens alle chromatineprocessen. Een cruciaal proces voor behoud van de integriteit van het genoom is de reparatie van DNA-dubbelstrengsbreuken (DSB). De belangrijkste route voor DSB-reparatie in menselijke cellen is *non-homologous end joining* (NHEJ). Voor de nucleosoom assemblage nabij de DNA beschadiging moeten de histonen worden samengebracht. *Aprataxin and Polynucleotide-kinase Like Factor* (APLF) is de NHEJ-DNA-reparatiefactor die hiervoor de histonchaperonnefunctie in zijn C-terminale zure domein ($APLF^{AD}$) herbergt.

Het onderwerp van dit proefschrift is de karakterisatie van de histonchaperonnefunctie van $APLF^{AD}$. Om beter te begrijpen hoe deze histonchaperonne, van histonbinding tot nucleosoom-assemblage, functioneert, wordt een multidisciplinaire benadering gebruikt. Doel van het onderzoek is een beter begrip van NHEJ-DNA-herstel en het mechanisme van nucleosoom-assemblage.

Hoofdstuk 1 geeft een algemene inleiding tot de basisbegrippen en -beginselen die centraal staan in dit proefschrift en begint met een structurele beschrijving van de histoneiwitten. De vier kernhistonen H2A, H2B, H3 en H4 zijn kleine, zeer basische eiwitten die dimeren en tetrameren, respectievelijk H2A-H2B en $(H3\text{-}H4)_2$, vormen. Twee H2A-H2B dimeren en één $(H3\text{-}H4)_2$ tetrameer vormen een histon-octameer, de eiwitkern van het nucleosoom, de fundamentele repeterende eenheid van chromatine. Na een korte bespreking van de nucleosoom-structuur, volgt een overzicht van de structuur en functie van histonchaperonne-eiwitten. Histonchaperonnes binden histonen, blokkeren ongewenste interacties met DNA en andere factoren, assisteren bij de aanvoer van histonen, en faciliteren een stapsgewijze opbouw van nucleosomen.

Hoofdstuk 2 geeft een gedetailleerd protocol voor het gebruik van *microscale thermophoresis* (MST) voor bestudering van histon-eiwit interacties, met name de interactie van $APLF^{AD}$ met de kernhistonen H2A-H2B en H3-H4. Met nadruk op de geringe behoefte aan materiaal, de gevoeligheid, snelheid en eenvoud van het MST experiment, focusseren we op het nauwkeurig en goed reproduceerbaar meten van bindingsaffiniteiten. We bespreken de belangrijkste stappen in ontwerp van het experiment, strategieën voor het detecteren en oplossen van testproblemen, de stapsgewijze optimalisatie van experimentele condities, evenals de uitvoering en analyse van de experimenten. De MST-resultaten laten zien dat $APLF^{AD}$ met hoge en vergelijkbare affiniteit aan zowel H2A-H2B als $(H3\text{-}H4)_2$ bindt, hetgeen suggereert dat $APLF^{AD}$ een generiek histonchaperonnedomein is. In beide gevallen laten de bindingscurves twee overgangen zien, wat twee afzonderlijke bindingsstappen suggereert, één met hoge affiniteit (in het nanomolaire

bereik) en één met lage (micromolaire bereik), hetgeen mogelijk van belang is voor het chaperonnemechanisme van APLF^{FAD}.

In **Hoofdstuk 3** onderzochten we de moleculaire basis van de histonchaperonnefunctie van APLF^{FAD}, in het bijzonder voor H2A-H2B. Behalve MST gebruikten we hiervoor een combinatie van kernspinresonantie (NMR, van *nuclear magnetic resonance*) spectroscopie, crosslinking, isotherme titratiecalorimetrie (ITC) en een functionele chaperonne-test. We laten zien dat APLF^{FAD} intrinsiek ongestructureerd is en met hoge affiniteit zowel aan H2A-H2B als H3-H4 bindt. APLF^{FAD} bindt H2A-H2B via een zuur histon-bindend domein (HBD) dat twee aromatische zijketens bevat die binden aan de twee α1-α2-patches op H2A-H2B. Op basis van onze resultaten, stellen we een structuurmodel voor waarin APLF^{FAD} H2A-H2B bindt door middel van elektrostatische interacties en de aromatische zijketens het DNA-interactieoppervlak van de histonen afdekken. In een chaperonne-assay toonden we aan dat APLF^{FAD} niet-specifieke complexvorming tussen H2A-H2B en DNA voorkomt, waarbij de aromatische zijketens een belangrijke rol spelen. Verder vonden we op het nucleosoomoppervlak in de αC-helix van H2B een tweede bindingsplaats voor APLF^{FAD}. Deze extra bindingsmodus speelt mogelijk een belangrijke rol in de overdracht van histoncomplexen van en naar DNA en andere chaperonnes. Onze resultaten suggereren dat APLF de mogelijkheid heeft om histoncomplexen tijdelijk op te slaan bij een DNA-beschadiging zodat deze later weer gebruikt kunnen worden om een nieuw nucleosoom op te bouwen.

In **Hoofdstuk 4** laten we zien dat APLF^{FAD} een extra bindingsplaats heeft die specifiek is voor H3-H4. Analoog aan het bindingsdomein voor H2A-H2B, bevat dit gebied twee aromatische aminozuurresiduen die in dit geval binden aan de α1-α2-patch van H3. Met behulp van verschillende technieken laten we zien dat twee APLF^{FAD}-moleculen gelijktijdig binden aan H2A-H2B en H3-H4 om stabiele complexen te vormen met histon-octameren. Met behulp van data-gedreven docking, laten we zien dat de vier aromatische residuen zo gerangschikt zijn dat ze tegelijk binden aan de α1-α2-patches van H2A, H2B en H3 en de histonen in hun uiteindelijke nucleosoom configuratie brengen en op hetzelfde moment een reeks van elektrostatische interacties met het DNA-bindings-oppervlak van de histon octamer mogelijk maken. We noemen dit APLF^{FAD}-gebonden histon-octameercomplex het "chaperonosoom". Met behulp van een functionele chaperonne-assay laten we zien dat APLF^{FAD} de histone-octameer op het DNA positioneert via een mechanisme waarin de aromatische residuen van APLF^{FAD} een grote rol spelen. Het structuurmodel van het APLF^{FAD}-histon-complex en een mutatie-analyse geeft goede onderbouwing van het mechanisme van de chaperonne-activiteit: allereerst bindt het DNA aan een vrije DNA-bindingsplaats op H4 in het chaperonosoom, waarna het DNA zich rond de histon-octameer wikkelt en het de twee APLF^{FAD}-moleculen verwijdert. Daarmee breidt APLF het NHEJ DNA-reparatie-complex uit met de mogelijkheid om de histon-octameer tijdelijk op te slaan dichtbij een DNA-beschadiging om vervolgens de nucleosoom-assemblage te initiëren en bij te dragen aan het DNA-herstel. Dit laat zien dat de histonen in een gecontroleerde pre-assemblage op het DNA geplaatst kunnen worden waarbij het histon-octameer in zijn geheel en niet stapsgewijs wordt overgedragen.

Hoofdstuk 5 geeft een algemene discussie gebaseerd op het belangrijkste resultaat van dit proefschrift, namelijk de vorming van het histon-octameer-complex door APLF^{FAD}, het "chaperonosoom"-structuurmodel, met daarnaast een model voor nucleosoom-assemblage door middel van "octameer preassemblage". We wijzen op het belang van de aromatische ankers voor een functionele binding en stellen dit tegenover de niet-specifieke elektrostatische

interactie. We bespreken de voordelen van intrinsiek ongeordende eiwitten voor de vorming van het chaperonosoom. De beperkingen van het structuurmodel worden bediscussieerd aan de hand van een mogelijke rol voor het KR-motief van APLF^{FAD} in een additionele interactie met de histonen. Dit motief bindt mogelijk aan de zure patch op H2A-H2B en in de gleuf bij H2B-H4, hetgeen bijdraagt aan de stabilisatie van het histon-octameer. Verder bespreken we het chaperonosoom-assemblage-mechanisme en wijzen op de rol van enthalpie-entropie-compensatie voor een geordende nucleosoom-assemblage. Na te wijzen op het gemeenschappelijke modulaire karakter van het chaperonosoom, het nucleosoom en de histon-octameer, bespreken we histonoverdracht en nucleosoom-assemblage-mechanismen van andere histonchaperonnes. We leggen een link naar chaperonnes in eiwitvouwing en nemen het chaperonosoom op in een model van het NHEJ DNA-reparatiecomplex voor de binding, opslag en depositie van het histon-octameer op DNA. Ten slotte doen we voorstellen voor mogelijke rollen van het chaperonosoom in toekomstige studies aan chromatine.

Samenvattend, in dit proefschrift geven we een gedetailleerde karakterisatie van de histonchaperonnefunctie van APLF^{FAD}, dat uitmondt in een model van een histonchaperonne-gebonden histon-octameer-complex dat we het "chaperonosoom" hebben genoemd en dat het mechanisme van nucleosoom-assemblage door APLF kan verklaren. Met een multidisciplinaire aanpak hebben we een nucleosoom-assemblagemechanisme ontwikkeld dat gebruik maakt van pre-assemblage en overdracht van een volledig histon-octameer. Deze bevindingen geven tal van mogelijkheden voor toekomstig onderzoek naar de histonchaperonnefunctie in gezondheid en ziekte. Daarom concludeer ik dat voor histonchaperonne-onderzoek

"... dit niet het einde is. Het is zelfs niet het begin van het einde. Maar het is misschien wel het einde van het begin."

(Winston Churchill in zijn toespraak *The Bright Gleam of Victory* op 10 november 1942, in het Mansion House, Londen, Verenigd Koninkrijk)*.

* Winston S. Churchill, The End of the Beginning, Cassell and Company Ltd, London, 1943.

Thanks a hundred to my chaperones

It is a difficult but important task to thank every person who helped make this thesis possible. This work would not have been possible without hundreds of people probably. It is more than just four years of research. The life around it plays a role, too.

Gratitude does not come naturally to many people but it can be a key to a good and balanced life. The journalist and author A. J. Jacobs wrote a book about it (Thanks a Thousand: A Gratitude Journey, Simon & Schuster/TED, 2018) in which he tells us about it. Scientific research shows that being grateful can make our lives happier, more impactful, it improves human relationships and compassion (connects us and makes us more generous and kinder to strangers), heals the body, helps to lift depression and sleep better, and makes it easier to improve the diet and do physical exercise. This is a reminder of the interconnectedness of things.

A spectrum is a condition that is not limited to a specific set of values but can vary, without steps, across a continuum. Like everything else in life, also human nature lies on a spectrum, ranging anywhere from super bad to angelic, ultra-conservative to uber-liberal, humble to pretentious etc., all the extremes of any possible human characteristic and everything in between. The same is true for scientific knowledge and capabilities. In such a multidisciplinary project as the one described in this thesis, people from different parts of the spectra were involved. But as we are all chaperones, we can chaperone each other towards the right path.

With this, I would like to thank all my chaperones throughout the last years.

Of course, my project, work, success, and career would not have been possible without my promotor. Thank you so much **Prof. Dr. Rolf Boelens** for accepting me as your last PhD candidate, for all the lectures and wisdoms about science and life, for pushing to arrange my PhD defense, and for letting me go to all the different conferences and NMR workshops. I learnt a lot on those trips and also some good new people. A big thanks to my co-promotor and supervisor throughout these years, **Dr. Hugo van Ingen.** Thank you for all your support. It is amazing how many scripts you can pull out of your sleeve. Thank you very much for letting us write together all the manuscripts, papers, and thesis chapters. Thank you also for letting me do my lab work on my own, in my own time, until I finally had the essential results of some very difficult and challenging assays. I learnt a tremendous amount about these processes. Thank you very much for all the proofreading and editing of this thesis. It was a key for the success of my project that you managed to come to Utrecht. Thanks for making the collaborations happen in my last official PhD year. That and all the equipment that was added to our lab when you got your position in Utrecht were absolute key factors for the success of the chaperonosome story. Thank you very much for writing an application so that I could give my chaperone talk at the Bijvoet Symposium 2019. It would have been such a pity if, after so many years, the people of the Bijvoet Center would have missed out on this one-of-a-kind performance. Thank you very much for pushing to get my application through for the FEBS YSF and Congress 2019 for which I was selected in the end to give two talks (at the YSF and the Congress). At the YSF, I also won my first ever scientific award (Best-talk-award) for my chaperone story which encouraged me to give the same talk again with a different message at the end a few days later at the Congress. Both talks were very well-received and represented a

major impact on these meetings and the reactions I got from the audience and people were just incredible. It was also because of the freedom that you gave me in my thinking process and preparation of talks, as well as some challenging questions that made it possible for me to come up with the chaperone story. With these attitudes, both my promotor and co-promotor were very good scientific chaperones throughout these years.

I would like to thank my thesis reading and defense committee for putting the effort into reading and evaluating this thesis: **Dr. Francesca Mattiroli**, **Prof. Dr. Inneke Braakman** (who was so kind to agree on short notice to be in my thesis reading committee after somebody else had to cancel), **Prof. Dr. Titia Sixma**, **Prof. Dr. Haico van Attikum**, **Prof. Dr. Guido van den Ackerveken**, **Prof. Dr. Willem Kegel**, and **Dr. Stefan Rüdiger**. Also thanks to the chair at my defense **Prof. Dr. Hans Kamerling**.

Thanks to all my office mates which changed a couple of times throughout the years, but luckily, I was never alone and it is nice to have people come around, even if it is for my office mates, and have some conversations. Thanks to **Agnes (Aha) Adler** for being such a friendly new office mate and for the new ("insider") jokes you have introduced ("Was ist tiefer: Tasse, Oder, Teller? Oder!" :D). It is amazing to see how much about science you know at your young age and how you can manage so many things in a short amount of time. Thanks to **Dr. Cecilia Pinto** for the nice evening with dinner and games you invited some of us for in Amersfoort. You were also a chaperone that brought people together to get lunch which was nice to see. Thanks to **Dr. Deni Mance** for your friendliness and kind conversations. It was a good experience to do the NMR teaching with a DNP expert and PhD of the year like you. Thanks to the office mate I shared my office with for the longest time here, **Siddarth (Sid) Narasimhan**, for all the support throughout these years. Your knowledge of trivia is amazing. You are a connoisseur of the art of living (great food, coffee, BBQ) with all that you have been through during your time here. Your language skills are amazing. It is great to see how you can get dedicated and follow through with things, be it a private or scientific challenge, losing weight, becoming fit, learning a language that is essential for your future, or changing your citizenship.

Interestingly, all my office mates have been from the solid-state NMR part of the group and of course I would like to thank everyone else of that group, too. Thanks to **Prof. Dr. Marc Baldus** for making it possible that all these nice people could work here. Thanks to **Dr. Elwin van der Cruijsen** for greeting friendly when you are around. It is great to see what you have achieved with your PhD. Thanks to the visiting scientist **Dr. Guoqing Jia** for your interest in pretty much everything in the lab, interesting questions and conversations at the lunch table. Thank you also for the Chinese hot pot you invited some of us for as a farewell at your place. Thanks to **Dr. Marie Renault** for always being so kind and friendly. Thanks to **Dr. Shengqi Xiang** for your NMR teaching efforts. Thanks to **Dr. Mohammed Kaplan** for being so friendly and easy-going. Your work and publications are amazing, especially what you have managed to do at Caltech with a new technique. Your fluency in Dutch and your musical talents are an inspiration. Thanks to **Alessandra (Ale) Lucini Paioni** for all the times when you fetched me for a coffee break or to get lunch. You are so friendly and funny, humble and shy, an expert in DNP and a chaperone that brings people together at housewarming and birthday parties. Thank you for supporting my theatre plays. Thanks also to your boyfriend **Dr. Ewan Henry** for making a nice compliment about my "Forrest Gump" short scene performance during the theatre course you were so kind to come and participate in. It was amazing to see how fit you both are, running 10 km at the "Utrecht Singelloop" 2018 in under an hour. Thanks to **Barend Elenbaas** for being so kind and funny. Your lunch eating acts, German accent speeches, and

jokes are hilarious. Thank you for your kind words after my first "chaperone story" group presentation in 2018. That encouraged me to continue with it and also to congratulate others on their good presentations and other achievements. I have heard and seen on video that you are amazing with the saxophone, so continue to inspire people with that talent. Thanks to **Helena (Heli) Leona Ehren** for bringing some "Koelsch" culture to the group. Thanks for being so kind to come and talk to me, ask if I wanted to go for coffee, walks and to get food. Thanks for your strength and for walking with us the "Night of the refugee" 2019 for which also your boyfriend **Benedikt Pluskat** joined who I would like to thank for being so kind and funny. It was amazing to see how you both mastered that walk with ease and fun. Thanks to the visiting PhD candidate **Federico Fontana** for being kind and telling about your sports activities and vacations. Thanks to **Reinier (Reiner) Damman** for being so kind and making conversation with me at lunches and coffee breaks. You are very much down-to-earth, sophisticated, well-organized, and social. Your dancing skills which you show at some borrels from time to time are amazing. Thanks to **Yanzhang (Jon) Luo** for the funny moments in acting and making all the PhD defense videos for the people of our group. You are very talented as a director and producer. Thanks for walking with us the "Night of the refugee" 2019. It was great to see how strong you are to walk through the pain that built up during that walk. Thanks also to you and your wife **Jane** for coming to see some of my theatre performances. Thanks to **João Medeiros Silva** for all the fun. You are a great hard worker. Thanks for all the trivia you told me about and the introduction of some nice educational channels. Thanks to **Rhythm Shukla** for being so caring, funny, and social. It is amazing to see how you are so young, yet, already have so much life experience. Thanks for telling all those inspiring stories of yours about sports, activities, and the army experiences you were lucky to gather because of your father who is an officer in the Indian army. Thanks to **David Beriashvili** for being so friendly, curious, interested in our work and funny. Thank you so much **Dr. Meaghan Ward** for all the "Oh hey, how is it going?" :D. Thank you for all the activities and fun, bringing us together for food, games, cinema, babysitting. Of course thank you for bringing **Fionn (Mookie) Skoog**, that little sunshine, into our lives. Thank you, **Fionn**, for being so funny, active, independent, and well-behaved. You have made us beam with joy from the first time we saw you. Thank you, **Meg**, for entrusting me with walking him in his buggy and keeping an eye on him and carrying him at your place. Thank you for sending me those funny videos of him, they always put me into a good mood. Thank you for introducing me to bouldering. That is a tough sport and I admire you for being able to do it. Thank you for letting me run with you at the "Singelloop Utrecht" 2018. Seeing how you prepared for that and then running it only six months after getting **Fionn**, is a great inspiration and you have my biggest respect and admiration for that. Thanks of course also to your husband **Chris (Skoog) Skoog** for always being so cool, friendly, down-to-earth and inviting to your home for eating, games, and festive gatherings.

Our NMR Spectroscopy Research Group has always been a very big one because it has consisted of three to four sub-groups. One of them is the computational or HADDOCK group. Thanks to **Prof. Dr. Alexandre Bonvin** or "Captain HADDOCK" for the friendliness, insights, and support. It was a very good experience to use HADDOCK to build the models of the complexes generated for this thesis. It helped a lot in understanding the interactions and mechanisms involved. Thank you for calling me "Mr. Chaperones" after my talk at the Bijvoet Symposium 2019 where as the chair after my talk you realized and mentioned to the audience that you were also the chaperone of that session. That was a nice move to show again that chaperones are indeed everywhere. Thanks also to all the members of the HADDOCK group that I got to know or meet over the years and who made the group meetings, lunches, lab outings and other activities so much more enjoyable. Thanks to **Dr. Adrien Melquiond** for

being so kind and showing how one can do sports and have three kids while still doing a good job at work. Thanks for that compliment about the funny picture from my office that I sent on WhatsApp as a response to your New Year's picture with your feet up enjoying Indonesia. Thanks also for letting me paint a part of the inside of your new house and pick up that old cupboard. It is always nice to help someone. There, I also learnt a new trick for how to transport such a heavy cupboard by **Dr. Jörg Schaarschmidt** who I thank for showing me some of your home improvement skills and tricks. Thanks also to the third of the "postdoc dads" **Dr. Mikael Trellet** for always being kind and funny at the lunches. Thanks to the latter two "postdoc dads" for coming to my theatre performance of "Murder on the orient express". Thanks to **Dr. Brian Jimenez**, **Dr. Rodrigo Vargas Honorato**, and **Jorge Roel Touris** for being so kind and funny with positive attitude, for the funny conversations, insights, and moments, and some nice eye catchers in your presentations, and **Francesco Ambrosetti** for being kind and calm and helpful when I asked you about some of your Pymol figures. Thanks to **Dr. Irina Moreira** for greeting friendly when you were around and for congratulating our theatre play performance of "Murder on the orient express". Thanks to **Farzaneh Meimandi** for being so kind and introducing your baby daughter **Rosha** to us during a borrel with tasty Iranian food which reminded me a bit of Macedonian food and showed once again how closely connected we are in this world even if we might be geographically far apart. Thanks to **Dr. Li Xue** for being so friendly and supporting my theatre plays, for the delicious Chinese dinner you prepared for some of us as a housewarming party of your new place, and for playing squash with me which was a lot of fun and very good exercise. Thanks to **Panagiotis (Panos) Koukos** for being kind and asking how I was, if I wanted to go to get food, making compliments about my dressing style and my presentations. Thanks to **Dr. Zeynep Kürkçüoğlu** for always being so nice to me even when you come back for farewell borrels to the group. Thank you for bringing Turkish culture to the group and for being interested in my theatre activities. Thanks to the newest postdocs of the group, **Dr. Zuzana Jandova** for being so kind and funny, and **Dr. Siri van Keulen** for being so kind and bringing us together for fun, exciting, and entertaining game evenings. With that, you have the attribute of a chaperone. Thanks to **Dr. João Rodrigues** for letting me come to and friendly appreciating my presence at your PhD defense party when I was new here in my first week in Utrecht. Also when you come back you greet friendly and always have time for a short chat and advise. It was nice to see how in the one talk I saw from you here you connected your work with human behavior by comparing peptides with babies :D. Thanks to **Dr. Gydo van Zundert** for the fun conversations during lunches, "linners", "lunners", "dinches", and "dunches". Thanks also for including me in the PhD video for **Mohammed** and for making compliments about my acting skills there and thanks also for coming to my play of "Murder on the orient express". Thanks to **Charlotte van Noort** for being so kind, for showing me the trick of sitting in the buffet car of the train and for having a conversation with me on the train on the way to Germany, and for walking with us the "Night of the refugee" 2019. Thanks to **Dr. Cunliang Geng** for always being so kind, supportive, and helpful whenever I had some questions about HADDOCK or scripts. Thank you for sharing with me your stories from your studies in China and for bringing Chinese culture into our lives in the form of music, food, and festivals (the "Chinese New Year Gala" 2016 will always be remembered). Your association "protein and peptide" to describe a card from the game "Dixit" as one that brings humans and science together will always be remembered. Thank you so much **Dr. Anna Vangone** for being so kind right from the start. As a chaperone, you brought people together at birthday parties, game nights, and social events. Most importantly, it is because of you that I found my way to theatre, one of my biggest positive life changing events here. I will never forget that. You were an amazing "Madame LeBouc" on the side of "Detective Poirot" in "Murder on the orient express". Thank you also for the Sinterklaas borrels that you organized. I was very touched that

I received a poem for my first one of those just a few days after I had arrived in December 2014. Thanks for being so kind when you come back to Utrecht, you always try to meet and have a chat with your former colleagues.

I would like to thank all the students I met in our group. Thanks to **Ramon van den Bos** for being so kind and funny right from the start. Thanks to **Alma Svatos** for being so friendly at the beginning of my time here and then again when we met at the ICMRBS 2018 in Dublin. Thanks to **Apfrida Kendek** for being so kind. It was great to see how you work so independently. Thanks to **Benjamin Vermeer** for being so kind and friendly and asking for advice in the lab. Thanks to **Danique Ammerlaan** for being so kind and presenting and discussing your poster to me at the Bijvoet Symposium 2019. Thanks to **Bram Vermeulen** for being friendly and contributing to our "Night of the refugee" 2019 campaign. I wish you and all the other students good luck for your future career, among others **Sam de Vos**, **Ouissam Hsine**, **Zhengyue Zhang**, **Marijne Schijns**, **Yuri Vekelenburg**, **Mees Molenaar**, and **Jelmer Eerland**.

Nothing around the lab would be possible without the staff members. Thanks to **Dr. Andrei Gurinov** for sharing your experiences from your times abroad with us by showing pictures and telling stories. Thanks also to your wife **Dr. Svetlana Pylaeva** for giving a presentation with such a nice title ("My name is Bond. Hydrogen Bond") which was a nice beginning of my probably final scientific year 2019 here. Thanks to **Barbara Hendricx** for being so kind, interested, helpful and supportive as secretary and of course in your new position in which you help us get through with our thesis defense procedures. Thanks to **Geeske Badart** for being so friendly, helpful and supportive. You are an inspiration with your enthusiasm and how you make things happen and bring about positive change at our institute. Thanks to **Dr. Gerrit Gerwig** for not hesitating and driving me in your car to the UCU campus on my first day in Utrecht so that I could pick up my keys to my studio. Thanks to **Dr. Gert Folkers** and **Ing. Mark Daniëls** for the advice in the lab. Thanks to **Dr. Hans Wienk** for your open ears, advice, and support with NMR experiments, writing, and discussions. Thanks to **Ing. Johan van der Zwan** for being so kind and humble and always helpful. Thanks to **Dr. Klaartje Houben** for asking me to give that "Molecular Machines" NMR course which helped me to understand some new things about NMR and that I like teaching, which was helpful at that early stage of my PhD. Thank you for showing that a career and family are manageable at the same time. Thanks to **Dr. Markus Weingarth** for all the occasional conversations especially during lonely weekends in the lab, for supporting young scientists, asking me about solution NMR which shows your appreciation of my experience, for being interested in my project, and challenging my future perspectives in academic sciences which helped me to understand what I am missing but also what my strengths are. Thank you for your kind words after my presentations at the Bijvoet Symposium 2019 and FEBS Congress 2019. Thanks to **Prof. Dr. Rob Kaptein** for always being and greeting friendly and being so helpful with funding the lab day-outs and Sinterklaas borrels that I (co-)organized.

I undertook this PhD project as Marie Curie Fellow of the Initial Training Network and Innovative Doctoral Programme called "ManiFold" funded by the European Union via its 7th Framework Programme and I would like to thank the people who were part of that. Thanks to **Dr. Stefan Rüdiger** for writing the grant, managing and organizing the ManiFold programme and all around that. It was by pure chance that I found the open position. But maybe it was actually destiny so that I could come up with this very special chaperone story. Thanks to all the other participants of the programme, most of which have already graduated. Thanks to **Dr.**

Tania Moràn Luengo for always being so kind and social. It is an inspiration to see how you always bring so many different people together and how you always have a positive attitude and a smile on your face. Thanks to **Dr. Anna Chatsisvili** for being so kind and friendly. You are an open and positive person and the quality of your work is fantastic. Thanks to **Dr. Yang Yang** for always being so kind. It is amazing to see what kind of work you managed and that you got your daughter during your PhD. It was heartwarming to see **Suri** at your defense. Thanks to **Dr. Camilla de Nardis** for being so kind. You are an inspiration with your engagement for a better environment and sustainable lifestyle. Thanks to **Dr. Daniel Fonseca** for being friendly and social. Your scientific knowledge which you showed with your questions after scientific talks amazed me. Thanks to **Dr. Jonas Dörr** for letting us ManiFolders get together at your place for the regular dinners and meetings and also for being friendly and supporting us PhD candidates through your work as PhD representative. Thanks to **Dr. Philip Lössl** for the nice time in the ManiFold project, it is great to see how much work you managed. Thanks to **Manikam (Saran) Sadasivam Saravanan** for always being friendly and for driving us to the AiO evening in the center of Utrecht in your car. Thanks to **Dr. Martina Radli** for being so friendly and for joining me in the trips to do MST in Leiden. I know you are a fantastic singer and you inspire people with your talent. Also your thesis title, cover, molecular cell article and your creativity with the structures of Hsp90 are fantastic. Thanks to **Dr. Nadia Leloup** for always being so kind and giving me a thesis book of yours with a nice comment. Thank you for coming to my theatre play of "Murder on the orient express", I am glad that you liked it. Thank you very much for introducing me to yoga. Still today, I use my experience of that in exercises I do to stay healthy. With your knowledge about this discipline, your commitment to it and the fact that you became a yoga teacher during your PhD, you are an inspiration. Thanks also to **Klemen Dolinar** for setting the start of the project and for setting the way free for me to come. My finding this position meant finding the key to a whole new understanding of chaperones like never before and defining the purpose of my life.

Collaborations are very important in science and I was fortunate to have had some good ones for my project. Thanks to **Prof. Dr. Marcellus Ubbink** for the allowance to use the ITC instrument in your group in Leiden without any complication nor interference. It was during one of those experiments, when one of the injection heat peaks of a mutant construct came down that I knew I had determined the nucleosome assembly mechanism of the chaperonosome. Thanks to **Anneloes Blok** for being such a cool and helpful technician about my usage of the ITC instrument in Leiden. You never complained about me measuring too much or changing and extending my measurement times. Thanks to **Dr. Domenico Fasci** from the **Prof. Dr. Albert Heck** group for being so kind. You took all the samples I gave you without resistance and you conducted all the necessary mass spectrometry experiments with them. That was a key collaboration for my project. Thanks to **Dr. Francesca Mattiroli** for the fruitful discussions about histone chaperones and your kind words about the quality of my data and presentation at the Bijvoet Symposium 2019. Thanks to **Prof. Dr. Haico van Attikum** for the collaboration and the kind email exchanges and also to the technicians from your group, **Kees Vreeken** and **Wouter Wiegant**, for the collaboration and the hard work you did for the project. Thanks to **Dr. Bert Janssen** for allowing that I can do SEC MALLS experiments in your laboratory and to **Matthieu Zeronian** for making time available and helping me out with those experiments. Thanks to **Dr. Dmitri Svergun** for the collaboration on the SAXS experiments and **Dr. Melissa Graewert** for the hard work you did for the project by conducting the SAXS measurements and analyzing the data. Thanks to **Dr. Vlad Cocojaru** for the insights about nucleosome dynamics from your computational work. Thanks to **Dr. Xiaohu Guo** from

the **Prof. Dr. Titia Sixma** group for the collaboration in setting up all the crystal trials and thank you for the great insights into crystallography.

A big thanks to the members of the group I was in. Thanks to **Clara van Emmerik** for being so kind and for your kind words about my presentations at NMR DG 2016, our group meetings, CHAINS 2017, and the Bijvoet Symposium 2019, and your interest in my project. Thanks also for laughing at my jokes and funny things that I said as you were one of the few who got them ;). It is amazing on how many different things you worked on and wrote about during your PhD and still have a good work-life balance. It is nice to see that you like games, escape rooms, and you have a great musical talent which I hope to be able to still see some day live. It is great that you found a new job for right after your PhD. Thanks to **Heyi Zhang** for being so cool and funny, for your fluent presentations, for sharing the beautiful meaning of your name which means "unity, oneness" which is exactly what a chaperone brings about, and for sharing interesting facts about China. You have broadened my horizon. Thanks to **Ulric le Paige** for the nice experimental discussions and advice. Also thank you for your funny lectures, moments, and jokes. Thanks to "Hey, yo" **Dr. Velten Horn** for always being so kind and supportive with all the fruitful and helpful discussions. It was good to have someone from Germany around. Thanks to **Vincenzo Lobbia** for all the insider information you have about the things that are going on at the institute and for the funny and memorable moments during the game evenings. It is amazing to see how well you have your experiments planned so that you can have a good work-life balance. Thanks to **Dr. Maryam Faridounnia** for being so friendly, for your encouraging wisdom and advice, and for giving me the hammer that says "The last argument". When I look at it, I know that not all has been said, yet, and it keeps me going. Thank you also for citing my NAR paper in your review.

Thanks also to all the PhD candidates from the Bijvoet Center who made the time here more enjoyable through social activities at for example AiO evenings and Bijvoet Symposia and for making nice comments after my talk at the Bijvoet Symposium 2019. Among others, thanks to **Viviana Neviani** for always being so kind and friendly with a smile on your face. It was nice to see how you kept your positive attitude throughout you project even after setbacks. Thanks to **Dr. Luca Ferrari** and **Magdalena Wawrzyniuk** for always being so friendly and asking for my advice at the beginning of my time here. Thanks to **Robert Englmeier** for making that nice compliment about my Bijvoet Symposium 2019 presentation when we met by chance at the bike shed one day after that. Such a nice reaction is not a given nowadays. Also thanks to all the other PhD students/postdocs I have had the chance to meet or talk to, among others **Dr. Mercedes Ramírez Escudero**, **Lucas Chataigner**, **Wout Oosterheert**, **Karla Ivette De la O Becerra**, **Nadine Prust**, **Marcel van Willigen**, and **Margreet Koopman**.

One of the greatest experiences outside of my PhD thesis during my time here was theatre and I would like to thank the people who made that a great experience. Thank you so much **Alexandra Elroy**, my theatre coach, teacher, and director. You gave me a voice when I had none by putting me in the middle of that stage in "Murder on the orient express" as the main character "Detective Poirot", in the short scenes as an impatient police agent, out-of-control robot, and my favorite "Forrest Gump", and in "A midsummer night's dream" as "Egeus" and unforgettable "Mustardseed", two completely different characters, and there were even people who did not recognize I played both roles. This theatre experience improved my life, friendships, self-confidence, and it helped me improve to become the presenter that gives award-winning scientific talks that touch hundreds of people. Your "isolation" and performance preparation exercises have helped me with this, so I hope you do not mind that I have used

them for scientific talk preparations, too ;). Your vision and creativity, with which you build a play around a cast, are an inspiration. Thanks to all the cast and crew of "Murder on the orient express" for making it so enjoyable and fun, among others **Sophia Berendt** (a great and super funny "Dr. Constantine", assistant to "Detective Poirot"), **Andrea Ferrazzo**, **Tina Lešnik**, **Jody Thornton**, **Türkü Köksel**, **Bariş Özkale**, **Lotte van der Velden**, **Luying Hou**, **Dr. Tania Moràn Luengo**, and of course again **Dr. Anna Vangone** as wonderful "Madame LeBouc" because of whom I started with theatre in the first place. Thanks to all the cast and crew of "A midsummer night's dream" for making it so enjoyable and fun, among others **Alise van Heerwaarde** (the flutist who encouraged "Mustardseed" to sing and supported him so well while he was joking around and singing), **Anneloes Vermeer** (cool daughter "Hermia" of "Egeus" who brought us all together to cook and eat together after theatre Saturday and watch the play during a get-together with the cast), **Esther van der Werf** (unforgettable "Queen Titania" and an inspiration with your multiple talents in acting and singing), **Marly Terwisscha** (a fantastic "Puck"), **Manon Julicher**, **Igor Magaraggia**, and **Athena Papantoniou**.

Sometimes one meets special people at places outside of the institute like for example conferences, workshops etc. Thanks to **Suraj Manrao** for being so kind to talk to me while we were walking to the opening of the ICMRBS 2018 at the UCD in Dublin. It is amazing to see that you support young scientists with your poster prizes at that and others conferences. Thanks to **Prof. Dr. Karolin Luger** for letting me talk to you about histone chaperones over lunch at the nucleosome conference in Heidelberg in 2017 and for coming with such enthusiasm to my poster and talking in-depth about my research there. A big thanks to **Dr. Marta Brucka** from the EMBO NMR workshop close to Berlin for the inspirational time when I got to visit Geneva, one of the most beautiful places I have ever been to with the longest bike tour I have ever made on a single day even though I live in the Netherlands which is the bike country :-J. With your active lifestyle, love for languages, culture, different places and life in general, you are an inspiration. Thanks to the people I met at the FEBS YSF and Congress 2019, amongst others **Hovakim Grabski**, **Dr. Andrew (Drew) Hammond** (who has with his gene drives the most incredible technology in his hands to eradicate malaria, absolutely fascinating!), **Olívia Petrvalskà**, **Mira Hammad**, **Egor Diakonov**, **Ksenia Skobeleva**, **Ilia Korobko**, **David López Martinez**, **Anna Jagusiak, Victoria Barygina, Marco Cavaco, Marcin Makowski, Gonzalo Pérez-Mejías, Francisco Rivero-Rodríguez, Cene Skubic, Aneta Smidova, Agata Szade, Iva Uzelac** and **Tomasz Tronina** and many more who were either as participants or organizers great chaperones throughout these meetings and who encouraged me with a Best-talk-award and their kind words that my chaperone story is worth telling, can reach and inspire people. Thanks to **"an angel"** that I do not know but I remember when you looked back at me from your bike while I was biking while holding an unhandy bag. Because you slowed down I had to slow down, too, the bag got stuck behind my leg which made my bike suddenly turn a 90° left and off the bike lane. Luckily nobody was trying to overtake me otherwise there would have been an accident, and I somehow managed to get to a stand just before the bus lane next to the Janskerkhof bus stop. You are my angel because if you had not slowed me down there, the same thing might have happened a few meters later and I would have actually landed on the bus lane with no chance if a bus was just about to pass.

Also the people I met in and outside science before coming to Utrecht have still an impact on me today. The PhD time has been a hard time for me. I have tried to take in any hint of support and inspiration that could keep me going. I could always count on some old friends from Frankfurt. Thanks to **Daria Schulz** and **Khai-Thai Duong** for all the years of friendship. It is always nice to know that there is an old friend still in Frankfurt. Thanks to Khai-Thai for making

me go to Nepal. That was a valuable experience for my life. It is amazing what kind of a help organization you have built up. Thanks to the children from **Buddhist Child Home**. We were at your house when the earthquake hit us. That saved our lifes. You kids are so full of joy and appreciation. I wish you all the best in the world. Thank you so much **Dr. Orla Slattery** for introducing me to independent lab work as my first ever supervisor. You are one of the nicest people I have ever met in science. With your friendliness you were always a delight to talk to, work with and a great inspiration. Thanks to **Prof. Dr. Volker Dötsch** for your support throughout my diploma studies, thesis, up to my application for the PhD position in Utrecht. Thanks to **Dr. Daniel Coutandin, Dr. Jan Heering, Dr. Sebastian Richers, Dr. Jean Aymard Nzigou Mandouckou and Larissa Angebauer** for your support during my diploma thesis, your scientific and life insights. That helped me to keep my head up in that difficult time. Your dedication and approach to your work are an inspiration. Thanks to **Dr. Nina Ripin** for your company during our long working days in the lab in Frankfurt. Your dedication, thoughts about and plans for the future of young scientists and science are an inspiration. Another experience that shaped my character was during my time in the Federal Defence Forces of Germany just before I went for my PhD to Utrecht and I would like to thank my comrades during basic military training, among others **Maria Hoppe**, **Franz Massini**, **Laura Lohbrunner**, **Jörg Polling, Martin Neumann and Charlie Merkle**. Of course also thanks to **Captain Steffen Puhlmann**, my commander during basic military training, who made it possible that I could get time off to go to my interview for this PhD position.

And finally, I want to thank the person that made my life so much more worth living during my PhD. I cannot thank you enough **Schatzi (Miranda (Shehrazade) Jekhmane)**. The fact that I cannot write a single word of acknowledgment for you without tears in my eyes says it all. Thank you for everything. You are such a fantastic person. Thank you for always sitting next to me at lunch, for calling me "Schatzi", for all the walks in the botanical gardens, for walking twice the "Night of the refugee" with me in 2018 and 2019, for showing me the Nijmeegse Vierdaagse and the festivities around it and for visiting my home town Frankfurt (all some of the nicest days for me ever). Thank you for cheering for us when we ran the Utrecht Singelloop 2018 and for me again at the Goudse Singelloop 2019. Thank you for inviting some of us for a Moroccan dinner at your place in Gouda, it was delicious and reminded me of Macedonian food, again showing how closely different parts of the world can be connected. Thank you for inviting many of us to your Moroccan wedding, that was a very nice experience. Your strength, life experience, love for life, people and especially cats are an inspiration. Of course also thanks to your husband **Roman Dingjan** for being so kind, inviting and talking to me outside at your Moroccan wedding, and for being so accepting of my friendship with Schatzi.

Finally, it is time to thank my **family**, all my grandparents, aunts, uncles, cousins, their spouses and children. And most importantly **my parents and brother** without which my life would not have been possible in the first place (Picture 4).

Picture 4. My family, the best chaperones. (A) Thanks to my **brother Dejan**, 5 years older than me, who has always been there to take care of me, support me and stand up for me. He helped me grow up strong and clever. Until today, I see him as one of the most intelligent people I have ever known. **(B) and (C)** My humble parents who made a good life possible for their children and who have helped many people in their lives. They taught me to be a good person and hard worker. They showed me that one can achieve everything with dedication and hard work. **(B)** My **mother Kadifka** grew up in a small village in central North Macedonia. As a child, she had to work very hard. Among other things, she had to get up in the middle of the night to work in the fields before going to school. She is the strongest woman I have ever known. **(C)** My **father Boriz** who grew up in a small village in the south of North Macedonia. As a child, he grew up with a big family of farmers, all living under the same roof. He is a humble man, always willing to put extra effort to help people in their most difficult times while setting his own life aside.

In the end, I would like to thank you, the reader of this book. I hope you enjoyed it. I see science as a public service for the good and wellbeing of the world and the people. But it has to be brought closer to them. A closer connection has to be made between science and people and between people themselves. Because we are all one world and dependent on each other. My chaperone story is aimed at making such a connection. To explain to the people out there, parents, caretakers, teachers etc. who are chaperones themselves, why we scientists call these molecules that we study "chaperones", too. My colorful story is aimed at bringing peace. I see the world different which allowed me to have many twists in my perspective which in turn made it possible for me to determine the mechanism of the chaperonosome and to make the connection to human chaperones and the ones involved in protein folding (Picture 5). So, how can you remember the chaperonosome mechanism? You just have to think about the roller coaster: The chaperone hugs the children and releases them properly and safely, one after the other and onto the roller coaster of life.

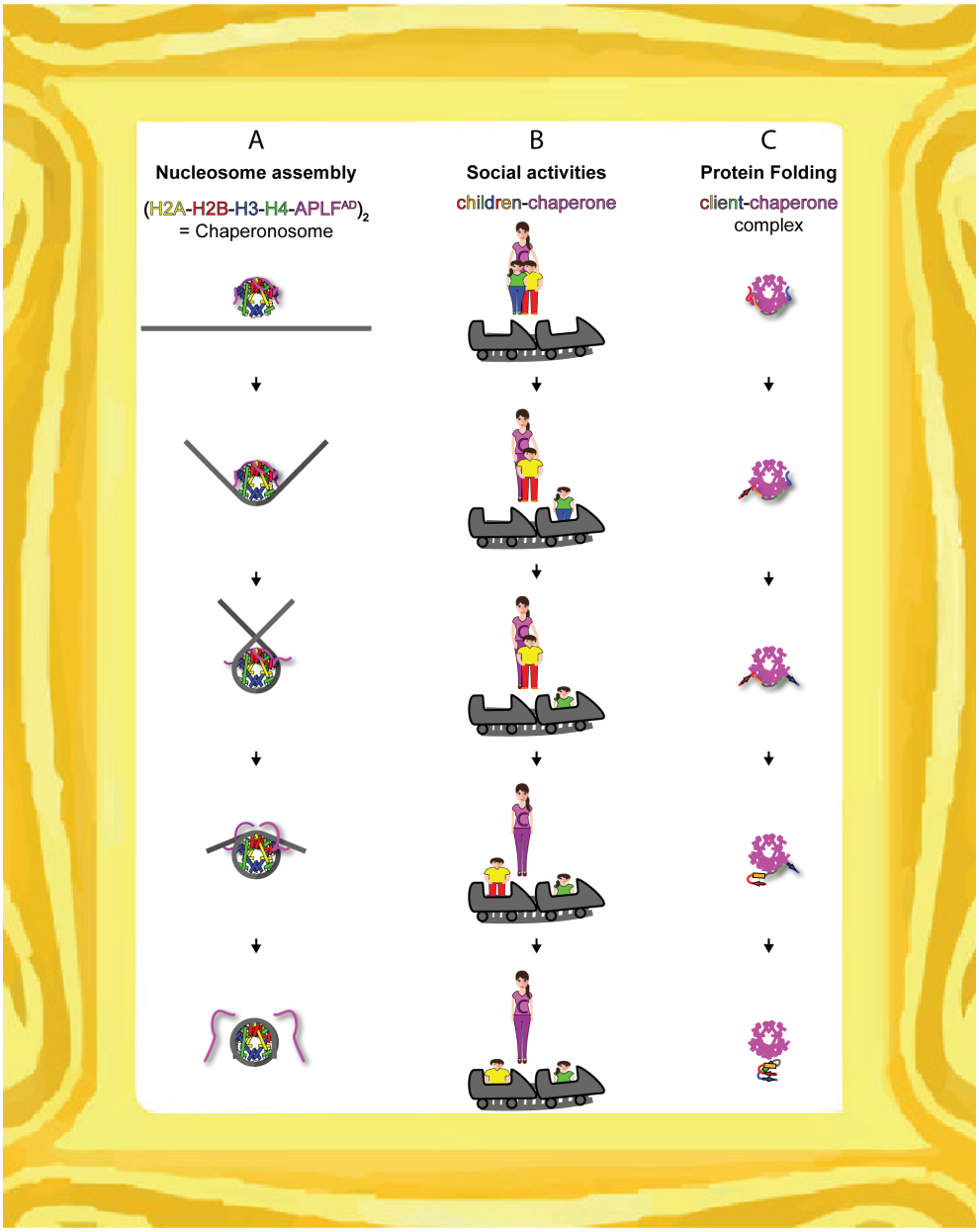

Picture 5. All chaperones function in the same way. The chaperonosome mechanism (A) works just like human chaperoning (B) and protein folding (C): The chaperone hugs the children and puts them, one after the other, properly and safely onto the roller coaster of life.

In the end, I would like to leave you with the final picture of "chaperone" that I have from finding the chaperonosome because I think we can learn a lot from it.

Do you remember I told you in **Chapter 1** that the histones form dimers and tetramers through a so-called handshake motif? And, whereas separated alone, I showed you in **Chapter 4** that they are brought together by the chaperone (The final picture A). I would suggest that we should follow this example and put all of our hands together (The final picture B) to bring all of the divided parts of the world together (The final picture C) and make it a better place for us all to live. Because we are all chaperones of this planet. We form its "chaperonosphere" to protect it.

The final picture. We are one. The chaperone brings the histones together (A), so let us put our hands together (B) to bring all the divided parts of the world together (C) and make it a better place for us all to live.

"Chaperone". Are you now familiar with this term? This is almost the end of this book. And, after all that you have read and seen, I would like to ask you to figure out one more time what you associate with, or the picture that you have of "chaperone". In order to do so, I would like to ask you to do the following.

Take a pen or pencils and draw or paint for yourself in the empty picture frame you see on the next page your own personal final picture that describes what you associate with the term "chaperone". You can also brainstorm and the picture can contain bullet points, whole sentences, diagrams or anything that comes to your mind about "chaperone". And once you have that picture and you are satisfied with it, you can continue with reading on the next page. Are you ready? Then, please, draw your own personal final picture of "chaperone".

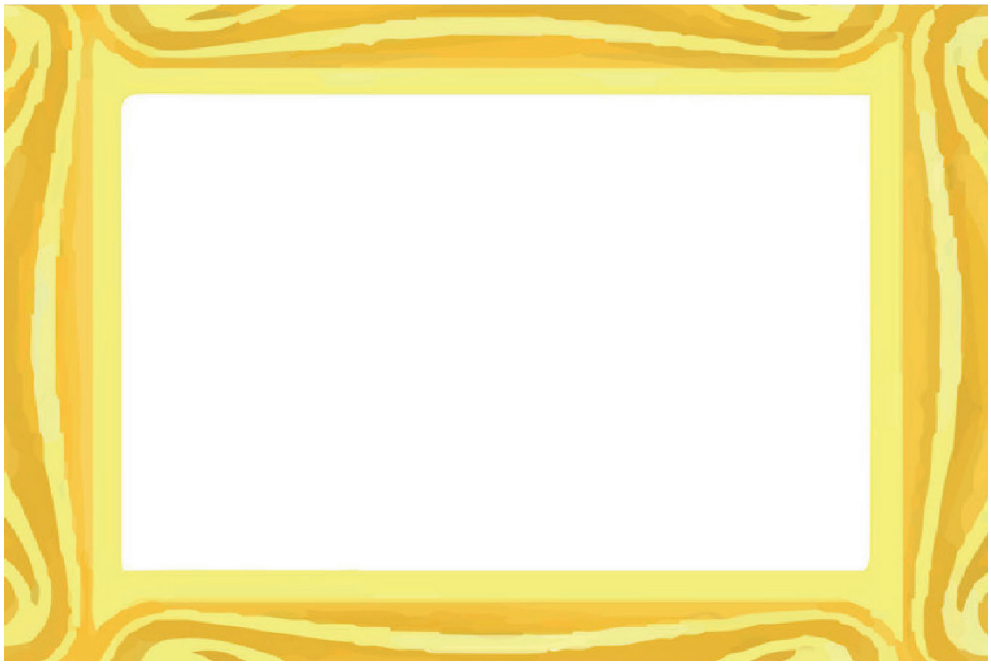

Now that you have your final picture of "chaperone", I would like to ask you to answer for yourself one question:

When you compare your final picture to the one that you drew at the beginning of this thesis:

Are they the same?

Thank you!

Can you finally see?

List of Publications

PhD-related publications:

Corbeski, I., Horn, V., van der Valk, R.A., le Paige, U.B., Dame, R.T. and van Ingen, H. (2018) Microscale Thermophoresis Analysis of Chromatin Interactions. *Methods Mol Biol*, 1837, 177-197.

Corbeski, I., Dolinar, K., Wienk, H., Boelens, R. and van Ingen, H. (2018) DNA repair factor APLF acts as a H2A-H2B histone chaperone through binding its DNA interaction surface. *Nucleic Acids Res*, **46**, 7138-7152.

Corbeski, I., Graewert, M.A., Fasci, D., Wiegant, W., Vreeken, K., Mattiroli, F., Wienk, H., Svergun, D.I., Heck, A.J.R., Van Attikum, H., Boelens, R. and van Ingen, H. (2019) A chaperone that assembles the histone octamer to promote its deposition onto DNA. *In preparation*.

Publications from previous research work:

Luh, L.M., Hänsel, R., Löhr, F., Kirchner, D.K., Krauskopf, K., Pitzius, S., Schäfer, B., Tufar, P., Corbeski, I., Güntert, P., Dötsch, V. (2013) Molecular crowding drives active Pin1 into nonspecific complexes with endogenous proteins prior to substrate recognition. *J Am Chem Soc*, **135**, 13796-13803.

Hänsel, R., Luh, L.M., Corbeski, I., Trantirek, L. and Dötsch, V. (2014) In-cell NMR and EPR spectroscopy of biomacromolecules. *Angew Chem Int Ed Engl*, **53**, 10300-10314.

About the Author

Ivan Corbeski was born on September 10th, 1986, in Skopje, Republic of North Macedonia (then Yugoslavia). In 1992, he moved with his family to Frankfurt am Main, Germany, where he grew up and went through school education. He obtained his diploma (equivalent to master) in biochemistry with distinction from the Goethe University Frankfurt, Germany, in 2014. The research resulting in his diploma thesis was conducted at the Institute of Biophysical Chemistry and Biomolecular Magnetic Resonance Center of the Goethe University under the supervision of Prof. Dr. Volker Dötsch and was titled: "Kinetic and Thermodynamic Characterization of Enzyme Dynamics under Macromolecular Crowding Conditions and in a Cellular Environment by CPMG Relaxation Dispersion NMR Spectroscopy". After that, Ivan voluntarily joined the Federal Defence Forces of Germany, nuclear/biological/chemical defence division, where he successfully completed basic military training with a special certificate that "attests to him that he shows the highest degree of commitment, team spirit, and endurance". He then moved to Utrecht, Netherlands, to pursue a PhD in the field of structural biology at the NMR Spectroscopy Research Group, Bijvoet Center for Biomolecular Research, Utrecht University, in the group of Prof. Dr. Rolf Boelens, who is also his promotor, and under the supervision of Dr. Hugo van Ingen. Ivan undertook as Marie Curie Fellow the project titled "Mechanism of Nucleosome Disassembly by Histone Chaperones" of the Initial Training Network and Innovative Doctoral Programme called "ManiFold" funded by the European Union via its 7th Framework Programme. The results of that research are presented in this thesis.